Synthesis, Structural Characterization and Tuning Electronic Properties in Planar and Large Porphyrinoids

विद्या वाचस्पति की
उपाधि की अपेक्षाओं की आंशिक पूर्ति में प्रस्तुत शोध प्रबंध

A thesis submitted in partial fulfillment of the requirements of the degree of Doctor of Philosophy

द्वारा / By
प्रगति शुक्ला / Pragati Shukla

पंजीकरण सं. / Registration No.: २०१८३५७४ / 20183574

शोध प्रबंध पर्यवेक्षक / Thesis Supervisor:
वी. जी. आनंद / V. G. Anand

भारतीय विज्ञान शिक्षा एवं अनुसंधान संस्थान पुणे
INDIAN INSTITUTE OF SCIENCE EDUCATION AND RESEARCH PUNE
2024

Dedicated to

My parents

Smt. Kusum Shukla and Shri. Atul Shukla

My husband Mr. Prashank Pandey

भारतीयविज्ञानशिक्षाएवंअनुसंधानसंस्थान, पुणे
INDIAN INSTITUTE OF SCIENCE EDUCATION AND RESEARCH (IISER), PUNE

CERTIFICATE

Certified that the work incorporated in the thesis entitled "*Synthesis, Structural Characterization and Tuning Electronic Properties in Planar and Large Porphyrinoids*" submitted by *Ms. Pragati Shukla* was carried out by the candidate, under my supervision. The work presented here or any part of it has not been included in any other thesis submitted previously for the award of any degree or diploma from any other University or institution.

Date: 15th Jan 2024

Dr. V. G. Anand

Research Supervisor

DECLARATION

I declare that this written submission represents my ideas in my own words and where others' ideas have been included, I have adequately cited and referenced the original sources. I also declare that I have adhered to all principles of academic honesty and integrity and have not misrepresented or fabricated or falsified any idea/data/fact/source in my submission. I understand that violation of the above will be cause for disciplinary action by the Institute and can also evoke penal action from the sources which have thus not been properly cited or from whom proper permission has not been taken when needed.

Date: 15th Jan 2024

Pragati Shukla

20183574

Acknowledgement

My profound gratitude goes to my thesis advisor, Prof. V. G. Anand, for his constant guidance, inspiration, and support. His immense knowledge and timely discussion regarding the projects enabled me to finish this study and compose my thesis. I wholeheartedly thank to him for his friendly nature and encouragement. I would like to thank his wife, Mrs. Padma Priya Anand, for her kindness and affectionate behavior.

I am thankful to former directors Prof. K. N. Ganesh and Prof. Jayant Udagaonkar, as well as current director Prof. Sunil S. Bhagwat, for providing excellent research facilities and a wonderful research environment at IISER Pune.

I would like to sincerely thank my Research Advisory Committee members Dr. Jayaraj Nithyanandhan (NCL, Pune) and Dr. Moumita Majumdar (IISER, Pune) for their suggestions and advice throughout my doctoral journey.

I am grateful to Dr. Rajesh G. Gonnade (NCL, Pune) for his prompt assistance and crystal-solving recommendations. I am extremely thankful to Prof. Ramakrishna G. Bhat especially for his suggestions, support, and inspiring remarks throughout my degree. I am also grateful to the former and current Chair Chemistry, as well as all the IISER Pune faculty members.

I want to express my heartfelt appreciation to all my past and present lab mates for sharing their knowledge. It gives me great pleasure to thank Dr. Madan, Dr. Ashok, Dr. Rakesh, Dr. Udaya, Dr. Prachi, Dr. Brijesh, Dr. Sujit, Dr. Tarunpreet, Dr. Sunita, Mr. Markose, Mr. Vishnu, Mr. Ramesh, Mr. Rakesh, and Ms. Nikita for making the lab a pleasant place to work and for guiding me to improve my research skills. I would like to give special thanks to Dr. Madan Ambhore for his constant support and suggestions related to project works.

I would like to thank all the staff members of IISER Pune, especially Mr. Tushar, Mr. Mayuresh, Mr. Mahesh, Mrs. Megha, Mrs. Hema, Mr. Ganesh, Mr. Sanjay, Mrs. Amruta, Mrs. Bhagyashree, Mr. Yatish, Ms. Dnyaneshwar for their timely help and concern.

My special thanks to Dr. Sandeep Mishra (for NMR experiments and suggestions), Mr. Praveen, Mr. Nitin, Mr. Ravindra, Mr. Sandeep Kanade and Mr. Suresh for instrumental support. I am also thankful to Mrs. Nisha Kurkure for her support related to cluster facilities.

I am forever thankful to my batchmates Akanksha M., Pooja, Jabed, Deepak, Nirmala, Utreshwar and Akanksha for their continuous encouragement and support. We had a great time and made memories to last a lifetime. I am also grateful to my IISER Pune friends, seniors and juniors for their help and friendly nature during my doctoral journey.

I am also grateful to my IIT Kanpur labmates, particularly Dr. Tapas, and my IISER Mohali colleagues. They all helped me in both direct and indirect ways. I am thankful to Dr. Nidhi and Ms. Tanuja (NCL Pune) for their scientific discussion and friendly behaviour.

I am also thankful to my previous school teachers, college faculties and staff members to always being helpful to me for my studies. I am especially thankful to Dr. Daniel, Dr. jyotsana for believing in my abilities and sharing knowledge.

I am deeply thankful to my grandmother (late Mrs. Ramshakhi Shukla) for sowing the seed of knowledge and kindling the lamp of my dreams. No words can ever express how grateful I am to my mother, Mrs. Kusum Shukla, and father, Mr. Atul Shukla, for believing in me and allowing me to pursue my career. My greatest gratitude goes to my husband, Mr. Prashank Pandey, and my brothers (Mr. Prateek and Mr. Yash), as well as the entire family members, for their unwavering love and support throughout my career.

Due appreciation is offered to them, whose names were unintentionally left despite their constant assistance during my PhD journey.

My final and warmest thanks to IISER Pune for the research funding and fellowship, as well as for realizing my aspiration of being called a Dr.

Yours

Pragati Shukla

Table of Contents

Synopsis

The thesis is entitled “Synthesis, Structural Characterization and Tuning Electronic Properties in Planar and Large Porphyrinoids”. These larger porphyrinoids have a greater number of heterocyclic units and *meso* positions in comparison to the parent porphyrin ring. The replacement of a pyrrole unit with thiophene/furan/selenophene results in the core modification of the parent porphyrin. Therefore, expansion and modification of the ring affect the electronic and structural properties in these macrocycles. This thesis mainly focuses on the expanded planar and core modified porphyinoids including hexaphyrin, octaphyrins and decaphyrins. These macrocycles were synthesized through multistep synthesis utilizing small precursor units. As the macrocycle's conjugated backbone enhances its redox nature, the oxidation of these macrocycles was thoroughly studied. The isolation of these macrocycles were done by column chromatography and characterized through mass spectrometry, 1D and 2D NMR spectroscopy, UV-vis absorption spectroscopy, X-ray single crystal diffractometer, cyclic voltammetry and spectroelectrochemistry. Quantum chemical calculation provides additional support for the observed experimental findings.

This thesis comprises of five chapters. The first chapter provides a literature overview of porphyrins and isophlorins, including their structural and electronic properties. Subsequently, the reports on expanded porphyrinoids and discussion related to their synthesis and structural properties are detailed. It includes the strategic modification in expanded porphyrinoids to study the structure dynamics. This chapter well describe the properties of porphyrinoids to stabilize the radicaloid species and further its enhanced two -photon absorption values.

The second chapter of this thesis describes the intriguing properties of expanded porphyrinoids as Huckel and Mobius aromaticity. It describes the transformation of Huckel to Mobius macrocycle with the effect of pH, solvent, kinetic and thermodynamics conditions. It includes the synthesis of planar and core-modified hexaphyrin with 30π electrons. It has two pyrrole and four furan rings in the conjugated network, and expressed as Huckel aromatic macrocycle. Unexpectedly, the two electrons reversible ring oxidation of 30π Huckel aromatic hexaphyrin led to the formation of 28π Mobius aromatic hexaphyrin. Along with NMR and single crystal studies, computational analysis of both hexaphyrins provide insight into their aromatic behavior through AICD plots and NICS values. This aromatic transition was accomplished via an unstable intermediate radical cation, as confirmed by spectro-electrochemical experiments.

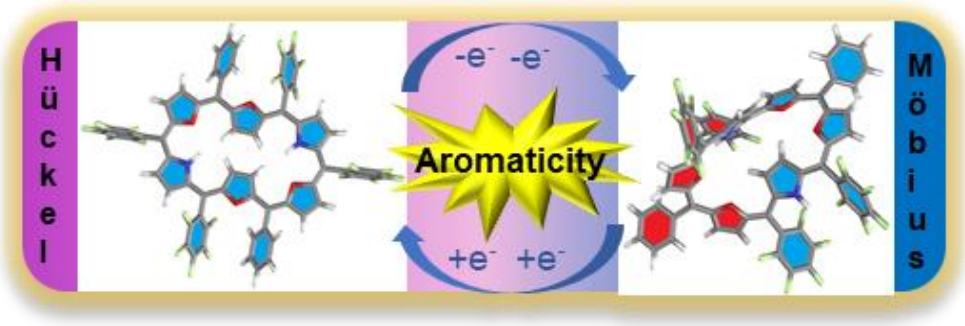

The synthesis of four and eight membered isophlorinoids, including all of the furan units in the ring is thoroughly described in the third chapter of the thesis. These antiaromatic macrocycles include 20π and 40π electrons in the conjugated backbone. The octaphyrin exhibits the intriguing characteristics of solvatomorphism, presenting different solid-state conformations depending on the solvent of crystallization. In contrast, the functionalized *meso*-position, i.e., *p*-Br-phenyl, in these isophlorins makes them active in coupling reactions, and thus they could form the porphyrin-isophlorin dimer when coupled with borylated porphyrins.

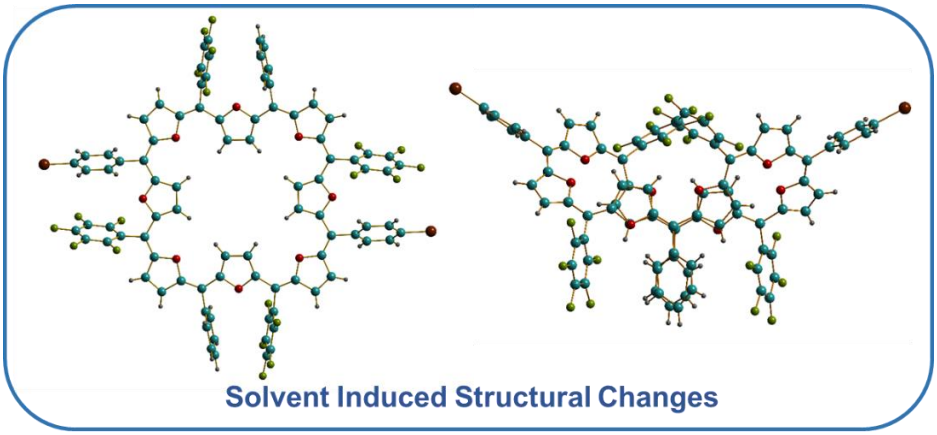

The fourth chapter of the thesis describes the synthesis of larger and planar decaphyrins with 44π and 46π electrons, which were synthesized with fewer *meso*-positions and non-pyrrolic heterocyclic units. These are the first reports of decaphyrins with planar topology that have been analysed by single crystal x-ray diffraction. Experimental studies of 46π decaphyrins demonstrate its diradicaloid character with a *g* value of 2.0054 in EPR measurements. While computational studies revealed a small $\Delta E_{(S\text{-}T)}$ gap and 69% diradicaloid character for the macrocycle. The synthesised decaphyrins displayed reversible 2-electron ring oxidation processes and all the possible electronic stages of these decaphyrins were characterized by spectroelectrochemistry.

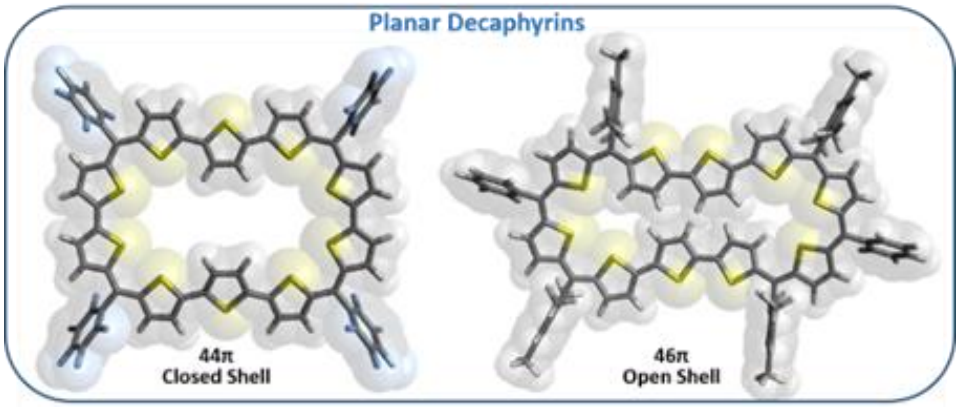

The 5th chapter explains the well-versed strategy to synthesis the first example of porphyrin-isophlorin dimer through the Suzukii-Miyuara cross coupling of functionalized isophlorin and porphyrins. The electronic coupling between 20π isophlorin and 18π porphyrin was studied by UV-vis absorption and NMR experiments. Interestingly the isophlorin-porphyrin dimer undergo the oxidation and form dication of the dimer. This dimer could act as captivating materials for investigating electron transfer mechanism in artificial photosynthesis and also in optoelectronis.

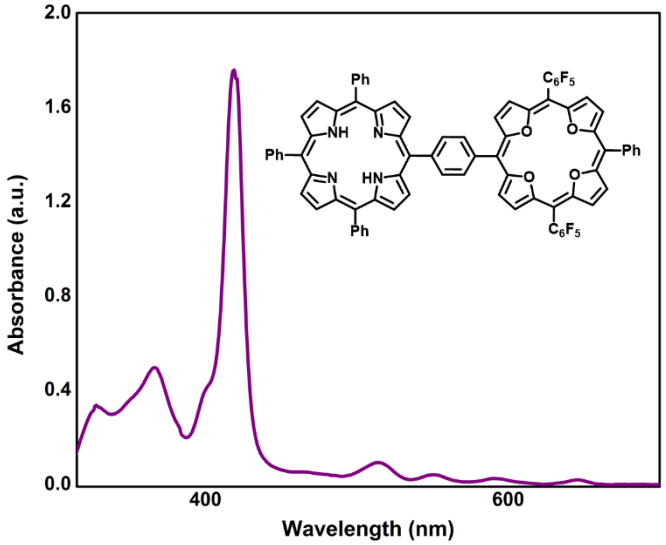

In summary, this thesis demonstrates the synthesis of aromatic and antiaromatic models of expanded porphyrinoids. The tailoring of electronic and structural properties of expanded porphyrinoids discovers the possibility of diradicaloid character and solvatomorphism in these expanded derivatives.

CHAPTER 1

Introduction

Porphyrin compounds have attracted substantial attention due to their importance in biology such as metalloenzymes, complexing agents, and medicinal applications.[1] Porphyrins have a basic structure made up of four pyrrole rings joined by four methine carbons. Out of total 22π electrons only 18π electrons are involved in the conjugation as the flow of electrons in porphyrin **I.4** goes through inner macrocyclic core. Due to its planar and conjugated structure, it exhibited diatropic ring current and satisfies Huckel's (4n+2) requirements for aromaticity.[2] In 1960, during the study of chlorophyll[3], R. B. Woodward suggest the formation of porphyrin through the condensation of pyrrole **I.1** with formaldehyde in presence of protic acid. Reaction proceeded with the formation of porphyrinogen **I.2**, which further gets oxidized to a 18π porphyrin **I.4** (scheme-1.1).

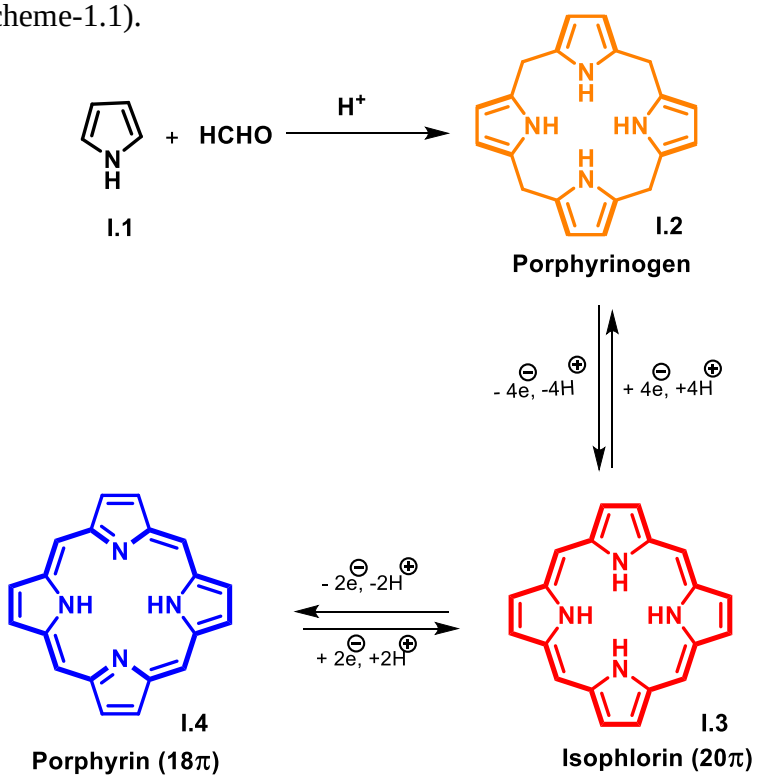

Scheme-1.1: Synthesis of porphyrin **I.4** from pyrrole and formaldehyde.

In the above process (scheme-1.1), R. B. Woodward proposed an intermediate **I.3** with 20π electrons in conjugation. The **I.3** considered as the N,N'-dihydroporphyrin and conjugation flow is supposedly only through the sp^2 carbon skeleton framework. The inner protons of isophlorin **I.3** produce steric congestion due to nonbonding interaction of H--H bond[4], resulting in electronic destabilization and hence causing instability in its current form. **I.3**.

Vogel's group pioneered the strategic synthesis and isolation of isophlorin and its analogues. Therefore, they simultaneously worked to synthesize the furan **I.5**, thiophene **I.6**, and selenophene analogues of porphyrin as its dicationic form, in an attempt to study isostructural macrocycle bearing 18π electrons.[5] These dicationic analogues **I.5**, **I.6**, **I.7** resemble porphyrin in terms of their π-electron counts and the deshielding of outer protons. These molecules demonstrate porphyrin's ability to maintain cyclic π-conjugation despite steric congestion.

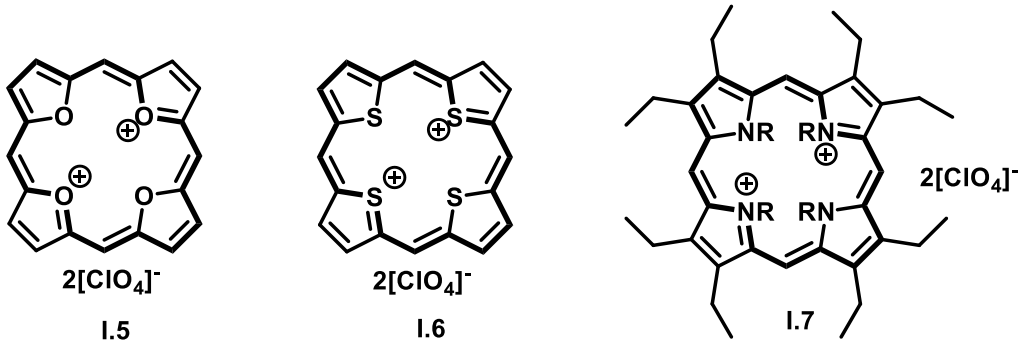

Fig. 1.1: The 18π dicationic species of porphyrin and its analogues.

In continuation of these studies, Vogel and group reported the synthesis of 20π isophlorin[4] **I.8** from its dicationic porphyrin **I.7**, through two electron reduction in presence of anthracene-sodium in THF at -78 °C (Scheme 1.2). But a major shortcoming was the quick and subtle two-electron oxidation of **I.8** to its dicationic porphyrin, **I.7**. Therefore the synthesis of 20π isophlorin was not facile through this procedure. Similarly, the dicationic tetraoxaisophlorin **I.5** was subjected to reduction in presence of K in THF, to yield the 20π isophlorin as black colored crystals.[6] An upfield chemical shift was observed for the synthesized tetraoxaisophlorin and hence it confirmed the paratropic ring current of 20π isophlorin. But again, a drawback was its air sensitive nature, as it could only be stored at a lower temperature such as -78 °C.

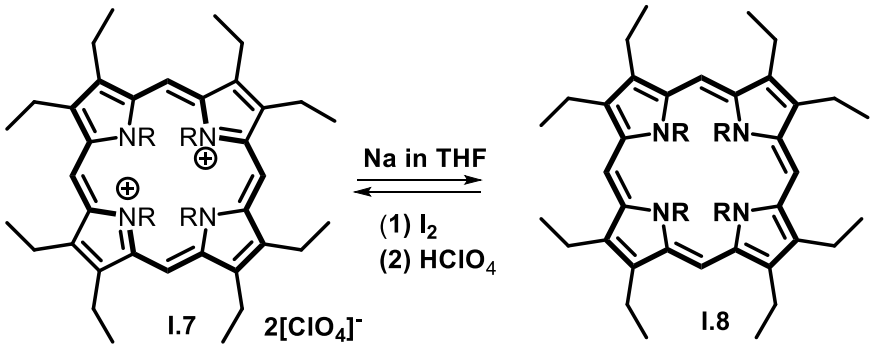

Scheme 1.2: Conversion of 18π **I.7** into 20π isophlorin **I.8.**

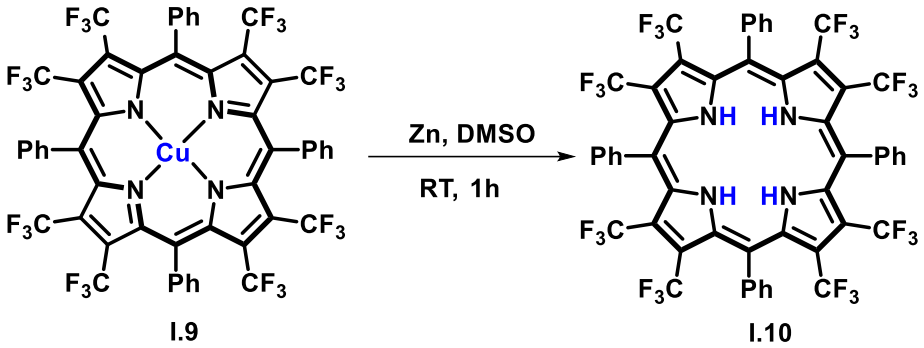

Scheme.1.3: Reduction of **I.9** with Zn to 20π isophlorin **I.10**.

Further, in the year 2007, Chen and co-workers reported the synthesis of 20π *β*-tetrakis(trifluoromethyl)-*meso*-tetraphenylporphyrins[7] **I.10** by the reduction of Cu(II) *β*-tetrakis(trifluoromethyl)-*meso*-tetraphenylporphyrin **I.9** with zinc powder in DMSO (Scheme 1.3). Although **I.10** was relatively stable compared to **I.8**, but it adopted a nonplanar (saddle shape) structure as revealed from its single crystal X-ray analysis. Thus **I.10** does not exhibit significant paratropicity in its ^{1}H NMR. In the ongoing study of stabilizing 20π isophlorin, many reported isophlorins[8a-c] are either air-sensitive or non-planar in nature. Ultimately, Anand and co-workers successfully reported the first synthesis of planar and stable isophlorin[9] **I.12** with a strategic change, in which the nitrogen of the inner core was substituted with divalent elements such as furan and sulphur. The **I.12** was synthesized by the acid assisted self-condensation of 2-pentafluorophenylhydroxymethyl **I.11**, followed by oxidation with $FeCl_3$ (Scheme 1.4).

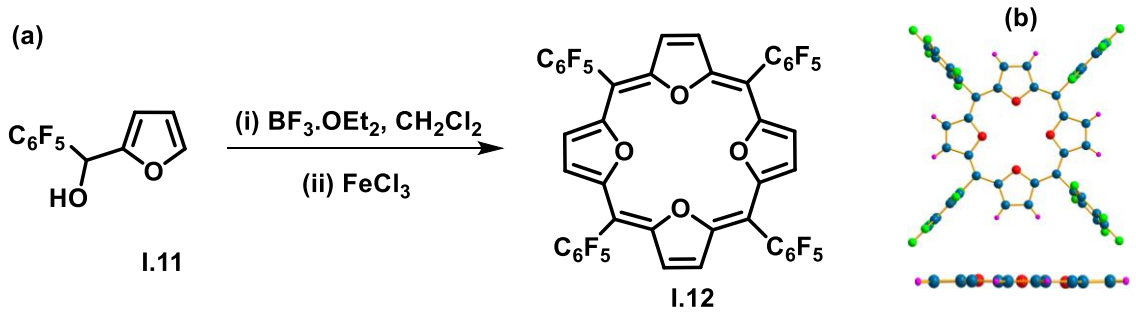

Scheme 1.4: (a) Condensation reaction for preparation of **I.12 (b)** Molecular structure of **I.12** obtained from single crystal X-ray diffraction.

The molecular structure of **I.12** displayed the perfectly planar topology and its outer eight β C-H protons were resonating at δ 2.49 ppm and confirmed its antiaromatic character (unlike the

porphyrin β C-H resonate at δ = 8.2 ppm). The *meso*-substituted pentafluorophenyl rings in **I.12,** enhance the stability of the isophlorin ring. Further, **I.12** displayed the electronic absorption at 320 and 357 nm as an intense peak along with weaker absorptions between 400-500 nm. It demonstrated that the core alteration of porphyrin is an effective technique for stabilizing the 20π isophlorins.

Along with extensive research into porphyrins and their derivatives, X-ray studies of bacteria photosynthetic antenna systems prompted scientists to investigate multiporphyrin arrays in order to emulate the photosynthesis reaction center and gain a better understanding of electron transfer mechanisms.[10] Thus several covalently bonded porphyrin dimers, trimers, pentamers, and oligomers were synthesized to better understand the orientation or interaction of these two porphyrins during electron transfer activities.[11,12] To perturb the spectral properties, the directly linked diporphyrins **I.13** and the porphyrins linked with some spacer **I.14** were synthesized. Further the properties such as exciton coupling, stock shift, and quantum yield were examined to compare with the original systems.

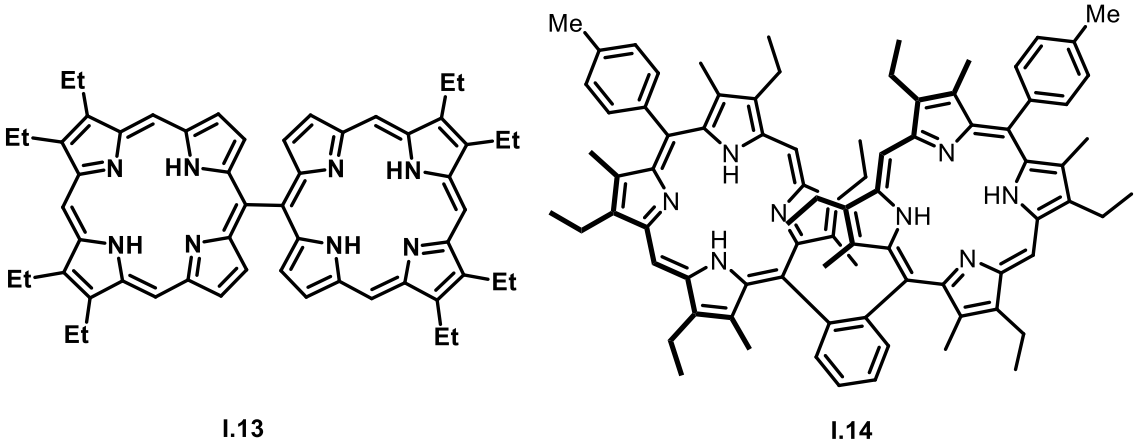

I.13 **I.14**

Fig. 1.2: Porphyrin dimer **I.13** and **I.14**.

Additionally, these porphyrins go through an oxidative coupling reaction that creates an array of porphyrins, which leads to the formation of porphyrin molecular tape.[13] Remarkably, these characteristics have been studied extensively in the aromatic system but not in the antiaromatic systems. Anand and co-workers reported the first instance of isophlorin dimer[14] **I.15**. It was the first synthesized example of a *meso-meso* directly connected antiaromatic isophlorin dimer **1.15**. The dimer **I.15** was obtained by crystallization of *meso*-free tetraoxa isophlorin in the

presence of C_{60} fullerenes in toluene. Aside from their structural value, porphyrin dimers and isophlorin dimers could be more effectively used in optoelectronic devices.

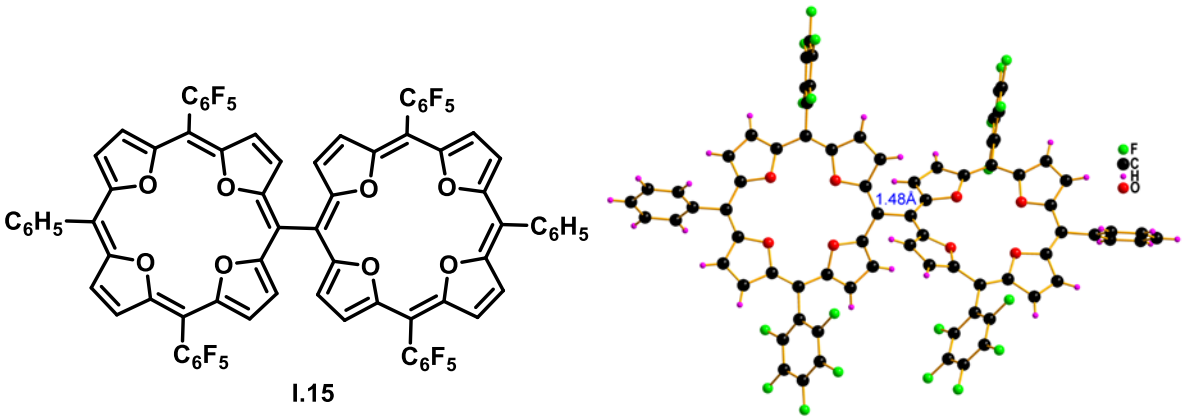

I.15

Fig. 1.3: Possible chem draw structure of **I.15** (left) and Molecular structure of **I.15** (right)**.**

Another notable feature of porphyrin is ring expansion. The expansion of π electrons can be achieved by increasing the number of heterocyclic rings or the *meso* positions. Sessler and co-workers reported a pentapyrrolic **I.16** macrocycle[15b] consisting the five pyrrole rings in conjugation and named as Sapphyrin[15a] (due to its dark blue color). **I.16** has one extra pyrrole ring than porphyrin **I.4**, resulting in a total of 22 π electrons in conjugation. Because of increased conjugation, they show a prominent Soret-like band at 456 nm, as well as Q-bands at 626, 668, and 714 nm. This Sapphyrin **I.16** has a larger core size of 5.5 A° than porphyrin (about 4 A°), making it a potential anion receptor for fluoride anion.

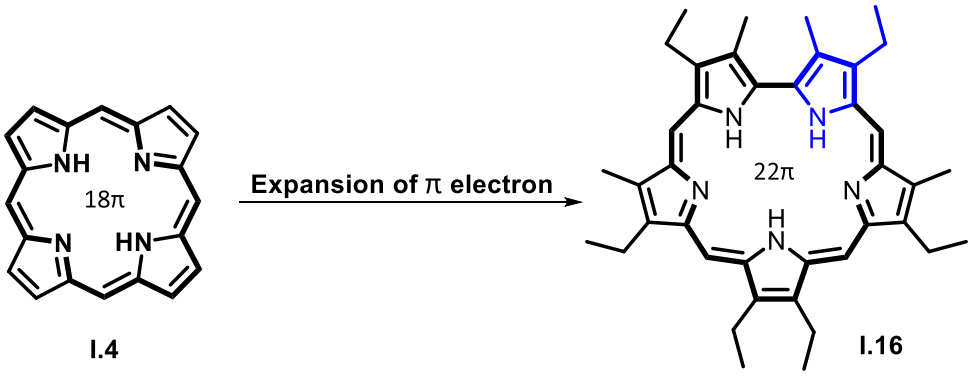

I.4 I.16

Fig 1.4: Ring expansion from 18π porphyrin **I.4** to 22π sapphyrin **I.16**.

Furthermore, these expanded porphyrinoids have potential applications in photodynamic therapy, anion detection, and models of aromaticity.[16] Hence D. Dolphin reported a series of sapphyrins, *meso*-diphenylpentaphyrin **I.19** and *meso*-hexaphenylhexaphyrin[17] **I.20** by condensation of the small precursor like 5-phenyldipyrromethane and 5,10-diphenyltripyrrane **I.17** (Scheme 1.5).

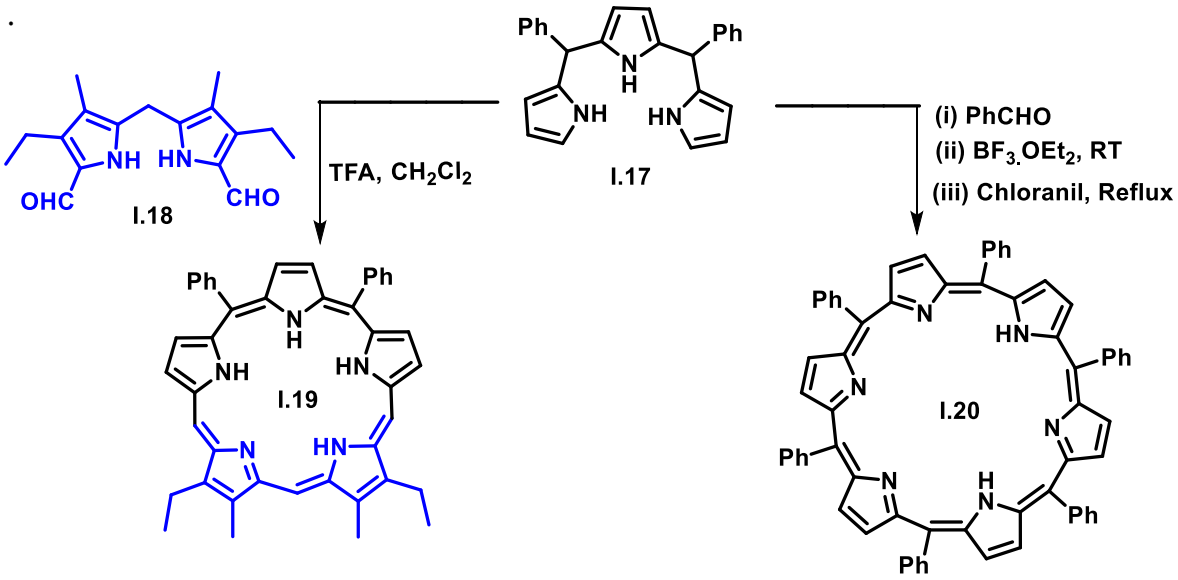

Scheme 1.5: Synthesis of pentaphyrin **I.19** and hexaphyrin **I.20.**

The hexaphyrin **I.20** was synthesized with acid catalysed reaction of 5,10-diphenyltripyrrane, **I.17,** with the benzaldehyde followed by oxidation with chloranil and macrocycle formation was confirmed by mass spectrometry. Due to pH dependent nature and non-static conformation, the further characterization of hexaphyrin **I.20** was hampered. Then two years later, in 1999 Cavaleiro and co-workers reported the successful synthesis of hexaphyrins with Rothemund method using pyrrole and pentafluorobenzaldehde.[18] The hexapyrrolic macrocycle was found as **I.21** and **I.22**; these two states of hexaphyrin were interconvertible with oxidizing and reducing agents such as DDQ and $NaBH_4$ respectively. These macrocycles exhibited the red shifted Soret-like absorption band with a λ_{max} in the region between 560-595 nm. Single crystal X-ray diffraction analysis revealed an usual rectangular structure of macrocycle **I.21**, consisting of six consistently spaced and organized pyrrole rings between six *meso*-methine carbon atoms. The non-planar conformation of the ring is prevented by the inversion of two pyrrole rings in the molecular structure.

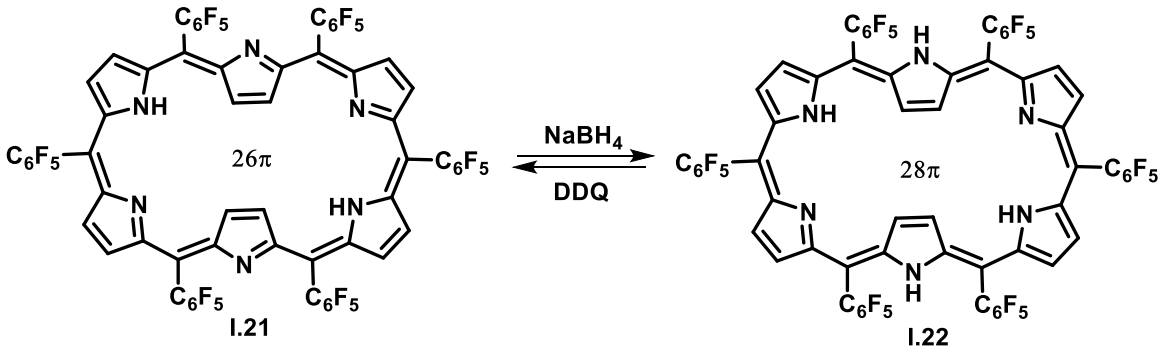

Scheme 1.6: Reversible redox transformation of between 26π and 28π hexaphyrin **I.21** and **I.22**.

Thus, extensive analysis of expanded porphyrinoids revealed a considerable difference in their electrical and structural properties when compared to the parent 18π porphyrin. Among expanded porphyrinoids, octaphyrin is a type of macrocyclic compound that consists of eight pyrrole rings connected by methine bridges. The octaphyrins **I.23** and **I.24**, which have variable bridging units were synthesized by E. Vogel and co-workers.[19] Regardless of their bridging units, both octaphyrins were found to lack any ring current effect, leading to the adoption of the figure-of-eight conformations.

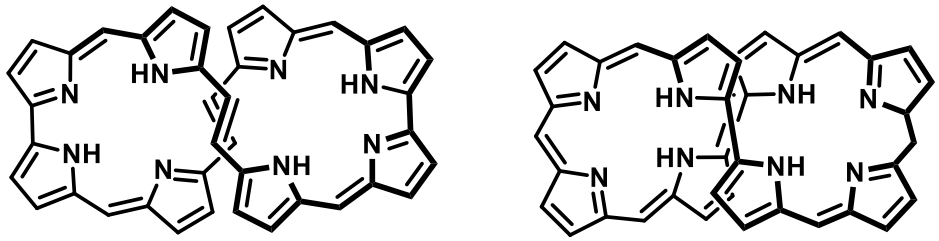

I.23 **I.24**

Fig. 1.5: Twisted Octaphyrins **I.23** and **I.24** reported by E. Vogel.

Continuing with the larger porphyrinoids, Osuka and co-workers reported the one-pot synthesis of a number of macrocycles[20], including pentaphyrin, hexaphyrin, heptaphyrin, octaphyrin, nonaphyrin, decaphyrin, and dodecaphyrins. (Scheme 1.7).

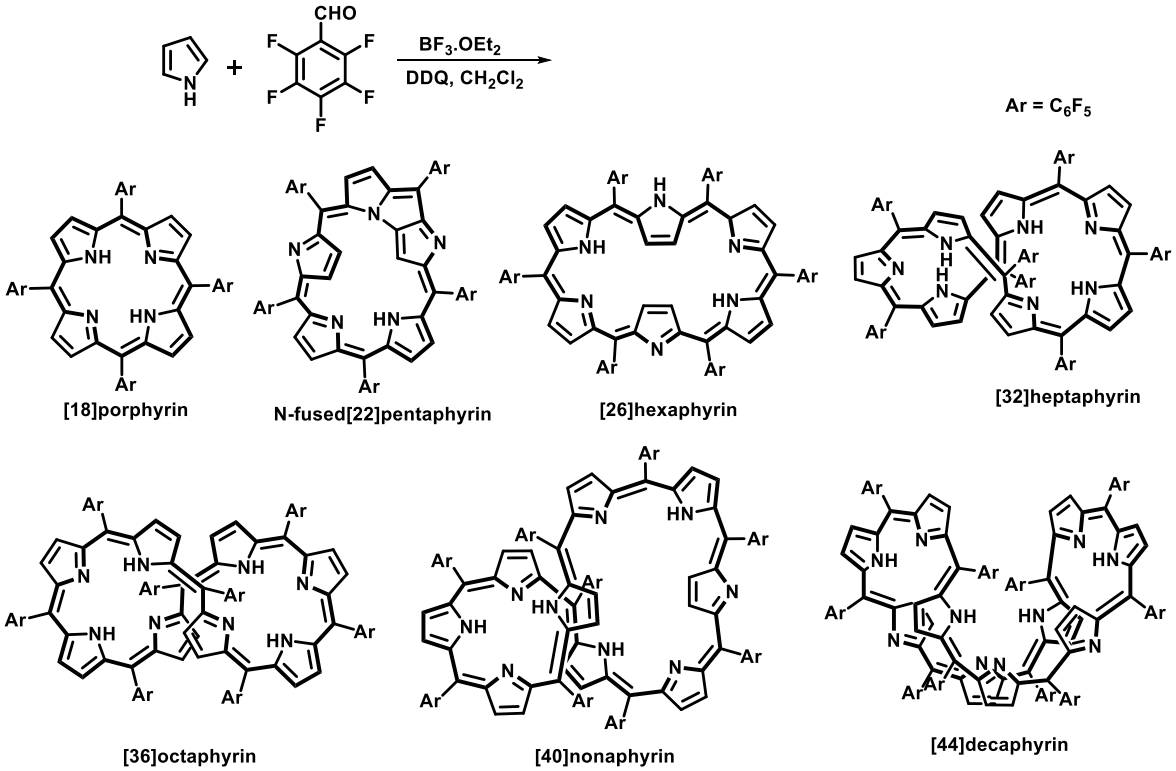

Scheme1.7: Series of expanded porphyrinoids.

The observed structural analysis revealed that these macrocycles have a planar topology up to six member rings, but beyond that, the molecule's flexibility increases significantly due to the increased number of heterocyclic rings and bridging carbons. Thus there is no ring current effect in such macrocycles. As a result, higher membered macrocycles adopt the non-planar conformations.

The intrinsic N-H interaction between the imine and amine type nitrogen in the cavity causes nonplanarity in higher membered porphyrinoids. Planarity in these macrocycles might be achieved through core modification, as nitrogen could be exchanged with alternate divalent elements such as O, S, or Se to overcome steric limitations. Thus, Latos Grazynski and group reported core-modified octaphyrin[21] **I.26** by substituting four pyrrole rings in a conventional octaphyrin with four thiophene rings. The **I.26** was synthesized (Scheme 1.8) with acid mediated condensation of pyrrole **I.1** with 2,5-bis(p-tolylhydroxymethyl) thiophene **I.25**, however, structural characterisation of **I.25** frequently resulted in the characterization of non-planar conformation.

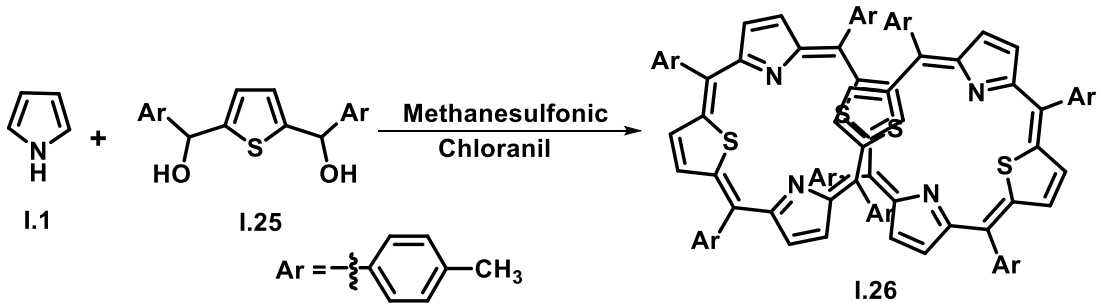

Scheme 1.8: Synthesis of core-modified octaphyrin **I.26**.

Therefore, replacing a few pyrrole rings with other heterocycle rings is not the only essential requirement to block the fluxional behaviour. As a result, in 1999, Sessler and group reported the 32π octaphyrin **I.27**, which containsonly two *meso* carbons and remaining pyrroles were directly coupled to each other.[22a] Hence, structure of **I.27** adopted a relatively planar conformation. Later, Chandrashekhar and co-workers reported the core modified octaphyrin[22b] **I.28** contained four pyrrole and four thiophene rings in the conjugation, connected through four *meso*-methine carbon. This 34π octaphyrin [1.0.1.0.1.0.1.0] **I.28** was synthesized through the oxidative coupling of (5,15-dimesityl-20,21- dithio-1-norbilane) and its electronic absorption spectrum displayed the intense Soret-like band at 598 nm accompanied with three of Q-like absorptions between 700-900 nm. Thus **I.28** displayed a strong diatropic ring current and X-ray diffraction studies of its single crystal revealeda planar conformation. Hence the core

alteration and ring inversion combined with a reduced number of *meso* positions, aids the macrocycle in achieving planarity. Later, Anand and co-workers described an all furan containing antiaromatic 40π octaphyrin[23] **I.29**, using a one pot reaction of furan and pentafluorobenzaldehde. Notably **I.29** displayed significant paratropicity in its ^{1}H NMR spectrum and the single crystal x-ray analysis revealed that out of the eight furan rings, four of them faced the macrocyclic core and molecular structure was entirely planar.

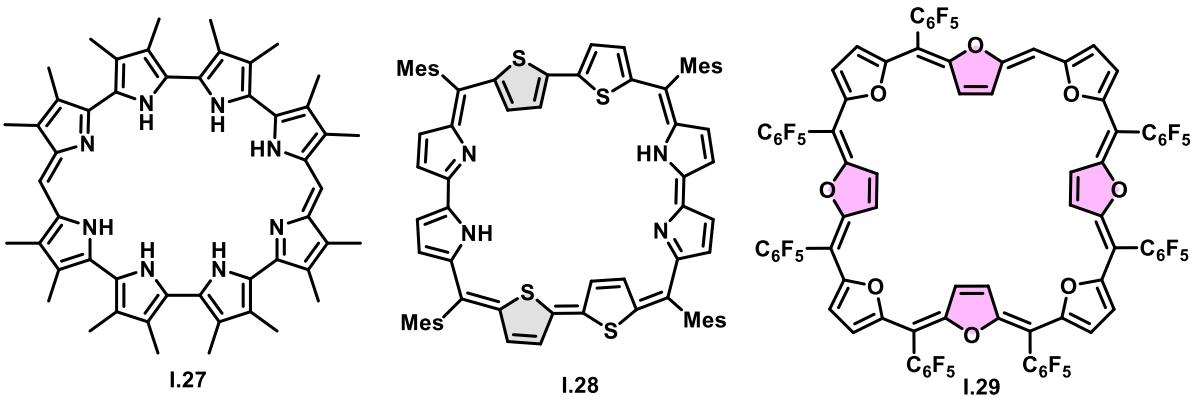

Fig. 1.6: Core-modified planar octaphyrins **I.27, I.28** and **I.29**.

Also, these expanded porphyrinoids are π electron rich macrocycles and hence they are more susceptible to reversible redox reactions. A reported example of nonaromatic octaphyrin **I.30** containing 36π electrons with figure-of-eight conformation undergoes deprotonation reaction and induces the structural changes in the macrocycle.[24]

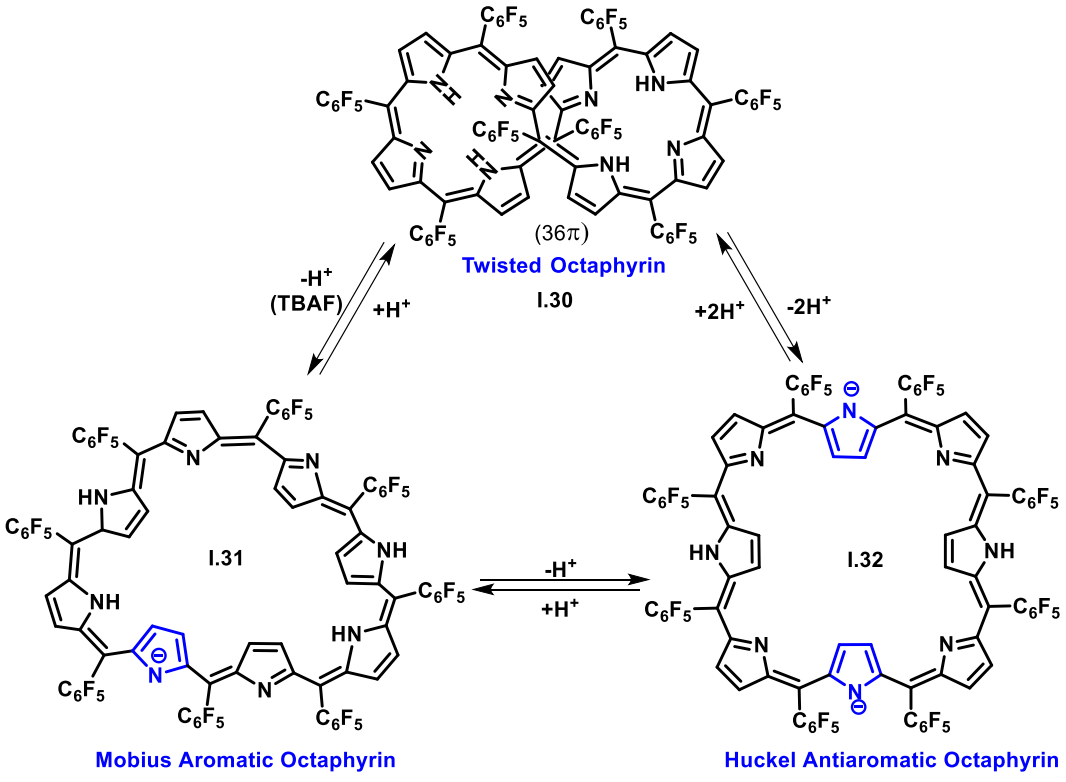

Scheme 1.9: Interconvertible redox behaviour of **I.30** to their corresponding state **1.31** and **I.32**.

Depending on the amount of base (tetrabutylammonium fluoride (TBAF)) needed to carry out the reaction, it formed 36π monoanion Mobius aromatic octaphyrin **I.31** and an increase in the equivalence of base lead to the isolation of 36π dianion planar Huckel antiaromatic octaphyrin **I.32**.

Therefore, it illustrates the potential use of porphyrinoids as models for investigating new chemistry linked to Mobius, Baird, and Huckel aromaticity and antiaromaticity. Several interesting examples are reported for Mobius aromatic porphyrinoids.[25] Firstly, it was observed in 28π di-*p*-benzi hexaphyrin[1.1.1.1.1.1] reported by Marcin and group.[25a] It was found to depend on the kinetic conditions, as the hexaphyrin adopts 28π Huckel antiaromatic topology **I.33** and twisted Mobius topology **I.34**. In Mobius form of hexaphyrin the two benzene rings were arranged in edge-to-face manner and its ^{1}H NMR reflected the deshielding of the outer protons.

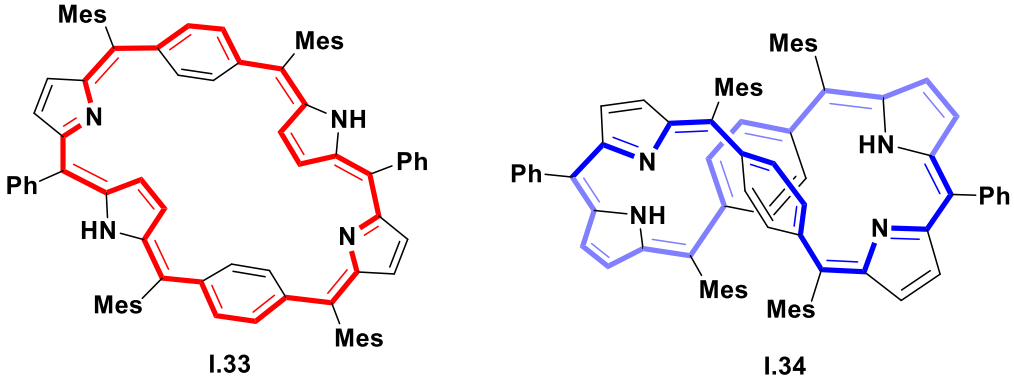

Fig. I.7: 28π di-*p*-benzi hexaphyrin with Huckel aromatic topology **I.33** and Mobius topology **I.34**.

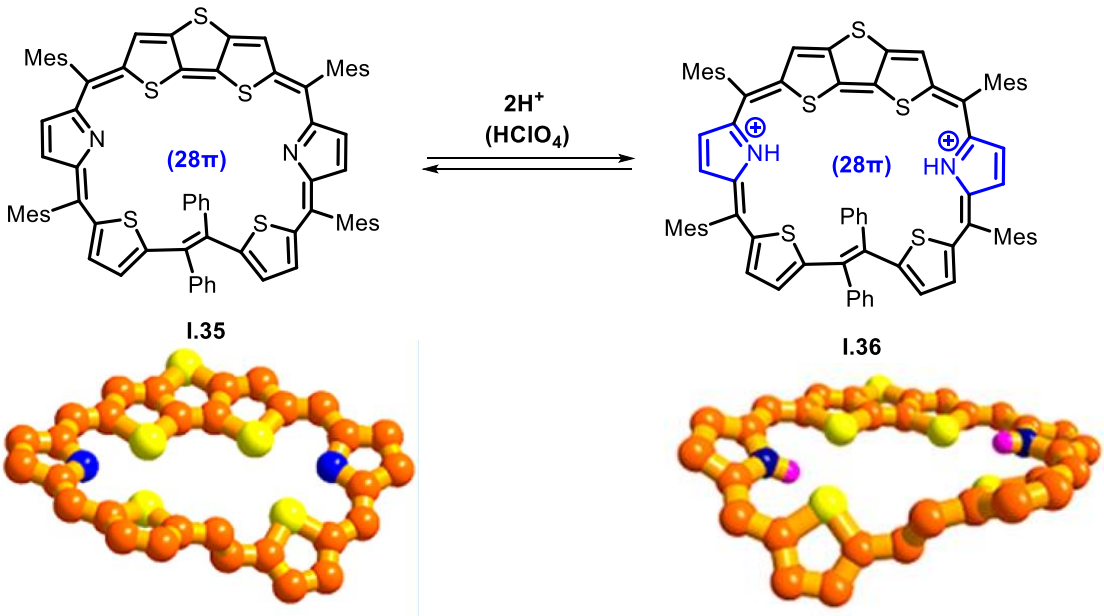

Fig.1.8: Conversion of nonaromatic **I.35** to Mobius aromatic Hexaphyrin **I.36**.

Further, the core modified hexaphyrin[26] incorporated dithieno-thiophene moiety, upon protonation was found to converts from 28π non aromatic **I.35** to 28π Mobius aromatic hexaphyrin **I.36** (Fig. 1.8). Therefore, the conversion of Huckel to Mobius aromatic molecule depends on thermodynamic parameters such as e pH, solvent and its kinetic conditions.

Thus, the porphyrinoids/isophlorinoids incoporating all pyrrole and combined pyrrole/furan/thiophene/selenophene exhibit a variety of structural behaviors, metal/anion complexing properties, and 4n/(4n+2)π redox couple. Also, that larger porphyrinoids are usually very flexible and solvent polarity usually plays a major role in triggering conformational changes in porphyrinoids. Therefore, they adopt different conformation in solid and solution states.[30d] In contrast, the macrocycle containing all of the thiophene units, exhibits a wide set of features due to its enhanced aromatic stabilization and electronic behavior. Peter Bauerle and group[27] reported a series of cyclic π-conjugated thiophene based macrocycles as (CnTs). Among them the ten membered cyclo[10]thiophene (C10T) **I.37**, revealed the syn-arrangement of all the thiophene units in almost circular form with inner diameter of 1.0 nm analysed by its molecule structure. Because of the ring strain, its optoelectronic properties and oxidation potentials affected drastically and hence in its oxidised form $C_{10}T^{2(+.)}$ $2SbCl_6^-$, **I.39**, was characterizes as a polaron-pair (Fig. I.9).

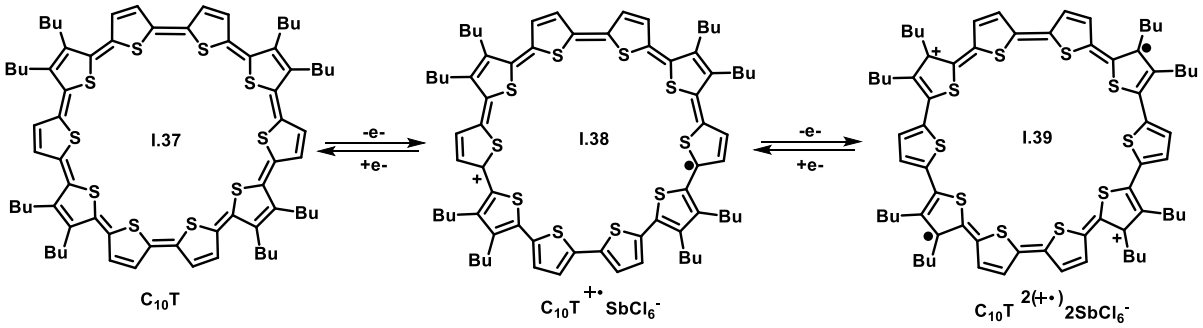

Fig. I.9: Electronic structure of $C_{10}T$ as a neutral molecule **I.37**, as radical cation $C_{10}T^{+.}$ **I.38** and as polaron pairs $C_{10}T^{2(+.)}$ **I.39**.

Thus, the isophlorinoids/porphyrinoids can be explored for stabilisation of radicaloid species and have a high potential as a organic semiconductors materials.[28] Considering the important of these molecules, Anand and co-workers reported the series of π-conjugated thiophene based macrocycles by the one pot reaction of thiophene and pentafluorobenzaldehyde in acidic medium, and followed by oxidation with $FeCl_3$ (Scheme-1.12a). These π-extended macrocycles were isolated as 4n/(4n+2)π and (4n+1)π electronic circuits.[29] The giant

isophlorinoids up to sixteen thiophene membered rings were isolated using multiple column chromatography and identified using a several spectroscopic techniques.

Interestingly, the five membered penta-thiophene macrocycle containing $(4n+1)\pi e^-$ was characterized as the neutral stable radical.[29a] Along with an open shell character, the macrocycle **I.40** was the amphoteric in nature, and hence it forms the $(4n+2)\pi$ aromatic anion **I.41** and $(4n)\pi$ monocationic **I.42** on reduction and oxidation respectively. All these chemically obtained macrocycles **I.40**, **I.41**, **I.42** were well studied with UV-vis, NMR and EPR spectroscopic techniques.

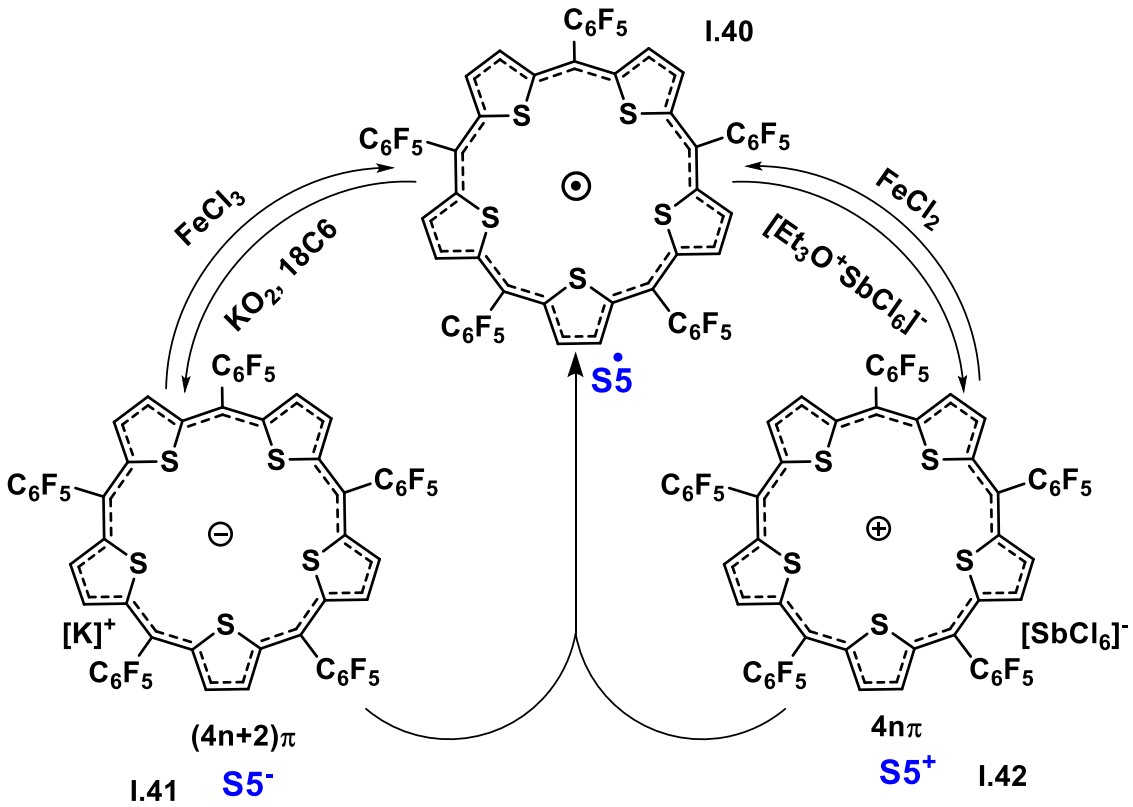

Fig. I.10: Amphoteric behaviour of pentathiophene radical **I.42.**

Further, Jishan Wu and co-workers explored the diradicaloid properties in porphyrinoids.[30] Recently they reported a 38π electrons containing octaphyrin **I.43** with an even number of *meso*-bridges, which displayed the diradical character. The diradical behaviour in the macrocycle was analysed with the extended absorption band in NIR region, broader ^{1}H NMR signals, magnetic susceptibility and electron paramagnetic resonance (EPR) signal.

In the resonance structures (Fig. I.11), the **I.43b** contribute for diradical form (open shell), as the gain in aromatisation energy is more due to increased number of benzenoidal thiophene moiety in **I.43b** (six aromatic thiophene) compare to closed shell, **I.43a** (with four aromatic thiophene).

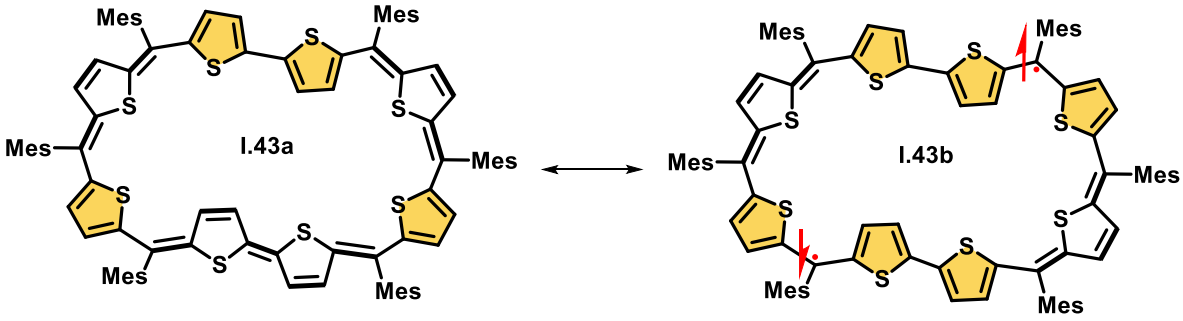

Fig. I.11: Resonance between the closed shell (Kekule) **I.43a** and open shell diradical **I.43b** from in **I.43** octaphyrin.

In quantum chemical calculation, the macrocycle **I.43a** has small $\Delta E_{S\text{-}T}$ = -2.70 kcal/mol with singlet ground state of the macrocycle. The diradical character was confirmed with the LUMO occupation number of 0.67 (NOON of 40%) calculated with Yamaguchi index. Remarkably, the effective spin delocalisation over the backbone of macrocycle enhanced its stability and also *meso*-mesityl groups kinetically block the radical.

Recently Anand and co-workers also reported a series of 38π octaphyrins[31] with varying heteroatoms in the ring and structural conformations of these octaphyrins changes drastically based on the link between these heteroatoms. All these octaphyrins **I.44, I.45** and **I.46** have open shell character and it confirmed with the EPR experiment and computational studies. Surprisingly, the **I.46** shows the y_0 of 0.47 compared to the planar structures **I.45** (y_0 of 0.24) and **I.44** (y_0 of 0.31).

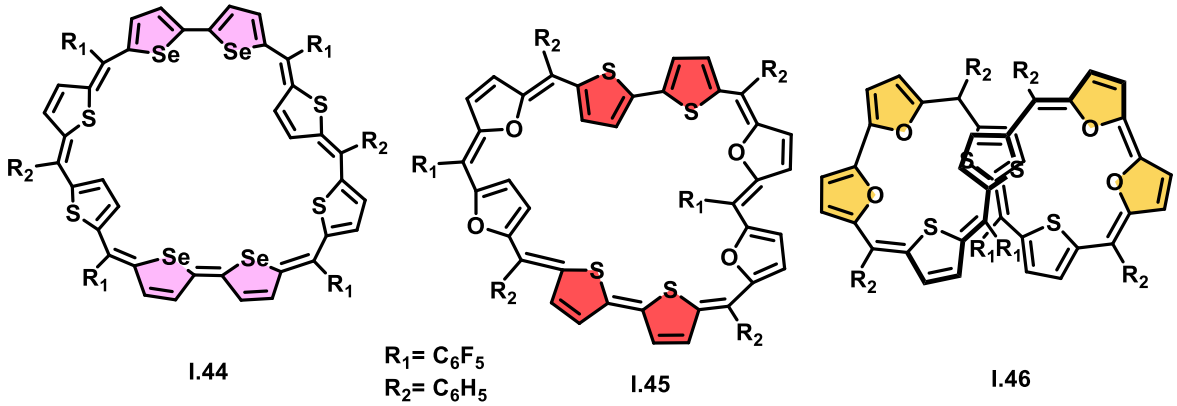

Fig. I.12: 38π expanded isophlorinoids **I.44**, **I.45** and **I.46**.

Osuka and Shinokubo group reported the stable non-Kekule type biradicaloid in 26π hexaphyrin **I.47**.[32] In **I.47** biradical, the unpaired electrons were delocalized over the tripyrrolic moiety which are connected with two *meso*-carbonyl carbons, further C_6F_5 provides the steric protection and these two factors enhanced the stability of the macrocycle in its biradical form. The EPR signal at g = 2.003 confirmed its biradical character and further computational calculations revealed 62% diradical character in **I.47**. Very Interestingly, it shows the two-photon absorption (TPA) cross section values of σ(2) = 3800 GM. As a result, porphyrinoids may be appealing molecules in the context of photonics and nanotechnology.

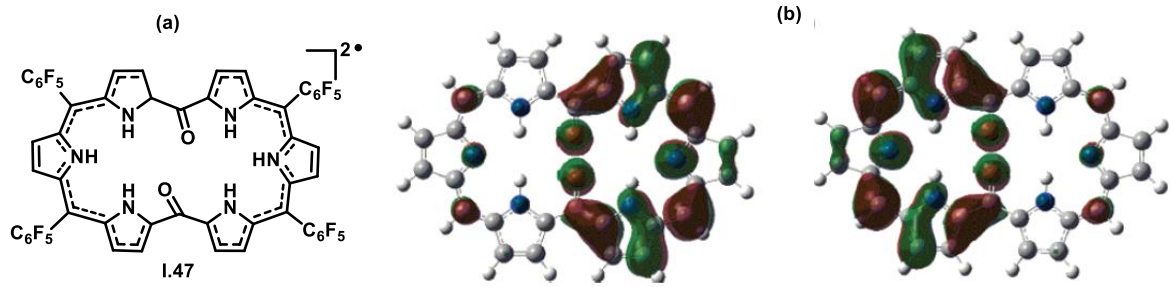

Fig. I.13: Biradicaloid nature of 26π diketohexaphyrin hexaphyrin **I.47** (a), SOMO orbital picture of **I.47**, α and β spin profile.

The increased TPA value is another consistent observation for singlet diradical compounds with intermediate diradical character (*y*) between (0 and 1).[33] Additionally, the diradical nature increases by the increase of conjugation in the molecule.[34] Hence the polycyclic hydrocarbons with diphenalenyl rings fused through central linkers like benzene, naphthalene, and anthracene, demonstrated higher diradical character due to increased conjugation (as a result of aromatic stabilisation).

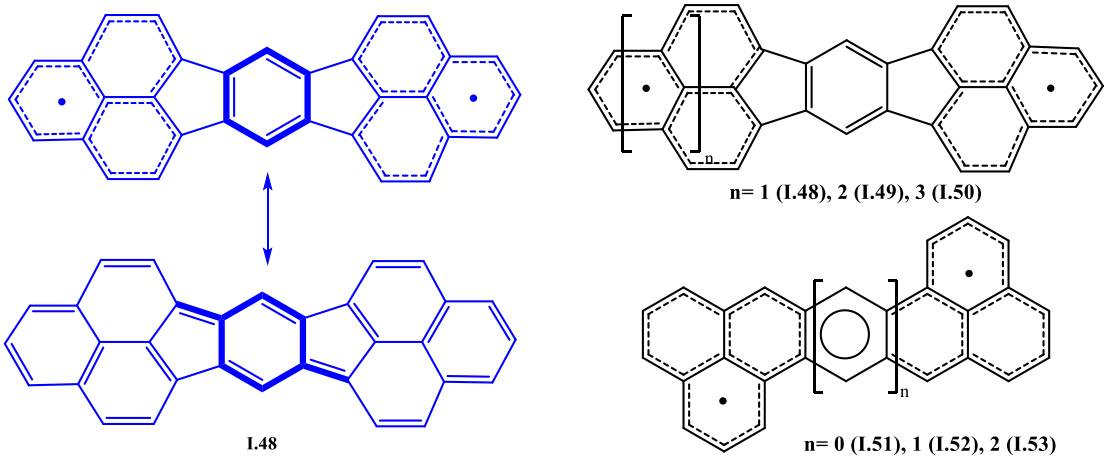

Fig. I.14: Polycyclic diphenalenyl radicals.

The value of diradical character (*y*) is 0.770 for **I.48**, 0.854 for **I.49** and 0.901for **I.50**. similarly, the diradical character of **I.51** < **I.52** < **I.53** increases due to better delocalised unpaired electrons.[35b] Hence, the length of conjugation in the ring governs the diradical nature of the molecule and subsequently affecting its two-photon absorption (TPA) value.

Sessler and co-workers reported higher expanded porphyrinoids with ten pyrrole rings, such as decaphyrin. The 40 decaphyrin [0.0.1.0.1.0.0.0.1.l], **I.56**, exists in tetra-cationic form and has been given the trivial name 'turcassin' since it reflects different colors in different solvents[35] (Scheme 1.10). Due to its extremely fluxional structure, the turcassin appeared to be a non-aromatic molecule with no ring current effect.

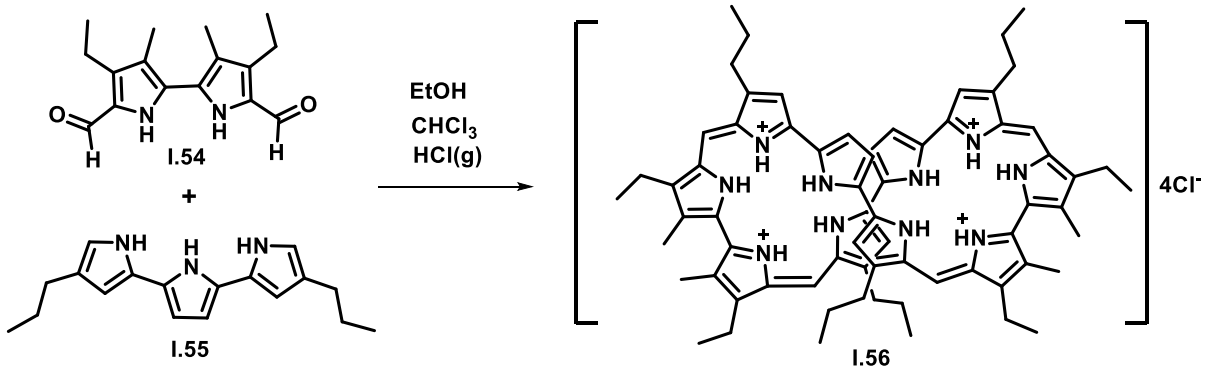

Scheme 1.10: Synthesis of first decaphyrin **I.56**.

Introducing planarity in giant porphyrinoids is a challenging task. Typically, due to their extremely fluxional nature, reported decaphyrin adopts the figure of eight conformation. The decaphyrin's structural modifications, which included a range of bridging units and templates, frequently resulted in a non-planar structure with a crescent-like form.[36]

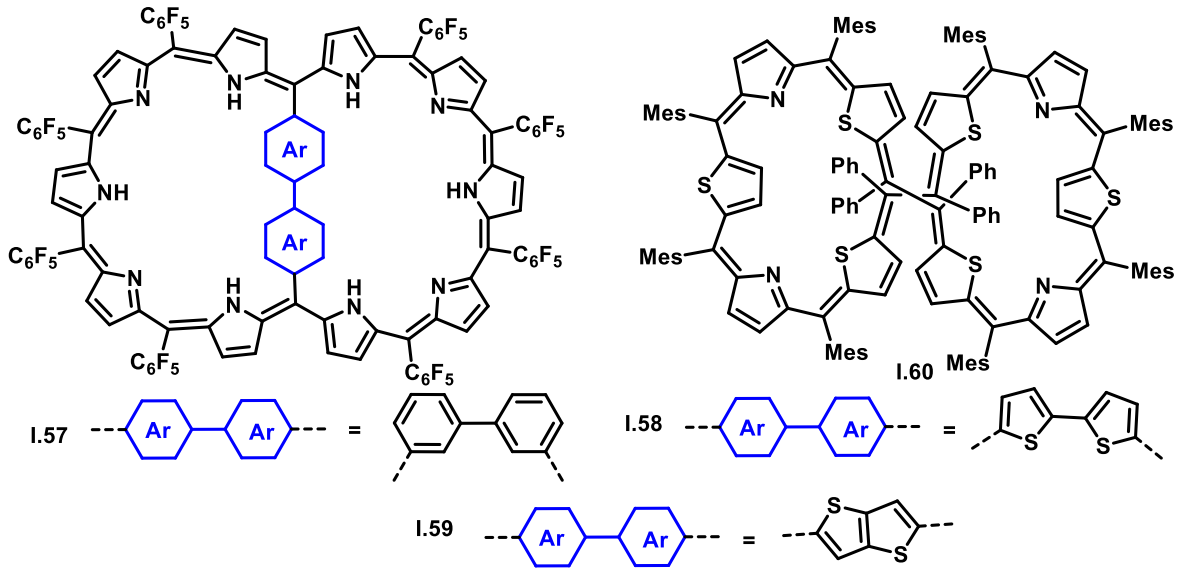

Fig. I.15: Bridged decaphyrins.

In 2006, Chandrashekar and co-workers reported the core modified decaphyrin with the reduced number of *meso* positions. The decaphyrins **I.62** and **I.63** were synthesized with the MacDonald type condensation of pentapyrrane **I.61** with benzaldehyde, resulting in the formation of ten-membered decaphyrins with [5+5] condensation reaction (Scheme 1.11). These decaphyrins sustain 42π electrons and its solution state study revealed the aromatic behaviour but molecular structure could not obtained for these decaphyrins. Due to their aromatic behaviour in solution states, these decaphyrins reflected the increased value of two-photon absorption cross-section value (σ_2)108000 GM for **I.62** and 106600 GM for **I.63** respectively.

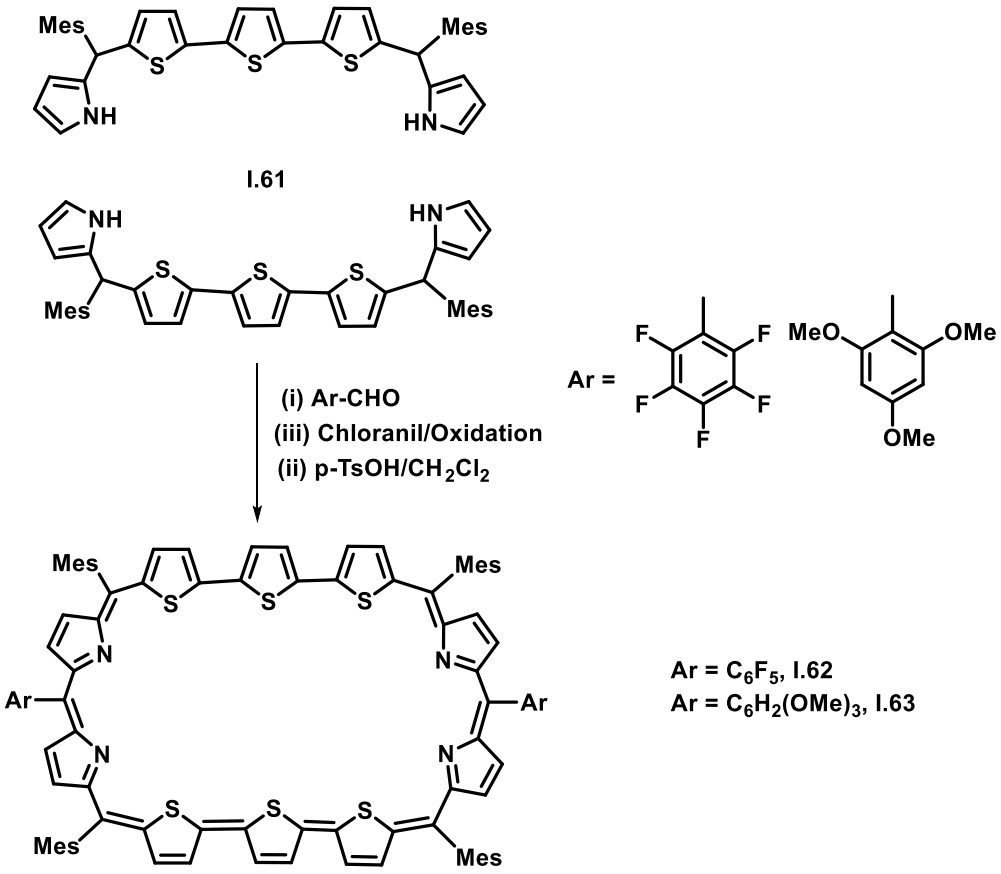

Scheme-1.11 synthesis of decaphyrin **I.62** and **I.63**.

Hence with growing importance of expanded porphyrinoids, recently, Anand and co-workers reported the 50π decaphyrin[29d] containing all the thiophene rings connected through ten *meso*-position (Scheme-1.12). Apparently, the solid-state analysis shows the two different conformations of decaphyrin **I.65** based on the solvent of crystallization. It adopts the twisted structure **I.65a** in acetonitrile while in benzene it was nearly planar **I.65b**.

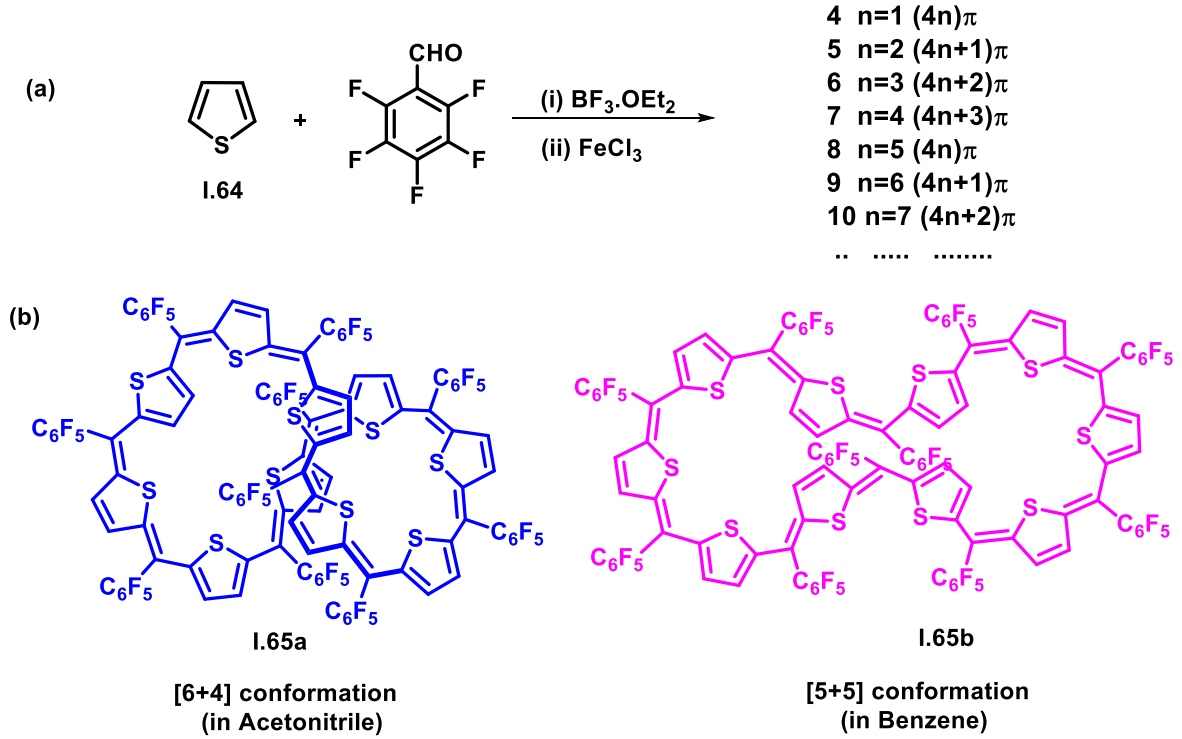

Scheme-1.12 (a) One pot reaction of thiophene and Pentafluorobenzaldehyde. (b) structural conformation of **I.65** decaphyrin.

In conclusion, porphyrinoids exhibit an array of structural and electrical features. In addition to the model systems, their remarkable qualities may find use in the development of optoelectronic devices and biological applications.

Aim of the Thesis

Porphyrinoids and isophlorinoids have drawn the interest of synthetic chemists due to their diverse structural, electronic, and redox properties. Their skeleton framework and larger π-conjugated circuits provide an opportunity to examine Huckel, Mobius and Baird type aromaticity. The larger expanded porphyrinoids frequently displayed the figure of eight conformation due to their fluxional nature. Furthermore, the structure of expanded porphyrinoids may change during crystallization due to their inherent fluxionality. As twisted and giant macrocycles have no ring current effect, hence determining aromaticity and antiaromaticity in larger-conjugated systems is a difficult task.

Therefore, the aim of this thesis is to explore the inherent characteristics of planar expanded isophlorinoids with 20π to 46π electrons and to describe the methods involved in their synthesis and characterization. The current study will mainly address core modified hexaphyrins, octaphyrins, and decaphyrins. The number of *meso* carbon and heterocyclic rings will be the same for the synthesis of planar hexaphyrins and octaphyrins. However, in order to attain planarity in giant isophlorinoid-like decaphyrins, the non-pyrrolic units and a lesser number of *meso* carbons in the ring will be involved. Furthermore, the role of heteroatoms in these decaphyrins will be studied, leading to the synthesis of decaphyrins with O/S/Se and with varying π electron counts. In terms of open shell properties (diradical character), of these thiophene-containing decaphyrins will be compared to previously reported octaphyrins.

Most crucially, the rational synthesis of isophlorin-porphyrin dimers will be carried out, and their orientation and interaction will be investigated further. Also, the redox behaviour of these synthesized macrocycles will be investigated using cyclic voltammetry and spectro-electrochemistry experiments, and the chemically accessible oxidized state will be thoroughly investigated. The molecule will be described as thoroughly as possible using single crystal X-ray diffraction studies in conjunction with various spectroscopic methods. For these macrocycle, additional quantum chemical calculations will be carried out in order to corroborate the experimental evidence. Creating enormous, planar macrocycles and studying their behaviours, such as aromaticity, solvatomorphism, and open shell character, is the overall goal.

Reference:

1. (a) *The Porphyrin Handbook*; Kadish, K. M., Smith, K. M., Guilard, R., Eds.; Academic Press: San Diego, CA, 2000-2003; Vols. 1-20. (b)

2. (a) E. Hückel, *Z. Physik*, **1931**, *70*, 204-286. (b) P. Garratt, Aromaticity; Wiley: New York, **1986**

3. R. Woodward, *Angew., Chem.*, **1960,** *72, 651-662*

4. M. Pohl, H. Schmickler, J. Lex, and E. Vogel *Angew. Chem. Int. Ed.*, **1991**, *30*, 1693-1696.

5. P. Rohrig, M. Sicken, B. Knipp, A. Herrmann, M. Pohl, H. Schmickler. J. Lex and E. Vogel *Angew. Chrm. Int. Ed. Engi.,* **1989,** *28, 12,* 1651-1652.

6. R. Bachmann, F. Gerson, G. Gescheidt, E. Vogel, *J. Am. Chem. Soc.* **1992**, *114*, 10855-10860.

7. C. Liu, D.M. Shen, and Q.Y.Chen, *J. Am. Chem. Soc*., **2007**,*129*, 5814-5815.

8. (a) J. A. Cissell, T. P. Vaid, A. L. Rheingold, *J. Am. Chem. Soc.* **2005**, *127*, 12212. (b) A. Weiss, M. C. Hodgson, P. D. W. Boyd, W. Siebert, P. J. Brothers, *Chem. Eur. J.* **2007**, *13*, 5982. (c) Y. Matano, T. Nakabuchi, S. Fujishige, H. Nakano, H. Imahori, *J. Am. Chem. Soc.* **2008**, *130*, 16446.

9. J. S. Reddy and V. G. Anand, *J. Am. Chem. Soc.*, **2008**, *103*, 3718.

10. Deisenhofer, J.; Epp, O.; Miki, K.; Huber, R.; Michel, H. *J. Mol. Biol.,* **1984**, *180*, 385-398.

11. T. Nagata, A. Osuka, and K. Maruyama *J. Am. Chem. Soc*., **1990**, *112*, 3054-3059

12. S. Nakajima, T. Nagata, K. Toriumi K. Maruyarna, and A. Osuka, *Angew. Chem. Int. Ed. Engl.* **1991**, *30*, 5, 582-584.

13. A. Tsuda and A. Osuka, *Science*, **2001**, *293*, 79-82.

14. B. K. Reddy, S. C. Gadekar and V. G. Anand, *Chem. Commun.*, **2016**, *52*, 3007-3009.

15. (a) V. J. Bauer, D. L. J. Clive, D.Dolphin, J. B. Paine, F. L. Harris, M. M. King, J. Loder, S.-W. C Wang, R. B. Woodward, *J. Am. Chem. Soc.* **1983**, *105*, 6429−6436 (b) M. J. Cyr, V. Lynch and J. L. Sessler, *J. Am. Chem. Soc.* **1990**, *112*, 2810-2813.

16. (a) T.J. Dougherty, *Photochem. Photobioi*. **1987**, *45*, 879-889. (b) M. Kongshaug, C. Rimington, J. F. Evensen, Q. Peng and J. Moan, *Int. J. Biochem.* **1990**, *22*, 1127-1131. (c) A. Jasat and D. Dolphin, *Chem. Rev*., **1997**, *97*, 2267-2340.
17. C. Bruckner, E. D. Sternberg, R. W. Boyle and D. Dolphin, *Chem. Commun*., **1997,** 1689-1690.
18. M. G. P. M. S. Neves, R. M. Martins, A. C. Tome, A. J. D. Silvestre, A. M. S. Silva, V. Félix, M. G. B. Drew and J. A. S. Cavaleiro *Chem. Commun.*, **1999**, 385-386.
19. M. Broring, J. Jendrny, L. Zander, H. Schmickler, J. Lex, Y. D. Wu, M. Nendel, J. Chen, D. **A.** Plattner, K. N. Houk and E. Vogel, *Angew. Chem.* **1995**, *107*, 2705-2709.
20. J. Y. Shin, H. Furuta, K. Yoza, S. Igarashi, and A.Osuka, *J. Am. Chem. Soc.*, **2001**, *123*, 7190-7191.
21. N. Sprutta and L. L.Grazyski, *Chem. Eur. J.*, **2001**, *23*, 5099-5112.
22. (a) Sessler, J. L.; Seidel, D.; Lynch, V. *J. Am. Chem. Soc*. **1999**, *121*, 8957. (b) V. G. Anand, S. K. Pushpan, S. Venkatraman, A. Dey, T. K. Chandrashekar, B. S. Joshi, R. Roy, W. Teng, and K. R. Senge *J. Am. Chem. Soc.* **2001**, *123*, 8620-8621.
23. J. S. Reddy, S. Mandal, and V. G. Anand, *Org. Lett***., 2006,** *8*, 5541-5543.
24. W. Y. Cha, T. Soya, T. Tanaka, H. Mori, Y. Hong, S. Lee, K. H. Park, A. Osuka, D. Kim, *Chem. Commun.,* **2016**, *52*, 6076-6078.
25. (a) M. Stepien, L. Latos-Grazynski, N. Sprutta, P. Chwalisz, L. Szterenberg, *Angew. Chem. Int. Ed.*, **2007**, *46*, 7869 -7873. (b) J. Sankar, S. Mori, S. Saito, H. Rath, M. Suzuki, Y. Inokuma, H. Shinokubo, K. S. Kim, Z. S. Yoon, J. Y. Shin, J. M. Lim, Y. Matsuzaki, O. Matsushita, A. Muranaka, N. Kobayashi, D. Kim, A. Osuka, *J. Am. Chem. Soc.*, **2008**, *130*, 13568-13579.
26. S. Dash, A. Ghosh, A. Srinivasan, C. H. Suresh, T. K. Chandrashekar *Org. Lett*., **2019**, *21*, 9637-9641.
27. F. Zhang, G. Gotz, E. M. Osteritz, M. Weil, B. Sarkar, W. Kaim and P. Bauerle, *Chem. Sci.*, **2011**, *2*, 781-784.
28. (a) E. M. Osteritz and P. Bauerle, *Adv. Mater*., **2001**, *13*, 243-246. (b) A. Bhaskar, G. Ramakrishna, K. Hagedorn, O. Varnavski, E. M. Osteritz, P. Bauerle and T. Goodson III, *J. Phys. Chem. B*., **2007**, *111*, 946-954.
29. (a) T.Y. Gopalakrishna, J. S. Reddy, and V. G. Anand, *Angew. Chem. Int. Ed.*, **2014**, *53*, 10984-10987. (b) hexaphyrin (c) octaphyrin (d) H. S. Udaya, A. K. Basavarajappa, T. Y. Gopalakrishna and V. G. Anand, *Chem. Commun.*, **2022**, *58*, 13931-13934.

30. (a) A. Rana, Y. Hong, T. Y. Gopalakrishna H. P Herng, T. Seng, P. Yadav, J. Ding, D. Kim, and J. Wu. *Angew. Chem. Int. Ed*. **2018**, *57*, 12534-12537. (b) Y. Ni, T. Y. Gopalkrishna, S. Wu and J. Wu, Angew., *Chem., Int. Ed.*, **2020**, *59*, 7414-7418.
31. M. D. Ambhore, P. Shukla, R. G. Gonnade and V. G. Anand, *Chem. Commun.*, **2022**, *58*, 8946-8949.
32. T. Koide, K. Furukawa, H. Shinokubo, J. Y. Shin, K. S. Kim, D. Kim, and A. Osuka, *J. Am. Chem. Soc.*, **2010**, *132*, 7246-7247.
33. K. Kamada, K. Ohta, T. Kubo, A. Shimizu, Y. Morita, K. Nakasuji, R. Kishi, S. Ohta, S. Furukawa, H. Takahashi, and M. Nakano, *Angew. Chem. Int. Ed.*, **2007**, *46*, 3544 -3546.
34. (a) Z. Zeng, X. Shi, C. Chi, J. T. Lopez Navarrete, J. Casado and J. Wu, *Chem. Soc. Rev.*, **2015**, *44*, 6578-6596. (b) M. Nakano, and B. Champagne, *J. Phys. Chem. Lett.*, **2015**, *6*, 3236-3256. (c) R. Kishi, S. Bonness, K. Yoneda, H, Takahashi, M. Nakano, E. Botek, B. Champagne, T. Kubo, K. Kamada, K. Ohta and T. Tsuneda, *J. Chem. Phys.*, **2010**, *132*, 094107.
35. S. J. Weghorn, V. Lynch, M. R. Johnson and J. L. Sessler, Angew. Chem. Int. Ed. Engl., **1994**, *33*, 1509-1511.
36. (a) V. G. Anand, S. Saito, S. Shimizu, and A. Osuka, *Angew. Chem. Int. Ed*., **2005**, *44*, 7244-7248. (b) T. Soya and A. Osuka, *Chem. Eur. J.*, **2019**, 25, 5173-5176. (c) T. Okujima, C. Ando, S. Agrawal, H. Matsumoto, S. Mori, K. Ohara, I. Hisaki, T. Nakae, M. Takase, H. Uno, and N. Kobayashi, *J. Am. Chem. Soc.*, **2016**, *138*, 7540-7543. (d) A. Ghosh, S. Dash, A. Srinivasan, C. H. Suresh, S. Peruncheralathan and T. K. Chandrashekar, *Org. Chem. Front.*, **2019**, *6*, 3746-3753. (e) H. Rath, V. Prabhuraja, T. K. Chandrashekar, A. Nag, D. Goswami, and B. S. Joshi, *Org. Lett.* **2006**, *8*, 2325-2328.

CHAPTER 2

Redox Assisted Reversible Aromaticity Transition between 30π Hückel and 28π Möbius Dication of a Core-Modified Isophlorinoid

2.1 Introduction

The cyclic, planar π-conjugated annulenes (CnHn) with (4n+2)π electrons are Huckel aromatic in nature.[1] They exhibit enhanced stability and unique electronic properties due to delocalization of their π electrons. On the other hand, planar annulenes with 4nπ electrons are Huckel antiaromatic, which means they are less stable and have higher reactivity.[2] This distinction is based on the Huckel rule, which helps us understand the aromaticity and antiaromaticity in planar π-conjugated systems. Whereas, in case of twisted annulenes, aromaticity can be defined with Mobius rule.[x] Based on Mobius band, Heilbronner's hypothesis that annulenes with an odd number of twist and 4nπ electrons will act as Mobius aromatic, furthermore annulenes with (4n+2)π electrons will be mobius antiaromatic in nature.[3] Withstanding a twist in the molecule without compromising the stability of the molecule is a tedious task.[4] Hence, compared to Huckel aromatic molecules, there are only limited reports on Mobius aromatic molecules. Therefore, the forty decades later to hypothesis, in 2001 Herges's group reported the first stable Mobius aromatic molecule **II.1** (Fig. 2.1), which was synthesized by photochemical reaction b/w two Huckel aromatic molecules.[5]

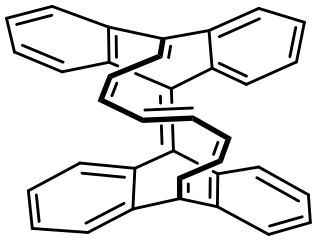

Fig. 2.1: First Mobius aromatic annulene **II.1**.

The flexible nature of porphyrinoids, provides an opportunity to sustain as Huckel, Mobius, and Baird aromatic/antiaromatic molecules.[6] In case of porphyrinoids based on thermodynamic, kinetic and pH dependent conditions, Huckel and Mobius transition could be achieved. Latos and coworkers reported Mobius aromaticity in 28π di-*p*-benzihexaphyrin, (Fig. 2.2) where in two benzene were arranged in edge to face manner, **II.3**, while the planar form **II.2** is Huckel antiaromatic.[7] In 2008, Osuka reported temperature dependent switching from Huckel to Mobius in 2,6-F_2-phenyl substituted 28π hexaphyrin. At lower temperatures Mobius form of **II.5** was stabilised and crystallized by slow evaporation method in 1,2-dichloroethane/ ethanol.[8] In the case of octaphyrin, pH dependent switching was observed upon treating Hückel non-antiaromatic 36πe^- octaphyrin in basic medium to form a 36π mono anionic Möbius aromatic species.[9]

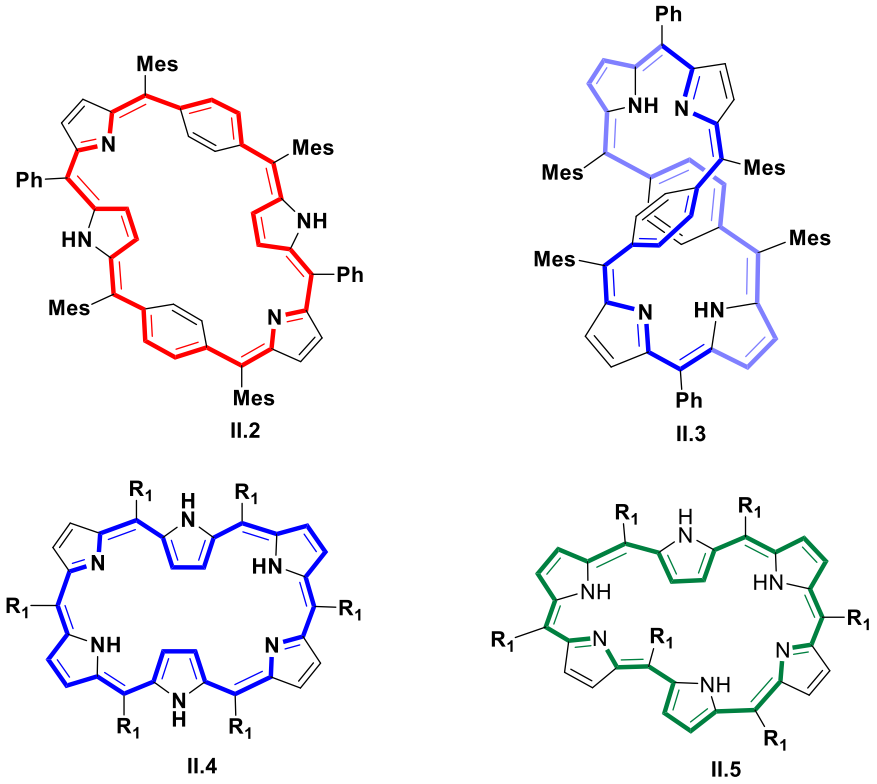

Fig. 2.2: Huckel topology, **II.2**, **II.4** and Mobius topology **II.3**, **II.5** in 28π hexaphyrin.

Aromatic-Antiaromatic transition could also be achieved by reversible redox of the molecule. Being electroactive in nature, 20π mono-pyrrole isophlorin[10] **II.6** undergoes two-electrons ring oxidization to yield the 18π dication **II.7** (Fig. 2.3). The overall reaction represents Huckel antiaromatic to Huckel aromatic transition. And it could be reversed by addition of Zn to the dicationic species **II.7**.[11]

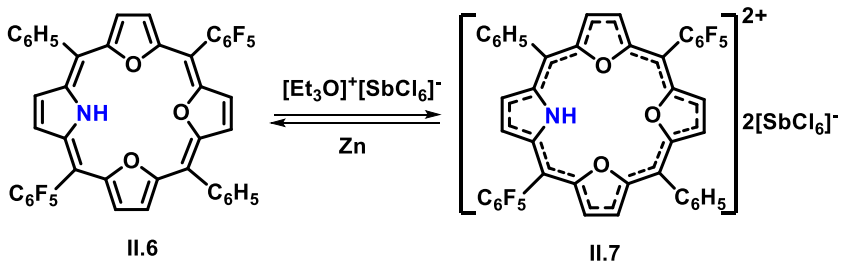

Fig. 2.3: Reversible redox between isophlorin **II.6** and porphyrin dication species **II.7**.

The higher analogues of porphyrin, hexaphyrin 26π was reported by Cavaleiro et al. It undergoes two electron reduction using simple reducing agent $TsNHNH_2$ to yield 28π hexaphyrin.[12] Recently, Anand and co-workers reported successive four electron reversible redox in case of thiophene and pyrrole based hexaphyrin.[13] The 28π Huckel antiaromatic hexaphyrin **II.8** undergoes two electron ring oxidation to form 26π Huckel's aromatic dication **II.9** and upon four electron reduction in presence of $Zn+NH_4Cl$ its forms 30π stable aromatic molecule **II.10** (Fig. 2.4). Both **II.9** [26π] and **II.10 [**30π] hexaphyrin are itself interconvertible in nature in the presence of oxidizing agent $[Et_3O]^+[SbCl_6]^-$ and reducing agent ($Zn+NH_4Cl$).

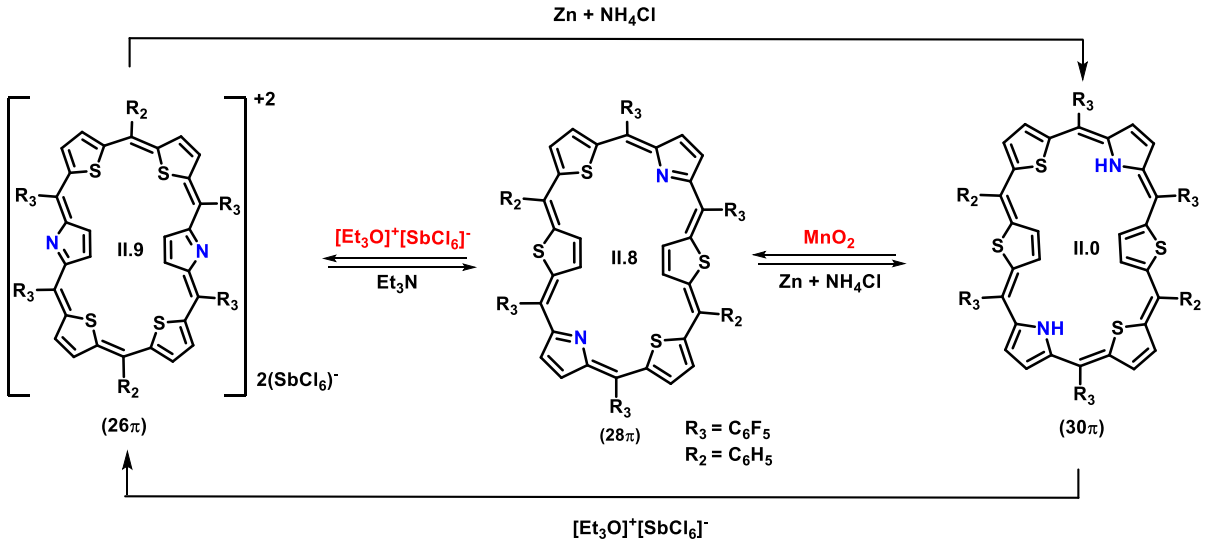

Fig. 2.4: Reversible redox couples in hexaphyrins **II.8**, **II.9** and **II.10** through PCET process.

In all above transformations either the macrocycles are identified as Huckel aromatic macrocycles.[7,8,9,14] But Huckel aromatic to mobius aromatic transition is rare and fascinating. In literature there are very few examples of 30π hexaphyrins, due to reduced stability of highly reduced 30π form of hexaphyrin. Replacing thiophene with furan in the 28π hexaphyrin[13] **II.8** yielded 30π stable aromatic isophlorinoids **II.11**. Unexpectedly its, reversible two electron oxidation process yielded the 28π Mobius aromatic dicationic species. To best of our knowledge this is the first report of topology change from Huckel to Mobius dication while retaining aromatic character in both the forms.

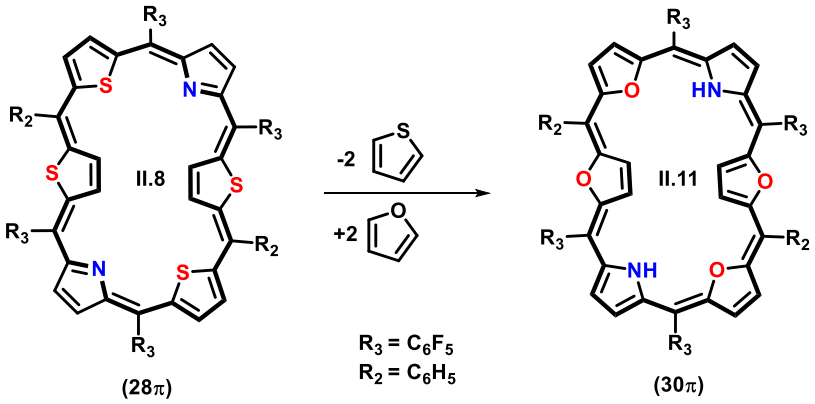

Scheme 2.1: Strategic modification in **II.8**, to synthesis 30π dioxa hexaphyrin **II.11.**

2.2 Synthesis and characterization of 30π dioxa core-modified hexaphyrin

Synthesis of hexaphyrin II.11

The 30π isophlorin II.11 was synthesised by acid mediated condensation of bifuryl dicarbinol **II.12**, and pyrrole under dark and inert condition and followed by oxidation using DDQ in open air atmosphere (scheme 2.2). The formation of desired compound was confirmed through MALDI-TOF/TOF spectrometry. Then, the reaction mixture was passed through a short bed of basic alumina column and the filtrate was concentrated under vacuum. Further isolation was done with neutral alumina column chromatography using 10% dichloromethane/hexane and size exclusion column chromatography was done in tetrahydrofuran. The hexaphyrin **II.11** was obtained as a green color solid in 2.5% yields.

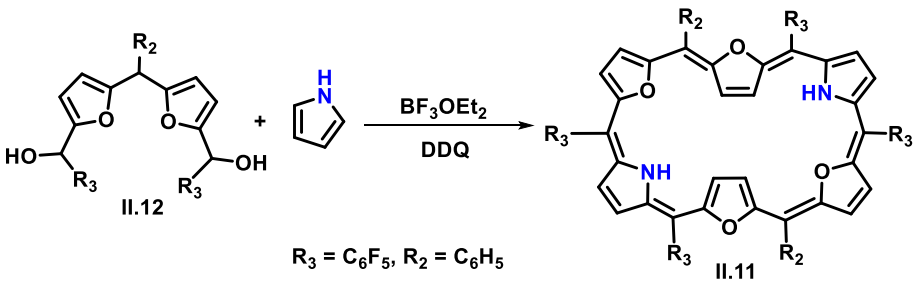

Scheme 2.2: Synthesis of core-modified 30π hexaphyrin **II.11.**

Characterization of Core- Modified Hexaphyrin II.11

The hexaphyrin was analysed through HRMS, UV-visible absorption spectroscopy, NMR spectroscopy, X-ray single crystal diffraction, cyclic voltammetry and spectroelectrochemistry studies**.**

HRMS Spectrum

The High-resolution mass spectrum (Fig. 2.5) displayed m/z of 644.0702 and 1288.1414 corresponding ($[M]^{2+}$ 644.07 and $[M]^{+}$ 1288.1417) for $C_{66}H_{24}F_{20}N_2O_4$.

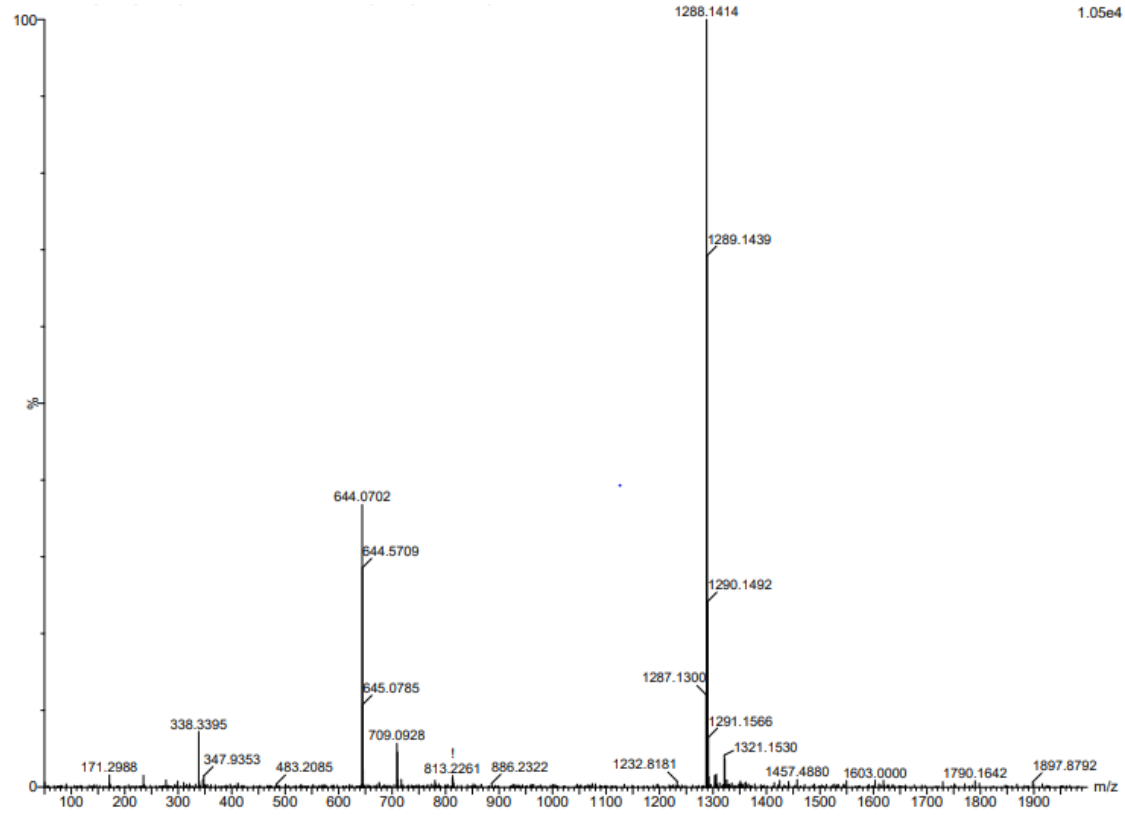

Fig. 2.5: High resolution mass spectrum (ESI-TOF) of **II.11.**

UV-visible Absorption Spectrum

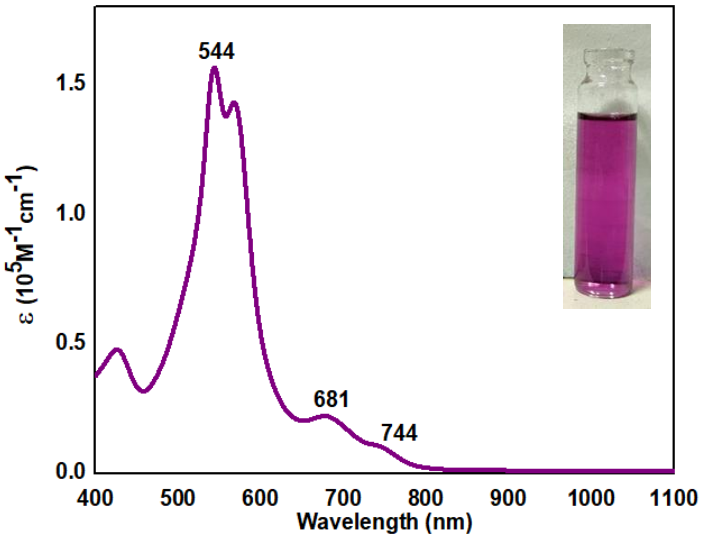

Fig. 2.6: UV-vis electronic absorption Spectrum of **II.11** in CH_2Cl_2.

The electronic absorption of the molecule was recorded in dry and distilled dichloromethane solvent (Fig. 2.6). It displayed an intense absorption peak at 544 nm (156500) with a shoulder peak at 568 nm (143100) followed by absorptions at 679 nm (21900) and 750 nm (10300). These represents the characteristics peaks of a porphyrinoid like macrocycle.

NMR Spectra of Hexaphyrin II.11

The ^{1}H NMR spectrum of the macrocycle was recorded in deuterated dimethyl sulfoxide at 298 K. It showed four distinct doublets in downfield region δ (8.74, 8.58, 8.42, 8.32 ppm) and two doublets δ (-0.66, -0.72 ppm) in upfield region corresponding to two protons each (Fig. 2.7). Macrocycle **II.11** has 30π electrons in conjugated backbone and exhibit diatropic ring current. So, protons at the peripheral of the ring are downfield shifted whereas, inner protons are upfield shifted. This large chemical shift difference between most shielded and deshielded protons corroborates its Huckel aromatic nature. The broad signal at δ +0.27 ppm was assigned to N-H proton which confirmed through ^{15}N-^{1}H correlation spectroscopy. There are two phenyl rings present in the macrocycle and this corresponding protons were found to resonate at δ 8.07 and 7.74 ppm with the integration of four and six protons respectively. This NMR pattern was suggestive the inversion of two heterocyclic rings. In the NOESY spectrum (Fig. 2.8) the correlation between signals at δ -0.72 and +0.26 ppm, confirmed the close proximity of N-H proton of pyrrole and the β-H of inverted heterocyclic unit. Along with three different sets of correlations were also present (i) 8.74 and 8.58 (ii) 8.42 and 8.32 (iii) 8.07 and 7.74 ppm (Fig. 2.8). ^{1}H-^{1}H COSY spectrum confirmed these three correlations between the protons of the macrocyclic ring (Fig. 2.9). ^{19}F NMR spectrum showing three different sets of single corresponding to *ortho, para* and *meta* fluorins of the pentafluorophenyl rings (Fig. 2.10).

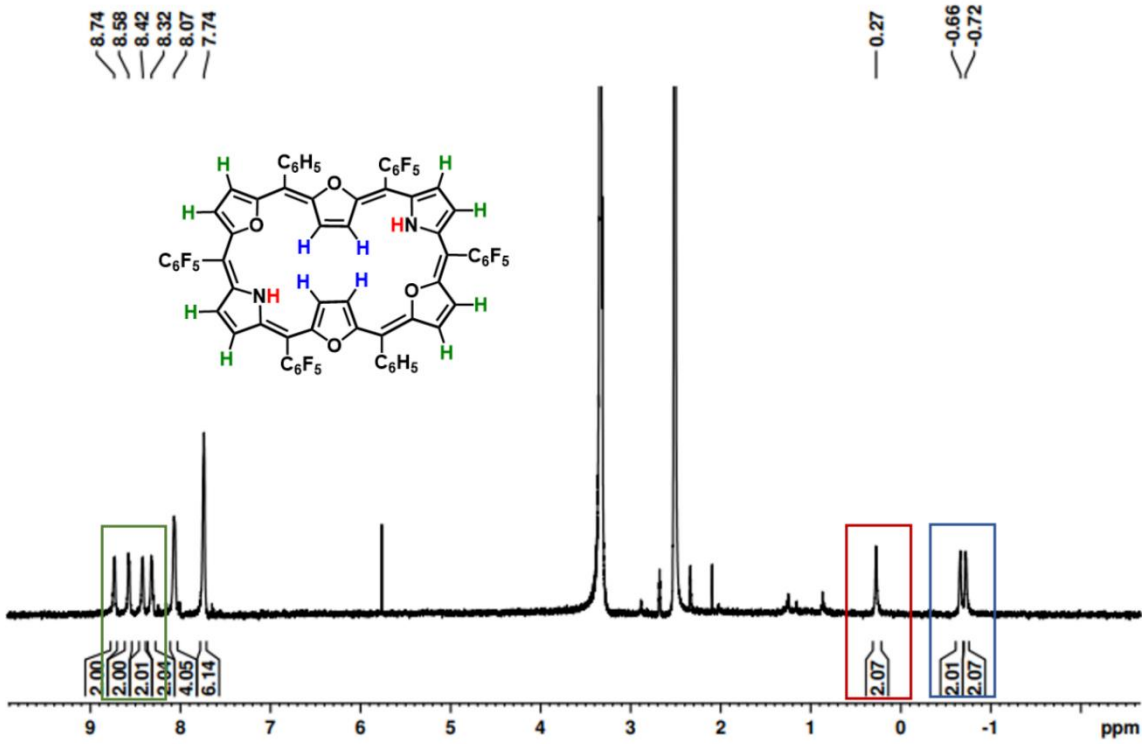

Fig. 2.7: ^{1}H NMR of **II.11** recorded with DMSO-d_6 at 298 K.

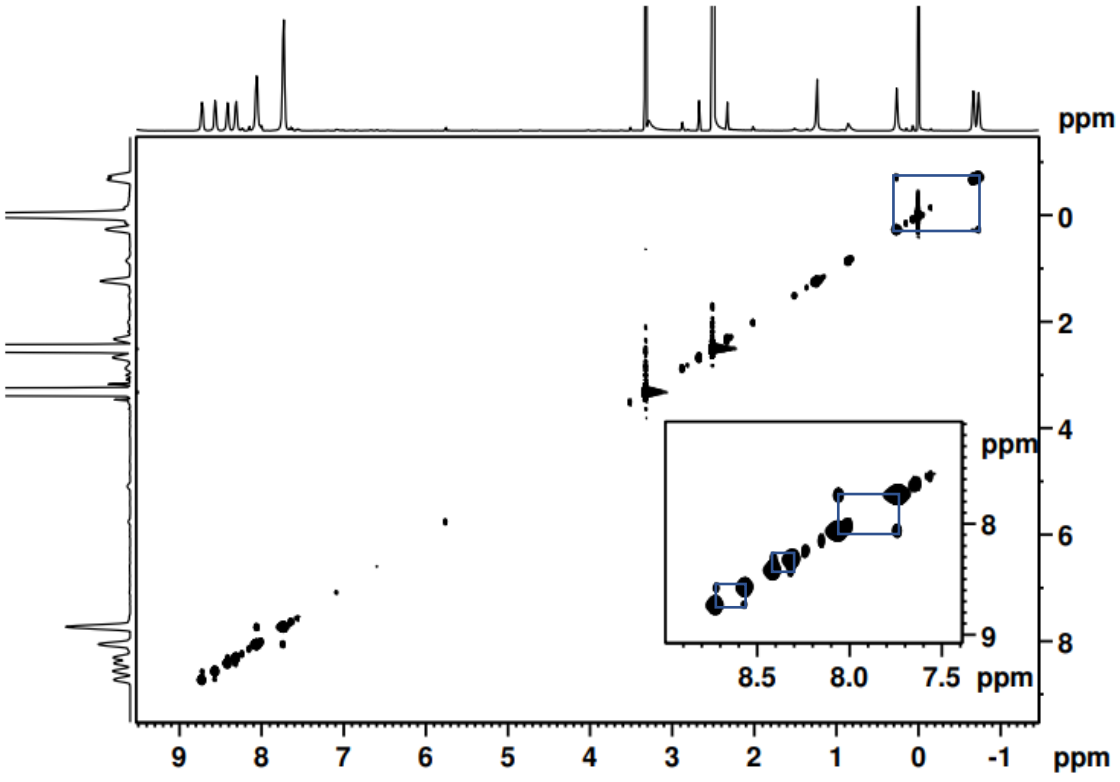

Fig. 2.8: NOESY spectrum of **II.11** in DMSO-d_6 at 298 K.

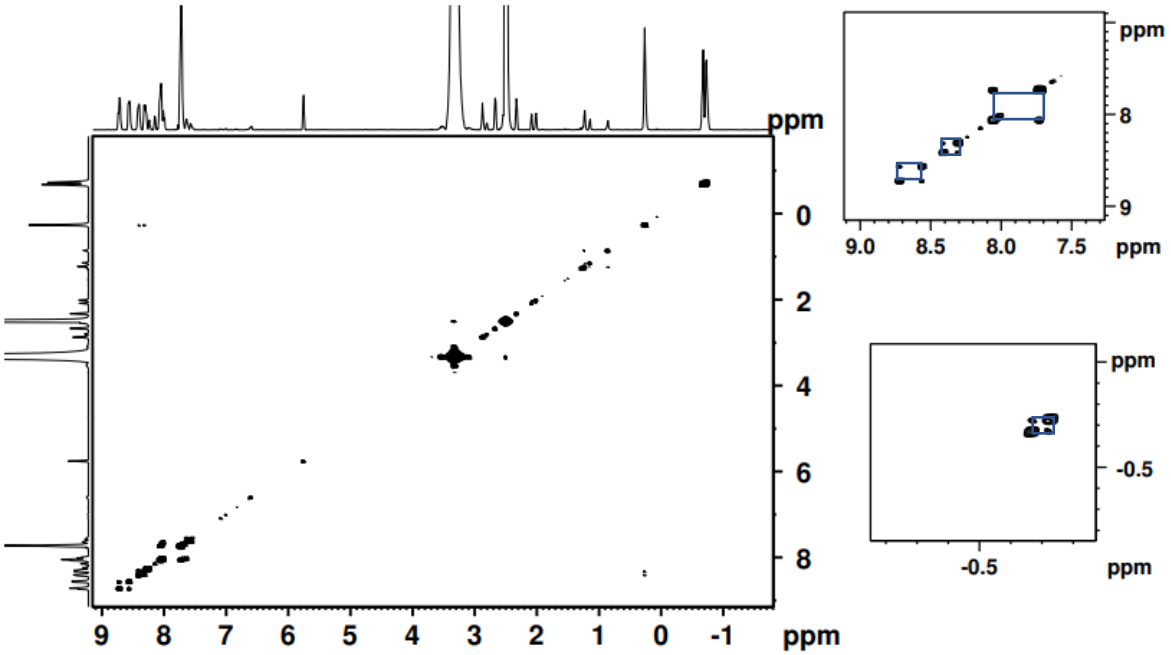

Fig. 2.9: ^{1}H- ^{1}H COSY spectrum of **II.11** in DMSO-d_6 at 298 K.

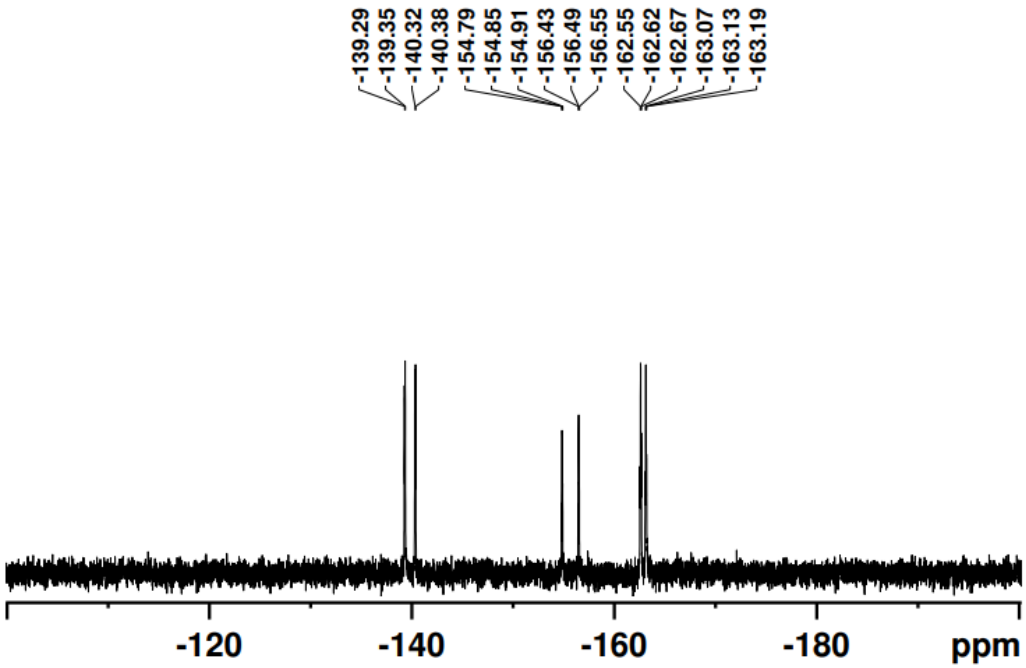

Fig. 2.10: ^{19}F NMR spectrum of **II.11** in DMSO-d_6 at 298 K.

Single Crystal X-ray analysis of II.11

The molecular structure of hexaphyrin was determined from single crystal X-ray analysis. Good quality crystals of the macrocycle were grown in dichloromethane/hexane solvent system by vapor diffusion method. The molecule crystallized in monoclinic P 21/n space group, with a rectangular topology, where all the heterocyclic rings were present in the same plane. Two diametric opposite furan rings were inverted and other four heterocyclic rings (two furan & two pyrrole) facing towards core of macrocyclic ring. All the six *meso* substituents were found perpendicular to the mean macrocyclic plane (Fig. 2.11). The N-H of the pyrrole rings shows the H-bonding interaction with oxygen of non-inverted furan ring with distance 2.415 Å. The assignment of proton signals in ^{1}H NMR spectrum are in sound agreement with molecular structure of hexaphyrin.

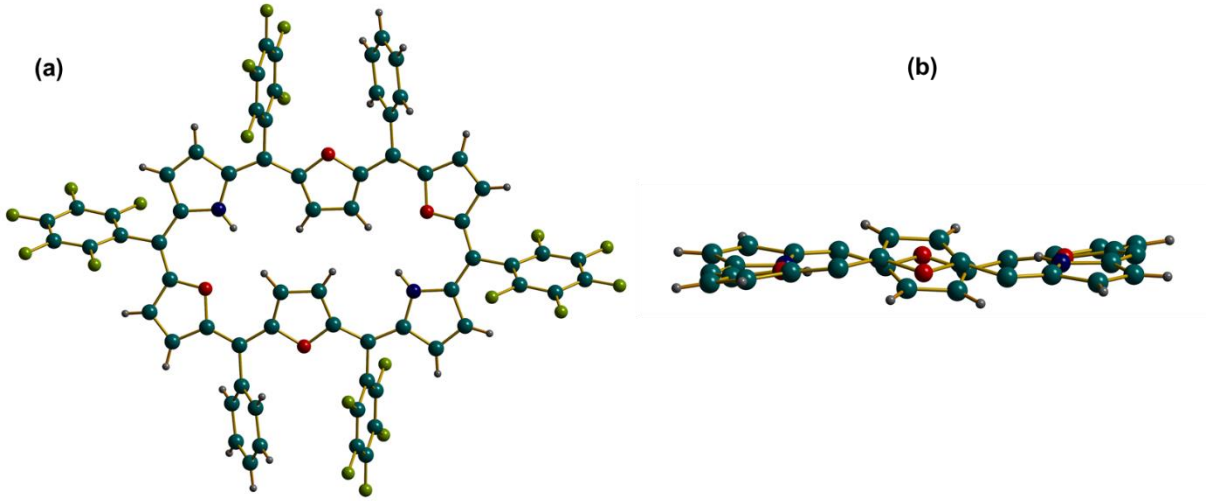

Fig. 2.11: Molecular structure of hexaphyrin **II.11** top view (a). Side view (b), all the *meso* substituents are omitted for clarity.

Cyclic Voltammetry Experiment

The previously reported core modified dithia hexaphyrin **II.8** displayed two oxidation peaks and two reduction peaks. After chemical oxidation 28π hexaphyrin was converted 26π dication species **II.9** of hexaphyrin and on reduction it yielded 30π aromatic hexaphyrin **II.10**.[13] Considering a similar redox nature, the potential of **II.11** was measured with cyclic voltammetry using platinum wire as counter electrode, glassy carbon as working electrode and calomel as reference electrode. The recorded CV displayed two reduction peaks at -0.47 and -

0.97 V along with four oxidations at 0.37 V, 0.51 V, 1.05 V, 1.34 V respectively. These potential values further supported by differential pulse voltammetry experiment (Fig. 2.12).

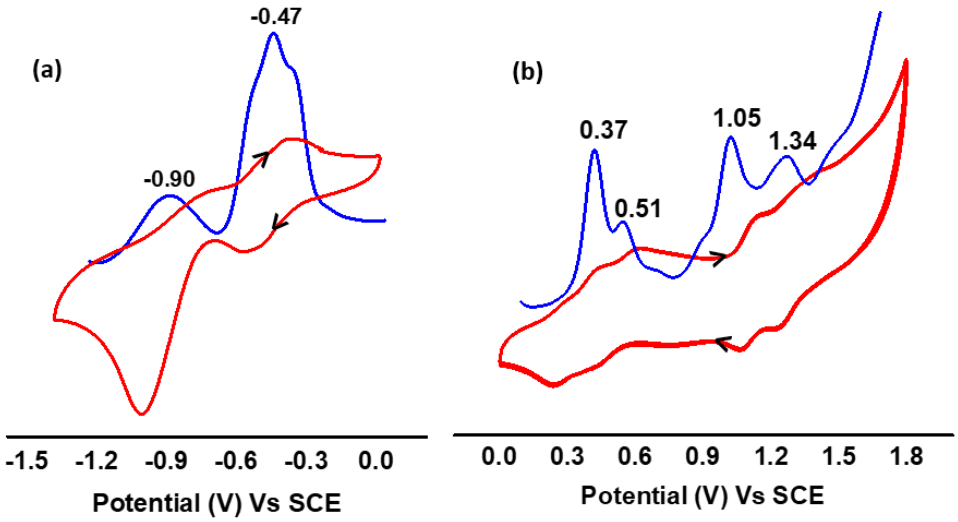

Fig. 2.12: Cyclic voltammetry (red lines) and Differential Pulse Voltammetry (blue lines) of **II.11**. (a) reduction (b) oxidation, using 0.1 M tetrabutylammonium perchlorate in dichloromethane with the scan rate of 100 mV/s.

2.3 Spectro-electrochemical experiment

To analyse the oxidized species of the molecule, the spectro-electrochemical measurements were performed using the same set of electrodes as (cyclic voltammetry experiment). With respect to time, the change in the electronic absorption was recorded after every 10 seconds at a particular applied potential.

On applying the potential of +0.46 V (beyond the first oxidation potential) on starting material **II.11**, new electronic absorption bands were observed at 373, 490 and 615 nm, and peak at 544 nm is diminishing (Fig. 2.13, a). On further increasing the potential to 1.18V, it shows a decrement in the absorption peak at 490 nm and other absorption peak appears at red shifted region at 595 nm and followed by peaks at lower energy region 805 and 867 nm (Fig. 2.13, b). An increase in the potential beyond 1.18V, did not induce any prominent change in the absorption pattern. Hence, only two oxidised states were observed. Further these two oxidation states were reversible in nature, which could seen by applying a potential in the reverse direction from (1.18 V to 0.46 V) and then towards (0.46 V to -0.2 V).

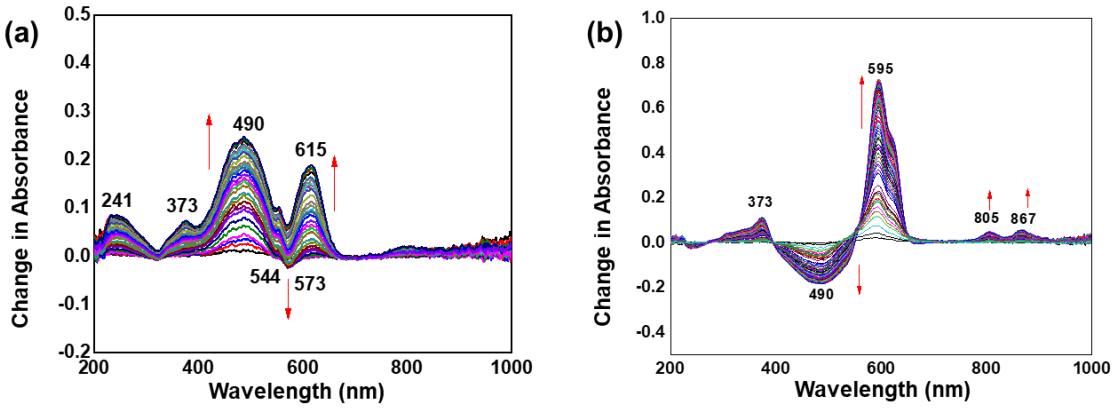

Fig 2.13: Spectroelectrochemical analysis of hexaphyrin **II.11** (a) Potential applied 0.46 V (b) potential applied 1.18 V.

2.4 Synthesis and Characterization of $[II.11]^{2+}$

UV-visible Absorption Spectroscopy

To support the spectro-electrochemistry studies, the hexaphyrin **II.11** was oxidised by $[Et_3O]^+[SbCl_6]^-$ (Meerwein's salt), a classic one electron oxidising agent for π-conjugated system.[15] On treating the hexaphyrin **II.11** with excess equivalent of $[Et_3O]^+[SbCl_6]^-$ in dried dichloromethane, color of the solution immediately changes from violet to blue (Scheme 2.3). Suggesting two-electron ring oxidation of the macrocycle. The oxidised species **$[II.11]^{2+}$** was isolated in quantitative yield as a golden color solid.

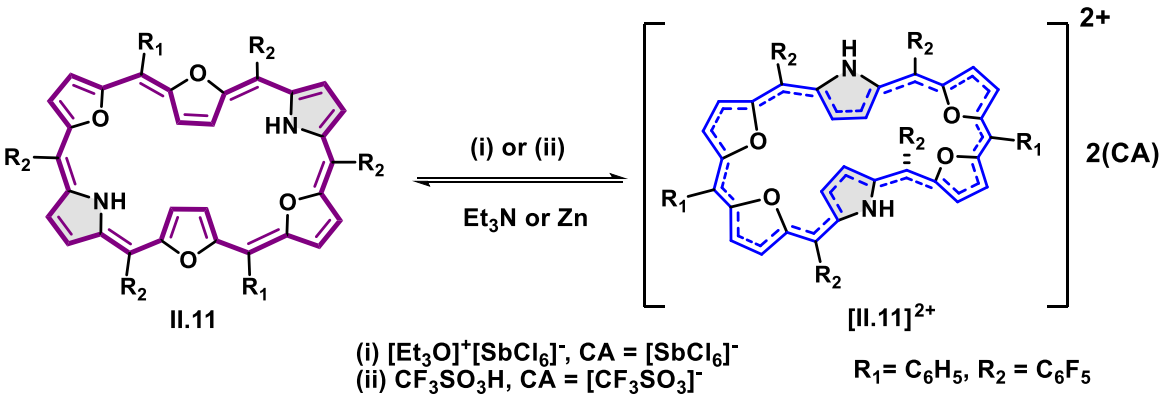

Scheme 2.3: Oxidation of 30π hexaphyrin **II.11** to its 28π dicationic species **$[II.11]^{2+}$**.

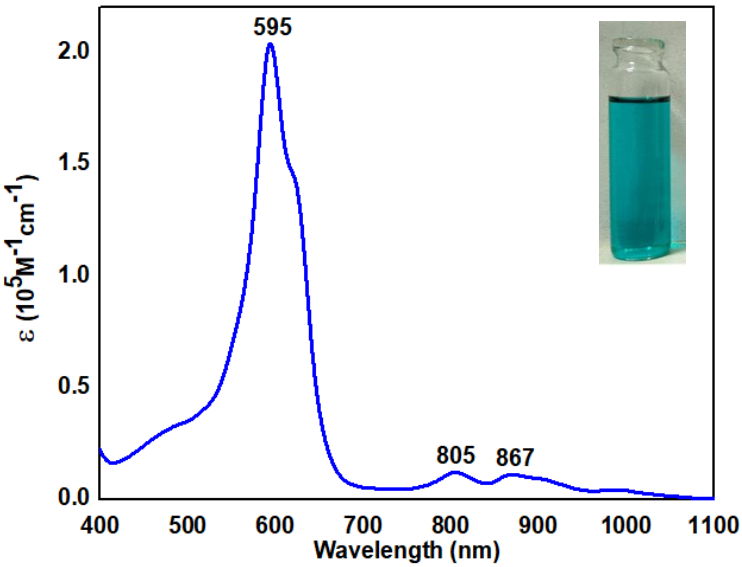

Fig 2.14: UV-vis absorption Spectrum of **[II.11]**$^{2+}$in dichloromethane.

The absorption spectrum of the blue colored compound **[II.11]**$^{2+}$ was recorded in dichloromethane and it shows a red shifted and intense band at 595 nm (203500) and followed by low energy bands at 805 nm (11700), 867 nm (10935) and 991 nm (4090) (Fig. 2.14). Such type of spectrum with intense Soret like absorption and three Q-peaks are typical of porphyrin like macrocycles. The observed absorption pattern upon chemical oxidation was found similar to electrochemical oxidation of molecule at a applied potential of 1.18V (Fig. 2.13, b). This oxidised species **[II.11]**$^{2+}$ was also obtained by treating the hexaphyrin **II.11** with triflic acid CF_3SO_3H. The color of the solution and electronic absorption was exactly similar to oxidised species **[II.11]**$^{2+}$ obtained with Meerwein salt. Hence $[Et_3O]^+[SbCl_6]^-$ and CF_3SO_3H yielded the same dicationic species. The reversible reduction of the dication can be chemically achieved by addition of triethylamine or Zn as a reducing agent to **[II.11]**$^{2+}$ and hence it undergoes two electron reduction to its free base hexaphyrin **II.11** (Scheme 2.3).

High Resolution Mass Spectrum of [II.11]$^{2+}$

The hexaphyrin **[II.11]**$^{2+}$ formed with chemical oxidation of **II.11**, revealed a peak m/2 at 644.0695 (calcd. for $(C_{66}H_{24}F_{20}N_2O_4)^{2+}$; $[M]^{2+}$ 644.0708) for the macrocycle, confirming the $2e^-$ ring oxidation of the hexaphyrin **II.11** (Fig. 2.15).

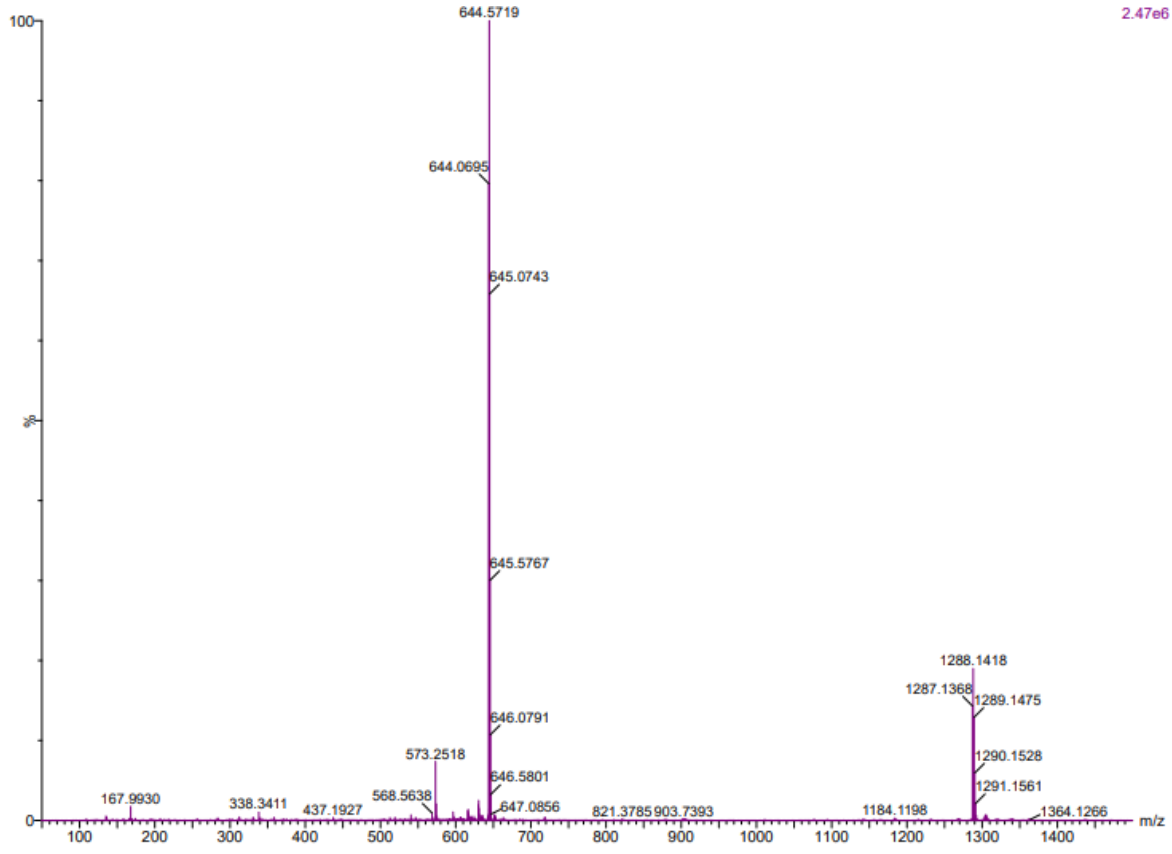

Fig 2.15: High resolution mass spectrum (ESI-TOF) of **[II.11]**$^{2+}$.

Single Crystal X-ray analysis of the [II.11]$^{2+}$

Several attempts were required to obtain good quality crystals of the dicationic species **[II.11]**$^{2+}$. The best quality crystal was obtained with diffusion of hexane into a solution of **[II.11]**$^{2+}$ in dichloromethane. Molecule crystallizes in monoclinic space group P 21/n, and adopted the twisted topology with two triflate counter anions associated with macrocyclic backbone (Fig. 2.16). In comparison to free base, all the heterocyclic rings deviated from its mean macrocyclic plane in the oxidised form. Hence, it resulted in disruption of ring current and attained a twisted topology for the macrocycle. The arrangement of heterocycles was changed significantly and two pyrrole rings positioned at diametric opposite position had arranged in edge-to-face manner. The N-H proton of the pyrrole ring remained intact in the macrocyclic core and hence suggesting the absence of PCET (proton coupled electron transfer) reaction. Instead only ring oxidation has taken place. The two positive charges on the macrocyclic were balanced by negative charge of two counter anions (triflate) (Fig. 2.16, b).

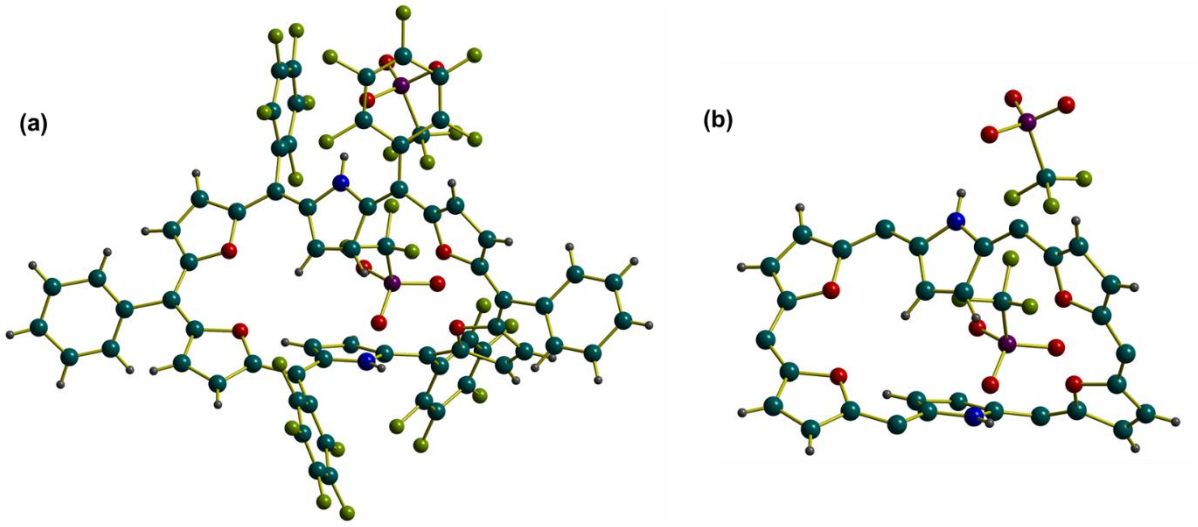

Fig. 2.16: Molecular structure of oxidised hexaphyrin **[II.11]**$^{2+}$ top view (a), side view (b) where all the *meso* substitution was omitted for clarity.

NMR Spectra of the Hexaphyrin [II.11]$^{2+}$

The macrocycle **II.11** follows (4n+2) π e$^-$ rule of Huckel aromatic system and displayed diatropic ring current effect. After two electron ring oxidation, it forms 28π e$^-$ electronic system and so according to Huckel rule it should have the paratropic ring current. The proton NMR spectrum of **[II.11]**$^{2+}$ at room temperature was not resolved and hence low temperature proton NMR was recorded which confirms fluxional nature (Fig. 2.17). Surprisingly, **[II.11]**$^{2+}$ displayed the diatropic ring current in proton NMR spectrum and secondly, the obtained crystal structure has the twisted topology therefore, it support the Mobius aromatic nature. On lowering the temperature to 193 K it exhibited signals in the at most shielded region at δ -1.64 ppm and -2.35 ppm, which belongs to the inverted pyrrole ring. The proton signals at δ 4.93 ppm and 5.10 ppm suggested moderate ring current of one heterocyclic ring. Two characteristic signals at δ 5.86 and 12.17 ppm for the N-H proton gets diminished with addition of D_2O to the sample. Other proton signals from four furan rings and two phenyl rings were present in between δ 6.88 ppm to 9.19 ppm. Hence, all the assigned proton signals were found in sound agreement with the molecular structure of **[II.11]**$^{2+}$ (Fig. 2.16).

In following spectrum the peaks between δ 0 to 4.3 ppm belongs to residual impurities, either from excess oxidising agents or ethyl chloride or diethyl ether which unfortunately could not be removed even after recrystallization also.

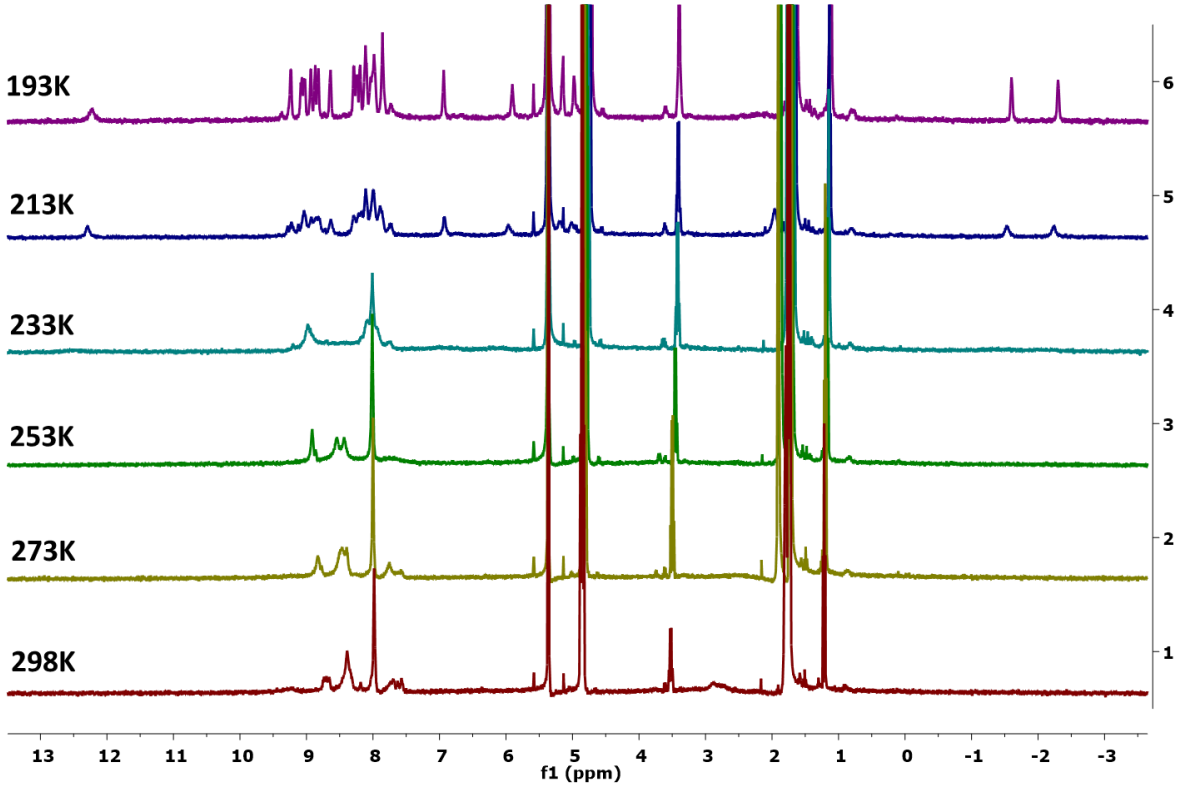

Fig. 2.17: Variable temperature ^{1}H NMR spectra of **[II.11]**$^{2+}$in dichloromethane-d_2.

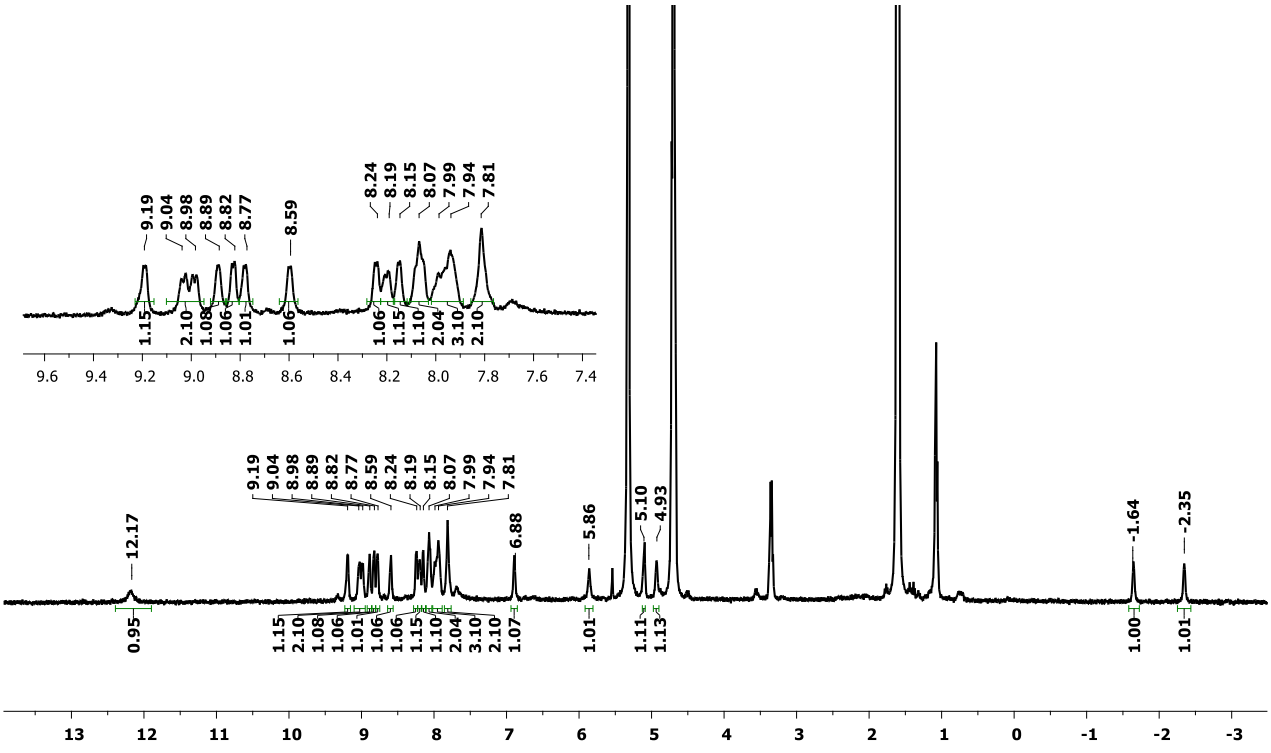

Fig. 2.18: ^{1}H NMR spectrum of **[II.11]**$^{2+}$ at 193 K in dichloromethane-d_2.

2.5 Quantum Chemical Calculations

To get more insight on aromaticity and antiaromaticity of the π- conjugated systems, the quantum mechanical calculations were performed for these molecules using Gaussian 09 rev D[16a]. These calculations were done with Density Functional Theory (DFT) using Becke's three-parameter hybrid exchange and Lee-Yang-Parr (B3LYP) function and the basis set 6-31G (d, p).[16b, 16c] Firstly, to the get optimised geometry of the macrocycle, the respective molecular structure obtained from single crystal x-ray diffraction was used as initial input.

To elucidate the experimental results on ring current (shielding and de-shielding) P.V.R Schleyer introduced the concept of calculating Nucleus Independent Chemical Shift (NICS) value.[17] It's a magnetic criterion to measure the extent of aromaticity for π-conjugated molecules. The NICS values were obtained using Gauge independent atomic orbital (GIOA) method. And the global ring centres for the NICS (0) values were labelled at the non-weighted mean centers of the macrocycles.

S. No.	NICS Value	Character
1	Negative	Aromatic
2	Positive	Antiaromatic
3	Around Zero	Non aromatic/ Antiaromatic

Table 2.1: NICS value and its associated character.

An estimated negative NICS (0) value -17.5 ppm for macrocycle **II.11** represents its strong aromatic behaviour and it supports the deshielding of protons in ^{1}H NMR spectrum. The macrocycle **[II.11]$^{2+}$** shows NICS (0) value of -9.57 ppm supporting the aromatic nature. A reduced value of NICS (0) compare to its parent macrocycle attributed to the relatively non-planar geometry and globalized dicationic charge on the macrocycle **[II.11]$^{2+}$**.

AICD (Anisotropy of the Induced Current Density) another magnetic criterion for estimating the aromaticity and antiaromaticity of the molecule. Herges and co-workers reported the theory of AICD to determine the ring current effect on delocalised π-conjugated system.[18] The AICD plot provides the direction and magnitude of ring current effect when external magnetic field applied orthogonal to the macrocyclic plane. The data obtained by CGST (continuous applying set of gauge transformation) method was plotted using POVRAY 3.7 visualisation software.

In AICD plot, molecule with clockwise direction of ring current represents its aromatic nature, whereas anticlockwise direction of ring current shows antiaromatic character of the molecule.

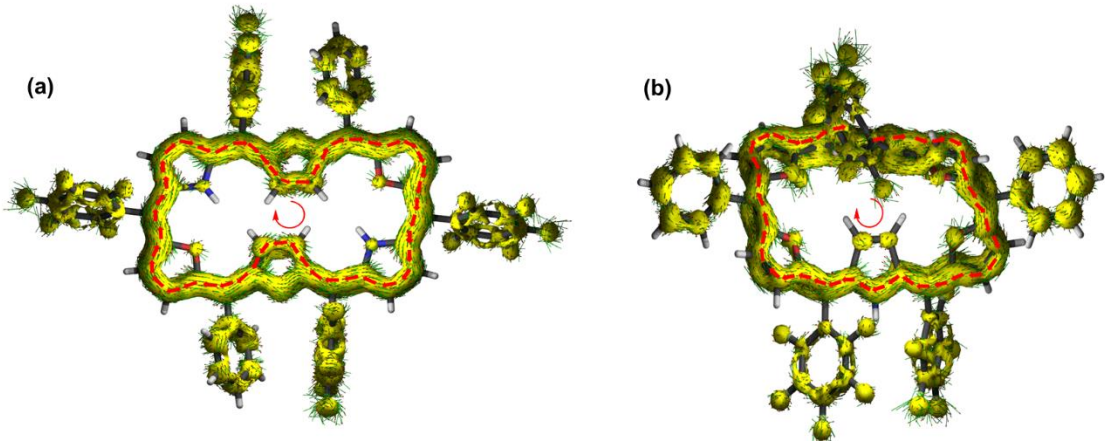

Fig. 2.19: AICD plot of macrocycle (a) **II.11** and (b) **[II.11]**$^{2+}$ at 0.06 iso value (πe^- only).

Macrocycle	NICS (0)	Ring Current	Characteristics
II.11	-17.5 ppm	Clockwise	Aromatic
[II.11]$^{2+}$	-9.57 ppm	Clockwise	Aromatic

Table 2.2: Estimated NICS values and AICD Plots measure of **II.11** and **[II.11]**$^{2+}$.

To simulate the steady-state absorption spectra, the TD-DFT (time dependent density functional theory) calculations using the B3LYP/631G (d, p) basis set was done for energy optimized structure. The obtained theoretical vertical excitation energies are in sound agreement with the electronic absorption obtained from UV-visible absorption spectroscopy.

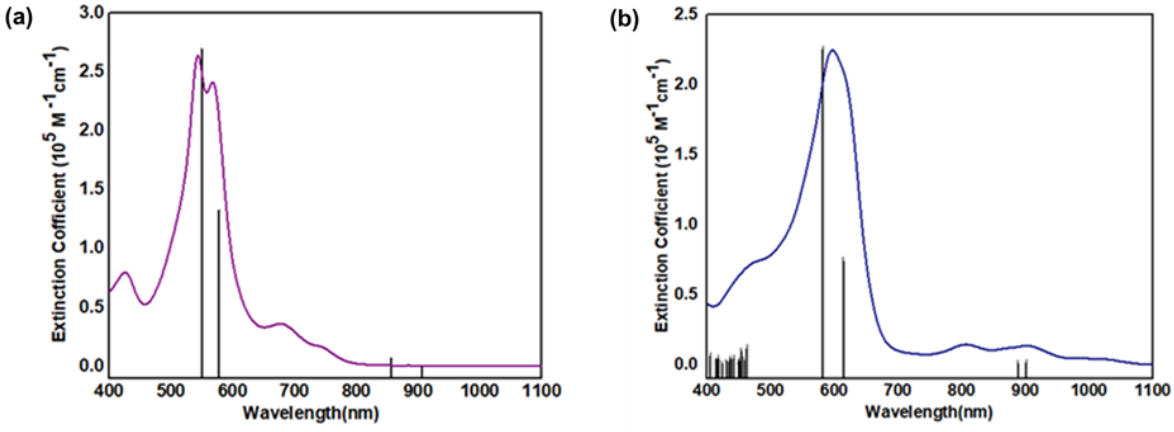

Fig. 2.20: The steady state absorption spectrum of the molecule recorded in dichloromethane (a) **II.11** (b) **[II.11]**$^{2+}$, with their corresponding theoretical vertical excitation energies obtained from TD-DFT calculations.

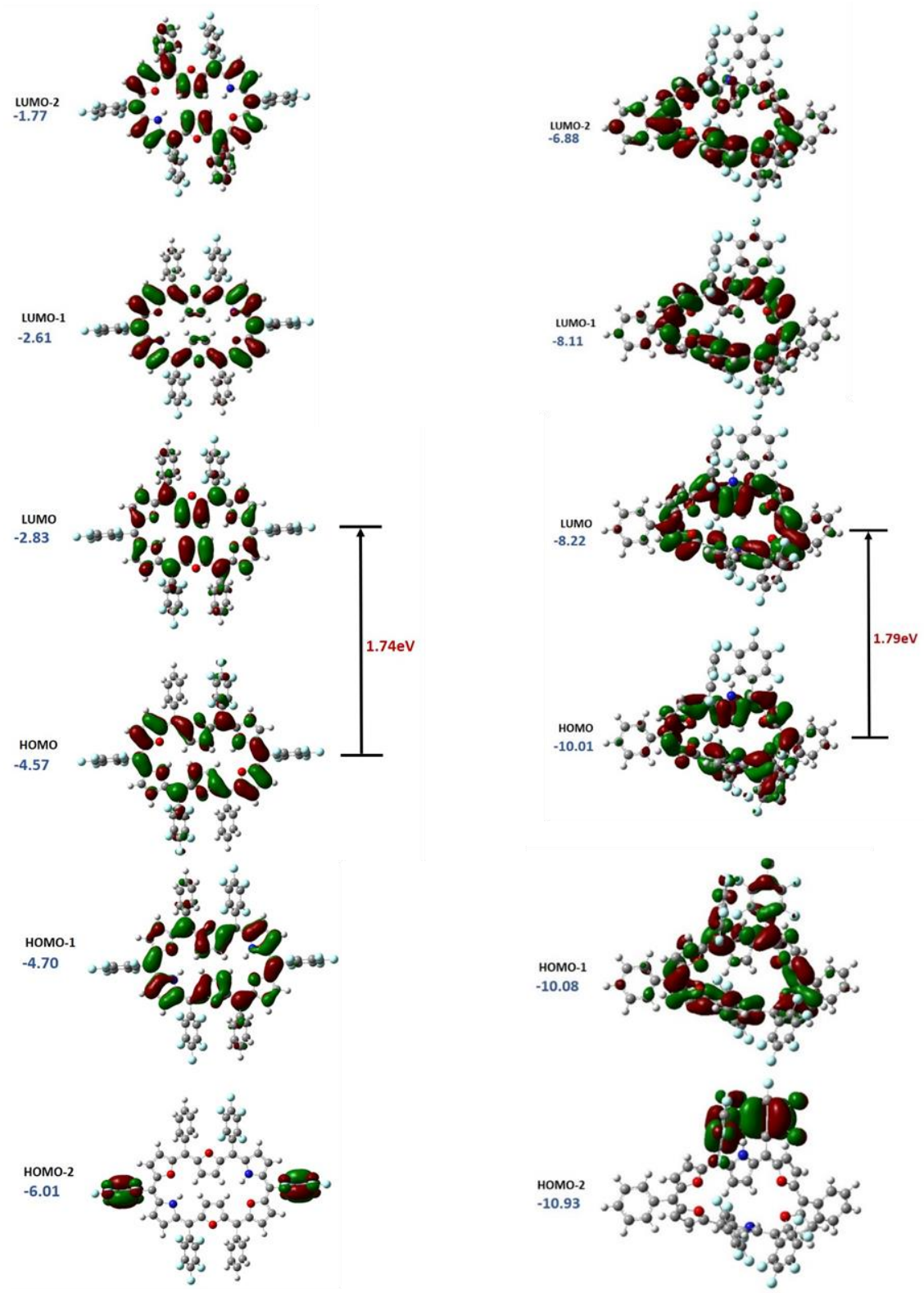

Fig. 2.21: Selected Frontier Molecular orbitals picture of **II.11** (left) **$[II.11]^{2+}$ (right).**

The HOMO-LUMO energy gap is almost same for **II.11** and **$[II.11]^{2+}$** 1.74 eV and 1.75 eV respectively. The experimental and computational data supports the aromatic character of

both the hexaphyrins. Hence dication **[II.11]**$^{2+}$ with 28π electrons in its circular pathway and seizing all the aromatic character, is Mobius aromatic in nature.

2.6 Conclusion

Using a simple strategic method, 30π dioxa hexaphyrin was synthesised with pyrrole and furan based precursors. Usually porphyrinoids has ability to undergo amine and imine interconversion but this 30π core-modified hexaphyrin obtained in highly reduced form where N-H remains intact and also macrocycle was found air and moisture stable. Being electroactive in nature, it shows reversible redox transition without affecting its aromaticity. The two electrons ring oxidation of 30π Huckel aromatic molecule to 28π Mobius aromatic dicationic molecule was observed. Both the macrocycles were characterized through several spectroscopic methods and X-ray diffraction of single crystal confirmed the topological change in the macrocycles. Further the aromatic nature was supported with quantum mechanical calculations, where both the macrocycles reflect the negative NICS (0) value and clockwise direction of ring current. The reversible aromatic transition was achieved chemically with addition of triethylamine or Zn and spectroelectrochemically by applying certain potential. The 28π Mobius dicationic hexaphyrin is a novel example of Mobius charge species, through which we can explore the new class of Mobius salts.

2.7 Experimental Section

All the air and moisture sensitive reactions were performed under nitrogen atmosphere in flame dried round bottom flask. The chemicals purchased from different brands were use as it is, except pyrrole (distilled prior to use). The solvent like tetrahydrofuran and dichloromethane were dried and distilled prior to use by sodium metal and P_2O_5 respectively. The column chromatography were performed using basic alumina and silica gel as per need. The size exclusion column packed in Bio-Beads S-X1 (BIO-RAD) was used for purification of final compound. WATERS G2 Synapt Mass Spectrometer was used to record High resolution mass spectrum (HRMS) of the compounds. Bruker 400 MHz spectrometers were used to record NMR spectrum of the molecules. The chemical shift value reported as delta scale in ppm values relative to deuterated solvents. The electronic absorption spectra of the molecules were recorded in Perkin-Elmer λ-35 UV−vis Spectro-photometer sample loaded in optical quart cuvette of 10 mm path length. X-ray single crystal diffraction analysis was performed with a

BRUKER KAPPA APEX II CCD Duo diffractometer at 100K using graphite monochromatic Mo K_α radiation (λ = 0.71073 Å). The software like SHELXL-97 was used to solved and refined the structures and further diamond software used to draw the crystal images of molecule. The CCDC (Cambridge Crystallographic Data Centre) deposition number for **II.11** = 2207874, **[II.11]**$^{2+}$ = 2207884 for detailed information of crystals.

The Cyclic Voltammetry (CV) and Differential Pulse Voltammetry (DPV) experiments to analyse the redox behaviour of molecule was performed in CH instrument Electrochemical Analyser. This setup comprises of three electrode cell (i) working electrode - glassy carbon (ii) reference electrode - calomel and (iii) counter electrode - platinum wire, using supporting electrolyte 0.1 M tetrabutylammonium perchlorate (prepared in freshly distilled dichloromethane).

The electrochemical absorption spectra were recorded in Ocean Insight FLAME Miniature Spectrometer by incorporation of CH Instrument Electrochemical Analyzer. The assembly of spectro-electrochemical cell kit contains purge tube 10 cm, teflon cap, thin layer quartz glass cell with 1 mm of optical path length, Pt gauze as working electrode, Pt wire as counter electrode and calomel as reference electrode. The experiment was perfomed in 0.1 M tetrabutylammonium perchlorate (supporting electrolyte) solution, prepared in freshly distilled dichloromethane.

Synthesis Procedure and Characterization

Hexaphyrin II.11

In flame dried 500 mL round bottom flask bifuryl dicarbinol, **II.12** (1.56 gm, 2.54 mmol) and freshly distilled pyrrole (162 mg, 0.167 mL 2.41 mmol) were added to the 250 mL of dried dichloromethane and solution was bubbled with nitrogen for 10 mins. To this stirred solution $BF_3.OEt_2$ (342.70 mg, 0.297 mL, 2.41 mmol) was added slowly under dark and nitrogen atmosphere, and stirr the reaction for 2 hours. Then 2,3-dichloro-5,6-dicyano-1,4-benzoquinone (DDQ) (1.92 gm, 8.45 mmol) was added and stirred in open air condition. After 2 hours reaction mixture was filtered through short bed of basic alumina column and further filtrate was concentrated under vacuum. Purification was done in neutral alumina column with 10% dichloromethane/hexane eluent. **II.11** appears as purple color in solution state and green color in solid state and isolated in 2.5% yield.

HRMS (ESI) m/z: 1288.1414 and 644.0702 (Calcd. for $C_{66}H_{24}F_{20}N_2O_4$; $[M]^+$ 1288.1417 and ; $[M]^{2+}$; 644.0708). UV-vis Absorption : (CH_2Cl_2), (conc = 10^{-5}), λ_{max} nm (ε, $M^{-1}cm^{-1}$): 544 (156500), 568 nm (143100), 677 (21900) and 740 nm (10300). ^{1}HNMR (400 MHz, in DMSO-d_6 at 298 K) δ: 8.74 (d, J = 4 Hz, 2H), 8.58 (d, J = 4 Hz, 2H), 8.42 (d, J = 4 Hz, 2H), 8.32 (d, J = 4 Hz, 2H), 8.07 (m, 4H), 7.74 (m, 6H), 0.27 (s, 2H), -0.66 (d, J = 4 Hz, 2H), -0.72 (d, J = 4 Hz, 2H). Crystal Data : $C_{66}H_{24}F_{20}N_2O_4$, Monoclinic, space group P 21/c , a = 14.494 (4) b = 15.607 (4), c = 11.617 (3) Å, α = 90, β = 93.538 (9), γ = 90, V = 2622.9 (12) Å^3, *Z* = 2, T = 100 (2) K , Dcalcd = 1.632 g cm^{-3}, R1 = 0.0423 (5059), *R*w (all data) = 0.1433 (6533) GOF = 0.927.

Hexaphyrin $[II.11]^{2+}$

(a). $[II.11]^{2+}.2[SbCl_6]^-$: The synthesis of dicationic molecule was achieved by addition of excess of Meerwein salt $[Et_3O]^+[SbCl_6]^-$ (152.80 mg, 349.14 µmol) to the solution of **II.11** (10 mg, 7.76 µmol) dissolved in 8 mL dry dichloromethane at -20°C and stirred for 20 minutes at same temperature. The dark blue coloured compound **$[II.11]^{2+}$** was formed, which was filtered and washed with pentane multiple times. Molecule obtained in quantitative yield, after recrystallization 95% as golden color solid.

(b). $[II.11]^{2+}.2[CF_3SO_3]^-$: The dicationic molecule **$[II.11]^{2+}$** with triflate ions were obtained upon addition of stoichiometric excess triflic acid (CF_3SO_3H) diluted in acetonitrile to a solution of **II.11** (in acetonitrile) at room temperature. It shows dark blue color solution same as obtained with addition of $[Et_3O]^+[SbCl_6]^-$ to **II.11**. Its electronic absorption and ^{1}H NMR spectrum were identical with **$[II.11]^{2+}.2[SbCl_6]^-$**.

HRMS (ESI) m/z: 644.0695 (Calcd for $[C_{66}H_{24}F_{20}N_2O_4]^{2+}$; $[M]^{2+}$, 644.0708). UV-vis absorption: (CH_2Cl_2), (conc = 10^{-5}), λ_{max} nm (ε, M^{-1} cm^{-1}): 595 nm (203500), 807 (11700), 868 (10935) and 991 nm (4090). ^{1}H NMR: (400 MHz, in Dichloromethane-d_2 at 193 K) δ: -2.35 (s, 1H), -1.64 (s, 1H), 4.93 (s, 1H), 5.10 (s, 1H) 5.86 (s, 1H), 6.88 (s, 1H), 7.81 (m, 2H) 7.94-7.99 (m, 3H), 8.07 (m,2H), 8.15 (s, 1H), 8.19 (s,1H) 8.24 (s,1H), 8.59 (s,1H), 8.77 (s, 1H) 8.82 (s, 1H), 8.89 (s, 1H), 8.98-9.04 (m, 2H), 9.19 (s, 1H), 12.17 (br s, 1H). Crystal Data: ($C_{66}H_{24}F_{20}N_2O_4$) 2(CF_3O_3S) monoclinic, space group P 21/n, a = 10.037 (6) b = 15.366 (9), c = 42.11(3) Å, α = 90, β = 94.515(15), γ = 90, V = 6474 (7) Å^3, T = 100 (2) K, *Z* = 4, , Dcalcd = 1.715 g cm−3, R1 = 0.1587 (3999) , *R*w (all data) = 0.4694 (12731), GOF = 1.093.

References

1. (a) E. Hückel*, Z. Physik,* **1931**, *70*, 204-286 (b) P. Garratt, Aromaticity; Wiley: New York, **1986**
2. R. Breslow, *Acc. Chem. Res.*, **1973**, *6*, 393-398
3. E. Heilbronner, *Tetrahedron Letters*, **1964**, *29*, 1923-1928.
4. (a) R. Herges*, Chem. Rev.*, **2006**, *106*, 4820-4842. (b) H. S. Rzepa, *Chem. Rev.,* **2005**, *105*, 3697-3715.
5. D. Ajami, O. Oeckler, A. Simon, R. Herges, *Nature,* **2003**, *426*, 819-821.
6. (a) A. Jasat, D. Dolphin, *Chem. Rev.,* **1997**, *97*, 2267-2340. (b) J. L. Sessler, D. Seidel, *Angew. Chem. Int. Ed.*, **2003**, *42* ,5134-5175.(c) T. Tanaka, A. Osuka, Chem. Rev., **2017**, *117*, 2584-2640. (d) S. Venkatraman, T.K. Chandrashekar *Acc. Chem. Res.*, **2003**, *36*, 676-691. (e) T. D. Lash, *Angew. Chem. Int. Ed.*, **2000**, *39*, 1763-1767.
7. M. Stepien, L. Latos-Grazynski, N. Sprutta, P. Chwalisz, L. Szterenberg, *Angew. Chem. Int. Ed.,* **2007**, *46*, 7869 -7873
8. J. Sankar, S. Mori, S. Saito, H. Rath, M. Suzuki, Y. Inokuma, H. Shinokubo, K. S. Kim, Z. S. Yoon, J. Y. Shin, J. M. Lim, Y. Matsuzaki, O. Matsushita, A. Muranaka, N. Kobayashi, D. Kim, A. Osuka, *J. Am. Chem. Soc.*, **2008**, *130*, 13568-13579.
9. W. Y. Cha, T. Soya, T. Tanaka, H. Mori, Y. Hong, S. Lee, K. H. Park, A. Osuka, D. Kim, *Chem. Commun.,* **2016**, *52*, 6076-6078.
10. (a) J. A. Cissell, T. P. Vaid, A. L. Rheingold*, J. Am. Chem. Soc.,* **2005**, *127*, 35, 12212–12213. (b) C. Liu, D. M. Shen, Q. Y. Chen, *J. Am. Chem. Soc*., **2007**, *129*, 5814-5815. (c) J. S. Reddy, V. G. Anand, *J. Am. Chem. Soc.,* **2008**, *130*, 3718–3719.
11. S. P. Panchal, S. C. Gadekar, V. G. Anand, *Angew. Chem. Int. Ed.*, **2016**, *55*, 7797-7800.
12. M. G. P. M. S. Neves, R. M. Martins, A. C. Tome, A. J. D. Silvestre, A. M. S. Silva, V. Félix, M. G. B. Drew, J. A. S. Cavaleiro *Chem. Commun.,* **1999**, 385-386.
13. M. D. Ambhore, A. K. Basavarajappa, V. G. Anand, Chem. Commun., **2019**, *55*, 6763-6766.
14. (a) M. Stepien, N. Sprutta, L. Latos-Grazynski, *Angew. Chem. Int. Ed.*, **2011**, *50*, 4288-4340. (b) S. Saito, A. Osuka, *Angew. Chem. Int. Ed.*, **2011**, *50,* 4342- 4373. (c) T. Tanaka, A. Osuka *Chem. Rev.*, **2017**, *117*, 2584-2640. (d) Y. M. Sung, J. Oh, W.

Y. Cha, W. Kim, J. M. Lim, M. C. Yoon, D. Kim, *Chem. Rev*., **2017**, *117*, 2257-2312.

15. R. Rathore, A. S. Kumar, S. V. Lindeman, J. K. Kochi, J. Org. Chem., **1998**, *63*, 5847-6682.
16. (a) Frisch, M. J.; et al. Gaussian 09, revision B.01; Gaussian, Inc.: Wallingford, CT, **2009**. (b) A. D.Becke, Phys. Rev. A, **1988**, *38*, 3098-3100. (c) C. Lee, W. Yang, R. G. Parr, Phys. Rev. B, **1988**, *37*, 785-789.
17. P. V. R. Schleyer, C. Maerker, A. Dransfeld, H. Jiao, N. J. R. van Eikema Hommes, J. Am. Chem. Soc. **1996**, *118, 26*, 6317-6318.
18. D. Geuenich, K. Hess, F. Kohler, R. Herges, Chem. Rev., **2005**, *105*, 3758-3772.

CHAPTER 3

Topological Changes in Octa-furan Macrocycle Driven by Solvatomorphism

3.1 Introduction

Monitoring the structural dynamics is a challenging task, as it has significant importance in the pharmaceutical products. Even a slight alteration in the molecular structure is known to cause drastic changes in the properties of a prodrug.[1,2] Also, the conformation of the molecule is strongly affected by the rate of nucleation, pH, crystallizing solvent, impurities, kinetic and thermodynamic situtions.[3,4] In tune with these properties of molecule, the word polymorphism is described as the existence of a compound in two or more distinct forms in solid-state arrangement. More precisely, the distinct molecular arrangement of same compound with varying amount of solvent or the type of solvent in crystal lattice is known as pseudopolymorphism or solvatopolymorphism.[5,6] These polymorphic properties are well studied with the small molecules or API's (active pharmaceutical drugs) [3,4,7] but are largely unexplored fluxional macrocycles such as porphyrinoids/isophlorinoids and their expanded congeners. As the larger porphyrinoids are usually very flexible, it can be expected that solvent polarity plays a major role in triggering conformational changes in these molecules and hence, they can be explored to study solvatopolymorphism.[8]

In this regards, a few examples of porphyrinoids whose, conformation changes due to reaction with oxidising/reducing agents has been reported recently.[9] For e.g., the ethylene bridge 32π hexaphyrin has a twisted conformation in free base form **III.1**, but upon oxidation to 32π dicationic species it adopts perfectly planar topology **III.2** with affect of pH variation.[9a]

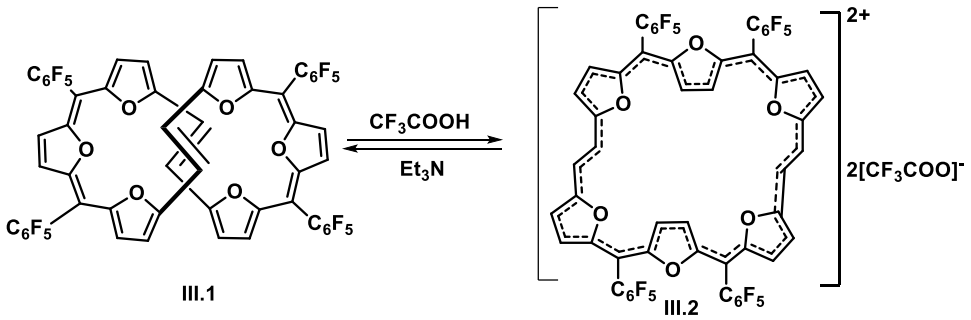

Fig. 3.1: Change in conformational dynamics in ethylene bridged hexaphyrin **III.1** on changing pH of the molecule.

Another interestingly example, the effect of pH in transformation of Huckel aromatic hexaphyrin to Mobius aromatic hexaphyrin has been recently observed as a consequence of oxidising agents like trifluoromethanesulfonic acid and Meerwein salt.[9d] Hence to study the

polymorphism in the macrocycle containing more the six heterocyclic ring, the octaphyrin was chosen as a promising example to study solvatopolymorphism. The previously reported 40π octa-furan[10] **III.6** was synthesized by acid mediated condensation of furan **III.3** and pentafluorobenzaldehyde **III.4** (Scheme 3.1).

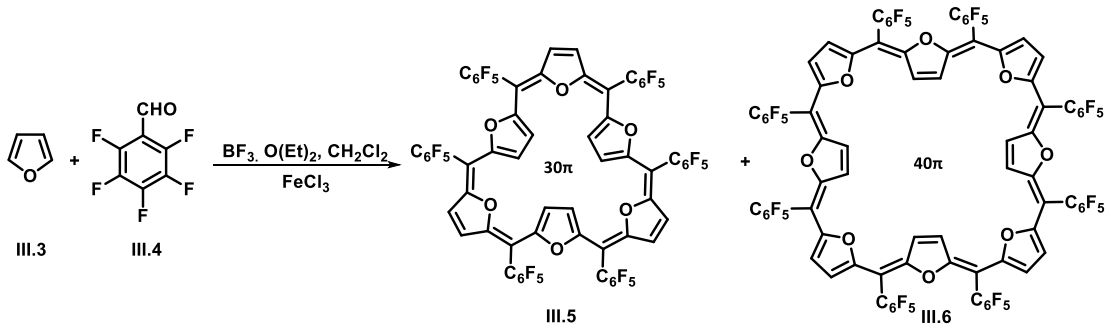

Scheme. 3.1: Synthesis of hexa-furan **III.5** and octa-furan **III.6** macrocycles.

In the above reaction, mainly two products, **III.5** and **III.6**, were isolated in 2 and 1% yields respectively. The ^{1}H NMR spectrum of macrocycle **III.6** displayed only two peaks, at δ 9.4 and 5.85 ppm corresponding to equal number of protons. Its single crystal obtained in chloroform/hexane, confirmed a rectangular topology for the macrocycle, where alternate furan rings were found to adopt ring inverted orientation. Out of eight furans, four furans were inverted and four furan rings were facing the core of macrocycle. Upon lowering the temperature there was no change in conformation of the macrocycle **III.6**. Although conformation of fluxional porphyrinoids is highly dependent on temperature, nature of the solvent and substitution in the ring are also known to alter the topological features. In an attempt to study the dynamics with respect to solvent of crystallization, **III.6** was crystallized with dichloromethane/hexane, but it results the same topology as obtained from crystallization of **III.6** from chloroform/hexane.

According to literature[4] even the substitution of functional group in molecule may affect the process of nucleation and hence the octaphyrin **III.10** was synthesized incorporating with Ph and Ph-Br groups at *meso* positions along with C_6F_5 groups. Thus, the octaphyrin **III.10** was synthesised with the acid catalysed condensation of monomers *meso*-p-bromophenyl dipyyromethane[11] **III.7** and furan dicarbinol[9d] **III.8** in the presence of boron trifluoro etherate and followed by oxidation with DDQ (Scheme 3.2).

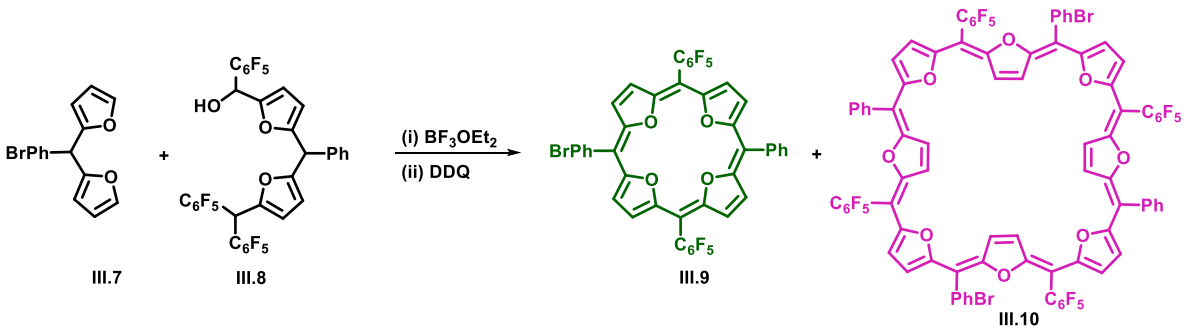

Scheme. 3.2: Synthesis of bromo-derivative tetraoxa-isophlorin **III.9** and octafuran octaphyrin **III.10**.

Analysis of the reaction mixture by MALDI-TOF/TOF mass spectrometry revealed the formation four membered **III.9** and eight membered **III.10** macrocycles, corresponding to [2+2] and [4+4] condensation of the precursor molecules (Fig. 3.2). The structure of macrocycles suggested 20π and 40π electrons correspond to the **III.9** and **III.10** respectively.

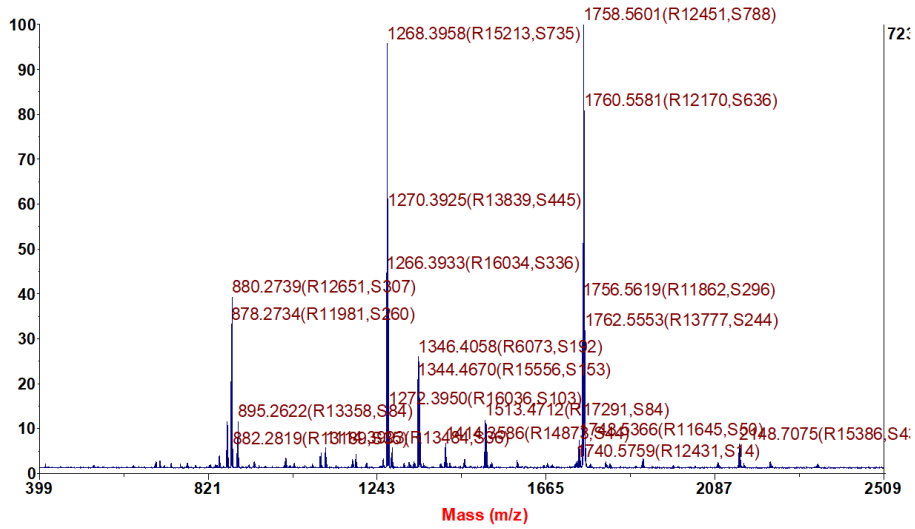

Fig. 3.2. MALDI-TOF/TOF mass spectrum of reaction mixture of isophlorins**.**

3.2 Characterisation of Macrocycle III.9

The tetraoxa-isophlorin macrocycle **III.9**, was characterized by HRMS, NMR, UV-vis absorption spectrum, cyclic voltammetry and spectro-electrochemical analysis.

HRMS Spectrum of III.9

The high-resolution mass spectrum (Fig. 3.3) displayed a value of m/z 878.0150 corresponding to ([M]$^+$ 878.0151, calculated for $C_{44}H_{17}BrF_{10}O_4$), confirming the exact composition in the macrocycle.

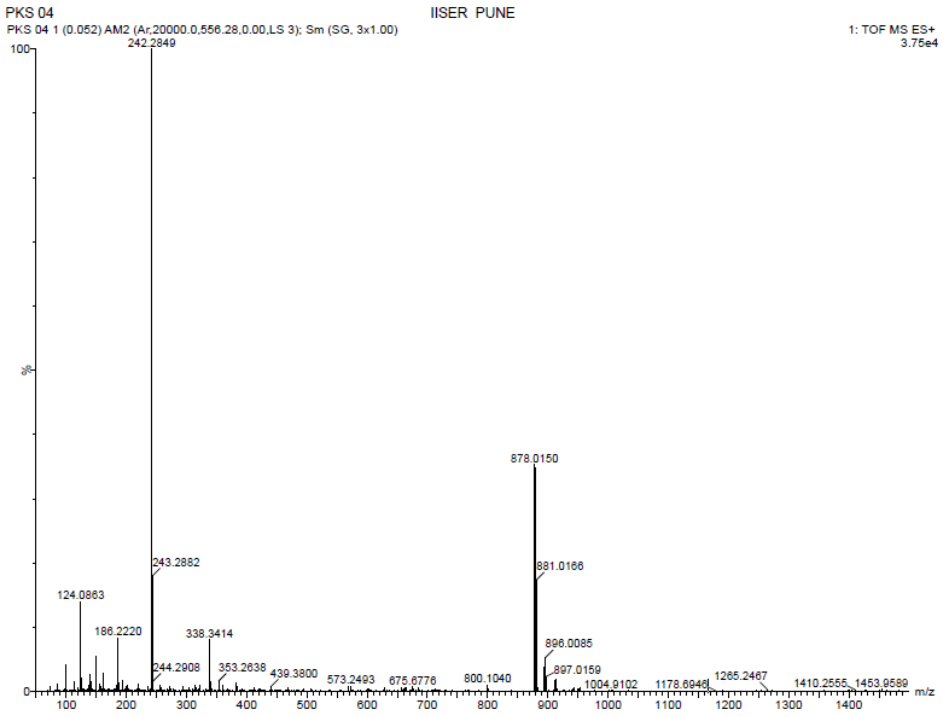

Fig. 3.3: High resolution mass spectrum (ESI-TOF) of **III.9**.

UV-Vis Absorption spectrum of III.9

The electronic absorbance of the macrocycle was recorded in dry and distilled dichloromethane solvent. A light green colored solution displayed strong absorption at 325 nm and 364 nm and followed by weaker absorptions at 437, 467 and 501 nm (Fig. 3.8). This absorption pattern is matching with previously reported 40π expanded isophlorin.[11]

NMR Spectrum of III.9

The macrocycle **III.9**, displayed a well resolved ^{1}H NMR spectrum at 298 K in deuterated toluene. Significantly, **III.9** revealed the paratropic ring current, as it contains 20π electrons along its conjugated pathway (Fig. 3.4). The four doublets in the region between δ 2-3 ppm corresponds to β C-H of furan rings in **III.9**. These four signals resonating at δ 2.57, 2.46, 2.26 and 2.21 ppm value corresponds to two protons each. The signals *meso*-substituents *p*-PhBr and Ph were resonating at δ 6.73, 6.04, 5.71 and 6.62 ppm corresponds to nine protons. The correlations between the adjacent protons of the ring were confirmed by two dimensional, ^{1}H-^{1}H COSY spectrum (Fig. 3.5). It appears as two sets of correlations between the protons (at 2.57, 2.21 & 2.46, 2.26) of heterocyclic rings. The correlation between protons δ 6.73 and 5.71 ppm confirmed the signals from *p*-PhBr ring. The additional correlations between the signals

at δ 6.04 and 6.62 ppm were assigned to the five protons of Ph rings. The upfield signals in the ^{1}H NMR spectrum supported the antiaromatic nature of 20π tetra-oxa isophlorin **III.9**.

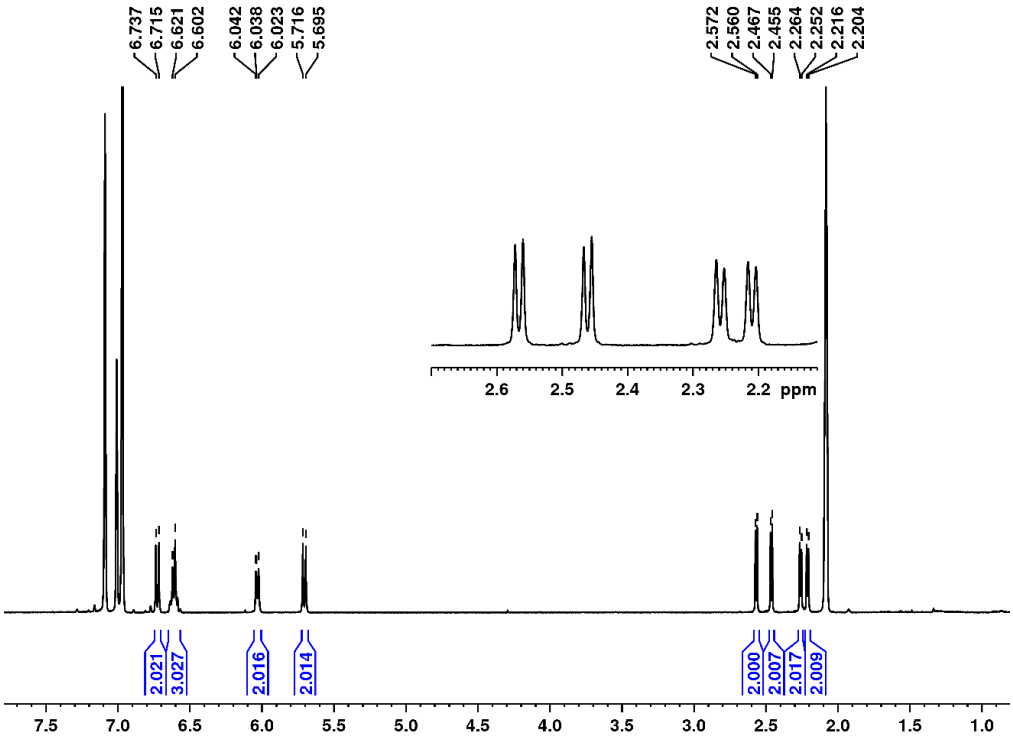

Fig. 3.4: ^{1}H NMR spectrum of **III.9** in toluene-d_8 recorded in 400 MHz machine at 298 K.

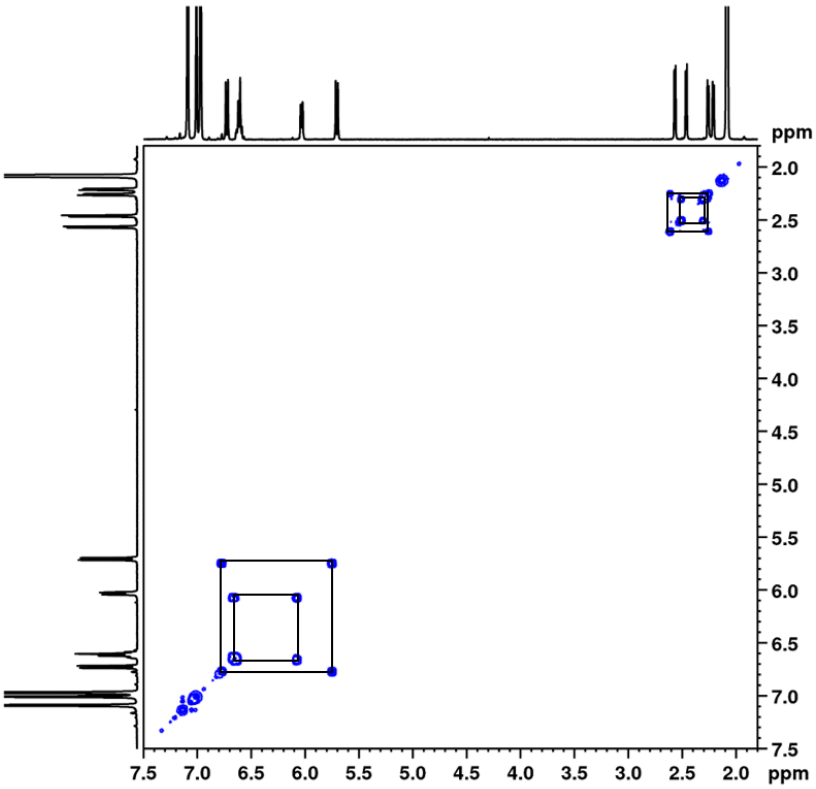

Fig. 3.5: ^{1}H-^{1}H COSY spectrum of **III.9** in toluene-d_8 at 298 K.

Cyclic Voltammetry Experiment of III.9

The macrocycle **III.9** is antiaromatic in nature and it is susceptible to show two-electron oxidation. As expected, in cyclic voltammetry it displayed two oxidation potentials and five reduction potentials (Fig. 3.6). The oxidation potentials were located at 0.38 and 0.70 V whereas, the reduction potentials were located at -0.36 V, -0.55 V, -0.94 V, -1.14 V and -1.36 V. The potential peaks of CV experiment were further supported by differential pulse voltammetry (DPV).

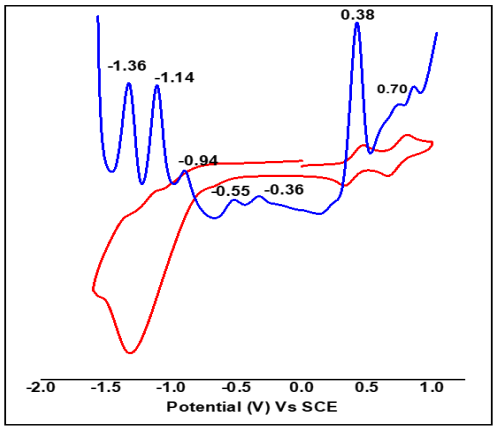

Fig. 3.6: Cyclic voltammetry (blue line) and Differential pulse voltammetry (red line) of **III.9**. For experiment 0.1M tetrabutylammonium perchlorate solution in dichloromethane was taken as the supporting electrolyte and scan rate100 mVs^{-1}.

3.3 Chemical Oxidation of III.9 to $[III.9]^{2+}$

The cyclic voltammetry experiment suggested, **III.9**, is susceptible for two electrons oxidation. Hence, **III.9**, was chemically oxidized with Meerwein salt[12] $[Et_3O]^+[SbCl_6]^-$ in dry and distilled dichloromethane (Scheme 3.3). The color of solution instantly changes from lighter green to darker green. The electronic absorbance of $\mathbf{[III.9]^{2+}}$ was red shifted compared to its free base form **III.9**. This oxidation reaction was found to be reversible and accomplished by the addition of base such as triethylamine to $\mathbf{[III.9]^{2+}}$.

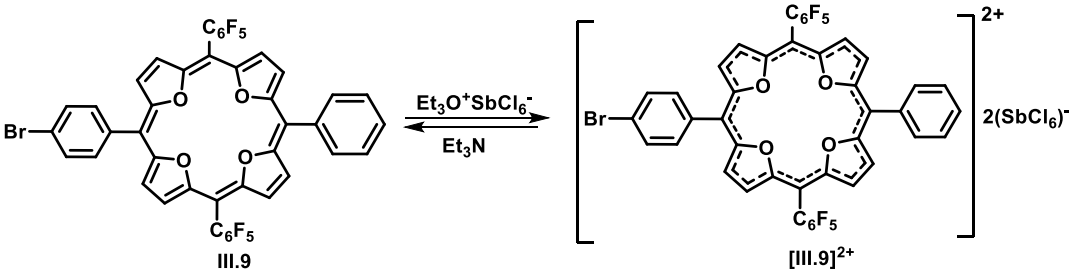

Scheme. 3.3: Reversible oxidation reaction of **III.9** and $\mathbf{[III.9]^{2+}}$.

3.4 Characterization of $[III.9]^{2+}$

The macrocycle **$[III.9]^{2+}$** was characterized by mass spectrometry, UV-Vis absorption, NMR spectroscopy and spectrochemical experiment.

HRMS spectrum of $[III.9]^{2+}$

The high-resolution mass spectrum (Fig. 3.7) of the **$[III.9]^{2+}$**, displayed an m/z value of 439.0057 calculated for ($[C_{44}H_{17}BrF_{10}O_4]^{2+}$: $[M]^{2+}$ 439.0075). The m/2 peak confirmed the two-electrons ring oxidation of 20π electrons **[III.9]** to its 18π dicationic species **$[III.9]^{2+}$**.

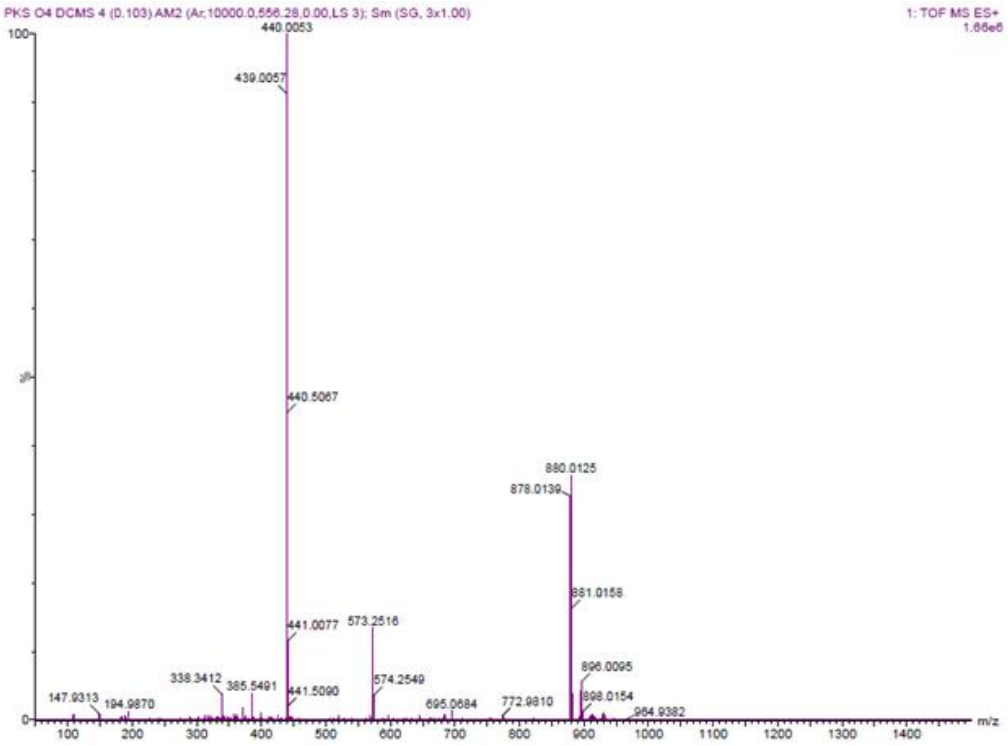

Fig. 3.7: High resolution mass spectrum (ESI-TOF) of **$[III.9]^{2+}$**.

UV-Visible Absorption Spectrum of $[III.9]^{2+}$

The absorption spectrum was recorded in dichloromethane (Fig. 3.8). The dicationic macrocycle **$[III.9]^{2+}$** displayed a more intense and red shifted absorption band compare to its free base form **III.9**. The λ_{max} appears at 403 nm and Q-band like peaks at 567, 618 and 767 nm and this spectral pattern matches with absorption of a typical 18π electron porphyrin derivatives. Hence, it further supports the two-electron ring oxidation of **[III.9]** to **$[III.9]^{2+}$**.

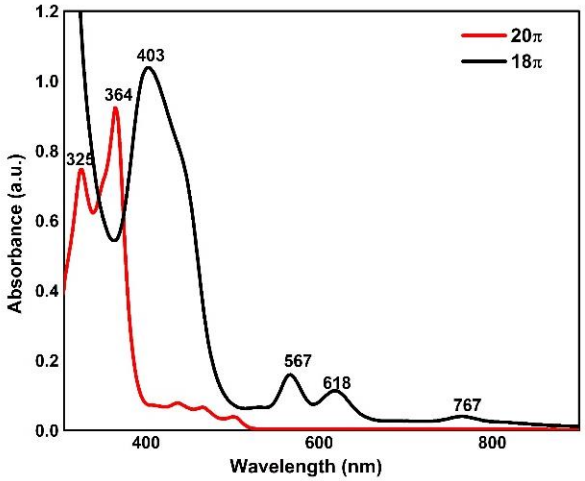

Fig. 3.8: UV-vis absorption spectrum of **III.9** (red lines) and **[III.9]**$^{2+}$ (black lines) recorded in dichloromethane.

NMR Spectrum of [III.9]$^{2+}$

The isophlorin **III.9**, consists of 20π electrons along its cyclic pathway and hence shows the paratropic ring current for the macrocycle (Fig. 3.4). Once it is chemically oxidised to its dicationic macrocycle **[III.9]**$^{2+}$, it consists of 18π electrons and hence the direction of ring current expected to be reverse with respect to free base **III.9**.

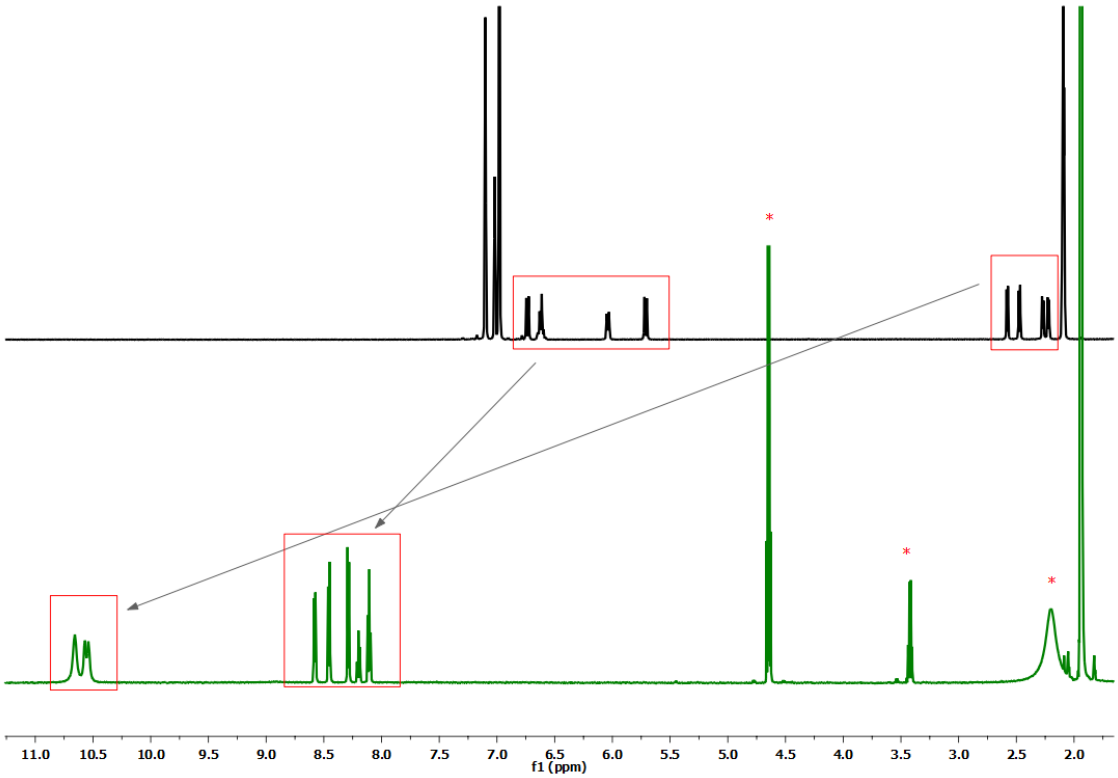

Fig. 3.9: ^{1}H NMR spectrum of **[III.9]** (black color spectrum) in toluene-d_8 and **[III.9]**$^{2+}$ (green color spectrum) in acetonitrile-d_3 recorded at 298 K. The other peaks with (*) are from residual solvents.

The ^{1}H NMR of **[III.9]$^{2+}$** was recorded at 298 K in acetonitrile-d_3 and it reveals the signals in downfield region. (Fig. 3.9) A broad singlet and one doublet corresponding to four protons each were assigned to β C-H of four heterocyclic furan rings. Here, the signals for *meso* substituents phenyl and 4-bromophenyl are more deshielded in comparison to its free base form **III.7** and they resonate as five peaks at δ 8.58, 8.46, 8.30, 8.20 and 8.11 ppm values for nine protons. Further, the correlation between these protons were confirmed by ^{1}H-^{1}H COSY spectrum (Fig. 3.10). The proton signals at downfield region were correlating each other and they belong to furan rings. Another correlation between the signals at δ 8.58, 8.20 and 8.11 ppm confirmed the contribution from *meso*-Ph ring. Additionally, the correlation of signals at δ 8.46 and 8.30 ppm, reflect the resonance from *p*-PhBr group.

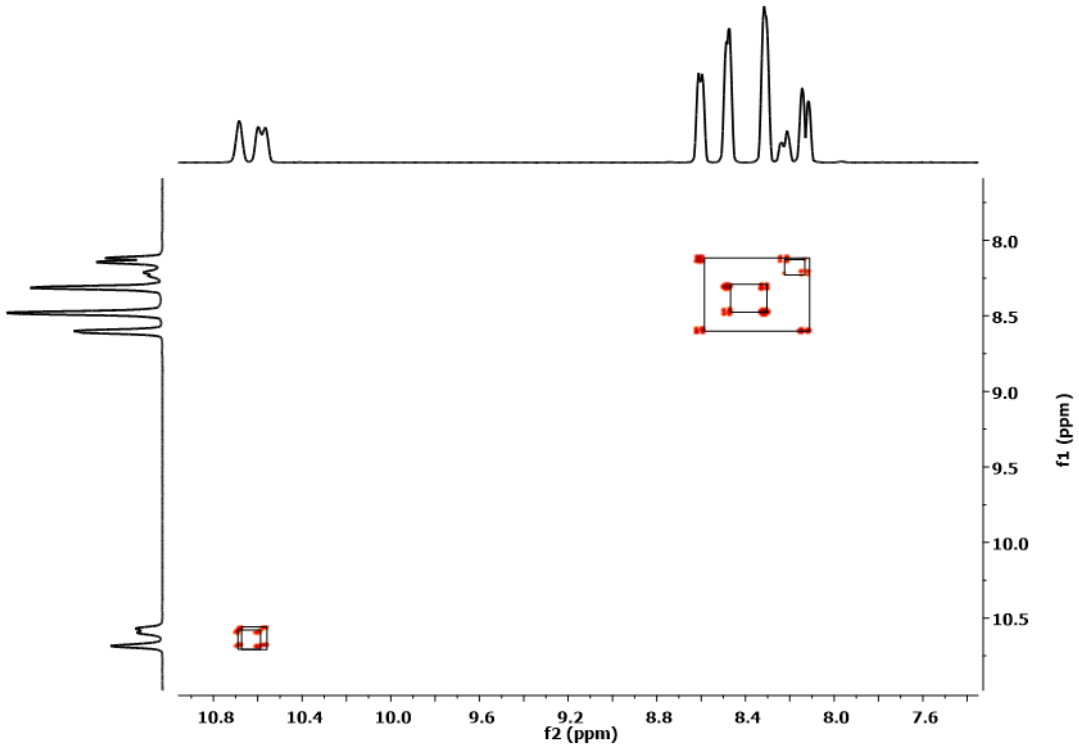

Fig. 3.10: ^{1}H-^{1}H COSY spectrum of **[III.9]$^{2+}$** in acetonitrile-d_3 at 298 K 600 MHz machine.

3.5 Spectro-electrochemical Analysis of III.9

The chemical oxidation of **III.9** was further validated with the spectroelectrochemistry measurements. For the experiment, the calomel electrode was used as reference electrode and Pt wire and Pt mess were used as counter and working electrode respectively. The electrolyte was 0.1M TBAP prepared in dry dichloromethane solvent. The spectra were recorded for 30 mins with 10s interval of time.

As the cyclic voltammetry (Fig. 3.6), suggest the two predominant oxidation peaks, hence on applying the potential of 0.9 V, which near to second oxidation potential in the neutral isophlorin **III.9**. It shows the depletion of the absorption peak at 325 nm and 364 nm and new peaks were emerging at 400 nm along with the peaks at higher wavelength region between 450-750 nm (Fig. 3.11). The newly formed peaks were getting more intense with time and these peaks corroborate with the UV-absorption peaks of **[III.9]**$^{2+}$. This experimental observation confirms the electrochemical conversion of **III.9** to dication **[III.9]**$^{2+}$.

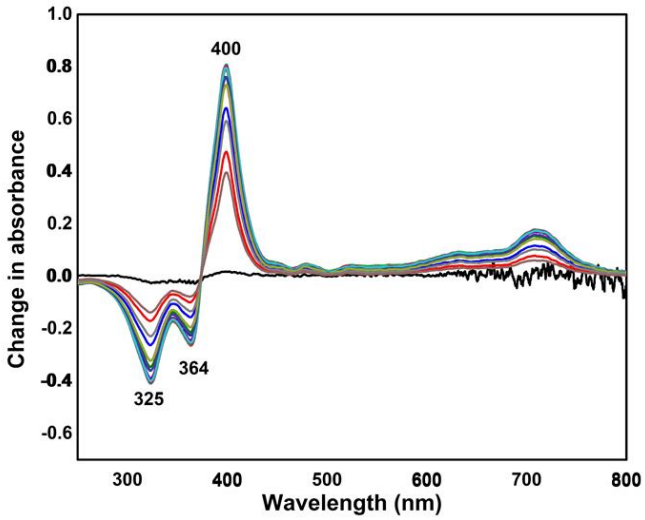

Fig. 3.11: Spectro-electrochemical analysis of Isophlorin **III.9** at applied potential of 0.90 V.

Thus, the 20π core-modified isophlorin **III.9** is redox active macrocycle, it could easily oxidize to its dicationic specie **[III.9]**$^{2+}$. And **[III.9]**$^{2+}$ can be reduced back to free base molecule **III.9**, with addition of electron donating agents such as triethyl amine or Zn dust. As **III.9** consists a functionalized *meso* position (*p*-PhBr), therefore, it could act as synthons for isophlorin-porphyrin dimer through cross-coupling reactions (detail discussion in Chapter 5).

3.6 Characterisation of Macrocycle III.10

The octa-furan **III.10** was characterized with HRMS, UV-vis, X-ray single crystal diffraction, cyclic voltammetry and differential pulse voltammetry experiments.

High-Resolution Mass Spectrum of III.10

The HRMS spectrum (Fig. 3.12) displayed a m/z at 1756.0217 and 878.0128 corresponding to ([M]$^{+}$: 1756.0301 and [M]$^{2+}$: 878.0150, Calcd. for $C_{88}H_{34}Br_2F_{20}O_8$) confirming the formation of desired macrocycle.

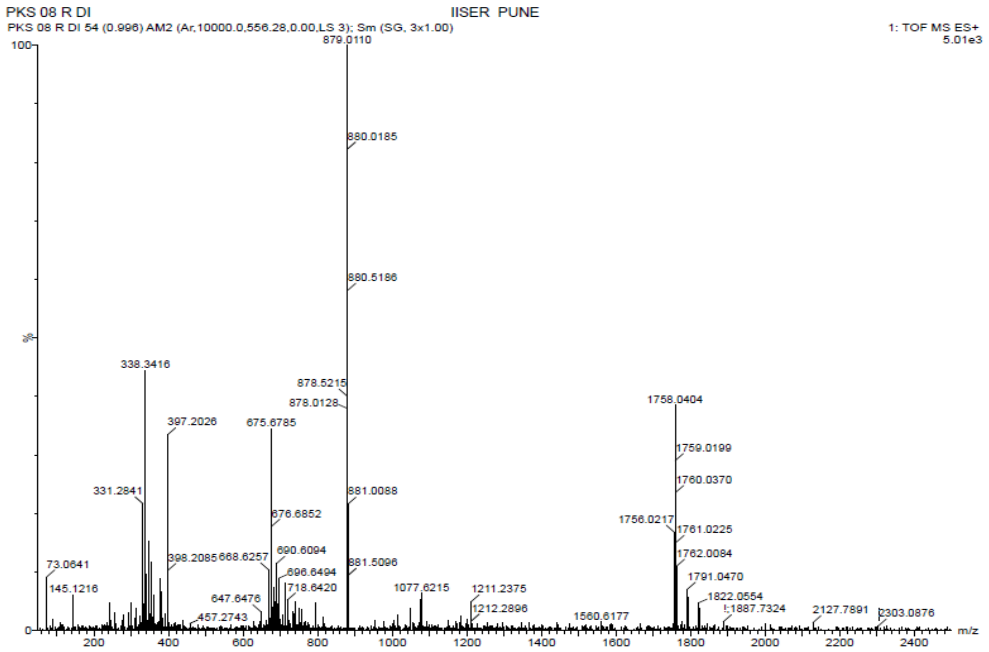

Fig. 3.12: High-resolution mass spectrum of **III.10**.

NMR Analysis of III.10

The macrocycle **III.10**, displayed broad ^{1}H NMR peaks in $CDCl_3$ at 298 K because of its suspected fluxional nature. With decrease in temperature beyond 298 K, the ^{1}H NMR signals started to yield a resolved ^{1}H NMR spectrum (Fig. 3.13).

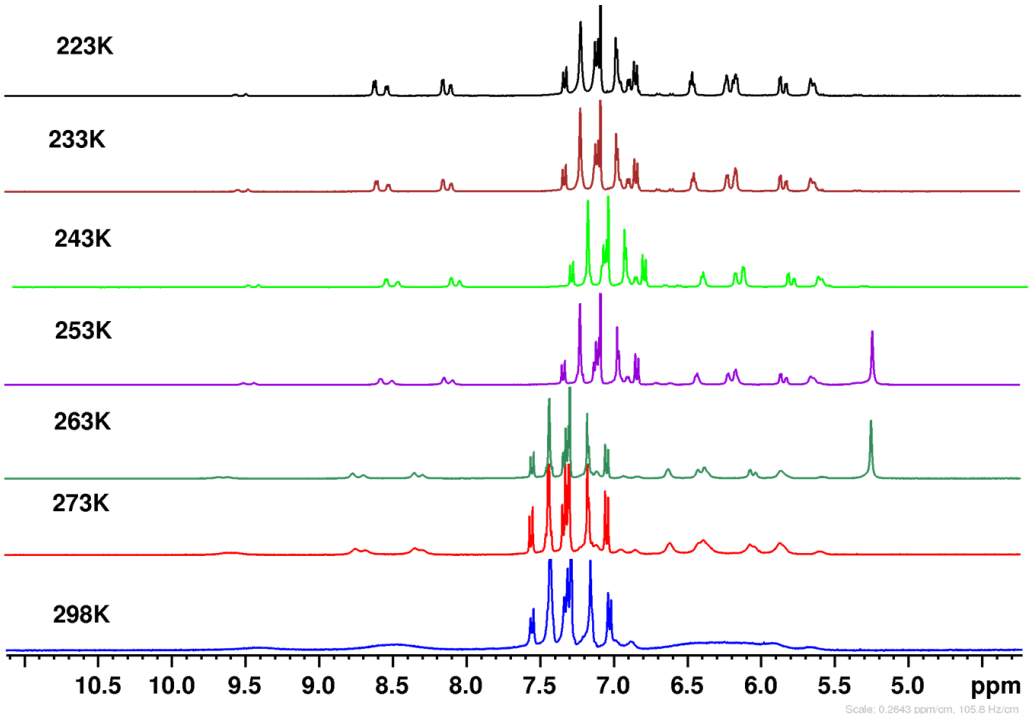

Fig. 3.13 VT ^{1}H NMR spectra of **III.10** in chloroform-*d*.

At 223 K, there are eight resonances appearing at δ 8.80, 8.33, 7.03, 6.63, 6.40, 6.34, 6.04 and 5.833 ppm with the integration of two protons each corresponding to sixteen β protons of the heterocyclic rings (Fig. 3.14). The signals with increased intensity resonating in between 7.15 ppm to 7.51 ppm belongs to *meso* phenyl protons of substituents (phenyl & 4-bromophenyl). The careful observation of ^{1}H NMR spectrum suggested the area under the curve for two protons contains two distinct type of doublet for each integration. Thus, suggesting the possibilities of two molecules being present in different ratio. The ^{1}H- ^{1}H COSY spectrum of the molecule **III.10** confirms the eight cross peaks corresponding to the sixteen protons of the furan rings (Fig. 3.15). To investigate further, the NMR of **III.10** was recorded in dichloromethane-d_2 with varying the temperature of the experiment (Fig. 3.16). The ^{1}H NMR spectra were almost similar with both the solvents chloroform and dichloromethane, but it was well resolved in chloroform-*d* (Fig. 3.17). Hence, the ambiguity regarding the presence of one or more conforms could be solved with single crystal diffraction analysis.

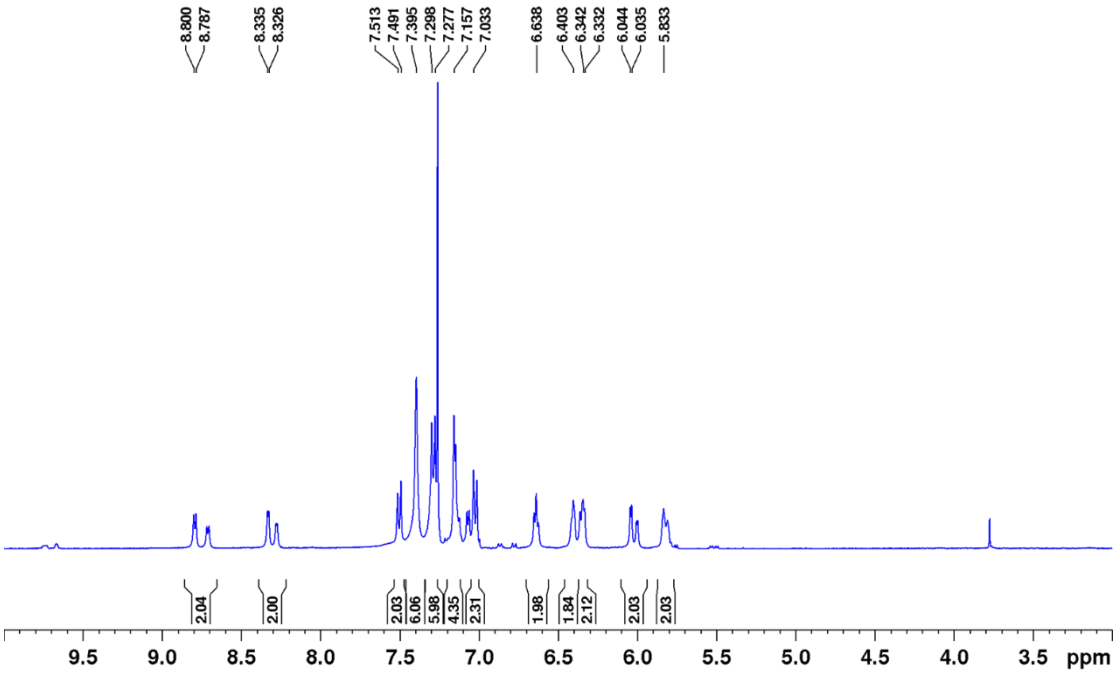

Fig. 3.14 ^{1}H NMR spectrum of **III.10** at 223 K in chloroform-*d*.

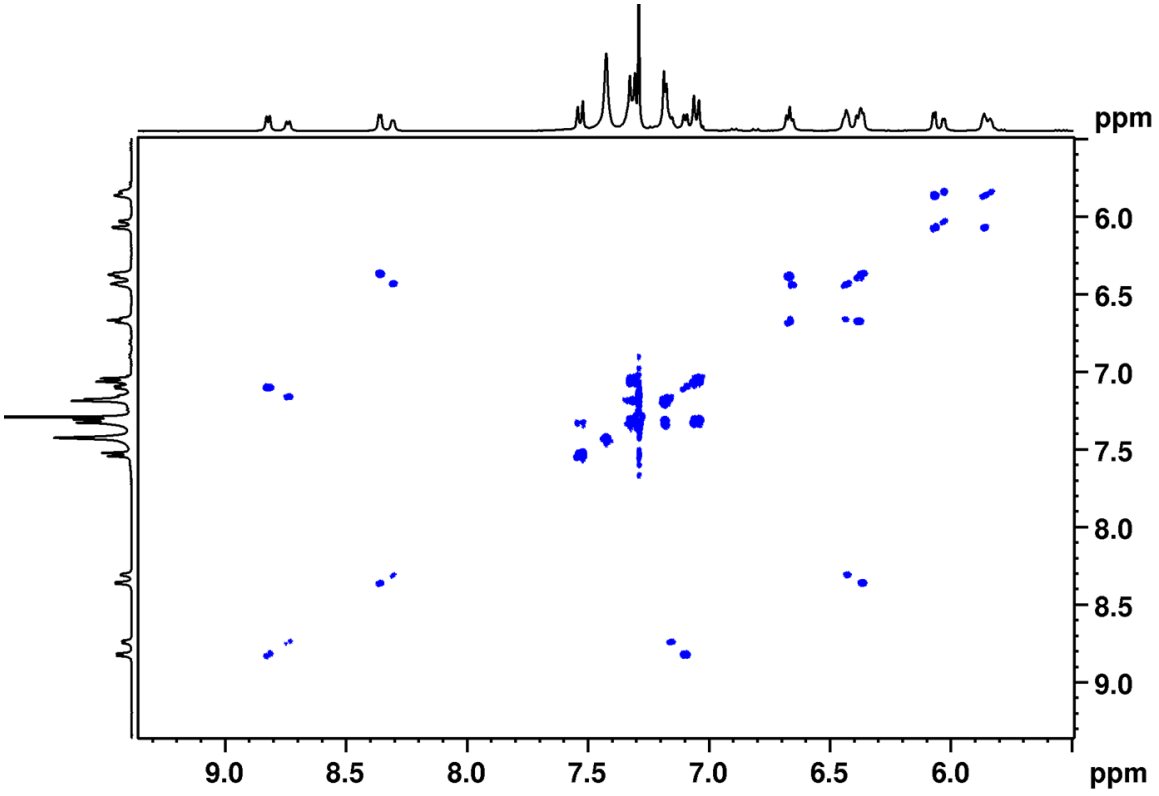

Fig. 3.15: ^{1}H- ^{1}H COSY spectrum of **III.10** in in chloroform-*d* at 223K.

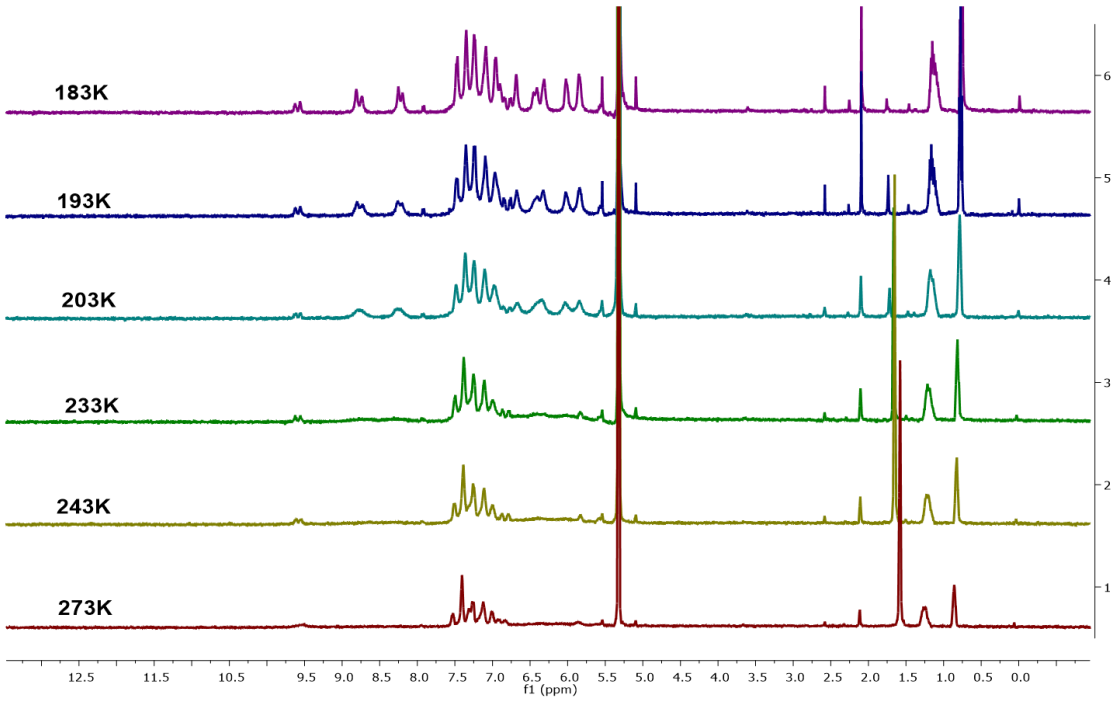

Fig. 3.16: VT ^{1}H NMR spectra of **III.10** in dichloromethane-d_2.

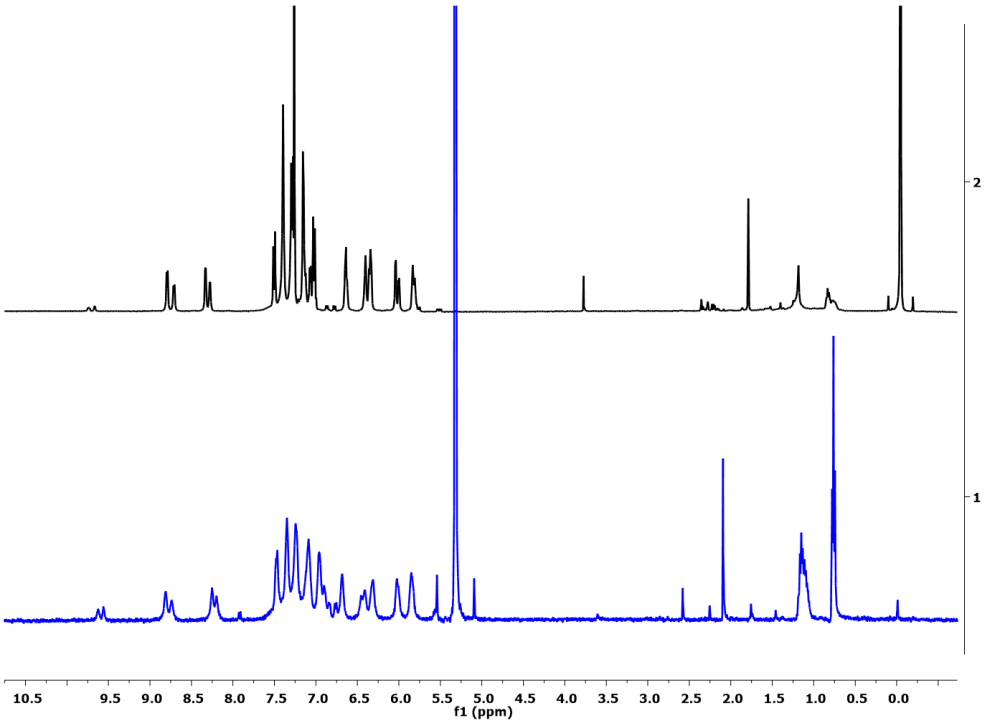

Fig. 3.17: Comparison of ^{1}H NMR spectra of **III.10** in chloroform-d (black spectrum) and dichloromethane-d_2 (blue spectrum) at temperature 223 K and 183 K respectively.

Single Crystal X-ray analysis of III.10

Multiple crystallization attempts were performed to obtain the good quality single crystals. The crystals obtained by solvent diffusion method in chloroform/methanol, revealed a rectangular shape of the molecule with three different *meso*-substituents present at near orthogonal position to the mean macrocyclic plane (Fig. 3.18).

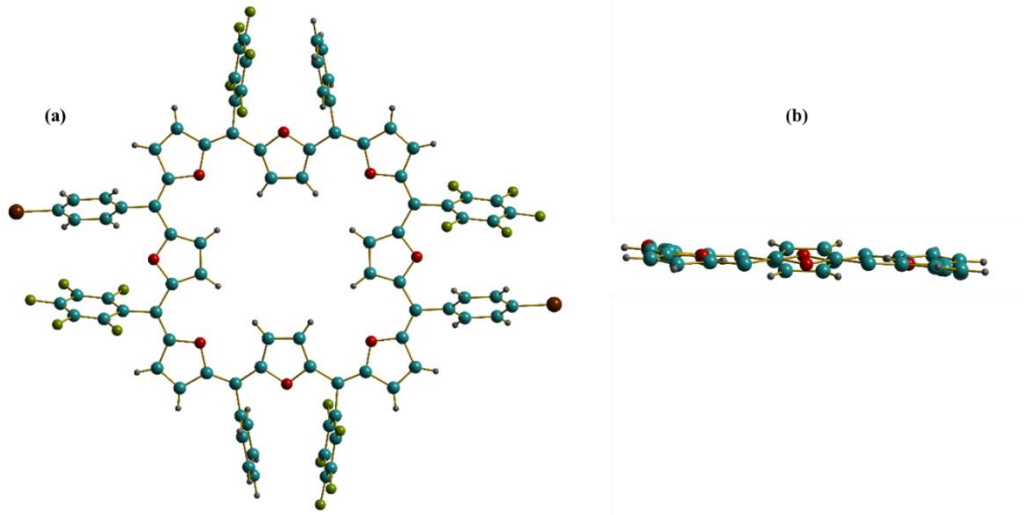

Fig. 3.18: Molecular structure of octaphyrin **III.10(a)** grown in $CHCl_3$/MeOH solvent system (a) top view and (b) side view, all the *meso* substituents are omitted for clarity.

In molecular structure **III.10(a)**, the arrangement of all furans were very similar to the molecular structure of **III.6**. In **III.10(a)** all the furan rings are present in the same plane and macrocycle adopted a perfect planar topology. The alternate furan rings were inverted, hence out of eight heterocyclic rings, the four rings were facing towards the core of macrocyclic. The phenyl ring and pentafluorophenyl rings were tilted toward each other because of C-H---F interaction present between these two rings.

Secondly, to investigate the solvatomorphism in **III.10** the multiple attempts were performed to get the solvatomorph of the molecule using various solvent combination and methods. Unfortunately, we could not get the good quality crystals in aromatic solvent systems. The best quality crystal in dichloromethane/methanol was obtained (Fig. 3.19). Surprisingly, conformation of the molecule **III.10(b)** was entirely different from the previous planar topology (Fig. 3.18). It had adopted a tub like shape, where two sub-porphyrins moieties were bridged through a furan dipyyromethane. Hence, **III.10(b)** adopted a nonplanar arrangement and it reflected the nonaromatic character. It was identified that macrocycle **III.10**, can adopt two different spatial arrangement in solid state with respect to the solvent of crystallization. Thus **III.10(b)** and **III.10(b)** are considered as solvatomorphs.

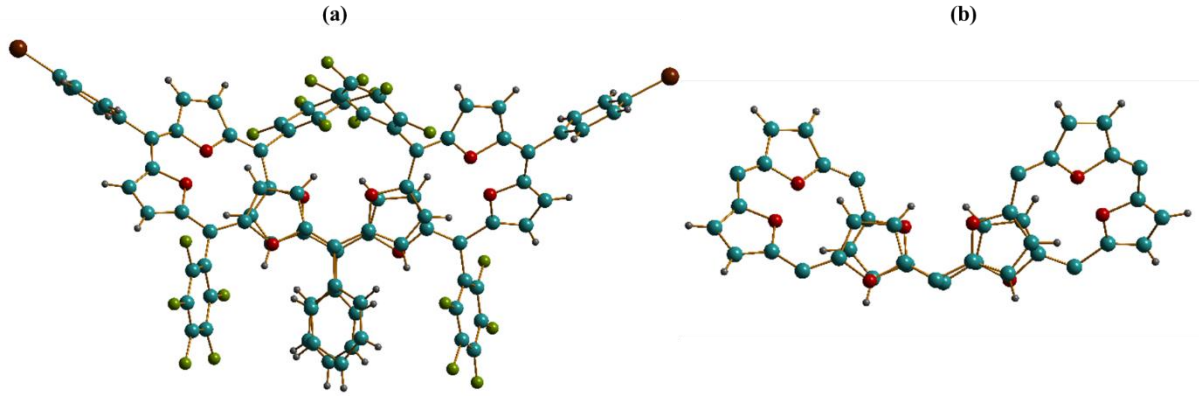

Fig. 3.19: Molecular structure of hexaphyrin **III.10** grown in CH_2Cl_2/MeOH solvent system (a) top view and (b) Side view, all the *meso* substituents are omitted for clarity.

UV-Vis Absorption spectrum of III.10

To study the electronic absorption features of the octafuran **III.10**, the spectrum was separately recorded in chloroform and dichloromethane solvent, both the spectrum revealed the similar absorption band features. It displayed an intense peak at 544 nm (Fig. 3.20). Therefore, it suggested the similar feature of **III.10** in solution state irrespective of solvent and this result

corroborate with the ^{1}H NMR spectrum study (unaffected with NMR solvents: chloroform and dichloromethane) (Fig. 3.17).

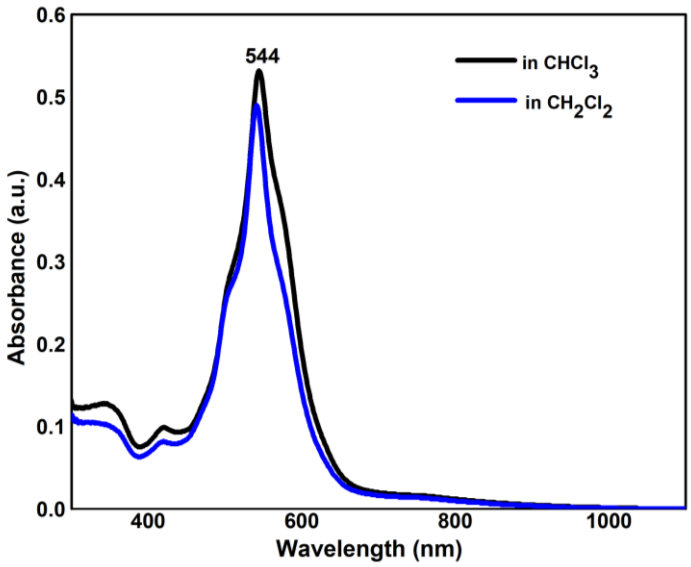

Fig 3.20: Electronic absorption Spectra of **III.10** in dichloromethane (blue colour) and chloroform (black color).

Cyclic Voltammetry Experiment of III.10

The cyclic voltammetry experiments revealed one broad reduction peak and one broad oxidation peak at -1.28 V and 0.68 V respectively (Fig. 3.21). Hence to study the redox behavior macrocycle **III.10** was subjected to chemical oxidation.

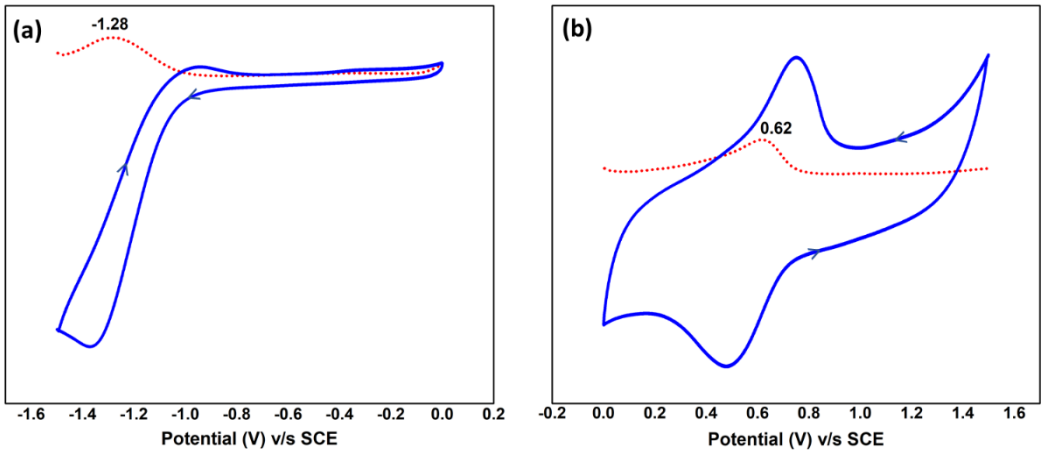

Fig. 3.21: Cyclic voltammetry (blue line) and Differential pulse voltammetry (red dotted line) of **III.10** in dichloromethane containing 0.1M tetrabutylammonium perchlorate (TBAP) as the supporting electrolyte recorded at 100 mVs^{-1}. (a) Reduction potentials (b) Oxidation potential.

3.7 Chemical Oxidation of III.10

Macrocyle **III.10** was chemically oxidized with excess of Meerwein salt[12] $[Et_3O]^+[SbCl_6]^-$ in dichloromethane (Scheme 3.4). A subtle color change from dark pink to green indicated the conversion of **III.10** to **[III.10]**$^{2+}$. Also, the absorptions peaks were red shifted from 541nm for **III.10** to 733 nm for **[III.10]**$^{2+}$, along with shoulder peak at 768 nm and a weak intense peak at 435 nm (Fig. 3.22).

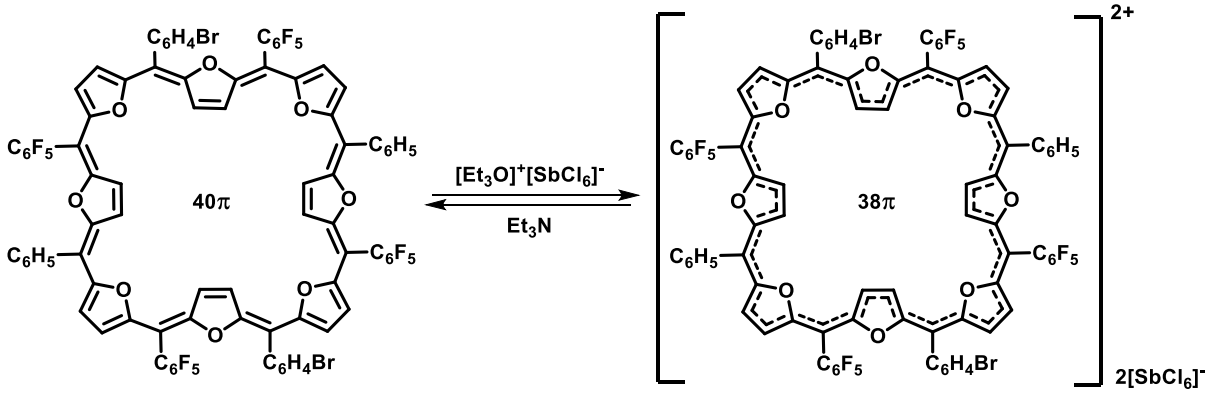

Scheme. 3.4: Chemical oxidation of **III.10** to **[III.10]**$^{2+}$ using Meerwein salt.

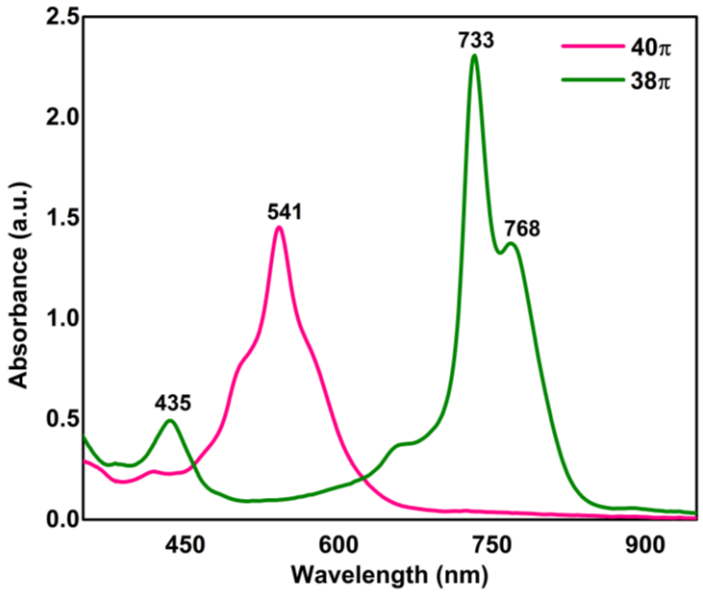

Fig. 3.22: UV absorption spectrum of **III.10** (pink color) to **[III.10]**$^{2+}$ (green color).

3.8 Characterization of dication [III.10]$^{2+}$

The macrocycle **[III.10]**$^{2+}$ was characterized with mass spectrum, UV-vis absorption spectrum and spectro-electrochemical measurements.

HRMS Spectrum of $[III.10]^{2+}$

The HRMS spectrum (Fig. 3.23) displayed am/z value of 878.0177 corresponding to ($[M]^{2+}$: 878.0150 Calcd. for $C_{88}H_{34}Br_2F_{20}O_8$) confirming the formation of desired dication **$[III.10]^{2+}$**.

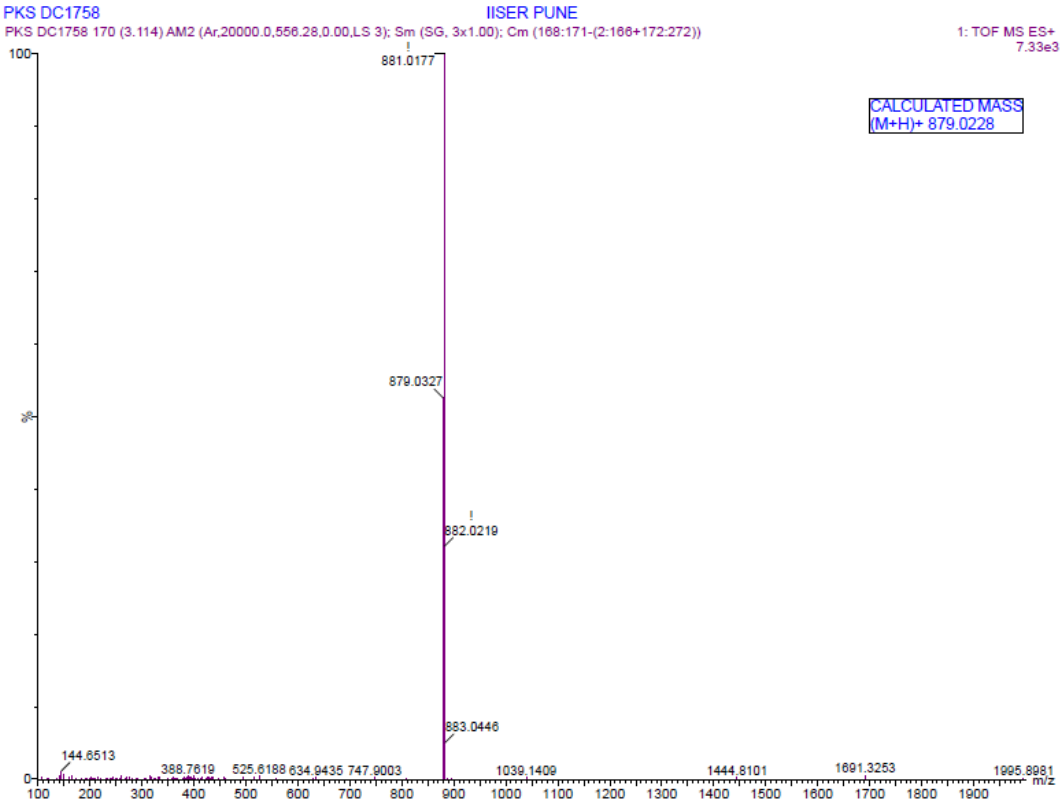

Fig. 3.23: High resolution mass spectrum of **$[III.10]^{2+}$**.

3.9 Spectro-electrochemical Analysis of III.10

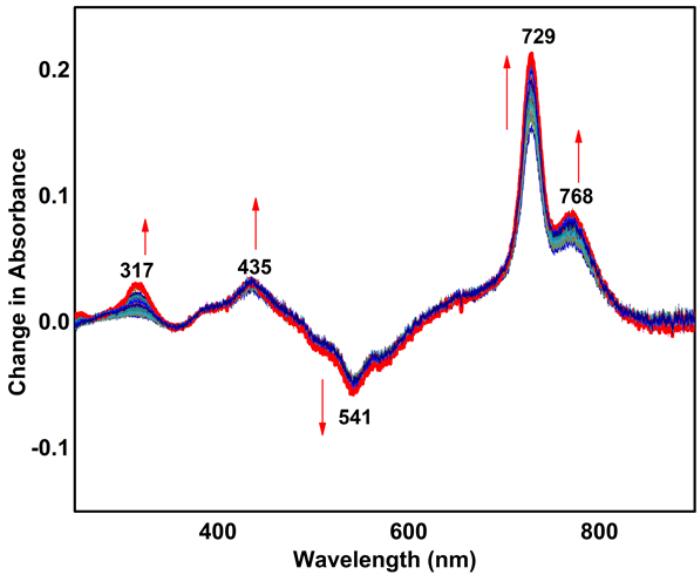

Fig 3.24: Spectroelectrochemical spectra of **III.10** at applied potential of 0.9 V.

Spectro-electrochemical study was performed for molecule **III.10**, at an applied potential of 0.9 V. It shows the decrement in the peak at 541 nm, whereas, the new absorption peaks appears in the region 729 nm and 768 nm along with the peak at 435 nm (Fig. 3.24). The newly formed peaks corroborate with absorption spectrum of **[III.10]**$^{2+}$ (Fig. 3.22). With increase in time, the significant changes in absorption peak intensity was not observed. Hence this was considered as the final oxidized state of molecule **III.10**.

3.10 Quantum Chemical Calculations

The initial state geometries were obtained by energy optimisation of molecular structure obtained from single crystal X-ray diffraction. The DFT calculations were performed using b3lyp/6-31G(d,p) basis set in Guassian 09 software using High performance supercomputer cluster 'Parambrahma' facility of IISER Pune.

Nuclear Independent Chemical Shift (NICS)

This magnetic criterion elucidates the shielding and de-shielding effect in the macrocycle. If the computed NICS value comes to negative the macrocycle hold the aromatic character, if the obtained value is positive then macrocycle considered as the antiaromatic in nature. If the value is near to 1 or 0, then macrocycle is classified as nonaromatic character. The computed NICS value for **III.10a** is +8.37 ppm hence it is antiaromatic in nature, whereas the +1.18 ppm value supports the nonaromatic nature of **III.10b** (Table 3.1).

Macrocycle	NICS (0) ppm	Character
III.10a	+ 8.37	Antiaromatic
III.10b	+1.18	nonaromatic

Table 3.1: Computated NICS values of the macrocycles

3.11 Conclusion

The 20π tetra-furan **III.9** and 40π octa-furan **III.10** isophlorinoids were synthesized and characterized with appropriate spectroscopic techniques and by X-ray diffraction. These isophlorinoids incorporate three different *meso* substituents like pentafluorophenyl, phenyl and 4-bromophenyl. These are air and moisture stable macrocycles and they have credential to

show the reversible redox properties and its redox behavior of these were very well studied by cyclic voltammetry and spectro-electrochemical measurements.

These *meso*-(4-bromophenyl) substituted isophlorinoid could be better synthons for the isophlorin-porphyrin dimer, where the C-Br can couple with other coupling partner through the metal catalyzed coupling reactions. Secondly, the octa-furan macrocycle shows the fascinating properties of solvatomorphism in chloroform and dichloromethane. It represents the extended possibility of giant isophlorinoids to display the polymorphism/pseudo-polymorphism.

3.12 Experimental Section

Synthesis of Characterization of III.9 and III.10

In round bottom 250 mL two neck flask, a mixture of bisfuran-2-ylmethane **III.7** (300 mg, 0.98 mmol) and difuro methanedicarbinol **III.8** (640.50 mg, 1.04 mmol) was added in 100mL of dried dichloromethane under nitrogen atmosphere. To this degassed solution $BF_3.OEt_2$ (122.13 mmL, 0.98 mmol) was added under dark, and resulting solution was stirred for 2 hours under nitrogen atmosphere. Then solution was opened to air and DDQ (561.59 mg, 2.47mmol) was added and stirred for additional 2 hours. The reaction was quenched with 2-3 drops of triethylamine, then reaction mixture was concentrated under reduced pressure. The MALDI-TOF/TOF mass spectrum confirms the formation of macrocycles **III.9** and **III.10**. The purification of compound was done with column chromatography in basic alumina using 15% CH_2Cl_2/hexane and followed by size exclusion column chromatography in toluene. The desired macrocycles**, III.10** was isolated in 10% yields as pink colored band and **III.9** was isolated as green color band in 7 % yields.

III.9: The high-resolution mass spectrum shows the value of m/z of 878.0150 calculated for $C_{44}H_{17}BrF_{10}O_4$ $[M]^+$ 878.0151. UV-Vis absorption spectrum (CH_2Cl_2), λ_{max} nm (ε, $M^{-1}cm^{-1}$) 325 nm, 364 nm, 437 nm, 467 nm and 501 nm. ^1H NMR: (400 MHz, $CDCl_3$, 298 K) δ 6.73 (d, J= 8.4 Hz, 2H), 6.60 (m, 3H), 6.04 (dd, J= 1.2 Hz, 6.4 Hz, 2H), 5.71 (d, J = 8.4 Hz, 2H), 2.57 (J = 4.8 Hz, 2H), 2.46 (J = 4.8 Hz, 2H), 2.26 (J = 4.8 Hz, 2H), 2.21 (J = 4.8 Hz, 2H).

III.10: HR-MS (ESI-TOF): The observed mass m/z of 1756.0217, and calculated for $C_{88}H_{34}Br_2F_{20}O_8$ $[M]^+$ 1756.0301. UV-Vis absorption (CH_2Cl_2): (conc = 10^{-6}), λ_{max} nm (ε, M^{-}

$^{1}cm^{-1}$) = 419 (31300), 506 (101800), 541 (187100). NMR Data: ^{1}H NMR: (400 MHz, $CDCl_3$, 223 K) δ 8.78-8.80 (dd, 2H), 8.32-8.33 (dd, 2H), 7.49-7.51 (dd, 2H), 6.06 (m, 6H), 7.29 (m, 6H), 7.15 (m, 4H), 7.03 (dd, 2H), 6.63 (dd, 2H), 6.40 (m, 2H), 6.33 (m,2H), 6.03-6.04 (dd, 2H), 5.83 (m,2H). Crystal data **III.10a:** $C_{88}H_{34}F_{20}Br_2O_8$, Monoclinic, space group P21/n , a = 14.32 (4) b = 9.13 (2), c = 28.93 (8) Å, α = 90, β = 103.64 (5), γ = 90, V = 3676 (17) $Å^3$, Z = 2, T = 273 K , Dcalcd = 1.589 g cm^{-3}, R1 = 0.0941 (3239), *R*w (all data) = 0.3020 (7663) GOF = 1.032. Crystal data **III.10b**: $C_{88}H_{34}F_{20}Br_2O_8$ (CH_2Cl_2) Monoclinic, space group P21/n , a = 15.086 (2) b = 15.967 (2), c = 20.247 (3) Å, α = 90, β = 98.958 (5), γ = 90, V = 4817.6 (11) $Å^3$, Z = 2, T = 273 K , Dcalcd = 1.271 g cm^{-3}, R1 = 0.0744 (15695), *R*w (all data) = 0.2140 (24000) GOF = 1.040.

Synthesis of $[III.9]^{2+}$

In 10 ml round bottom flask the 5 mg of **III.9** was dissolved in 5 mL of dry and distilled dichloromethane. Then stoichiometric excess of Meerwein salt, $[Et_3O]^+[SbCl_6]^-$ was added to the solution at -20 ºC. The immediate color of the solution changes from lighter green color to dark green. The reaction was stirred at same temperature additional for 20 mins and then slowly allow it to come in room temperature. Then reaction mixture was filtered and concentrated under vacuum and further washed multiple times with pentane and hexane. The desired dication was obtained in the quantity yield and recrystallized product was in 96% yields.

HRMS: The observed mass m/z 439.0057 for calculated $[M]^{2+}$ 439.0075 of $[C_{44}H_{17}BrF_{10}O_4]^{2+}$. UV-Vis absorption ($CH_2Cl_2$): (conc = 10^{-6}), λ_{max} nm (ε, $M^{-1}cm^{-1}$) 403 nm, 567 nm, 618 nm and 767 nm. NMR Data: ^{1}H NMR: (acetonitrile-d_3 at 298 K in 600 MHz) δ 10.65 (br, s, 4H), 10.57 (br, s, 2H), 10.53 (br, s, 2H), 8.58 (d, J = 4.8 Hz, 2H), 8.46 (d, J = 5.6 Hz, 2H), 8.30 (d, J = 5.6 Hz, 2H), 8.20 (m, 1H), 8.11(m, 2H).

Reference

1. L. Yu, S. M. Reutzel, G. A. Stephenson, *Pharm. Sci. Technol. Today* **1998,** *1*, 118-127.
2. Polymorphism in Pharmaceutical Solids; Brittain, H. G., Ed.; Marcel Dekker Inc.: New York, **1999**.
3. C. A. Mitchell, L. Yu, and M. D. Ward, *J. Am. Chem. Soc*., **2001**, *123*, 10830-10839.
4. E. Simone, G. Steele and Z. K. Nagy, *Cryst. Eng. Comm*., **2015**, *17*, 9370-9379.
5. A. Nangia, *Crystal Growth & Design,* **2006**, 6, *1*, 2-4.
6. G. R. Desiraju, *Cryst. Growth Des.*, **2004**, *4*, 1089.

7. D. Chopra and T. N. Guru Row, *Crystal Growth & Design*, **2006**, *6*, 1267-1270.

8. (a) N. Shivran, S. C. Gadekar and V. G. Anand, *Chem. Asian J.*, **2016**, *12*, 6-20. (b) H. S. Udaya, A. K. Basavarajappa, T. Y. Gopalakrishna and V. G. Anand, *Chem. Commun.*, **2022**, *58*, 13931-13934. (c) J. Sankar, S. Mori, S. Saito, H. Rath, M. Suzuki, Y. Inokuma, H. Shinokubo, K. S. Kim, Z. S. Yoon, J. Y. Shin, J. M. Lim, Y. Matsuzaki, O. Matsushita, A. Muranaka, N. Kobayashi, D. Kim, and A. Osuka, *J. Am. Chem. Soc.*, **2008**, *130*, 13568-13579.

9. (a) T. Y. Gopalakrishna, V. G. Anand, *Angew. Chem. Int. Ed*., **2014**, *53*, 6678-6682. (b) S. P. Panchal, S. C. Gadekar, V. G. Anand, *Angew. Chem. Int. Ed.*, **2016**, *55*, 7797-7800. (c) M. D. Ambhore, A. K. Basavarajappa, V. G. Anand, *Chem. Commun.*, **2019**, *55*, 6763-6766. (d) P. Shukla, M. D. Ambhore, V. G. Anand *Chem. Eur. J.* **2023**, e202203327.

10. J. S. Reddy, S. Mandal, and V. G. Anand, *Org. Lett.*, **2006**, *8*, 5541-5543.

11. J. S. Reddy and V. G. Anand, *J. Am. Chem. Soc*., **2008**, *130*, 3718-3719.

12. R. Rathore, A. S. Kumar, S. V. Lindeman, J. K. Kochi, *J. Org. Chem.*, **1998**, *63*, 5847-6682.

CHAPTER 4

Open Shell (4n+2)π and Closed Shell 4nπ Planar Core-Modified Decaphyrins

4.1 Introduction

Giant porphyrinoids[1] display excellent photo-physical properties and absorb in far-red region of the visible spectrum.[2] The higher analog of porphyrin decaphyrins, contains ten heterocycles with varying number of the π electron along the conjugated pathway of the molecule. By varying the number of *meso*-positions in the ring the decaphyrins can sustain 38π-50π electrons in the ring.[3, 4, 5, 6] Sessler and co-workers reported the first decaphyrin[4] as tetracationic, deca-pyrrole, **IV.1**, containing 40π electrons and named as Turcasarin (reflect different colors in different solvents). It was **IV.1** devoid of any ring current and hence it was nonaromatic in nature.

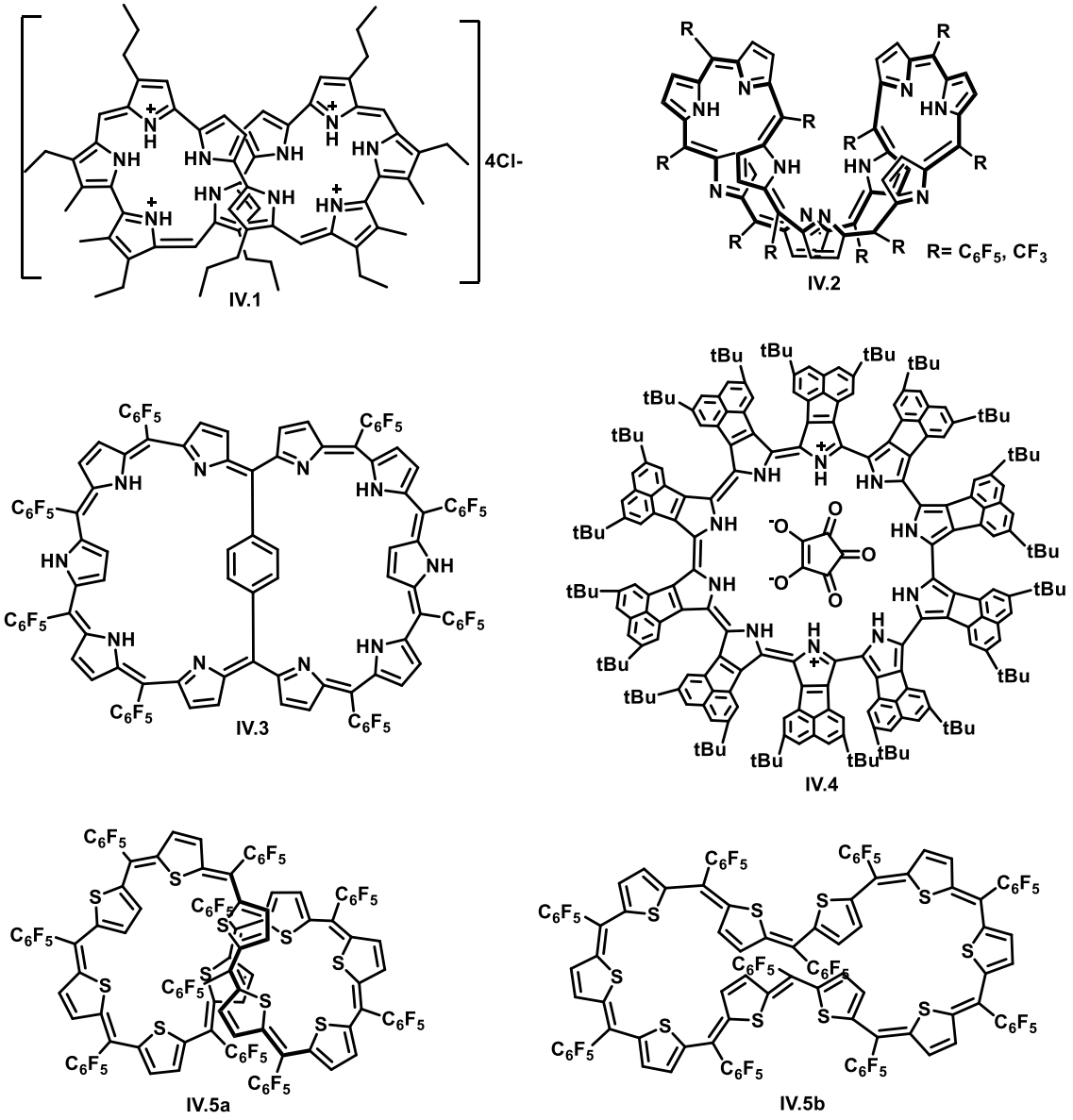

Fig. 4.1 Structures of decaphyrins.

In 2006 and 2008 Osuka and co-workers reported the decaphyrin **IV.2,** which contains ten pyrrole connected through ten *meso* carbons. Both the decaphyrins adoptes figure-of-eight configuration irrespective of the *meso* substituents CF_3 and C_6F_5.[5a, 5b] Because of highly fluxional nature these larger porphyrinoids attain the non-planar structure.[7] Few modifications in these porphyrinoids can lead to nonplanar macrocycles. The planarity in these decaphyrins was achieved by either with some bridging units[8a, 8b] **IV.3** or with an anion based template[3] **IV.4**. Due to lack of synthetic strategy, completely planar decaphyrin is not known till date.

Recently, Anand and co-workers reported a thiophene based decaphyrin, which adopted two different structures **IV.5a** and **IV.5b** based on solvent of crystallization.[9] In benzene, decaphyrin obtained a near planar topology **IV.5b**. It suggests, in non-pyrrolic decaphyrins the electronic and structure properties varies drastically[10] and hence they can adapt the planar structure. Similarly, 38π thiophene based octaphyrin **IV.6** reported by Jishan Wu adopted the rectangular structure where all the thiophene were lying in same plane. Due to aromatic stabilization **IV.6** displayed a significant diradical character.[11] The series of octaphyrins **IV.7**, **IV.8** with combination of multiple heteroatoms stabilised the reverse relationship between the diradical character and aromaticity.[12] Hence expanded porphyrinoids appear to be the best platform to stabilized the radicaloid species.

A literature survey of diradical reveals, the diradicals nature of the molecule increases with increase in the length of conjugation due to enhanced stabilization energy for e.g., linear oligothiophene, bisphenalenyls, etc.[13] Therefore, increasing the length of conjugation (adding thiophene units) in **IV.6** results in an increase in the diradical nature. Hence, using a synthetic protocol starting from small thiophene oligomers, several core-modified decaphyrins 44π and 46π could be synthesized with reduced number of bridging carbons.

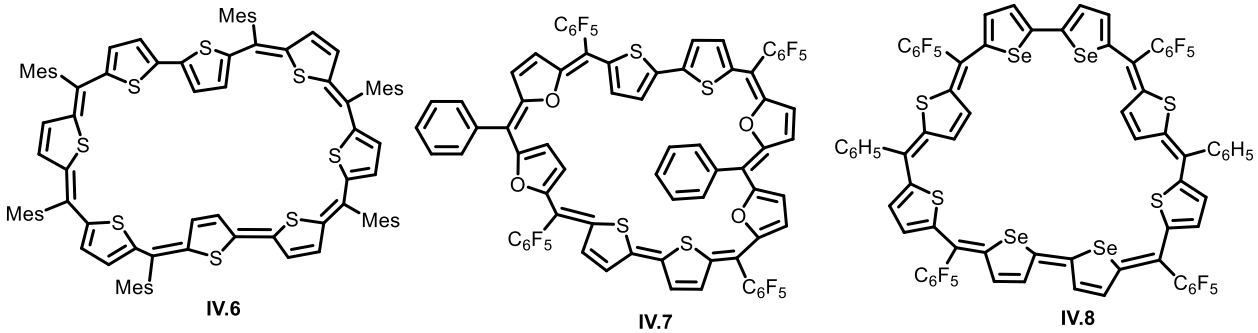

Fig. 4.2 Structures of octaphyrins with varying heteroatoms **IV.6, IV.7** and **IV.8**.

4.2 Synthesis of Decaphyrins

An attempt to synthesize decaphyrin was made by condensation of terthiophene diol, **IV.9**, and bithiophene, **IV.10**, in presence of boron trifluoride etherate and followed by oxidation with 2,3-Dichloro-5,6-dicyano-1,4-benzoquinone (DDQ). The MALDI-TOF/TOF mass spectrum confirmed the formation of desired molecule. After successful synthesis of **IV.13**, the selenophene and furan derivatives of decaphyrins **IV.14** and **IV.15** were also synthesised by the same reaction protocol using biselenophene **IV.11** and bifuran **IV.12** precursors (Scheme 4.1). After multiple column chromatography and size exclusion chromatography these decaphyrins were isolated in (7.2, 4.5 and 3.1%) yield respectively.

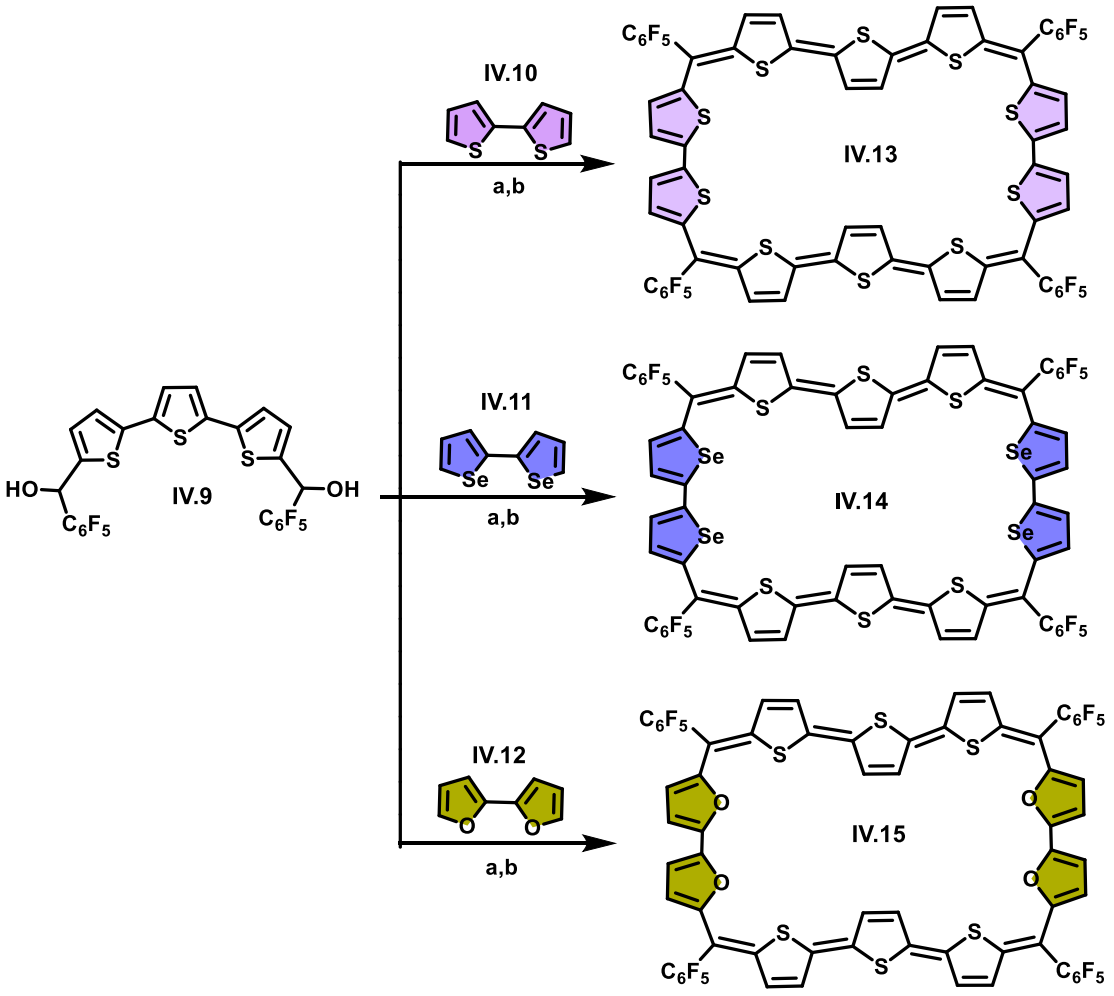

Scheme. 4.1 Synthesis of decaphyrins **IV.13**, **IV.14** and **IV.15**. (a) $BF_3.OEt_2$, dark, N_2 atmosphere 2h. (b) DDQ open air condition 2h.

4.3 Isolation and Characterization of Decaphyrin IV.13

Decaphyrin **IV.13** was synthesized by the reaction protocol described in (scheme.4.1). Preliminary analysis by the MALDI-TOF/TOF spectrometry suggested the formation of desired macrocycle **IV.13.** A green color shiny solid compound was isolated from column chromatography. Further, the molecule was characterised by HRMS, NMR spectroscopy, X-ray single crystal structure, cyclic voltammetry, spectroelectrochemistry and quantum chemical calculations.

HRMS Spectrum of IV.13

The HRMS displayed m/z of 1535.8490 (Calcd. for $C_{68}H_{20}F_{20}S_{10}$; $[M]^+$ 1535.8453) confirming the exact composition of macrocycle. **IV.13** (Fig. 4.3).

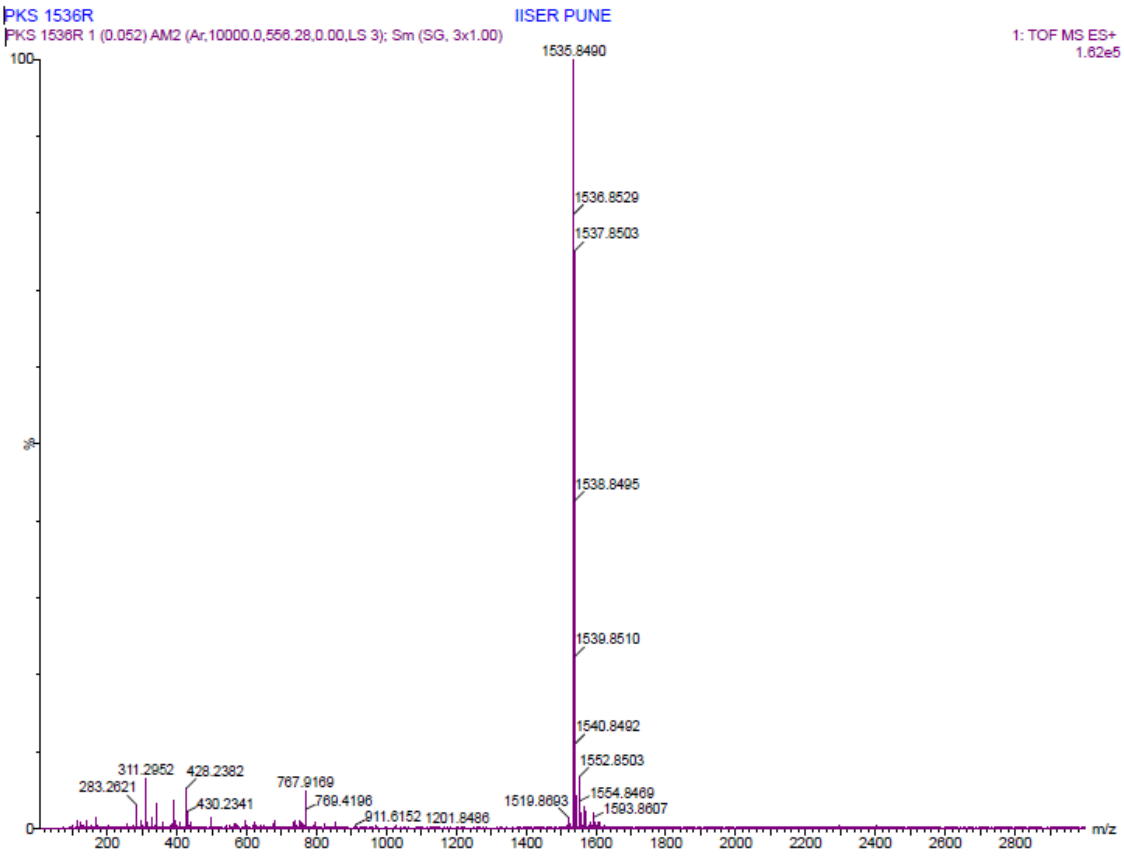

Fig. 4.3: High resolution mass spectrum (ESI-TOF) of **IV.13**.

UV-vis absorption spectrum of IV.13

The thiophene containing 44π decaphyrin **IV.13** showed an intense absorption at 602 nm (185000) and 507 nm (136500) along with a weak band at 559 nm (80500) in dry and distilled

dichloromethane solvent (Fig. 4.31 a). The absorption bands at higher wavelength implied the extended conjugation in the macrocycle.

NMR spectrum of IV.13

The spectrum of the molecule was recorded in deuterated chloroform at 298 K. The ^{1}H NMR spectrum reveals five signals including, a sharp singlet at δ 8.69 ppm and four doublets at δ 6.58, 6.55, 6.09 and 5.87 ppm corresponding to two protons each (Fig. 4.4). The reduced number of peaks represent the symmetrical nature of **IV.13** in solution state. As the 44π electrons flows in the ring therefore, according to Huckel's rule it should display the paratropicity. The outer protons are resonating at upfield region whereas one singlet at δ 8.69 ppm eqvivalent to four protons suggested the inversion of two thiophene rings. The small difference between the signals of most shielded and deshielded proton supports the weak paramagnetic ring current in **IV.13.** The 2D NMR spectrum revealed the coupling between the adjacent protons of the heterocycle. The ^{1}H-^{1}H COSY spectrum (Fig. 4.5) displayed two cross peaks between the proton which resonated at δ (6.58, 6.09 and 6.55, 5.87) ppm.

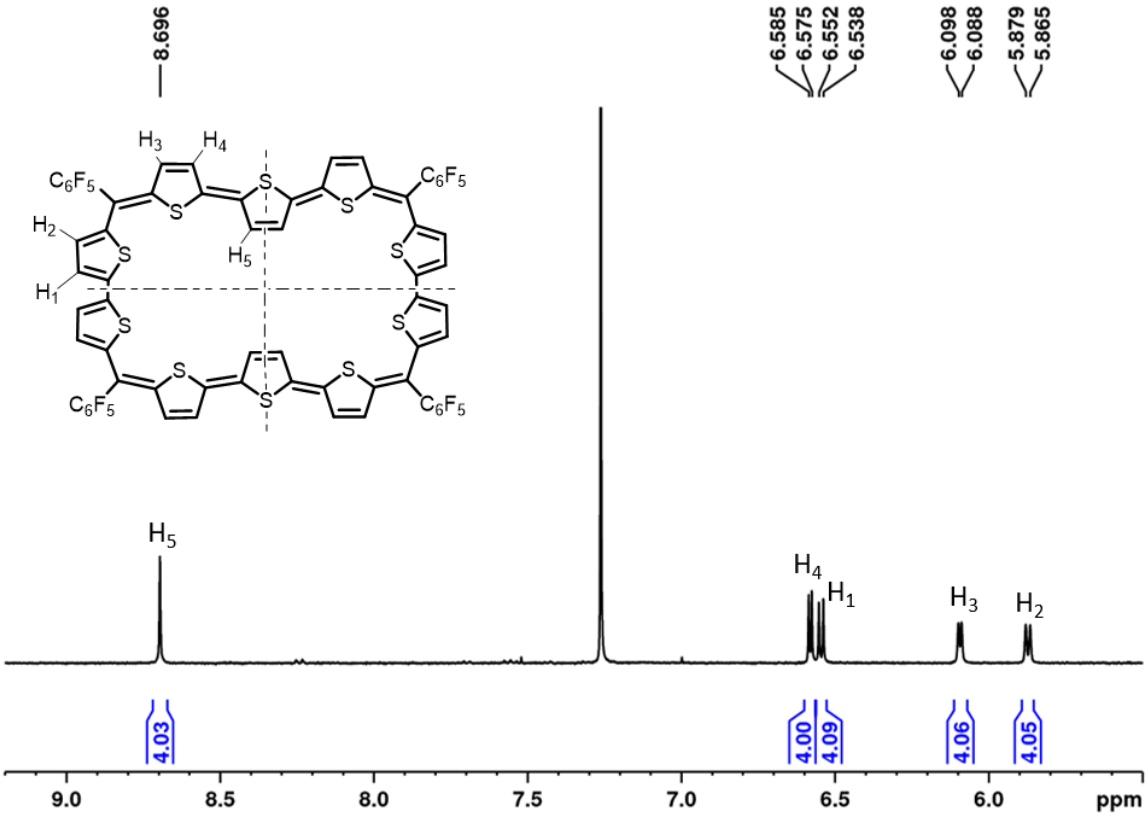

Fig. 4.4: ^{1}H NMR of **IV.13**.in $CDCl_3$ at 298 K.

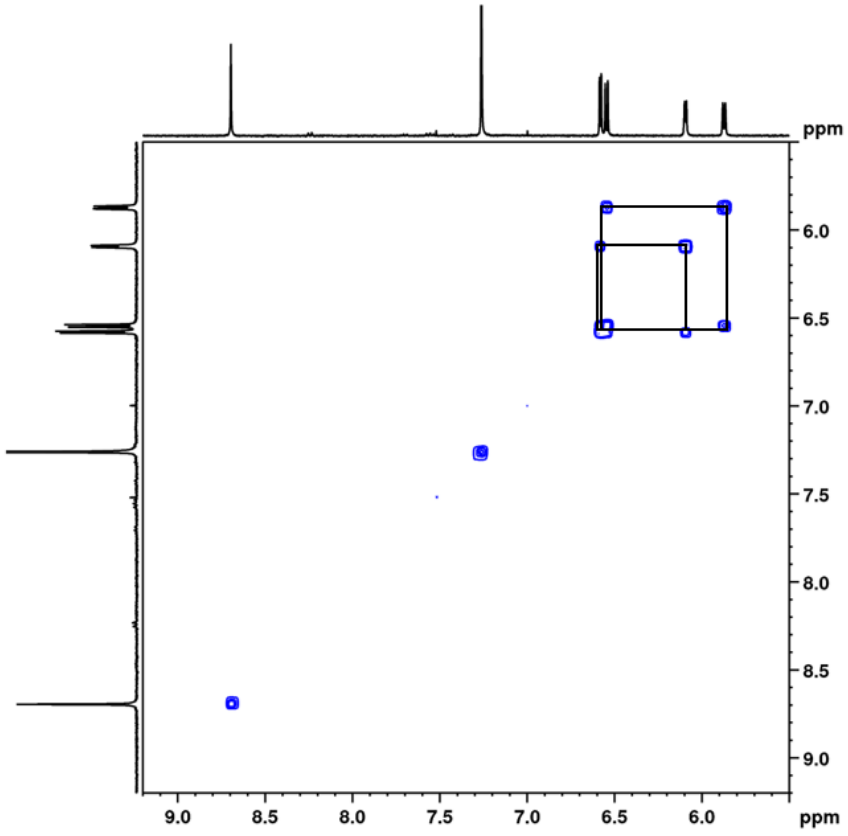

Fig. 4.5: ^{1}H-^{1}H COSY spectrum of **IV.13** in $CDCl_3$ at 298K.

Molecular Structure of IV.13

Good quality single crystals were grown by vapor diffusion of hexane into the solution of **IV.13** in chloroform. X-ray diffraction analysis revealed a rectangular structure of **IV.13**, with all the ten thiophene rings are in the same plane. (Fig. 4.6). The four *meso*-pentafluorophenyl rings were oriented almost perpendicular to the mean macrocyclic plane. Further, the molecular structure of **IV.13** was in agreement with the NMR finding. The central thiophene rings of terthiophene moieties were inverted and give rise to signal at δ 8.69 ppm. Remaining eight thiophenes were facing the core of macrocycle and hence the reflecting the signal at upfield region in the NMR as four well resolved doublets. The side view of the macrocyclic shows the planar nature of the ring.

Therefore, **IV.13** with 44π electron and planar molecular structure confirms to Huckel anti-aromatic nature of the molecule. This represents the first example of an expanded porphyrinoids (decaphyrin) which has adopted the planar topology instead of usual figure-of-eight topology.

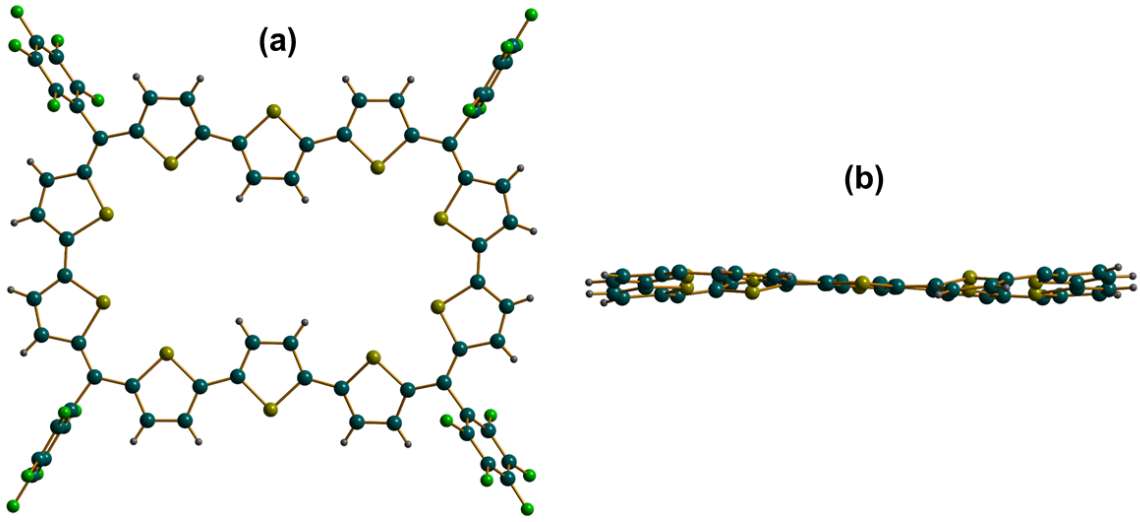

Fig. 4.6: Molecular structure of **IV.13** top view **(a)**, side view **(b)**, all the *meso* substitution were omitted for clarity.

4.4 Quantum Chemical Calculation of IV.13

Experimental results were further supported with the computational calculations. All the DFT calculations were performed in Gaussian 09 using the 6-31G(d,p) basis set. The X-ray molecular structure was taken as initial structure to get the geometry optimised structure. The Nuclear Independent Chemical Shift (NICS) was calculated at centre of the ring and 1 A° above and below the mean macrocyclic plane (Fig. 4.7).

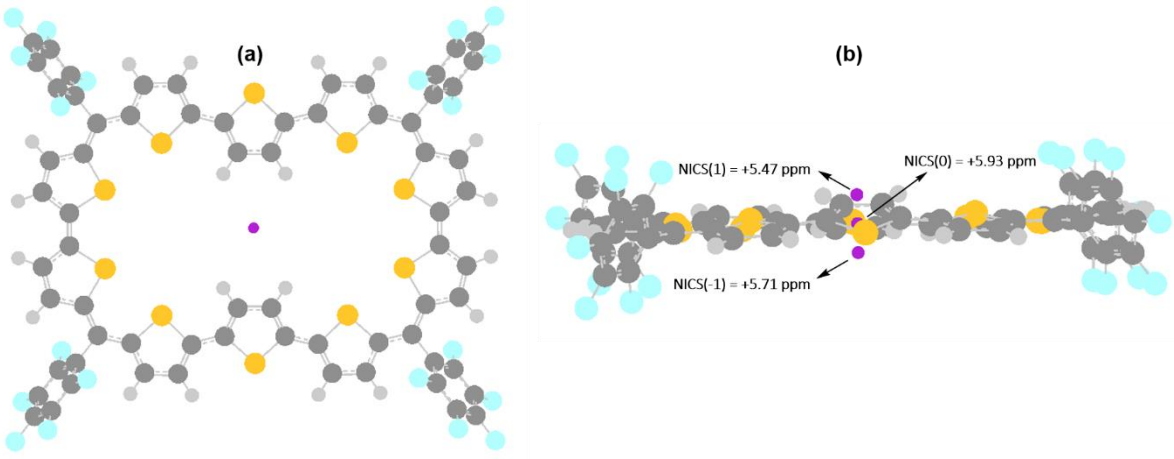

Fig. 4.7: NICS values of **IV.13** calculated using the standard GIAO (NMR=GIAO) at centre of the macrocycle and 1Å above and below the macrocyclic plane.

The AICD plot (Fig. 4.8) with moderate anticlockwise direction of ring current suggested Huckel antiaromatic characteristics of **IV.13**. The estimated geometrical descriptor of aromaticity/antiaromaticity, harmonic oscillator model of aromacitity (HOMA)[19] value was 0.75. The electronic aromacitity indices AV1245 and AV_{min} value for **IV.13** is 1.68 and 1.00 respectively. Hence all these calculations buttressed the antiaromatic character of **IV.13**. It has a small HOMO-LUMO energy gap of 1.25 eV for **IV.13** and corroborate with other reported antiaromatic macrocycles. Interestingly the diradical character of the macrocycle was calculated with the spin unrestricted UCAM-B3LYP /6-31G(d, p) level of theory and its shows zero percentage of diradical character and justifying its closed shell nature.

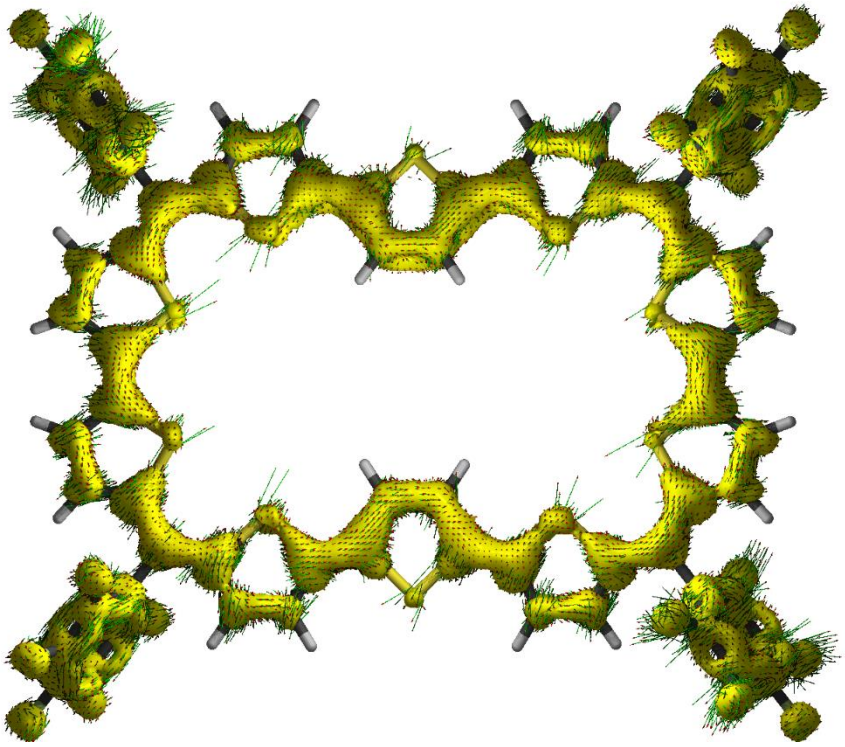

Fig. 4.8: Anisotropy of Induced Current Density (AICD) plot of **IV.13** (for π electrons only) at isovalue 0.08.

4.5 Isolation and Characterization of Decaphyrin IV.14

The selena derivative decaphyrin **IV.14** was isolated as a purple colored solid and it has less solubility compared to **IV.13**. The molecule **IV.14** was characterised by suitable spectroscopic techniques.

HRMS Spectrum of IV.14

The formation **IV.14** was confirmed by the High-Resolution Mass Spectrum (Fig. 4.9). The m/z value of 1727.6244 (Calcd. for $C_{68}H_{20}F_{20}S_6Se_4$; $[M]^+$ 1727.6231) revealed its exact composition.

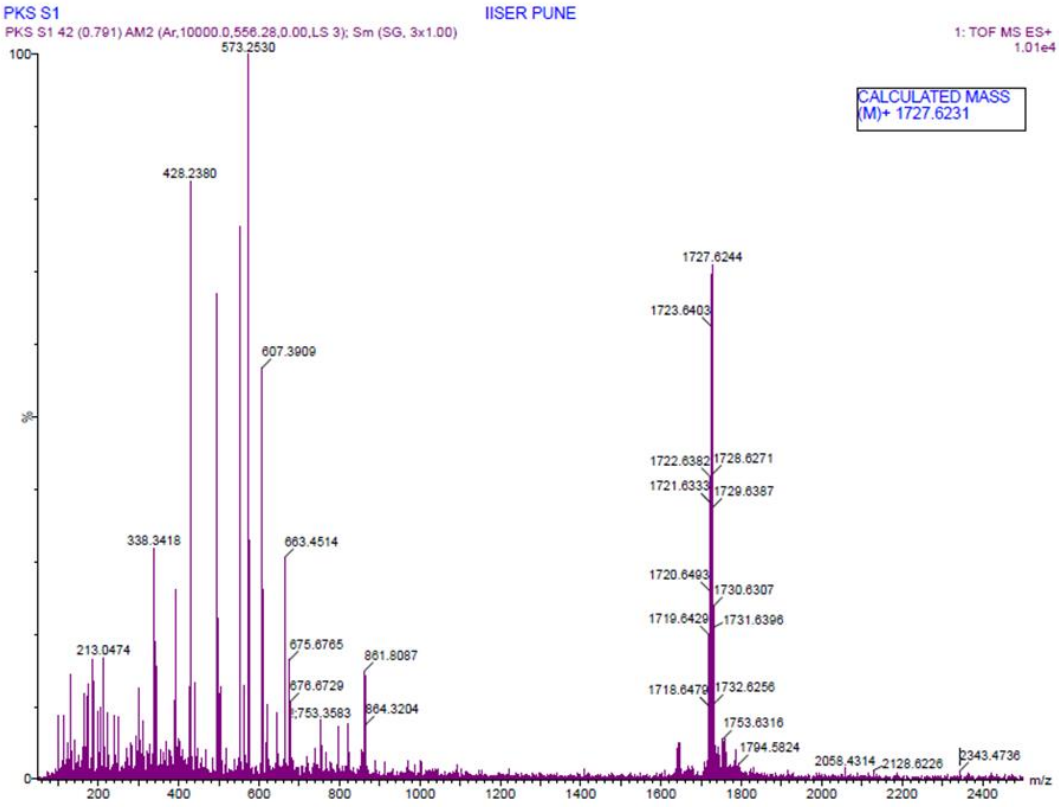

Fig. 4.9: High resolution mass spectrum (ESI-TOF) of **IV.14**.

NMR spectrum of IV.14

The decaphyrin **IV.14** displayed almost similar ^{1}H NMR pattern as **IV.13.** Hence, the molecular arrangement is also expected to be similar to **IV.13**. The ^{1}H NMR spectrum of **IV.14** was recorded in deuterated chloroform at 298 K. A singlet at δ 8.41 ppm for four protons, belongs to two inverted thiophene rings of the terthiophene moiety. The other four doublets resonating at δ 6.68 ,6.66, 6.21 and 6.05 ppm correspond to two protons each belonging to β C-H protons of outer thiophene and selenophene rings (Fig. 4.10).

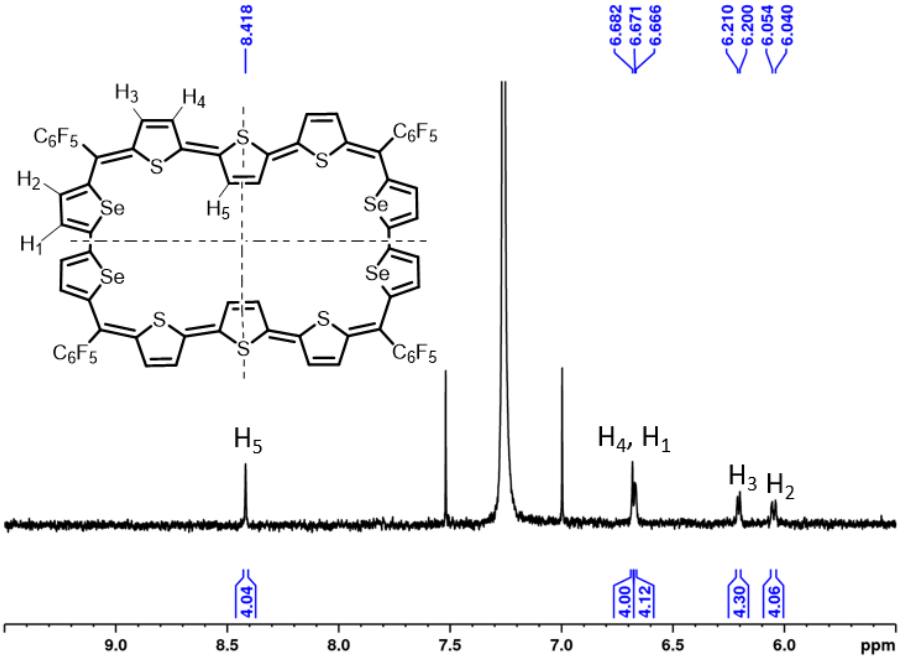

Fig. 4.10: ^{1}H NMR of **IV.14**.in $CDCl_3$ at 298 K.

UV-vis absorption spectrum of IV.14

Similar to **IV.13,** decaphyrin **IV.14** contains 44π electrons along its conjugation. Both **IV.13** and **IV.14** displayed the same color in solution state**.** Its electronic spectrum displayed an intense absorption at 589 nm (124700) along with bands at 547 nm (63700) and 505 nm (94900), (Fig. 4.31b).

4.6 Quantum Chemical Calculation of IV.14

The ground state geometry optimised structure revealed a planar topology as **IV.14** (Fig. 4.11). The calculated NICS value of +4.22 ppm suggested the weak antiaromatic characteristics. The HOMO-LUMO energy gap of 1.33 eV is comparable to HOMO-LUMO energy gap of **IV.13** 1.25 eV. Hence bi-selenophene **IV.14** revealed a similar character as **IV.13** in solid as well as solution state.

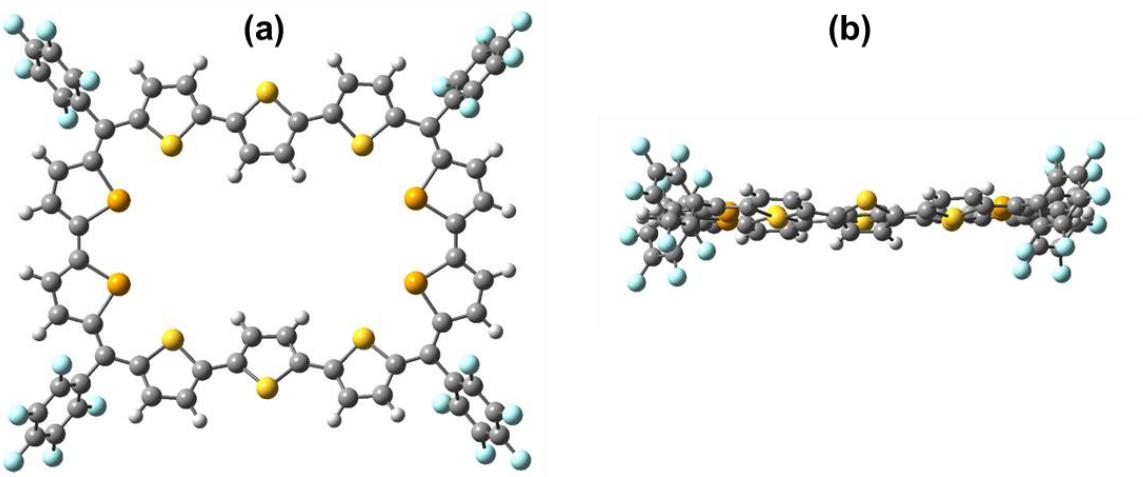

Fig. 4.11: Geometry optimised structure of **IV.14** obtained with B3LYP/6-31G(d, p) basis set.

4.7 Isolation and Characterization of Decaphyrin IV.15

The bifuran derivative of 44π decaphyrin **IV.15** was synthesized by the same protocol as discussed in scheme 4.1. The characterisation was done with appropriate spectroscopic techniques.

HRMS Spectrum of IV.15

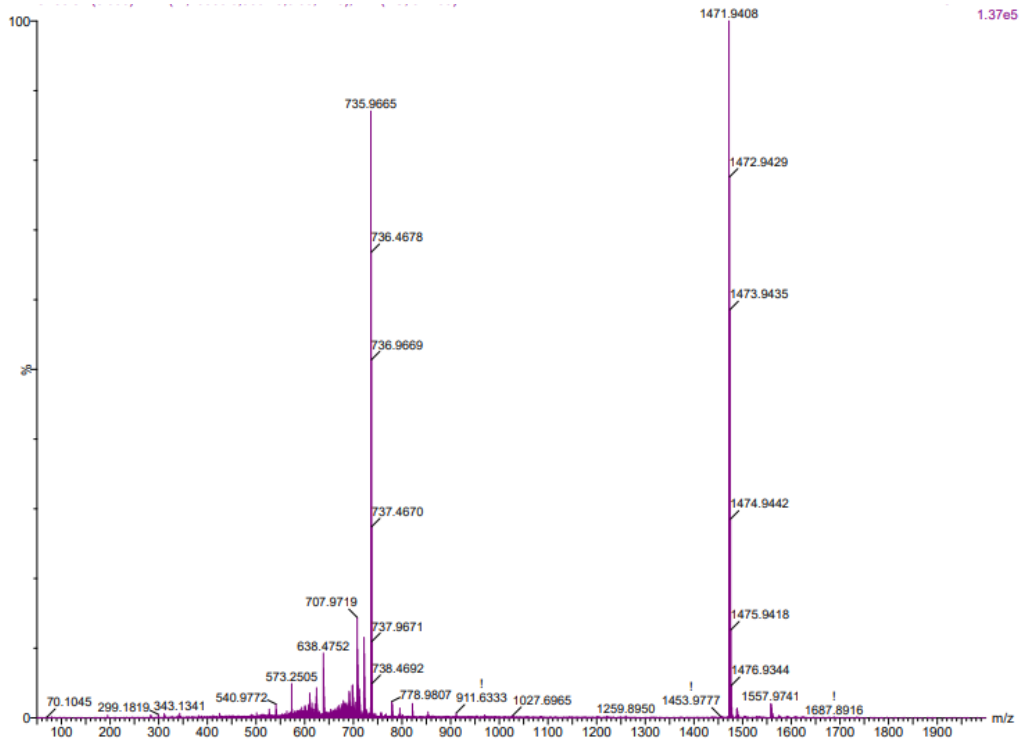

Fig. 4.12: High resolution mass spectrum (ESI-TOF) of **IV.15.**

The m/z of 1471.9408 along with m/2 of 735.9665 (Calcd. for $C_{68}F_{20}H_{20}S_6O_4$; $[M]^+$ 1471.9366 and $[M]^{2+}$ 735.9683) in HRMS spectrum (Fig. 4.12) confirmed the formation **IV.15**.

UV-vis absorption spectrum of IV.15

The macrocycle **IV.15** displayed as intense band at 494 nm (187000) accompanied by the absorption bands at 384 nm (112400), 583 nm (41200) and 624 nm (52900) in dichloromethane (Fig. 4.38). The furan derivative **IV.15** also showed a distinct absorption pattern compared to thiophene and selephene derivatives **IV.13, IV.14** implying overlapping of orbital due to small size of oxygen atom.

NMR spectrum of IV.15

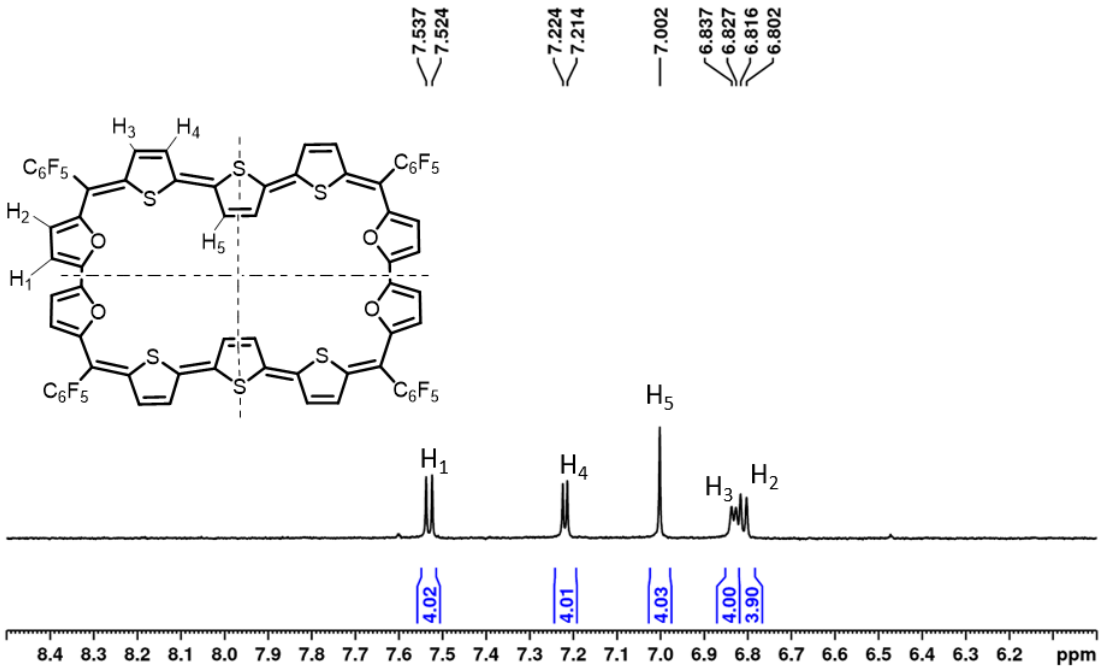

Fig. 4.13: ^{1}H NMR of **IV.15** in actone-d_6 at 298 K.

The solution state ^{1}H NMR spectrum in deuterated acetone solvent at room temperature, shows the resonance as four doublets at δ 7.53, 7.22, 6.83 and 6.81 ppm and one singlet at δ 7.00 ppm corresponding to four proton each (Fig. 4.13). Molecule **IV.15** revealed the insignificant ring current. The signal for inverted thiophene proton H_5 resonates at 7.00 ppm. In ^{1}H-^{1}H COSY spectrum H_5 did not reveal any correlation whereas two cross peaks δ (7.53 & 6.81) and (7.22

& 6.83) ppm represent the coupling of outer β C-H protons of the furan and thiophene (Fig. 4.14). The ^{1}H NMR spectrum pattern is similar to decaphyrins **IV.13** and **IV.14**, except a minor variation in the chemical shift values are varying significantly. Hence this observation predicts the molecular structure of **IV.15** very similar to **IV.13** in the solution state.

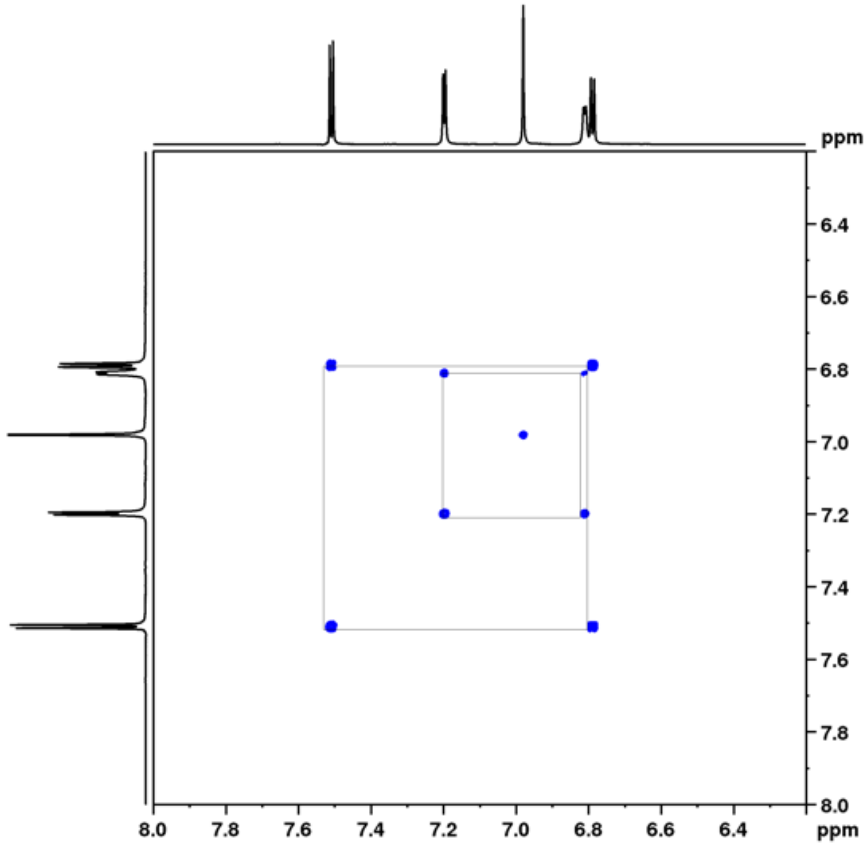

Fig. 4.14: ^{1}H-^{1}H COSY spectrum of **IV.15** in actone-d_6 at 298 K.

Molecular Structure of IV.15

In an attempt to crystallise **IV.15** using several solvent combinations and methods, good quality single crystals were grown in acetone and methanol by the vapor diffusion method. The single crystal X-ray diffraction analysis revealed a completely different structure in comparing to the solution state structure. Although similar to **IV.13**, the molecular arrangement of **IV.15** was planar but four of the thiophenes were inverted and facing outward to the macrocyclic plane. Whereas four furan units of bifuran were located at the corner of the macrocycle and other two thiophenes were facing the core of macrocycle. The four *meso*-pentafluorophenyl rings were oriented perpendicular to the conjugated backbone of **IV.15** (Fig. 4.15). Such observation of acquiring distinct arrangement of molecular framework in solid and solution state is common as reported in expanded porphyrinoids.

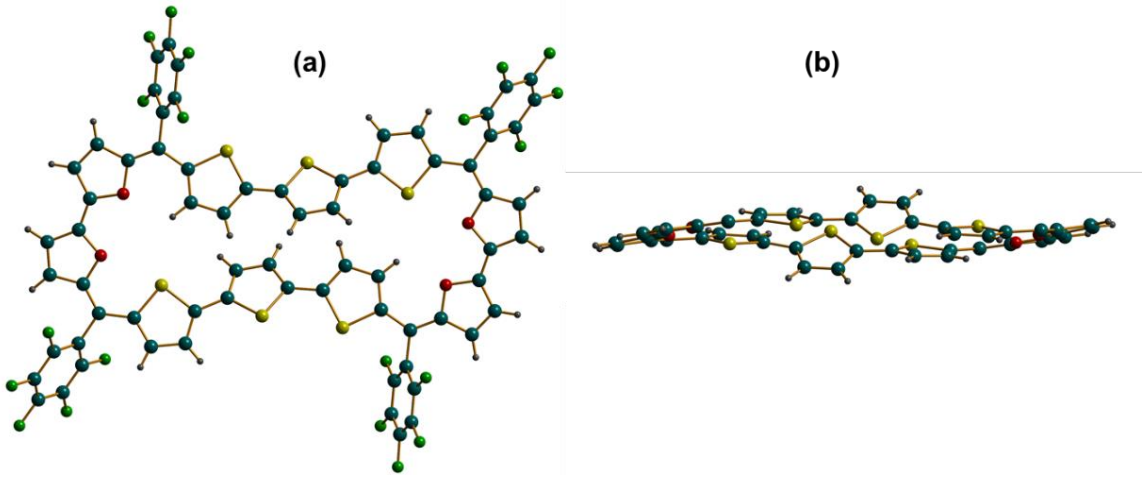

Fig. 4.15: Molecular structure of **IV.15** top view **(a)**, side view **(b)**, all the *meso* substitution were omitted for clarity.

All the synthesised 44π decaphyrins **IV.13**, **IV.14** and **IV.15** showed the well resolved ^{1}H NMR spectrum at room temperature and they follow the Huckel's rule of antiaromaticity. The solid state structure of **IV.15** showed completely different arrangement of atoms in comparision to **IV.13** and **IV.14** and it corroborates the fact the furan containing porphyrinoids always adopt different properties compare to thiophene and selenophene containing macrocycle. A detailed computational study revealed the closed shell character in all these three macrocycles.

4.8 Synthetic strategy for open shell decaphyrin IV.18

With the successful synthesis of 44π giant porphyrinoids with planar topology, a similar strategy to synthesis 46π decaphyrin was opted by condensation of the terthiophene **IV.17** and bithienyl dicarbinol **IV.16** (Scheme 4.2). In comparision to **IV.13**, the decaphyrin **IV.18** has two extra *meso*-methine positions and hence the number of πe^- will differ in both the decaphyrins and resulting to 46πe^- decaphyrin **IV.18** (Fig. 4.16).

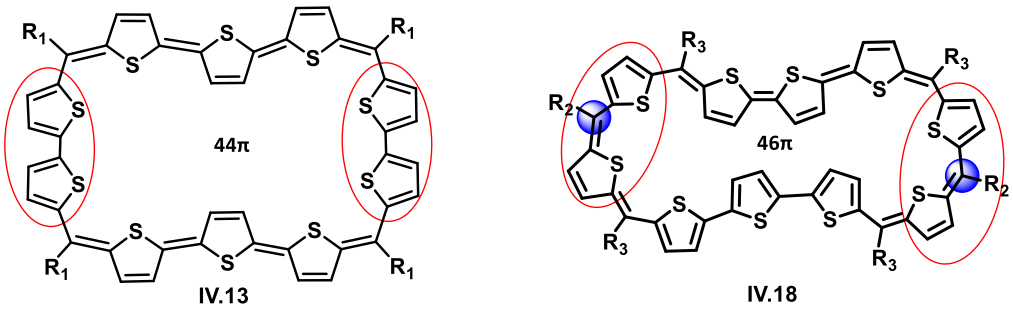

Fig. 4.16: Decaphyrin **IV.13** and **IV.18** with four and six *meso* positions.

4.9 Isolation and Characterization of Decaphyrin IV.18

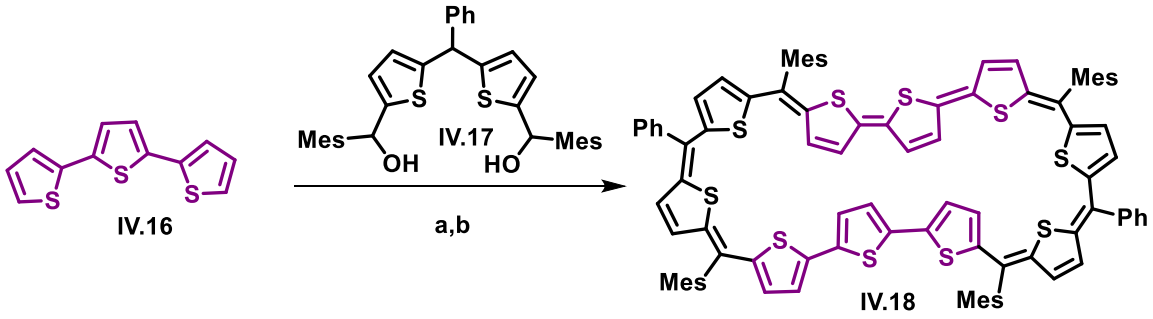

Scheme. 4.2 Cyclisation reaction for synthesis of decaphyrin **IV.18**. **(a)** $BF_3.OEt_2$, dark, N_2 atmosphere 2h. (b) DDQ open air condition 2h.

The preliminary analysis was done with MALDI-TOF/TOF spectrometry to confirm the formation of desired decaphyrin **IV.18** (Fig. 4.17). An intense blue colored compound was isolated from column chromatography in 5% ethyl acetate and hexane. In solid state this macrocycle appears as shiny brown solid.

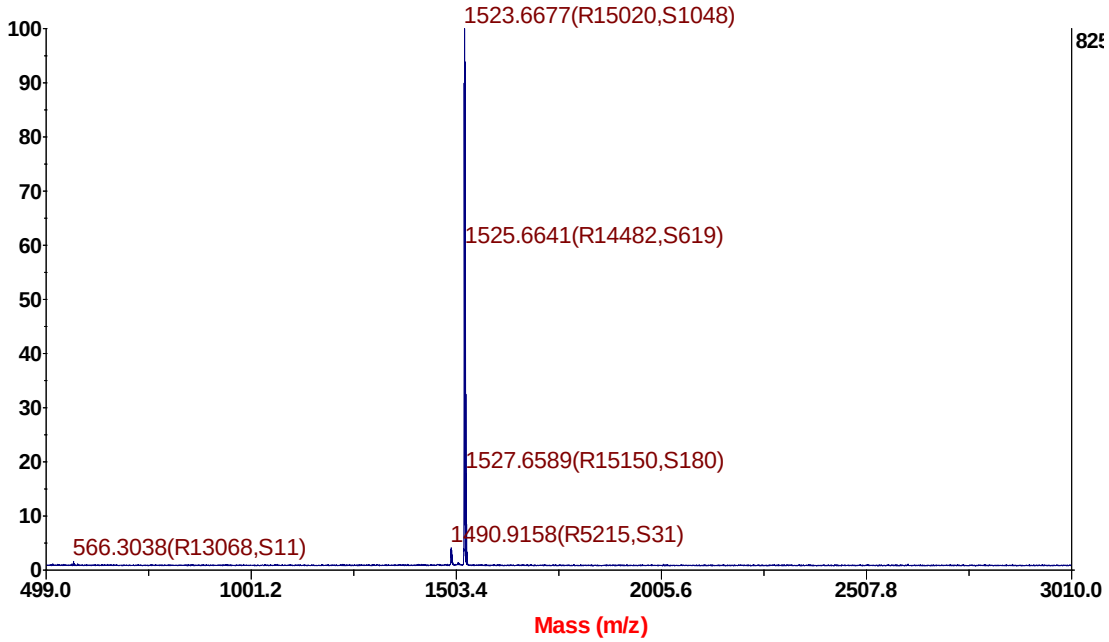

Fig. 4.17: MALDI-TOF/TOF mass spectrum of **IV.18.**

HRMS Spectrum of IV.18

High resolution mass spectrum analysis displayed m/z of 761.1470 and Calculated for $C_{94}H_{74}S_{10}$; $[M]^+$ 1522.2998 and $[M]^{2+}$ 761.1499 (Fig. 4.18).

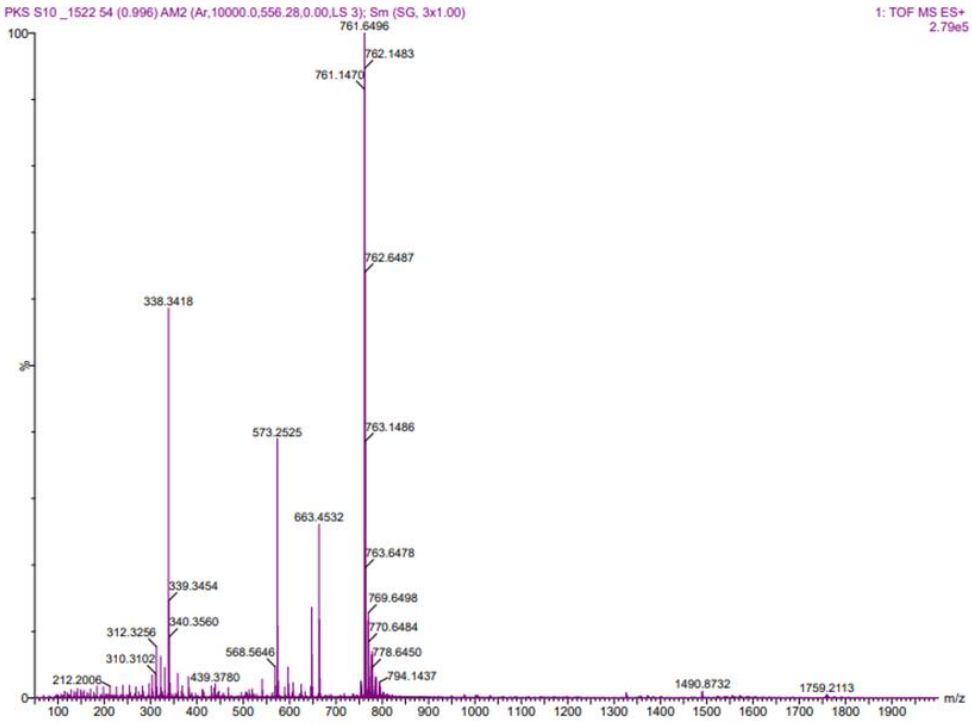

Fig. 4.18: High resolution mass spectrum (ESI-TOF) of **IV.18**.

UV-vis absorption spectrum of IV.18

The absorption spectrum of IV.18 was recorded in dry and distilled dichloromethane solvent. It showed unique absorption features compared to other decaphyrins. The most intense band in spectrum appears at 605 nm (153800) accompanied by two shoulder peaks at 546 nm (sh) and 664 nm (sh). Other peaks appeared at 432 nm (117800) and 725 nm (128700), the characteristics peak at 966 nm (112900) with extended and broad band suggested the possibility of radical species (Fig. 4.41).

NMR spectrum of IV.18

^{1}H NMR spectrum of **IV.18** was recorded in toluene-d_8 solvent. At room temperature the signals were broad and upon lowering the temperature upto 198 K there was not much change in signals (Fig. 4.19). But at 218 K, signals for mesityl protons were well resolved and methyl protons resonated at δ 2.39, 2.28, 2.12 ppm. The corresponding C-H resonated at δ 7.49 ppm and phenyl rings protons were observed at δ 7.25 ppm. The broad signals in region δ 8.35 to 6.20 ppm correspond to thiophene rings protons (Fig. 4.20). To analyse the conformational dynamics ^{1}H NMR spectrum was also recorded in THF-d_8 and chloroform-d solvents but significant change was not observed in any of these solvents.

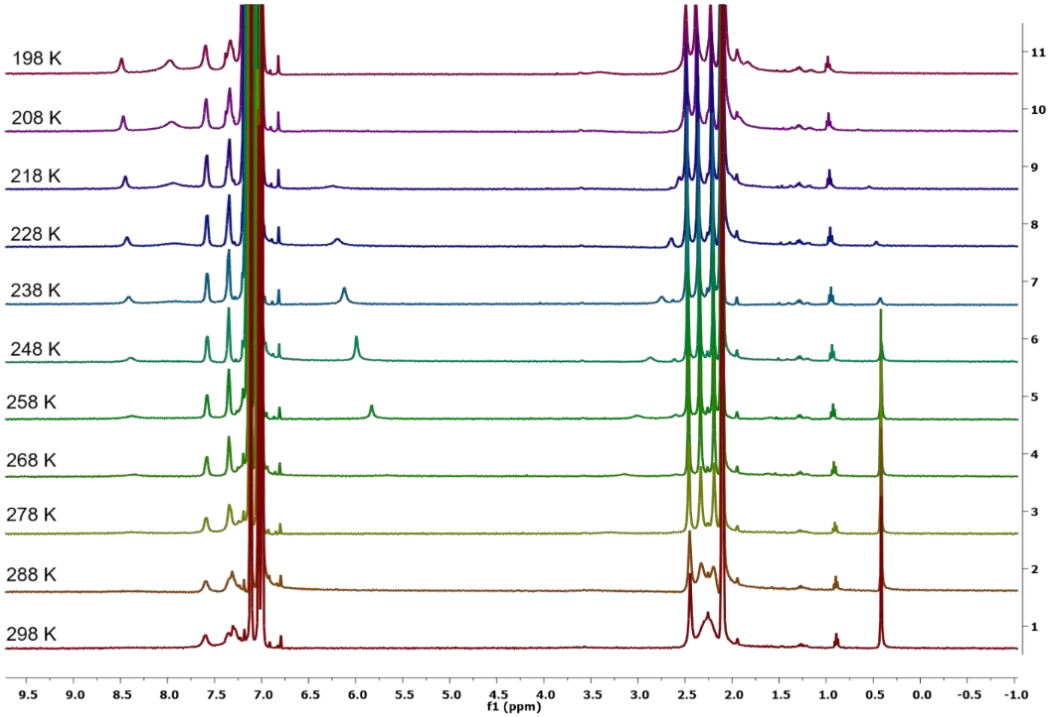

Fig. 4.19: Variable temperature ^{1}H NMR spectra of **IV.18** in toluene-d_8.

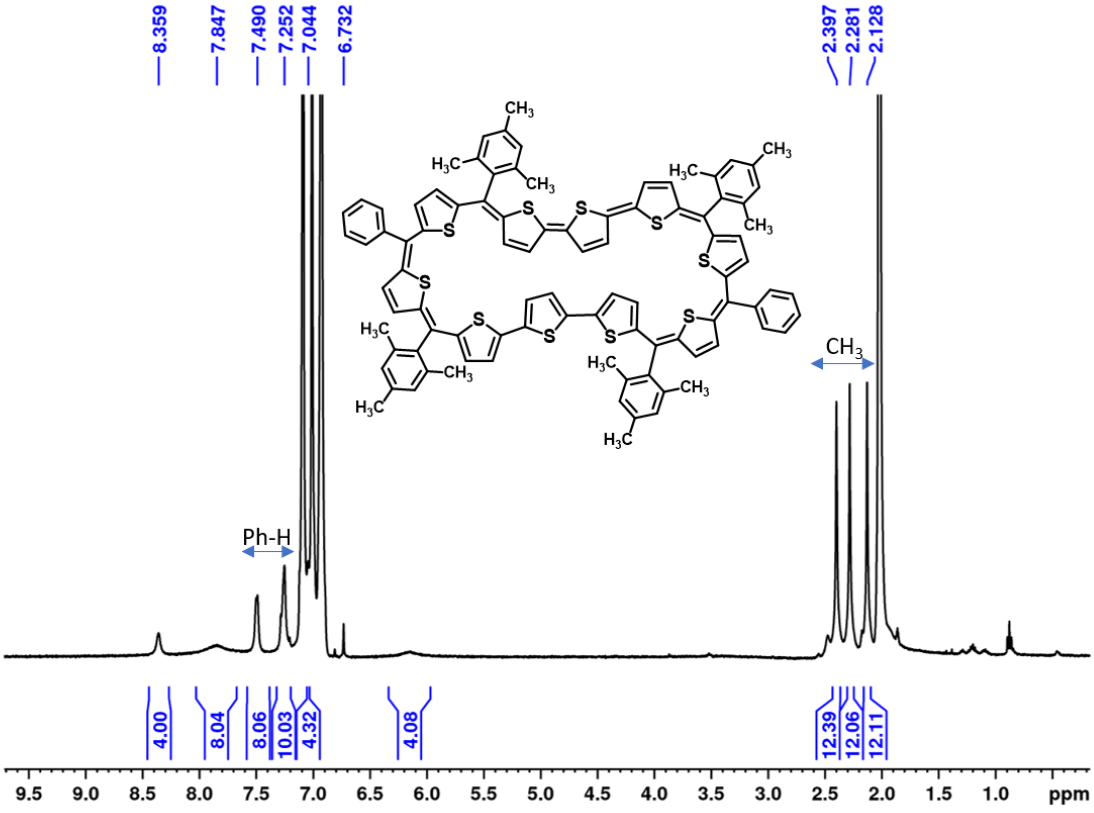

Fig. 4.20: ^{1}H NMR of spectrum of **IV.18** in toluene-d_8 at 218 K.

Molecular Structure of IV.18

To get insight on the arrangement of atoms in solid state, good quality single crystals were grown in benzene solvent. The obtained structure from X-ray diffraction analysis revealed monoclinic, space group P 21/c with a near planar arrangement of all the ten thiophene rings (Fig. 4.21). Unlike the 44π decaphyrins **IV.13**, the 46π **IV.18** adopted the rectangular shape with inversion of four thiophene rings. The two terthiophene units were arranged in parallely opposite position. To avoid the steric congestion, middle and side thiophenes of these two terthiophene units were facing opposite to the core of macrocyclic ring. Other six thiophenes were facing the center of macrocycle. The planar **IV.18** contains 46π electrons in the πe^- backbone of the macrocycle and fullfills the requirement of Huckel aromaticity.

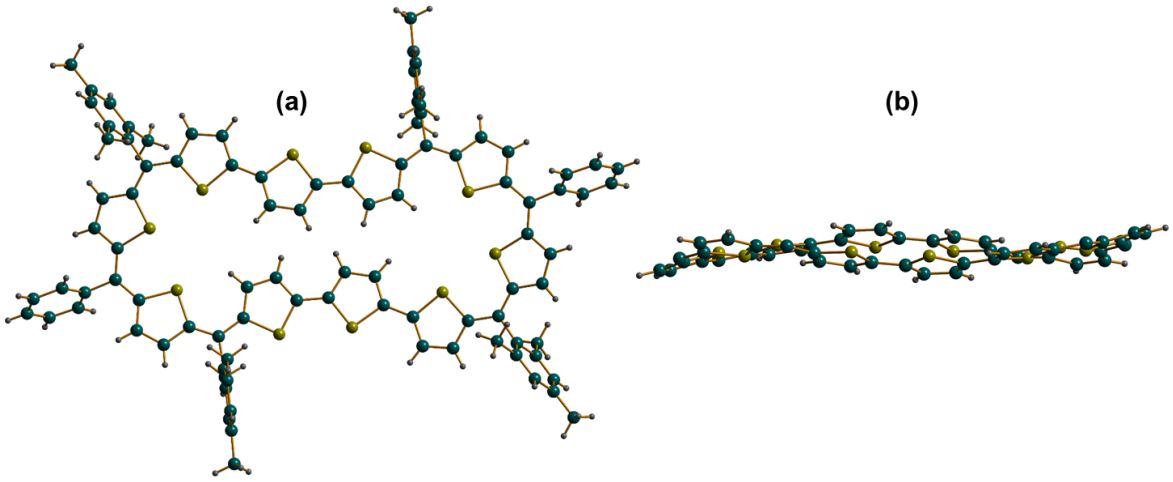

Fig. 4.21: Molecular structure of **IV.18** obtained from single crystal X-ray analysis.

Electron Spin Resonance (ESR) spectrum of IV.18

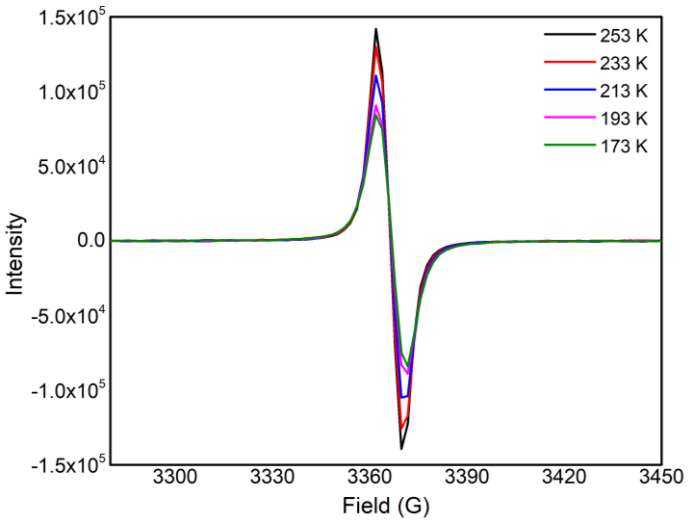

Fig. 4.22: Variable temperature ESR spectra of **IV.18.**

The broad ^{1}H NMR features was observed for **IV.18** even at temperature lower and higher than room temperature irrespective of NMR solvent. Suspecting its radical nature the Electron Spin Resonance (ESR) spectrum was recorded and it shows a broad feature less peak with a *g* value of 2.0054. A notable change in signal intensity was observed with varying the temperature (Fig. 4.22). The intensity of signals decreases with decrease in temperature along with absence of half field signal, confirms the singlet ground state of the decaphyrin **IV.18**.

4.10 Quantum Chemical Calculation of IV.18

The experimental results of **IV.18** was supported with the computational calculations. The DFT calculations was performed in Gaussian 09 software in High performance cluster facility of IISER Pune. The molecular structure (Fig. 4.21) obtained from single crystal X-ray analysis was chosen to get energy optimised structure of **IV.18**. The Anisotropy of Induced Current Density (AICD) plot (Fig. 4.23) was computed with the method developed by Herges. The clockwise direction of ring current and Nuclear Independent Chemical Shift NICS(0) value of -17.94 ppm (Fig. 4.24) confirmed the aromatic characteristics of **IV.18**. The harmonic oscillator model of aromacitity (HOMA)[19a] value 0.88, AV1245 and AV_{min}[19b, 19c] value was estimated to be 2.84 and 1.78 respectively.

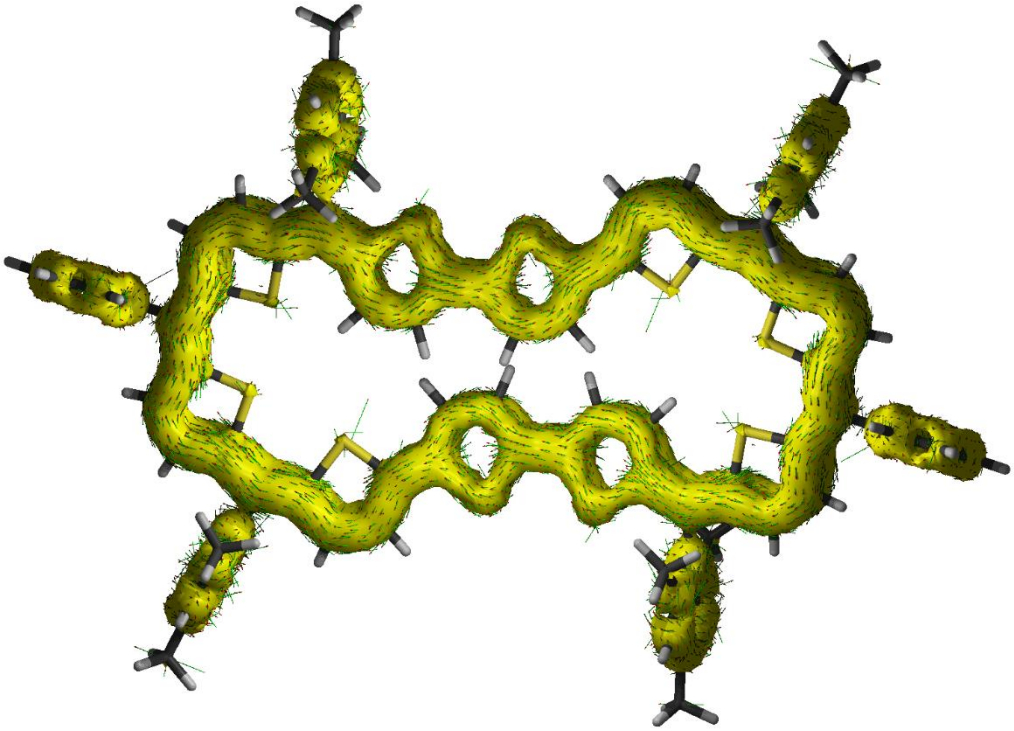

Fig. 4.23: AICD current density plot of **IV.18.**

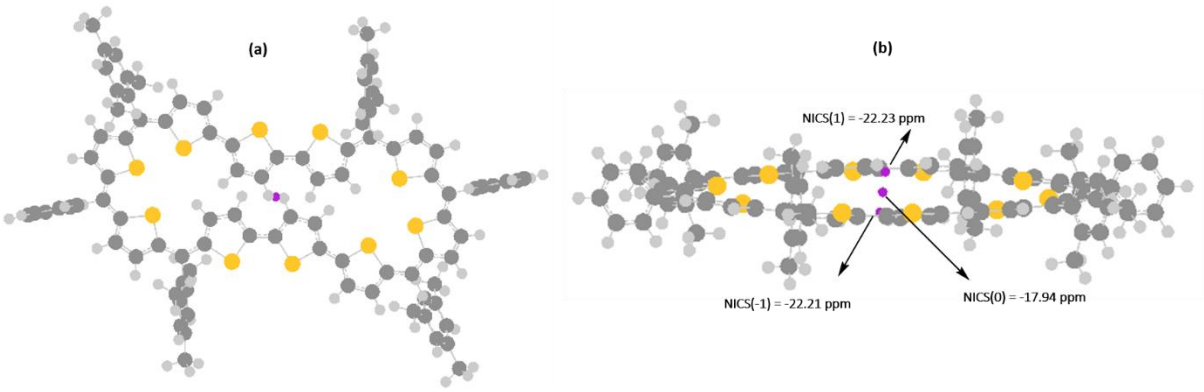

Fig. 4.24: NICS values of **IV.18** calculated using the standard GIAO (NMR=GIAO) at centre of the macrocycle and 1Å above and below the macrocyclic plane along z-axis.

Optimisation was done for singlet and triplet state of the molecule with spin unrestricted UCAM-B3LYP/6-31G(d,p) level of theory. The estimated singlet-triplet energy gap $\Delta E_{(S\text{-}T)}$ -2.19 kcal/mol, represents the singlet ground state of the molecule and this result buttress the experimental finding from EPR spectrum. The diradical nature of the molecule was calculated with Yamaguchi's scheme: $yi = 1 - (2T/(1 + T^* T))$, where $T = (nHOMO{-}i - nLUMO{+}i)/2$. The estimated Natural Orbital Occupation Number (NOON) value Y_0 is 69%, with the LUMO occupation of 0.84 (Table.4.2). The calculation implies the significant diradical character in the molecule **IV.18**.

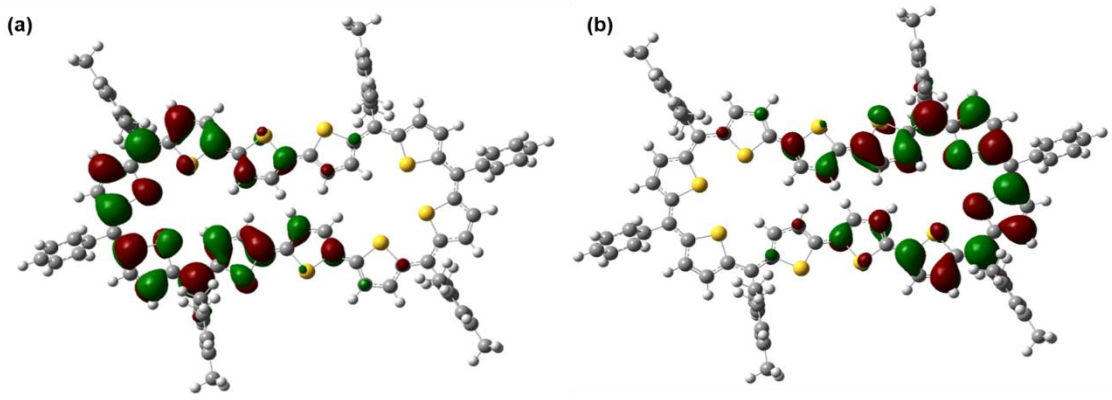

Fig. 4.25: Frontier SOMO diagram of **IV.18** (a) SOMO α spin (b) SOMO β spin, calculated using spin unrestricted UCAM-B3LYP /6-31g (d, p) of singlet ground state.

Further the Frontier Molecular Orbital profile of SOMO α and SOMO β (Fig. 4.25) confirmed the electron density of these two electrons are delocalised in two different halves of the **IV.18.** Spin density diagram (Fig. 4.26) represents the spin is delocalised over the aromatic backbone and hence suggesting good stability of the molecule **IV.18**.

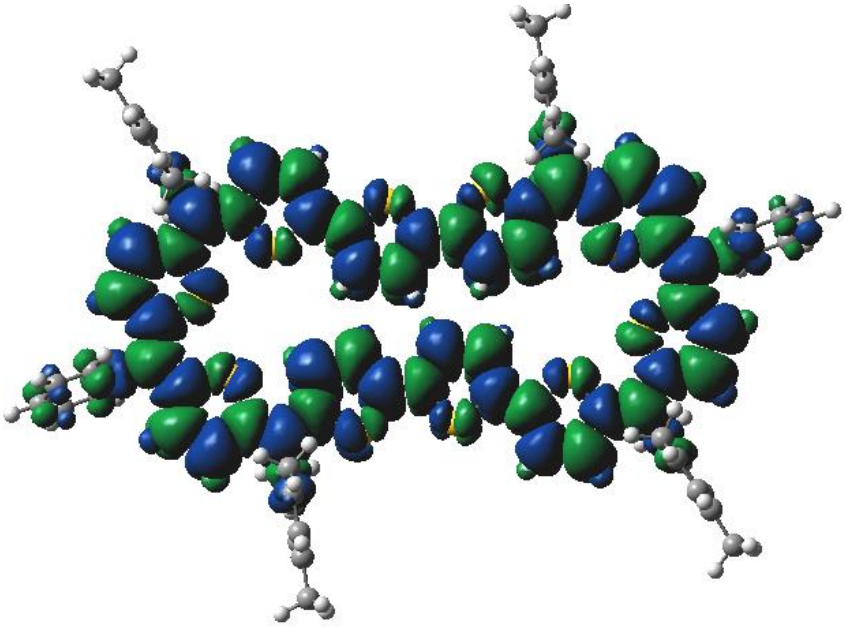

Fig. 4.26 Spin density diagram of **IV.18.**

Therefore, the detailed experimental and theoretical studies confirmed the singlet diradical nature of **IV.18**. Chemically, the four *meso*-mesityl substituents enhance the stabilities of **IV.18**. In fully conjugated form of macrocycle there is one benzenoidal terthiophene and one quinoidal terthiophene (Fig. 4.27). In diradical form, both terthiophene will get aromatic stabilisation by the recovery of benzeniodal form of terthiophene and hence it stabilizes the diradical form of **IV.18.**

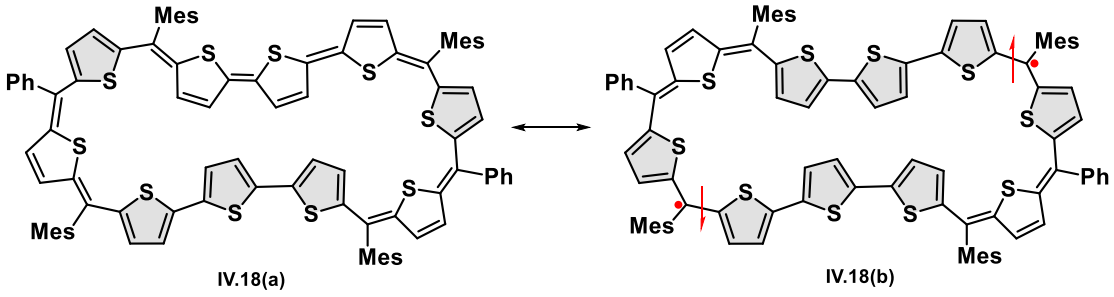

Fig. 4.27 Fully conjugated backbone IV.18(a) and diradical form IV.18(b) of **IV.18.**

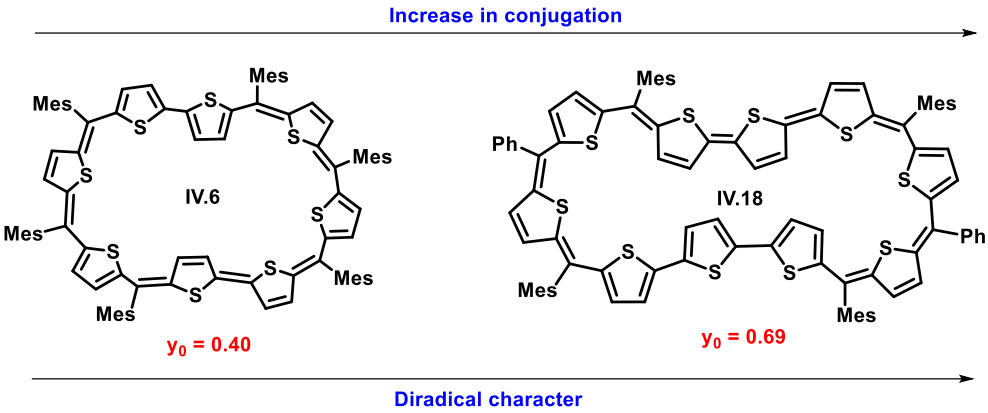

Fig. 4.28 Comparision of diradical characterization of **IV.6** and **IV.18**.

The study of diradical character prove that an increase in conjugation length of macrocycle from eight membered thiophene to ten membered thiophene increases the resonance in the ring and hence increase the diradical character (Fig. 4.28).

The synthesized decaphyrins have adopted the planar topology with incorporation of non-pyrrolic heterocyclic ring and reduced number of *meso*-substitutents. The 44π decaphyrins showed the closed shell nature whereas, the aromatic 46π decaphyrin displayed the notable value of diradical character. The delocalised πe^- clouds in these macrocycles makes them more susceptible towards redox reactions **IV.13**, **IV.14**, **IV.15** and **IV.18**.

Decaphyrin	No. of πe^-	λ_{max} (nm) $\varepsilon(M^{-1}cm^{-1})$	NICS(0) in ppm
IV.13	44	507(136500), 559(80500) and 602(185000)	+5.93
IV.14	44	505(94900), 547(63700) and 589(124700)	+4.22
IV.15	44	384(112400), 494(187000), 583(41200) and 624(52900)	+5.86
IV.18	46	432(117800), 546(sh), 605(153800), 664(sh), 725(128700) and 966(112900)	-17.94

Table 4.1 Decaphyrins with their electronic absorption and NICS(0) values.

4.11 Reversible Redox Properties of Decaphyrins

The cyclic voltammetry (CV) and differential pulse voltammetry (DPV) experiments revealed multiple redox peaks of these π conjugated molecules. Few redox states of these macrocycles were studied in details.

4.12 Redox Behaviour of IV.13 and IV.14

The electrochemical study of **IV.13** reveals the three oxidation peaks at 0.43, 1.03 and 1.32 V while two reduction potential at -0.89 and 1.30 V in cyclic voltammetry and DPV (Fig. 4.29) A very similar observation was obtained with selena derivative **IV.14**, it displayed three oxidation potential peaks at 0.49, 1.09 and 1.35 V and three reduction potential peak at -0.90, -1.25 and -1.42 V (Fig. 4.30).

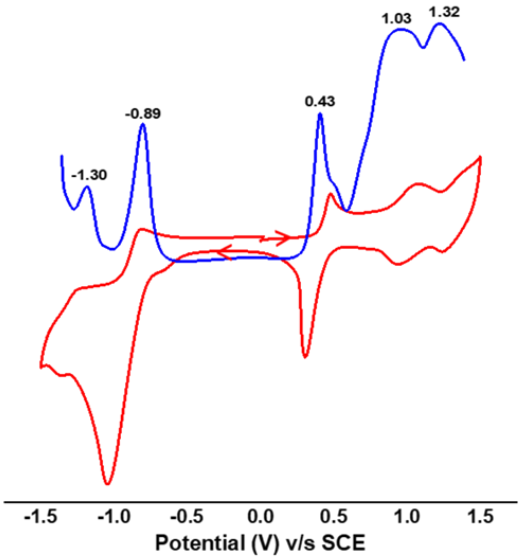

Fig. 4.29 Cyclic voltammetry (red line) and Differential Pulse Voltammetry (blue line) of **IV.13** recorded in 0.1 M solution of TBAP with scan rate 50 mV/s, using glassy carbon as working electrode, counter electrode (Pt) and standard calomel as reference electrode.

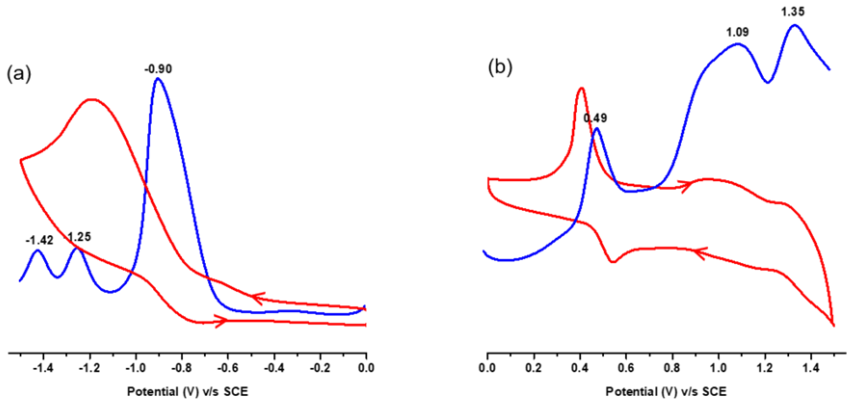

Fig. 4.30 CV (red lines) and DPV (blue lines) experiment of **IV.14** (a) reduction potentials (b) oxidation potentials. The three-electrode system: calomel as reference electrode, Pt wire as counter electrode and glassy carbon as working electrode.

Chemical Oxidation of IV.13 and IV.14

The chemical oxidation of **IV.13** and **IV.14** could be achieved with variety of oxidants like $[Et_3O]^+[SbCl_6]^-$, $NOBF_4$, $NOSbF_6$, triflic acid and TFA (scheme. 4.3). **IV.13** oxidised with $[Et_3O]^+[SbCl_6]^-$ displayed instant color change from purple to blue in dichloromethane (Fig. 4.31a). The oxidized species **[IV.13]$^{2+}$** precipitated out as a golden color compound in quantitative yield. In chemical oxidation of **IV.14**, with Meerwein salt or trifluoroacetic acid the color of the solution changes immediately and drastic change was observed in absorption spectrum with intense and red shift absorption for **[IV.14]$^{2+}$**(Fig. 4.31b). The oxidation process was completely reversible by addition of electron source such as triethylamine or Zn to dication. All the attempt to further characterization of **[IV.14]$^{2+}$** went futile.

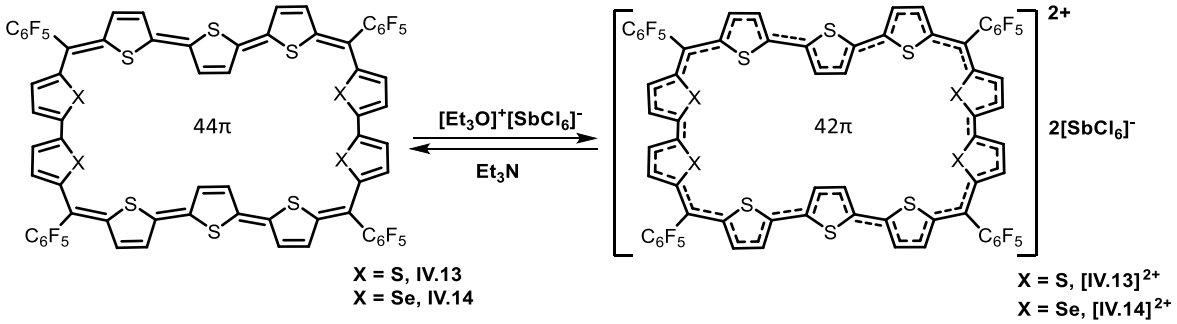

Scheme. 4.3 Reversible oxidation of **IV.13** and **IV.14** to its dication molecule **[IV.13]$^{2+}$**and **[IV.14]$^{2+}$**.

UV-vis absorption spectrum

[IV.13]$^{2+}$showed 170 nm red shifted absorption at 772 nm (450800) while **[IV.14]$^{2+}$** λ_{max} at 805 nm.

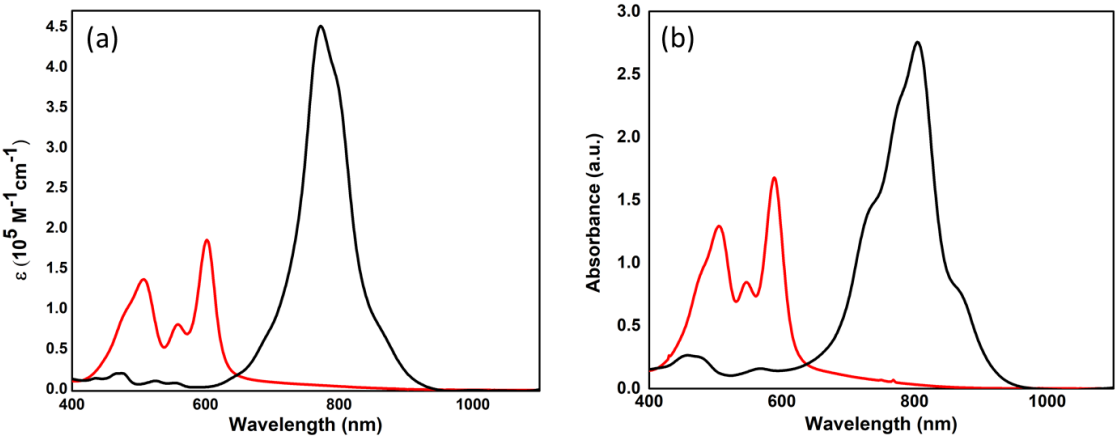

Fig. 4.31: UV-vis absorption spectrum of (a) **IV.13** (red line) and **[IV.13]$^{2+}$** (black line) (b) **IV.14** (red line) and **[IV.14]$^{2+}$** (blue line) recorded in dichloromethane.

HRMS Spectrum of $[IV.13]^{2+}$

The HRMS confirmed the formation of dicationic species **$[IV.13]^{2+}$** (Fig. 4.32) as m/z value of 767.9215 (Calcd. for $(C_{68}H_{20}F_{20}S_{10})^{2+}$; $[M]^{2+}$ 767.9226) revealed the di-positive charge on **$[IV.13]^{2+}$**. Hence it supports its $2e^-$ ring oxidation from 44π **IV.13** to 42π **$[IV.13]^{2+}$**. Unfortunately, the poor solubility and reversibility in polar solvents hampered the complete characterization of **$[IV.13]^{2+}$**.

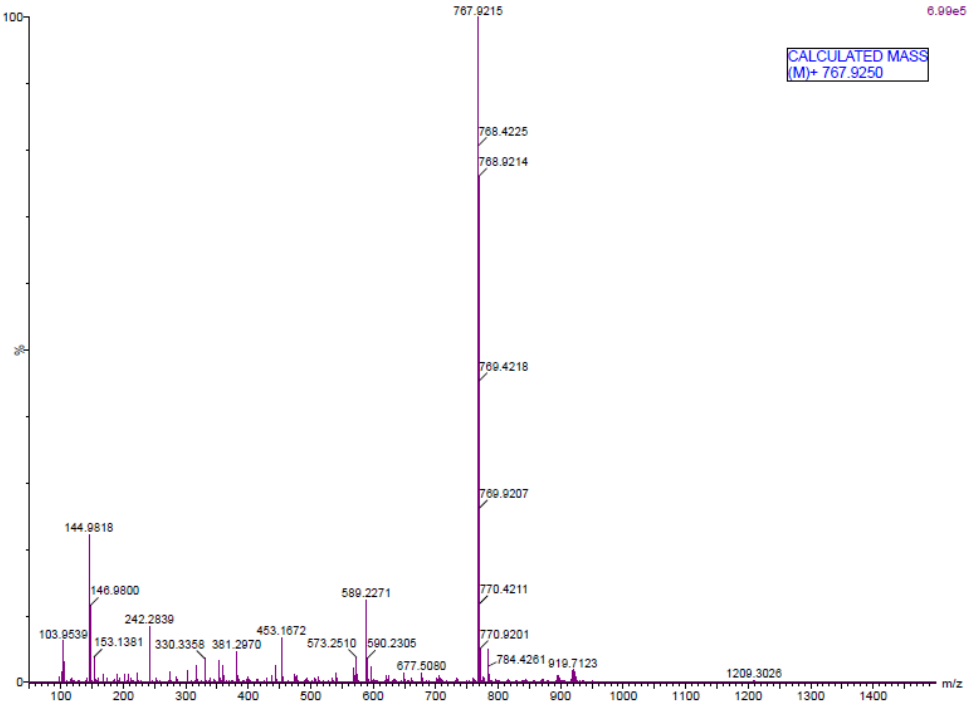

Fig. 4.32 HRMS spectrum of **$[IV.13]^{2+}$**.

Quantum Chemical Calculation of $[IV.13]^{2+}$

The optimised structure of **$[IV.13]^{2+}$** was obtained from DFT calculations, considering the molecule structure same as its free base **IV.13**, except the two positive charges on the ring. As the oxidised species contains the $42\pi e^-$, the calculated NICS(0) with B3LYP /6-31G(d, p) shown value of -13.95 ppm and confirms its aromatic nature. The small value of singlet-triplet energy gap $\Delta E_{(S\text{-}T)}$ -2.61 kcal/mol calculated using UCAM-B3LYP/6-31G(d,p) level of theory supports the possibility of diradical character. The Y_0 value of 0.50 and occupation number of LUMO 0.74 confirms the significant diradical character in the molecule (Table 4.2).

4.13 Redox Study of IV.15

The cyclic voltammetry experiment of **IV.15** using the same three electrode system as for **IV.13** and **IV.14**, revealed four oxidation peaks at 0.40, 0.75, 1.08 and 1.35 V along with one broad reduction peak at -0.88 V. These peaks are more pronounced with DPV (Fig. 4.33).

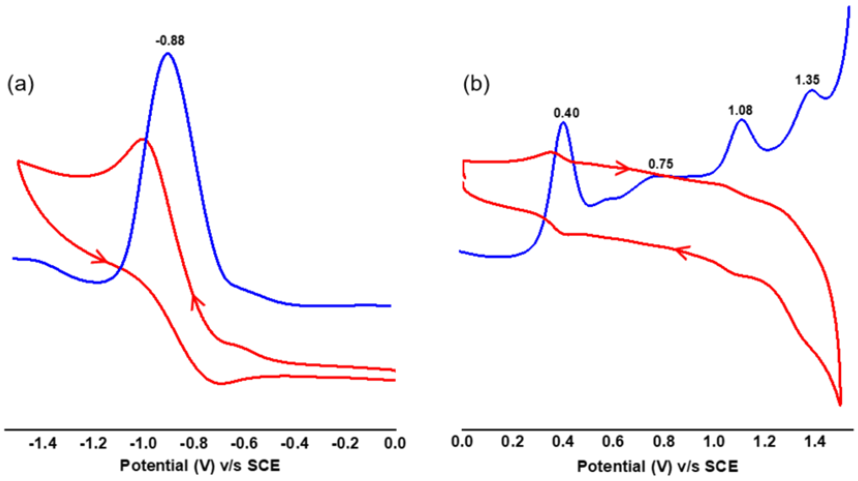

Fig. 4.33: CV (red lines) and DPV (blue lines) of **IV.15** (a) reduction potentials (b) oxidation potentials.

Chemical Oxidation of IV.15

The chemical oxidation of **IV.15** with $[Et_3O]^+[SbCl_6]^-$ in dichloromethane results in immediate color change from brownish green to yellowish green color (scheme 4.4). The dicationic molecule **[IV.15]**$^{2+}$ was isolated as a green colored compound in quantitative yield. **[IV.15]**$^{2+}$ shows the intense absorption at 768 nm (296000) along with peak at 457 nm (129400) (Fig. 4.34). It reflects the possibility of two electron oxidation of **IV.15**. This transformation is reversible and achieved by addition of electron donating reagents like Zn or Et_3N

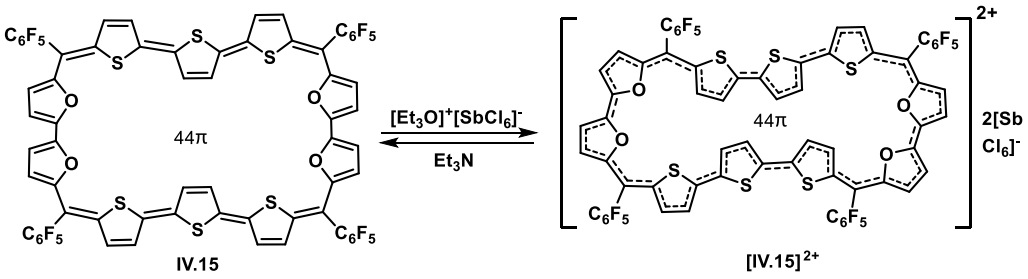

Scheme. 4.4: Chemical oxidation of **IV.15** to **[IV.15]**$^{2+}$.

HRMS Spectrum of $[IV.15]^{2+}$

HRMS analysis confirmed the formation of dication as m/z value 735.9675 (Calcd. for $(C_{68}F_{20}H_{20}S_6O_4)^{2+}$; $[M]^{2+}$ 735.9683) hence there is two positive charges delocalised over the ring (Fig. 4.34).

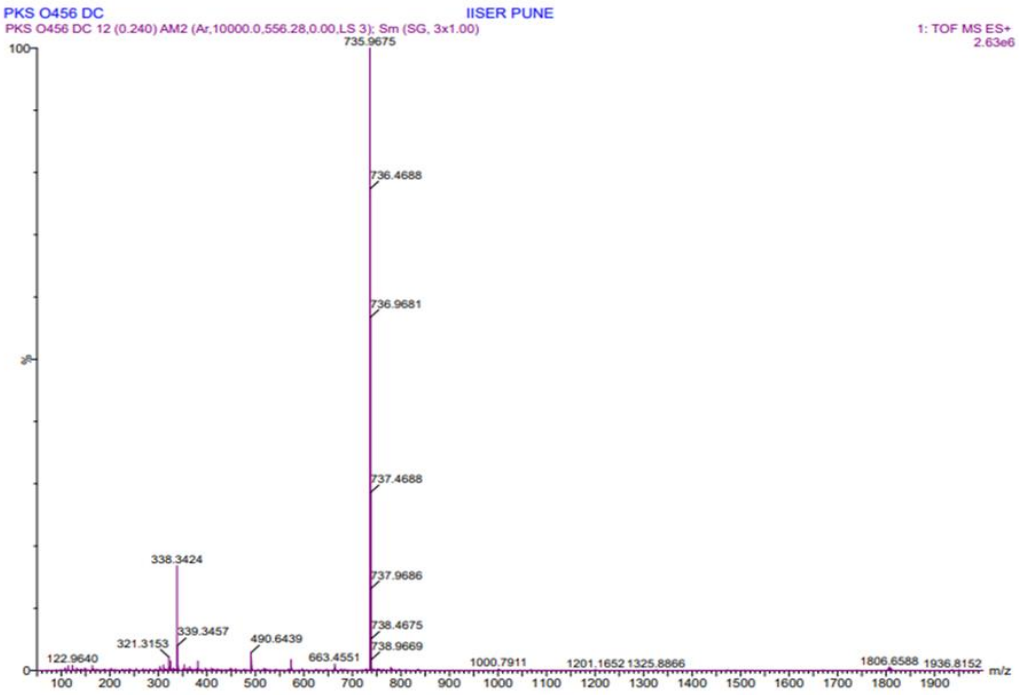

Fig. 4.34: High Resolution Mass Spectrum of **$[IV.15]^{2+}$**.

NMR analysis of $[IV.15]^{2+}$

The ^{1}H NMR spectrum of **$[IV.15]^{2+}$** reflect the well resolved signal in acetonitrile-d_3 at room temperature in 600 MHz spectrometer (Fig. 4.35). Compared to free base **IV.15**, (Fig. 4.13) where five signals were present for twenty protons corresponding to ten thiophenes, the ten distinct doublets are present for **$[IV.15]^{2+}$**. Hence increased number of signals suggest the reduced symmetry of **$[IV.15]^{2+}$** compare to free base **IV.15.** The dication $[IV.15]^{2+}$ contains $42\pi e^-$ therefore according to Huckel rule it should show diatropicity in the molecule. The six doublets at δ 8.50, 8.48, 7.84, 7.74, 7.65 and 7.57 ppm shows resonances corresponding to outer protons of ring, with three sets of correlations observed in 2D NMR. ^{1}H-^{1}H COSY spectrum (8.50 & 7.84), (8.48 & 7.65) and (7.74 & 7.57). The other four doublets at δ 6.96, 6.39, 6.10 and 4.69 ppm were found correlating to each other (Fig. 4.36). The detailed study from NMR suggest the dicationic molecule **$[IV.15]^{2+}$**, has adopted the similar molecular arrangement as of **IV.15** in the solid state (Fig. 4.15) in addition to two positive charges which are delocalized over the ring. Hence, **$[IV.15]^{2+}$** contains 42π electrons delocalized over the

backbone and two positive charges over the ring neutralized with the two counter anion of $[SbCl_6]^-$.

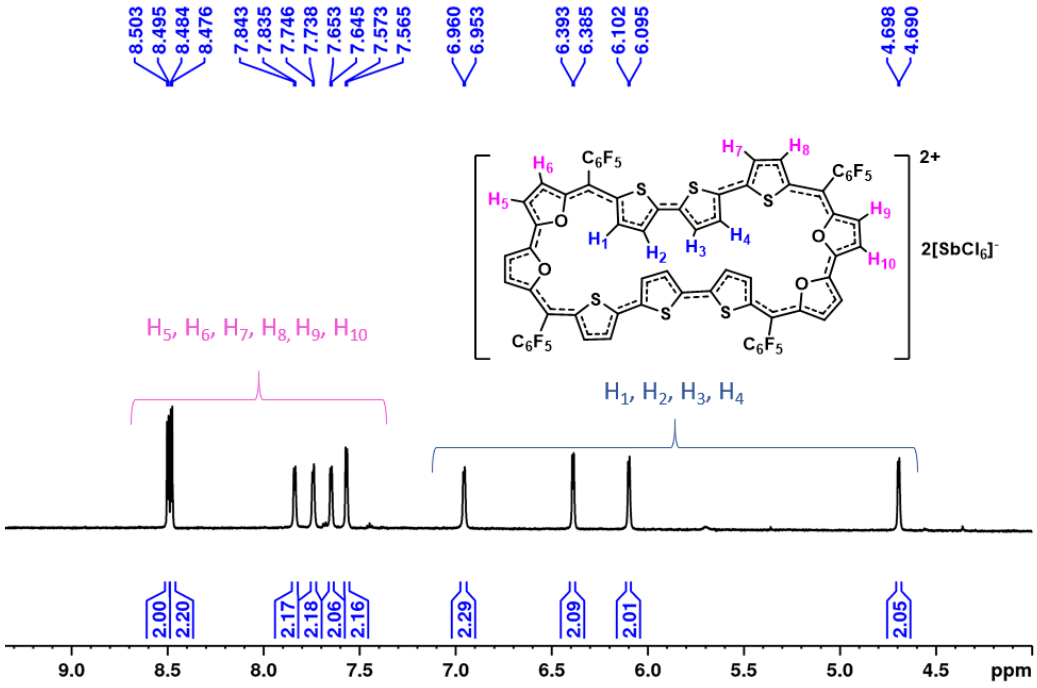

Fig. 4.35: ^{1}H NMR spectrum of **[IV.15]**$^{2+}$ in acetonitrile-d_3 at 298 K.

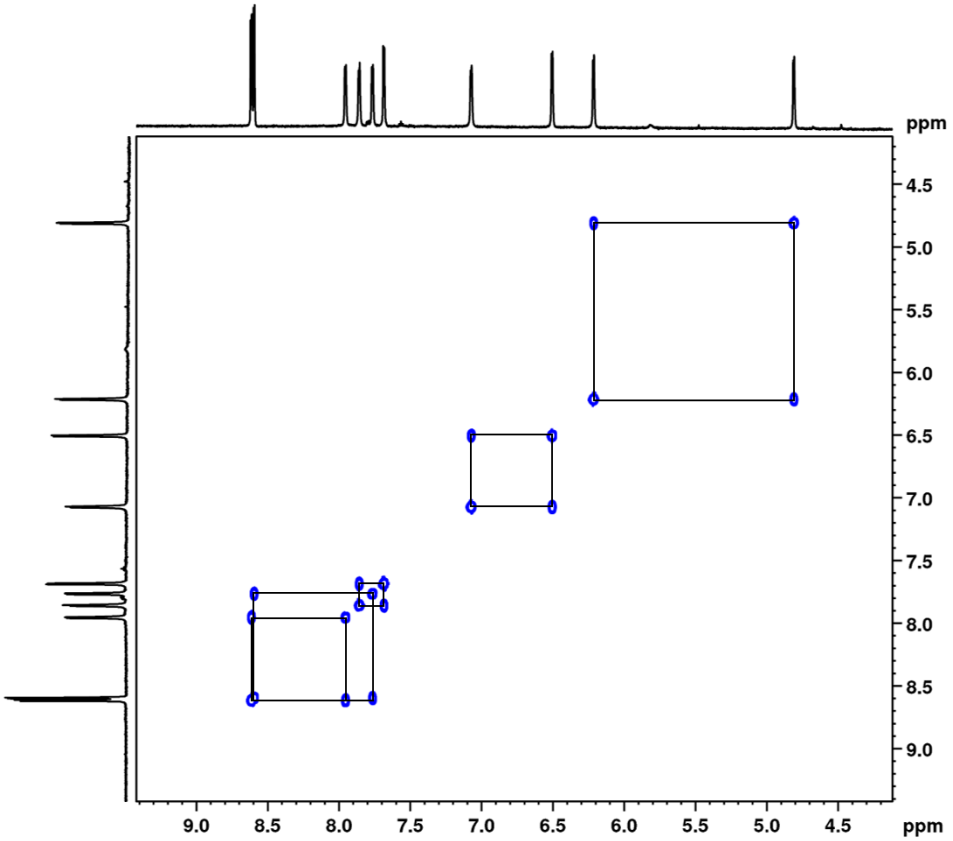

Fig. 4.36: ^{1}H-^{1}H COSY spectrum of **[IV.15]**$^{2+}$ in acetonitrile-d_3 at 298 K.

4.14 Spectro-electrochemical Analysis of [IV.15]

The 44π decaphyrin **IV.15** being electroactive in nature hence its conversion to dication **[IV.15]**$^{2+}$ could be studied with the spectroelectrochemistry. In reference with cyclic voltammetry experiment (Fig. 4.33) the oxidation potentials were applied to neutral molecule taken in 0.1M TBAP in dichloromethane. The assembly of spectroelectrochemical setup contains the quartz glass cell of 1 mm optical path length incorporated with set of three electrode Pt gauze, Pt wire and calomel as reference electrode. The absorbance spectrum was recorded at an the interval of 10s for the 45 mins.

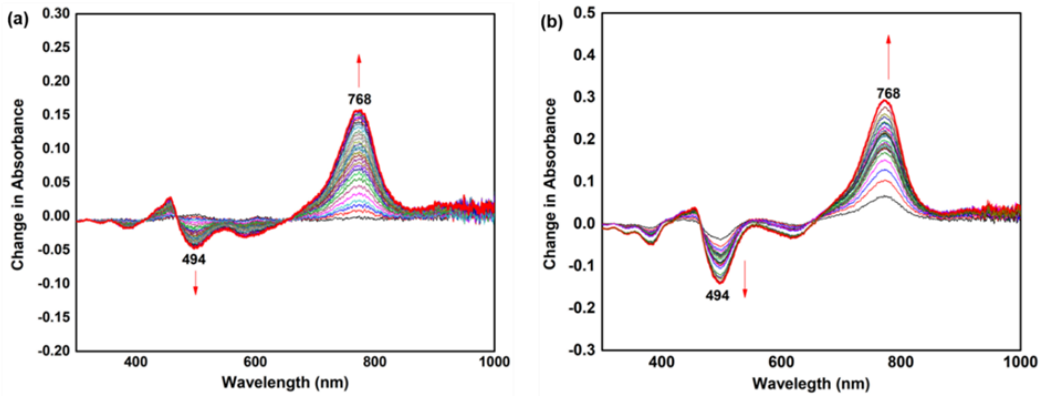

Fig. 4.37: Spectro-electrochemical measurement of **IV.15** (a) at 0.47 V and (b) 0.87 V.

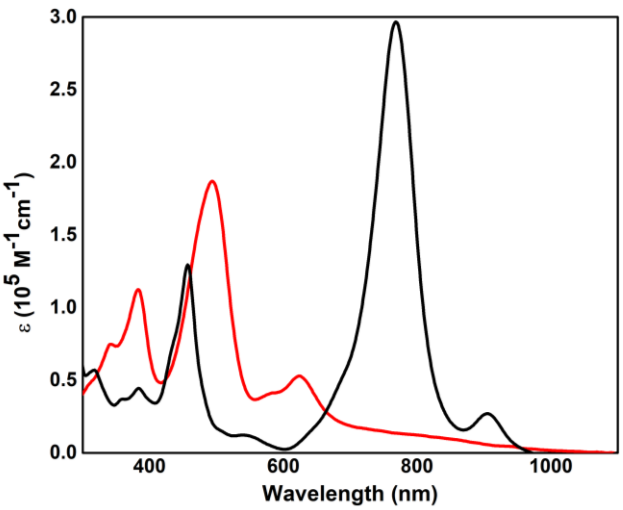

Fig. 4.38: UV-visible absorption spectra of [IV.15]$^{2+}$ (black spectrum) and IV.15 (red spectrum) in dichloromethane.

In spectroelectrochemistry experiment at applied potential of 0.47 V, slightly higher than first oxidation potential (0.40 V), the absorbance peak at 768 nm was emerging and intensity was increasing with increase in time. Whereas peak at 494 nm (belongs to free base decaphyrin) was diminishing with time (Fig. 4.37). Hence, it represents the conversion of **IV.15** to **[IV.15]**$^{2+}$

on applying the potential. At a higher potential 0.87 V, near to the second oxidation potential (0.75 V) a similar spectra pattern was observed hence suggested the stable dicationic state of the **IV.15**. The obtained results from spectroelectrochemistry is reminiscent with the chemical oxidation of **IV.15**.

Quantum Mechanical Studies

The geometrical optimised structure of **[IV.15]**$^{2+}$ was obtained with B3LYP /6-31G(d, p) level of theory. It reveals a nearly planar arrangement of all the rings (Fig. 4.39).

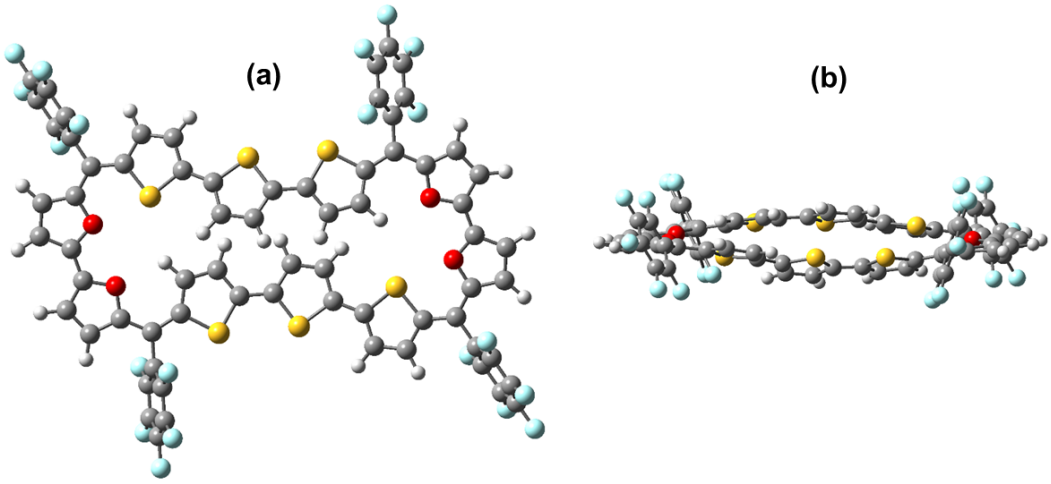

Fig. 4.39: Energy minimised geometry of **[IV.15]**$^{2+}$.

The calculated NICS value for **[IV.15]**$^{2+}$ was -17.82 ppm and it supports the aromatic behavior of dicationic molecule **[IV.15]**$^{2+}$ having 42π electron count in conjugation.

4.15 Redox Study of IV.18

Decaphyrin **IV.18** consist of 46π electrons and Huckel aromatic in character. The redox behaviour of **IV.18** was studied by cyclic voltammetry. It revealed four oxidation potentials at 0.45, 0.68, 0.76 and 1.18 V and the four reduction potentials -0.03, -0.28, -1.18, -1.32 V, which were predominately observed through differential pulse voltammetry experiment (Fig. 4.40). The CV predicts the possibility of two and four electrons oxidation of **IV.18**. Hence accordingly the chemical oxidation was studied.

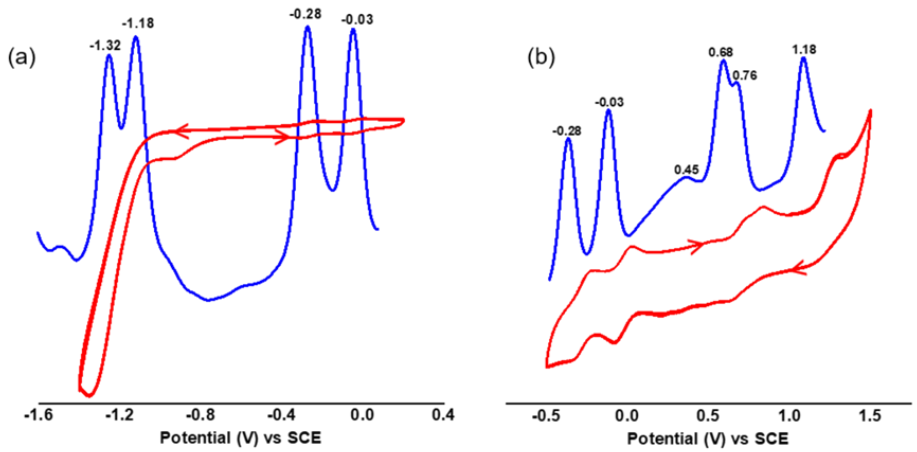

Fig. 4.40 CV (red lines) and DPV (blue lines) of **IV.18** (a) reduction potentials (b) oxidation potentials, using Ag/AgCl, Pt wire and glassy carbon scan rate 50 mV/s.

Chemical Oxidation of IV.18

Chemically the oxidation of **IV.18** to **[IV.18]**$^{2+}$ can be achieved either by the Meerwein salt $[Et_3O]^+[SbCl_6]^-$ or trifluoroacetic acid (TFA) and both results in instant color change from royal blue to green color and absorption was red shifted compared to free base form (Scheme 4.5). The oxidised specie **[IV.18]**$^{2+}$ was obtained by recrystallisation as golden color solid.

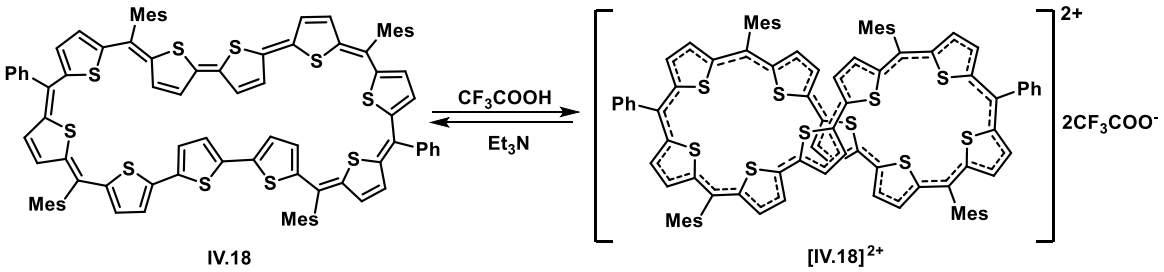

IV.18 [IV.18]$^{2+}$

Scheme. 4.5: Reversible redox reaction of **IV.18** and **[IV.18]**$^{2+}$.

4.16 Spectroscopic Characterisation of [IV.18]$^{2+}$

UV-vis absorption spectrum [IV.18]$^{2+}$

In electronic absorption study of molecule **[IV.18]**$^{2+}$ the λ_{max} appears at 698 nm (190100) along with absorptions at 470 nm (125200), 1008 (54000) and extended to the region 1600 nm (Fig. 4.41).

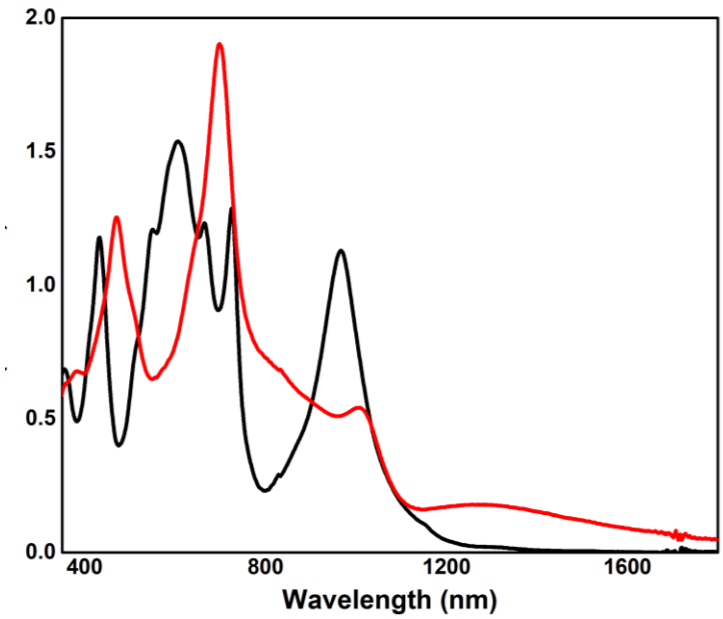

Fig. 4.41: UV-Vis-NIR absorption spectrum of **IV.18** and **[IV.18]$^{2+}$**.

HRMS Spectrum of [IV.18]$^{2+}$

The High-Resolution Mass Spectrum further confirmed the two positive charges on **[IV.18]$^{2+}$**. The found m/z mass of 761.1487 (Calcd. for $[C_{94}H_{74}S_{10}]^{2+}$; $[M]^{2+}$ 761.1499) clearly supported the formation of dicationic species (Fig. 4.42).

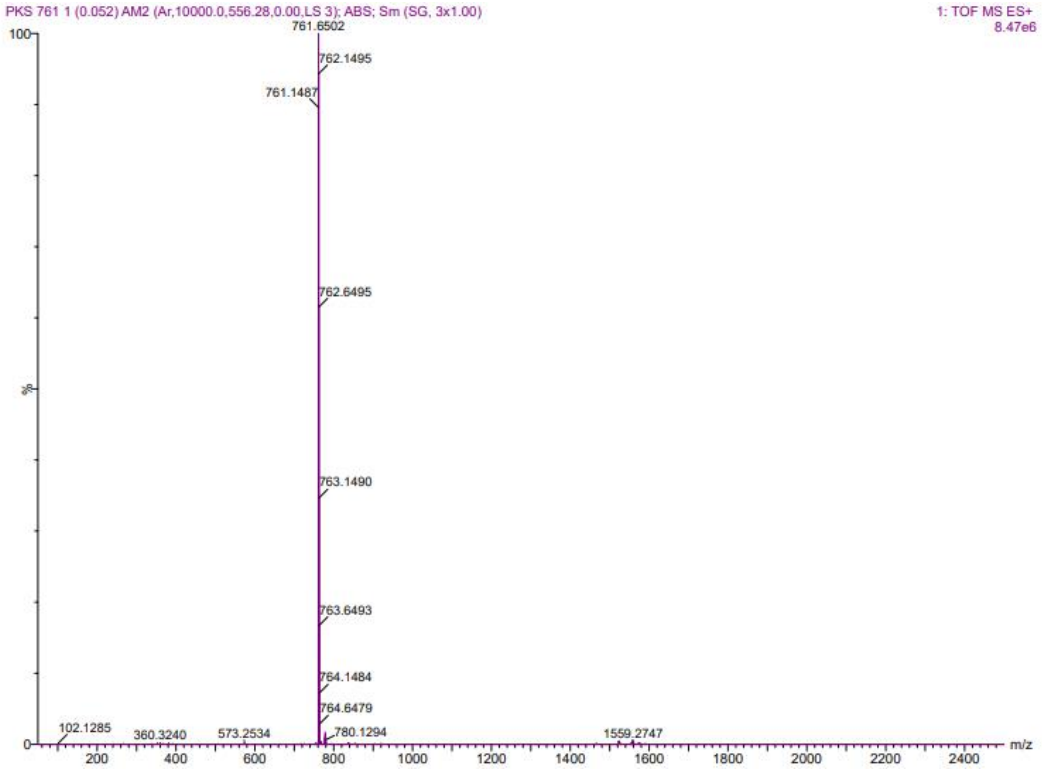

Fig. 4.42: High resolution mass spectrum (ESI-TOF) of **[IV.18]$^{2+}$**.

NMR study of [IV.18]$^{2+}$

^{1}H NMR spectrum was recorded in dichloromethane and being fluxional in nature the signals were not resolved at room temperature. Further on lowering the temperature the signals were revealed when NMR was recorded upto 193 K (Fig. 4.43). Interestingly, the number of proton signals increased in comparison to free base decaphyrin **IV.18**. At 203 K the distinct singlets in range of 6.75 to 8.12 ppm were observed for β-H protons and phenyl protons. The six signals at δ 2.99, 2.82, 2.41, 2.36, 1.49 and 1.41 ppm correspond to methyl protons of mesityl ring substituents (Fig. 4.44). Hence the increased number of proton signals suggests unsymmetrical arrangement of all the atoms in the molecule **[IV.18]$^{2+}$**. The 2D NMR spectrum (Fig. 4.45) of **[IV.18]$^{2+}$** showed the multiple cross peaks for adjacent protons of the heterocyclic ring but the NMR study was not informative to assign the absolute structure of macrocycle.

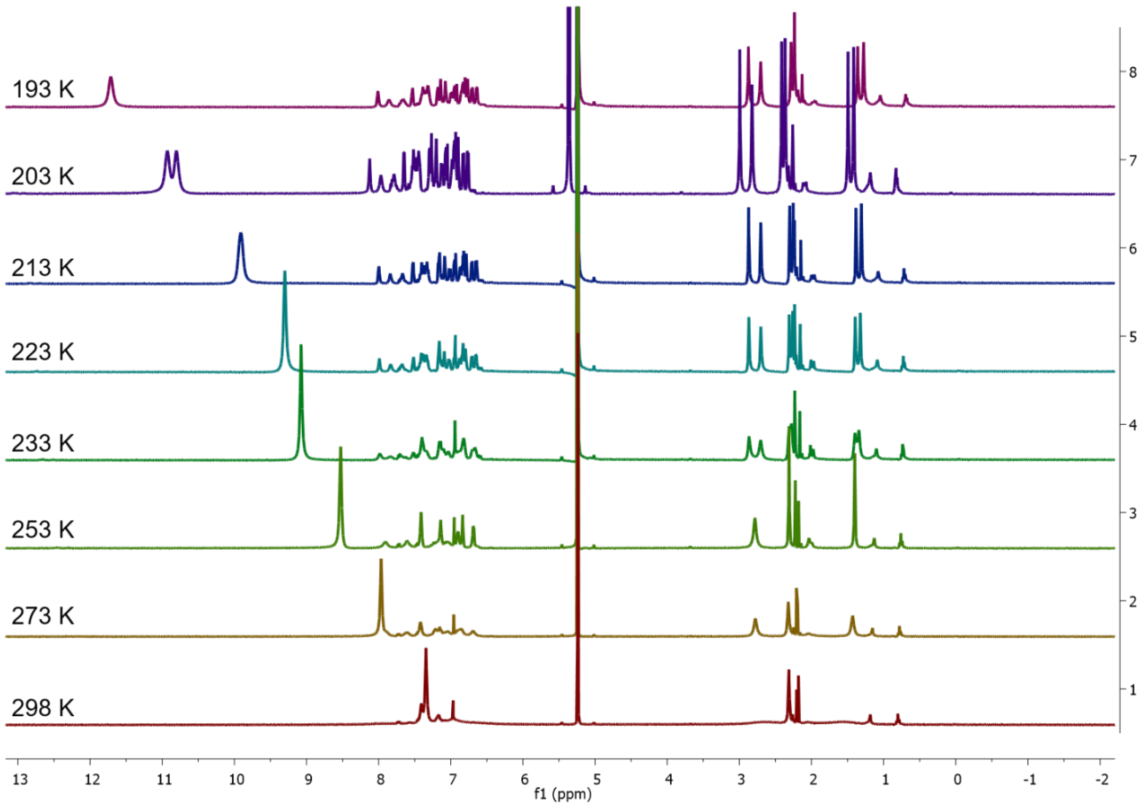

Fig. 4.43: Variable temperature ^{1}H NMR of **[IV.18]$^{2+}$** in dichloromethane-d_2.

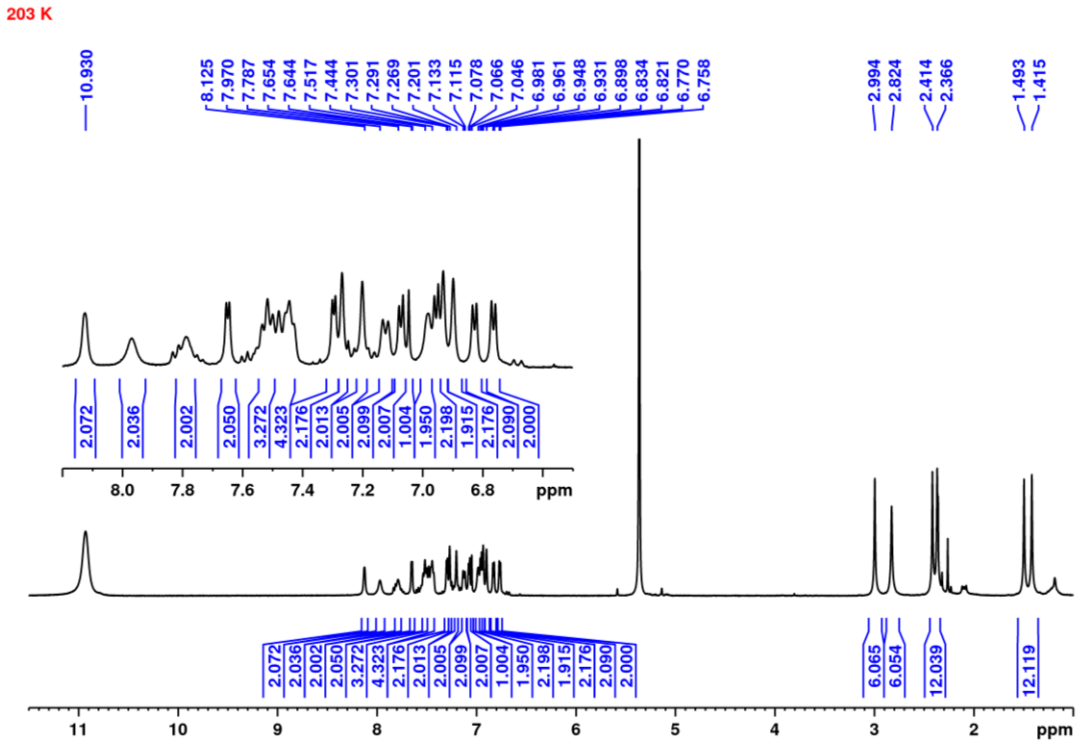

Fig. 4.44 ^{1}H NMR spectrum of **[IV.18]**$^{2+}$ in dichloromethane-d_2 at 203 K in 400 MHz. (Signal at δ ≈ 11.5 ppm corresponds to deuterated trifluoroacetic acid (CF_3COOD) added in excess to oxidize the macrocycle).

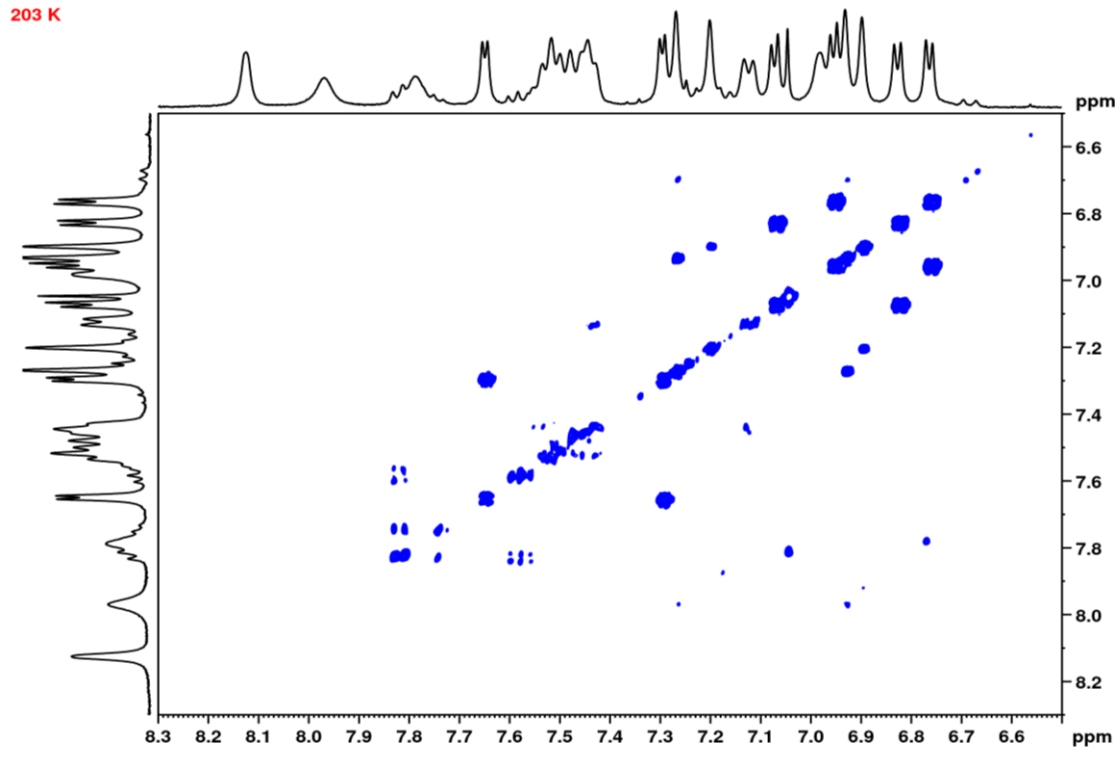

Fig. 4.45: ^{1}H-^{1}H COSY spectrum of **[IV.18]**$^{2+}$ in dichloromethane-d_2 at 203 K.

Molecular Structure of [IV.18]$^{2+}$

Multiple attempts were performed to grow good quality single crystal of dicationic macrocycle. The best possible crystal was obtained by solvent diffusion method in dichloromethane and heptane. The molecule crystallized in monoclinic, space group P 21/c.

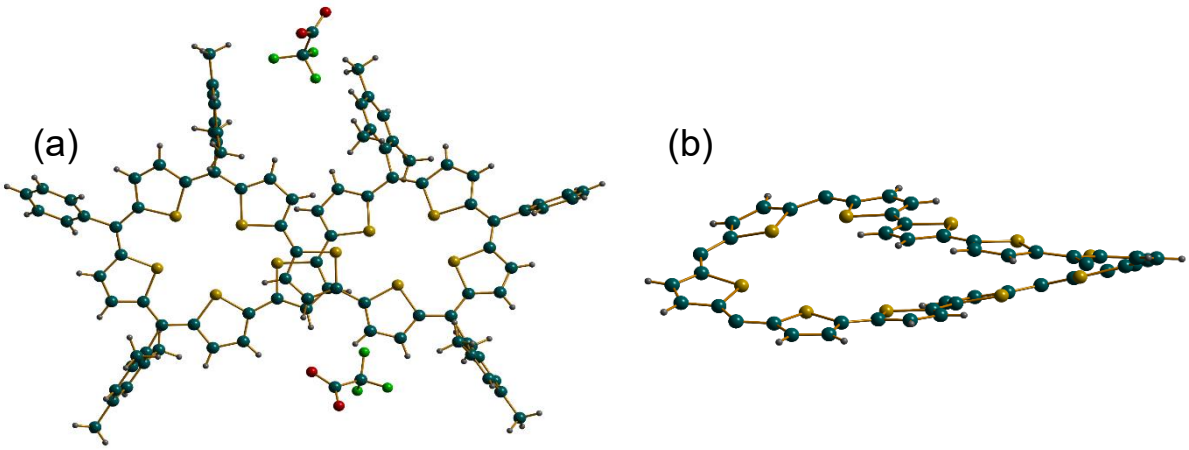

Fig. 4.46: X-ray single crystal analysis of **[IV.18]**$^{2+}$ (a) side view, two triflate anions are present (b) top view, *meso* substituents are omitted for clarity.

The nonplanar structure of macrocycle shows the deviation of thiophene ring from the planarity and the unusual criss-cross pattern of two terthiophene were observed which causes the unsymmetric structure in the molecule. The **[IV.18]**$^{2+}$ forms two different pockets of [5+5] conformation, where all the five rings were facing toward the macrocyclic core. The two trifluoroacetate anions were located above and below the macrocyclic plane, and it counter balance the two positive charges on the ring **[IV.18]**$^{2+}$. The single crystal structure confirmed the formation of dication of **IV.18**, the **[IV.18]**$^{2+}$ which contains the 44πe^- and nonplanar in nature hence hence satisfying characteristics of the non-antiaromatic macrocycle.

4.17 Spectro-electrochemical Analysis of [IV.18]

The electron transfer process between the **[IV.18]** and **[IV.18]**$^{2+}$ could also be achieved by spectro-electrochemical method. The process is similar to experiment performed for **[IV.15]** in Figure 4.37. On applying the potential equivalent to first and second oxidation potential respectively, similar spectral changes were obtained and hence confirmed the stable dicationic state. At 0.71V an increment in the intensity of peak at 699 nm and 470 nm while the absorption

peaks corresponding to neutral molecule **[IV.18]** region is vanishing with time. These observations support the oxidation of free base **IV.18** to dication **[IV.18]**$^{2+}$ on applying the certain potential (Figure 4.47).

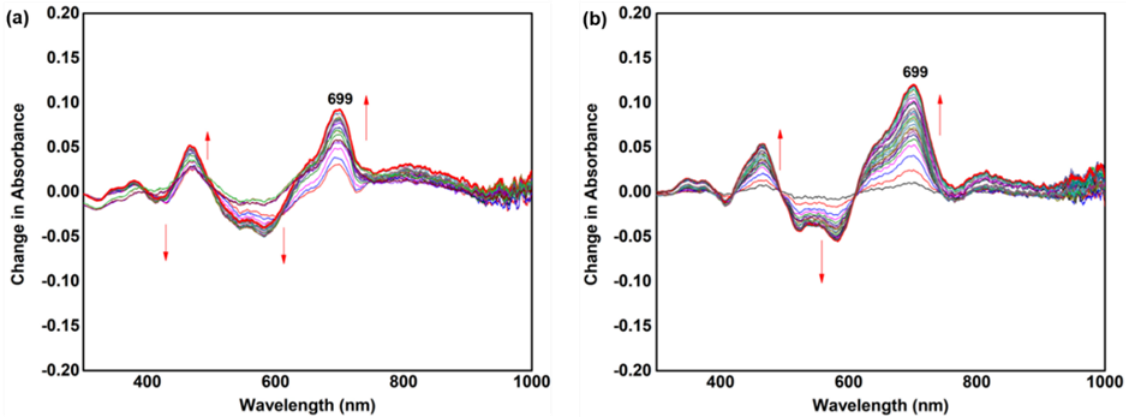

Fig. 4.47: Spectro-electrochemical analysis of **IV.18** (a) at potential 0.54 V and (b) at 0.71V.

Hence aromatic **IV.18** decaphyrin oxidised reversibly to non-antiaromatic **[IV.18]**$^{2+}$, via chemically and electrochemical and reversible transition could be achieved with reducing agents like triethylamine or Zn. The higher oxidised state of **IV.18** could be obtained by addition of strong oxidising agent $[NOSbF_6]^-$ and this conversion was also supported by spectroelectro-chemical observation.

Molecule	$\Delta E_{S\text{-}T}$ (kcal/mol)	Occupation Number of HOMO	Occupation Number of LUMO	y_0	y_1	y_2	NICS (ppm)
IV.13	-6.06	1.89	0.10	0.005	0.003	0	+5.93
[IV.13]$^{2+}$	-2.61	1.26	0.74	0.507	0.007	0.002	-13.95
[IV.18]	-2.19	1.16	0.84	0.692	0.020	0.009	-17.94

Table 4.2: Calculated singlet triplet energy gap $\Delta E_{S\text{-}T}$, occupation number of HOMO and LUMO, y_0, y_1. y_2 and NICS value of molecule **IV.13**, **[IV.13]**$^{2+}$ and **IV.18**.

4.18 Conclusion

The two distinct decaphyrins were obtained with 46π and 44π-electronic circuits incorporating the small thiophene precursor units. These molecules were then characterized using spectroscopic techniques. X-ray analysis revealed a planar topology for the decaphyrins. Interestingly, the 44π decaphyrin was identified as a closed-shell molecule, while the 46π

decaphyrin exhibited an open-shell character supported by the EPR studies. Further, these observations corroborate with quantum chemical calculations. The electrochemical studied reveals the multiple oxidation states of the macrocycles and these states are accessible using the suitable oxidising agents. The reversible two-electron ring oxidation of the 44π decaphyrins led to 42π dicationic species and it displayed moderate diradical character. These findings are in support with the fact the increase in the length of extended π conjugation in the ring, increases the diradical character. These studies provide valuable insights for the electronic structures and properties of these unique decaphyrin molecules. Further research on unexplored oxidation states are under process. With a better understanding of the various oxidation states and their properties, these extended porphyrins open a door for practical applications in the field of optoelectronics.

4.19 Experimental Section

Synthetic Procedure of IV.13

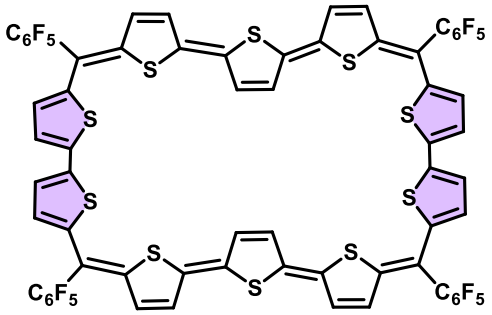

The mixture of terthiophene diol, **IV.9**, (202.26 mg, 315.78 μmol) and bithiophene, **IV.10**, (50 mg, 300.74 μmol) were stirred in 60 mL of dry dichloromethane under nitrogen atmosphere. The boron trifluoride diethyl etherate, $BF_3O(C_2H_5)_2$, (371.16 μmL, 300.74 μmol) was added to the resulting solution under dark and stirred for two hours. The oxidising agent 2,3-dichloro-5,6-dicyano-1,4-benzoquinone DDQ (238 mg, 1.05 mmol) was added to the mixture and the it was exposed to the open air for two hours. The MALDI-TOF/TOF spectrum confirms the formation of desired decaphyrin (2:2 condensation of monomers), along with other higher and lower masses product. The reaction mixture was passed with short bed of basic alumina coloum and filtrate was collected and further concerntrated under vacuum. Further purification was done in basic alumina column in 25% dichloromethane/hexane and followed with size

exclusion column in tetrahydrofuran and recrystallization. The purified decaphyrin IV.13 was obtained as metallic green solid in 7.2 % yield (16.8 mg).

Spectroscopic analysis: HRMS (ESI-TOF): *m/z* Calcd. for $C_{68}H_{20}F_{20}S_{10}$; $[M]^+$ 1535.8453; obtained, 1535.8490. ^1H NMR (400 MHz, $CDCl_3$, 298 K) δ: 8.69 (s, 4H), 6.58 (d, J = 4 Hz, 4H), 6.55 (d, J = 5.6 Hz, 4H), 6.09 (d, J = 4 Hz, 4H), 5.87 (d, J = 5.6 Hz, 4H). UV-vis absorption spectrum in dichloromethane: λ_{max} nm (ε, $M^{-1}cm^{-1}$): 507 nm (136500), 559 nm (80500) and 602 nm (185000).

Synthetic Procedure of IV.14

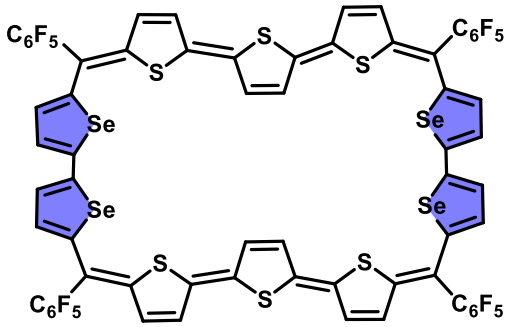

A similar reaction protocol was followed as **IV.13**. The reagents were used- terthiophene diol, **IV.9**, (200.97 mg, 313.75 µmol), biselenophene, **IV.11**, (80 mg, 307.60 µmol), boron trifluoride diethyl etherate (379.62 µmL, 307.60 µmol) and DDQ (244.39 mg, 1.08 mmol) in 60 mL dry dichloromethane. The desired decaphyrin **IV.14** was obtained as purple color solid in 4.5 % yield (11.9 mg).

Spectroscopic analysis: HRMS (ESI-TOF): m/z Calcd. for $C_{68}H_{20}F_{20}S_6Se_4$; $[M]^+$ 1727.6231; obtained, 1727.6244. ^1H NMR (400 MHz, $CDCl_3$, 298 K) δ: 8.41 (s, 4H), 6.68 (d, J = 4.4 Hz, 4H), 6.66 (s, 4H) 6.21 (d, J = 4Hz, 4H) and 6.05 (d, J = 5.6 Hz, 4H). UV-vis absorption spectrum recorded in dichloromethane: λ_{max} nm (ε, $M^{-1}cm^{-1}$): 589 nm (124700), 547 nm (63700) and 505 nm (94900).

Synthetic Procedure of IV.15

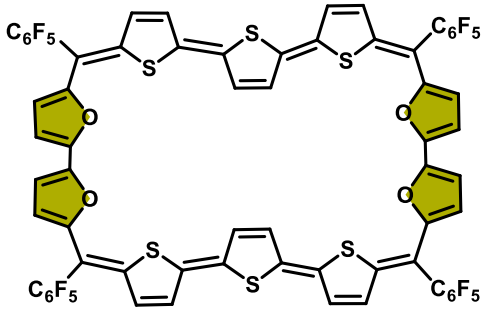

The reaction procedure for the synthesis of decaphyrin **IV.15** is similar to, **IV.13.** The reagents used: terthiophene diol, **IV.9**, (200.68 mg, 313.31 µmol), bifuran, **IV.12**, (41 mg, 305.66 µmol), $BF_3.OEt_2$ (377.24 µmL, 305.66 µmol) and DDQ (242.84 mg, 1.07 mmol) in 60 mL of dichloromethane. **IV.15** was isolated as metallic brownish-green solid in 3.1 % yield (6.9 mg).

Spectroscopic analysis: HR-MS (ESI-TOF): m/z Calcd. for $C_{68}F_{20}H_{20}S_6O_4$; $[M]^+$ 1471.9366 and $[M]^{2+}$ 735.9683; obtained, 1471.9408 and 735.9665. ^1H NMR (600 MHz, $(CD_3)CO$, 298 K) δ: 7.53 (d, J = 5.2 Hz, 4H), 7.22 (d, J = 4 Hz, 4H), 7.00 (s, 4H), 6.83 (d, J = 4 Hz, 4H), 6.81 (d, J = 5.6 Hz, 4H). UV-vis absorption spectrum in dichloromethane: λ_{max} nm (ε, $M^{-1}cm^{-1}$): 384 nm (112400), 494 nm (187000), 583 nm (41200) and 624 nm (52900).

Synthetic Procedure of $[IV.15]^{2+}$

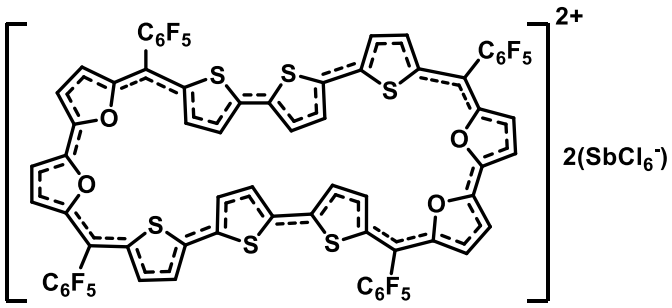

The dication of **$[IV.15]^{2+}$** was synthesised by addition of excess stoichiometric of Meerwein salt, $[Et_3O]^+[SbCl_6]^-$, in solution of **IV.15** in dichloromethane. The reaction was carried out at -20 °C. The instant color change was observed from brownish green to lighter green. Thereafter, the resulting solution was stirred for 25 mins at -20 °C. Then slowly allowed it to attain room temperature. The purple color solid formed, which further washed with pentane. The dicationic molecule **$[IV.15]^{2+}$** was obtained in quantitative yield (96%).

Spectroscopic analysis: HR-MS (ESI-TOF): *m/z* Calcd. for $(C_{68}F_{20}H_{20}S_6O_4)^{2+}$; $[M]^{2+}$ 735.9683; observed 735.9675. ^1H NMR (600 MHz, CD_3CN, 298 K) δ: 8.50 (d, *J* = 4.8 Hz, 2H), 8.48 (d, *J* = 4.8 Hz, 2H), 7.84 (d, *J* = 4.8 Hz, 2H), 7.74 (d, *J* = 4.8 Hz, 2H), 7.65 (d, *J* = 4.8 Hz, 2H), 7.57(d, *J* = 4.8 Hz, 2H), 6.96 (d, *J* = 4.2 Hz, 2H), 6.39 (d, *J* = 4.8 Hz, 2H), 6.10 (d, *J* = 4.2 Hz, 2H), 4.69 (d, *J* = 4.8 Hz, 2H). UV-vis absorption spectroscopy (CH_2Cl_2): λ_{max} nm (ε, $M^{-1}cm^{-1}$): 457 nm (129400) and 768 nm (296000).

Synthetic Procedure of IV.18

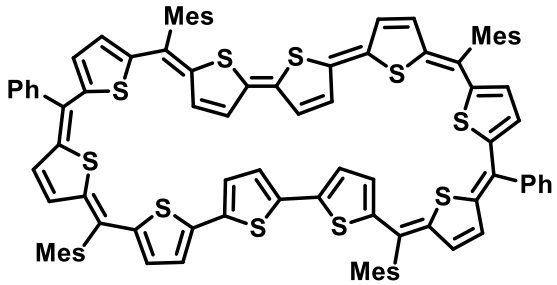

In a two-necked round bottom flask, ((phenylmethylene)bis(thiophene-5,2-diyl) bis((mesityl)methanol, **IV.17**, (567.53 mg, 1.03 mmol) and terthiophene, **IV.16**, (250.00 mg, 1.01 mmol) was charged and dissolved with 100 mL of dry dichloromethane under N_2 atmosphere. The BF_3OEt_2 (124.22 mmL, 1.01 mmol) was added drop wise and subsequently stirred for 2 hours under dark. Followed by addition of (124.22 mmL, 1.01 mmol) in open atmosphere condition for 2 hours. The resulting mixture was concentrated under vacuum and further purification was done in basic alumina column. After repetitive column and size exclusion chromatography in toluene, **IV.18** was isolated as brownish solid in yield 2.2% (17mg).

Spectroscopic analysis: HRMS (ESI-TOF): *m/z* Calcd. for $C_{94}H_{74}S_{10}$; $[M]^+$ 1522.2998 and $[M]^{2+}$ 761.1499; and observed 761.1470. ^{1}H NMR (400 MHz, toluene-d_8, 218 K) δ: 8.35 (s, 4H) 7.84 (br s, 8H), 7.49 (s, 8H), 7.25 (s, 10 H), 7.04 (s, 4H) 6.20 (br s, 4H). 2.39 (s, 12H, CH_3), 2.28 (s, 12H, CH_3), 2.12 (s, 12H, CH_3). UV-vis-NIR absorption spectrum (CH_2Cl_2): λ_{max} nm (ε, $M^{-1}cm^{-1}$): 432 nm (117800), 546 nm (sh), 605 nm (153800), 664 nm (sh), 725 nm (128700) and 966 nm (112900).

Synthetic Procedure of $[IV.18]^{2+}$

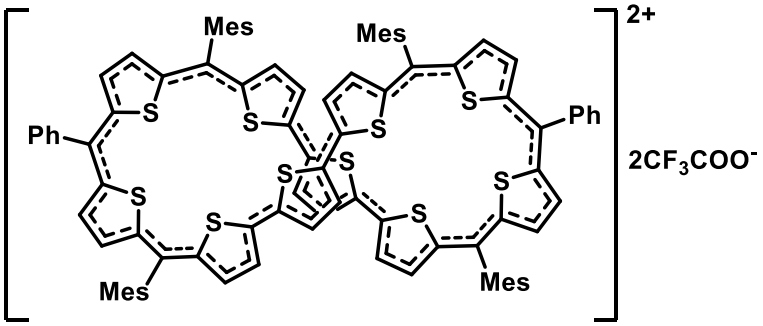

The synthesis of $[IV.18]^{2+}$ could be achieved by addition of a drop of trifluoroacetic acid in dichloromethane solution **IV.18**. The color of the solution immediately changes from blue to green and absorbance was shifted to red region and intense peak was observed.

Spectroscopic analysis: HR-MS (ESI-TOF): *m/z* Calcd. for $[C_{94}H_{74}S_{10}]^{2+}$; $[M]^{2+}$ 761.1499; observed 761.1487. ^{1}H NMR (400 MHz, dichloromethane-d_2, 203 K) δ: 8.12 (s, 2H), 7.97 (br s, 2H), 7.78 (br s, 2H), 7.65 (d, J= 4.12 Hz, 2H), 7.51(m, 3H), 7.44(m, 4H), 7.30 (d, J= 4.08 Hz, 2H), 7.26 (s, 2H), 7.20 (s, 2H), 7.13 (d, J= 7.04 Hz, 2H), 7.07 (d, J= 5.16 Hz, 2H), 7.04 (s, 1H), 6.98 (br s, 2H), 6.96 (d, J= 5.16 Hz, 2H), 6.93 (s, 2H), 6.89 (s, 2H), 6.83 (d, J=5.16, 2H), 6.77 (d, J= 5.12, 2H), 2.99 (s, 6H), 2.82 (s, 6H), 2.414 (d, 12H), 1.49 (d, 12H). UV-vis-NIR absorption spectrum (in CH_2Cl_2): λ_{max} nm (ε, $M^{-1}cm^{-1}$): 470 nm (125200), 698 nm (190100), 1008 (54000).

Compound	**IV.13**	**IV.15**	**IV.18**	**[IV.18]$^{2+}$**
Formula	$2(C_{68}H_{20}F_{20}S_{10})$	$C_{68}F_{20}H_{20}O_4S_6$	$C_{94}H_{74}S_{10}$	$(C_{94}H_{74}S_{10})^{2+}$
Temperature(K)	150(2)	100(2)	150(2)	150(2)
Crystal System	Triclinic	Monoclinic	Monoclinic	Monoclinic
Space group	P -1	P 21/c	P 21/c	P 21/c
Volume	5765 (3) Å^3	3138.6 (12) Å^3	5223 (2) Å^3	9255 (6) Å^3
a	12.453 (3)	18.288 (4)	18.258 (4)	23.966 (8)
b	21.757(6)	24.723 (5)	13.448 (3)	12.143 (4)
c	23.660 (6)	6.9501 (15)	21.934 (5)	32.204 (12)
α	66.193 (8)	90	90	90
β	79.426 (9)	92.813 (6)	104.115 (7)	99.057 (11)
γ	86.247 (8)	90	90	90
Z	3	2	2	4
Dcalc	1.329 g cm^{-3}	1.559 g cm^{-3}	0.969 g cm^{-3}	1.317 g cm^{-3}
R1	0.0893	0.0649	0.0754	0.0994
R2w	0.2642	0.1754	0.2407	0.3101
GOF	0.943	0.915	1.051	1.002

Table 4.3: X-ray crystal data of decaphyrins **IV.13, IV.15, IV.18 and [IV.18]$^{2+}$.**

References

1. D. Seidel and J. L. Sessler, *Angew. Chem. Int. Ed.*, **2003**, *42*, 5134-5175.

2. A. Jasat and D. Dolphin, *Chem. Rev*. **1997**, *97*, 2267 –2340

3. T. Okujima, C. Ando, S. Agrawal, H. Matsumoto, S. Mori, K. Ohara, I. Hisaki, T. Nakae, M. Takase, H. Uno, and N. Kobayashi, *J. Am. Chem. Soc.*, **2016**, *138*, 7540-7543.

4 J. L. Sessler, S. J. Weghorn, V. Lynch, and M. R. Johnson, *Angew. Chem. Int. Ed. Engl.*, **1994**, *33*, 1509-1511

5. (a) S. Shimizu, N. Aratani, and A. Osuka, *Chem. Eur. J.*, **2006**, *12*, 4909-4918. (b) Tanaka, Y.; Shin, J.-Y.; Osuka, A. *Eur. J. Org. Chem.* **2008**, 1341-1349.

6. A. Ghosh, S. Dash, A. Srinivasan, C. H. Suresh, S. Peruncheralathan and T. K. Chandrashekar, *Org. Chem. Front.*, **2019**, *6*, 3746-3753

7. N. Shivran, S. C. Gadekar, and V. G. Anand, *Chem. Asian J.* **2017**, *12*, 6-20.

8. (a) V. G. Anand, S. Saito, S. Shimizu, and A. Osuka, *Angew. Chem. Int. Ed.*, **2005**, *44*, 7244-7248T. Soya and A. Osuka *Chem. Eur. J*., **2019**, *25*, 5173 – 5176.

9. H. S. Udaya, A. K. Basavarajappa, T. Y. Gopalakrishna and V. G. Anand, *Chem. Commun.*, **2022**, *58*, 13931-13934.

10. H. Rath, V. Prabhuraja, T. K. Chandrashekar, A. Nag, D. Goswami, and B. S. Joshi, *Org. letters*, **2006**, *8*, 11, 2325-2328.

11. Y. Ni, T. Y. Gopalakrishna, S. Wu, and J. Wu, *Angew. Chem. Int. Ed.*, **2020**, *59*, 7414-7418.

12. M. D. Ambhore, P. Shukla, R. G. Gonnade and V. G. Anand, *Chem. Commun.*, **2022**, *58*, 8946-8949.

13. Z. Zeng, X. Shi, C. Chi, J. T. Lopez Navarrete, J. Casado and J. Wu, *Chem. Soc. Rev.*, **2015**, *44*, 6578-6596.

CHAPTER 5

Rational Synthesis of Phenylene Bridged Isophlorin-Porphyrin Dimer

5.1 Introduction

Porphyrin is 18π aromatic aza annulene macrocycle, found in many basic units of life such in chlorophyll, heomoglobin etc[1]. Similar to porphyrins, multiporphyrins arrays have gained significant attention as they are the synthetic models to mimic the biological light harvesting system and charge transfer processes of bacteria.[2] Extensive research has been carried out to study the interaction (or orientation) of two porphyrins in multiporphyrins, which affect the electron tranfer process in the artificial photosynthetic reaction centre[3]. Many covalently linked porphyrins dimer, trimers, pentamers were synthesised and characterised to further study their conformations and optical properties.[4] In dimers, these porphyrins were either linked with some spacer [3,4] **V.1** or they are *meso-meso* directly linked. Considering the importance of bridgeless porphyrins, in the year 1997 Osuka reported the first example of *meso-meso* connected dimer **V.2**, via oxidative coupling of zinc(II) 5,15-di(3,5-di-tert-butylphenyl)porphyrin[5]. In the same year Smith and co-workers reported a metal free porphyrin dimer[6], **V.3**. In extension of these dimers **V.4**, Osuka and co-workers reported an array of porphyrins which contains several porphyrin units and their oxidative coupling results in the formation of porphyrin molecular tape[7]. Hence these largely π-conjugated species could be better utilised as photonic materials and molecular devices as well.

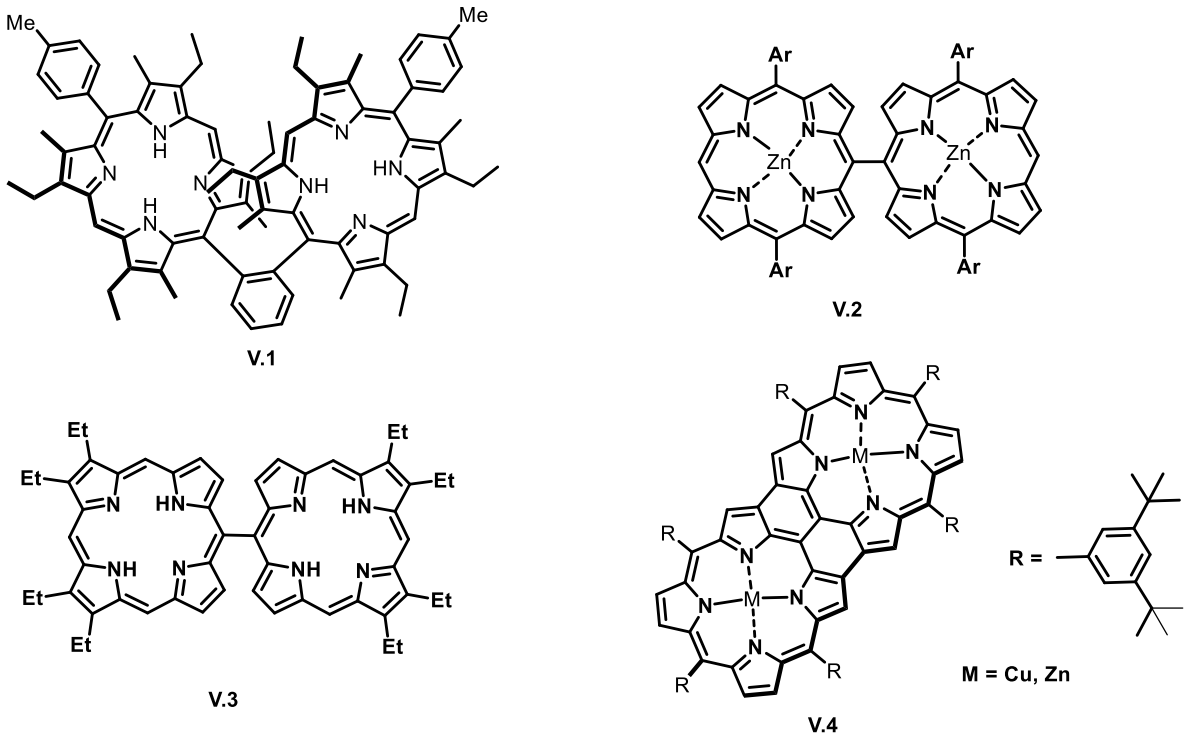

Fig 5.1: Porphyrin dimers.

In tune with porphyrin dimers, a serendipitious discovery of *meso-meso* linked antiaromatic tetraoxa isophlorin dimer **V.6** was reported by Anand and co-workers.[8] It was the first example reported by the coupling of two antiaromatic **V.5** monomer. During the course of crystallization of *meso*-free isophlorin **V.5** in presence of C_{60}- fullerene in toulene solvent, it yielded **V.6**, (Scheme 5.1), as the black colored crystals.

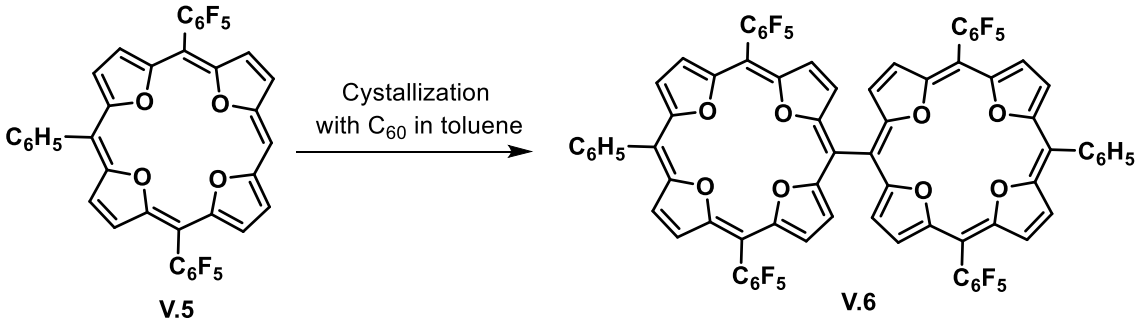

Scheme 5.1: Co-crystallization of isophlorin **V.5** with C_{60} fullerene.

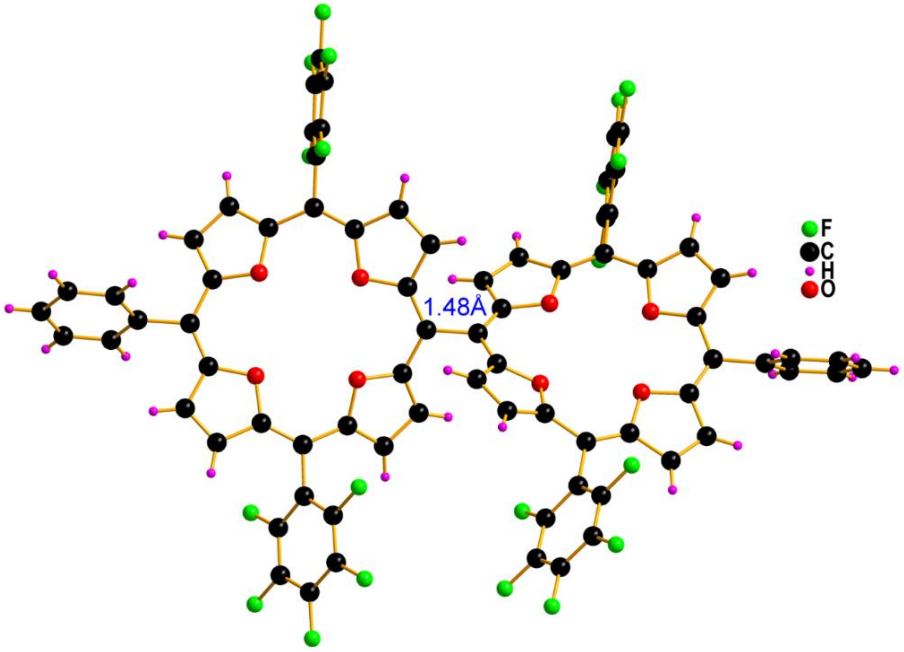

Fig. 5.2: Molecular structure of covalently linked isophlorin dimer **V.6**.

The X-ray diffraction analysis revealed, both the isophlorins were arranged in 35.57° to each other in **V.6**. **V.6** sustained its antiaromaticity as it resisted the formation of tetracation upon addition of the several oxidising agents. Hence, synthesis and characterisation of these antiaromatic synthons opens a new pathway to explore them as a potential organic electronic materials.

All these reported examples are either for porphyrin dimers or isophlorin dimer. But till date no examples of isophlorin-porphyrin dimer are reported in literature. The main interest for exploring the first phenylene bridged isophlorin and porphyrin dimer **V.7,** is to understand its electronic and redox properties. Consequently isophlorin-porphyrin coupled dimer consist of 20π and 18π electrons corresponding to isophlorin and porphyrin respectively. But due to synthetic challenge in functionalising the *meso* position of isophlorin, the 4-bromophenyl group was introduce at *meso* position of isophlorin **III.7** which can be further coupled with boronic acid derivative of porphyrin ring **V.10** (Scheme 5.2). Compared to porphyrin dimer and isophlorin dimer, the coupled isophlorin-porphyrin dimer could be the captivating material for study of electron transfer process as it contains two different electronic systems.

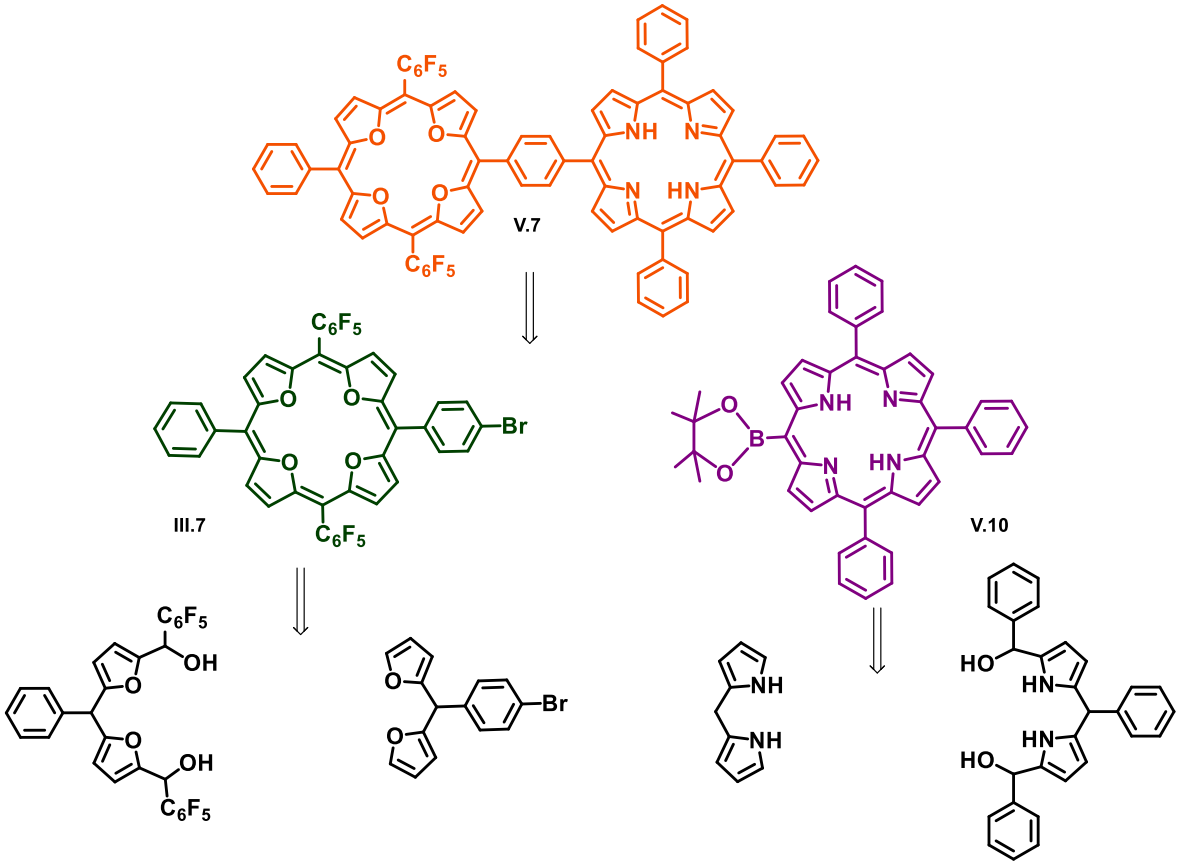

Scheme. 5.2: Retrosynthetic Pathway for Isophlorin-Porphyrin Dimer **V.7**.

The isophlorin **III.7** was synthesized by condensation of difuro dicarbinol with furan dipyrromethane under acidic conditions. The complete characterisation of **III.7** is discussed in detail in chapter 3. The macrocycle **III.7** contains 20π electrons in conjugation and displayed paratropic ring current. The calculated NICS (0) value for tetra-oxa isophlorin is +20.25 ppm

and it supports the antiaromatic character of **III.7**. The porphyrin **V.10** was obtained by the borylation of bromo porphyrin **V.9** through a reported procedure.[9] After multiple reactions and columns, the final compound **V.10** was isolated at 54% yields. The synthetic scheme is given below.

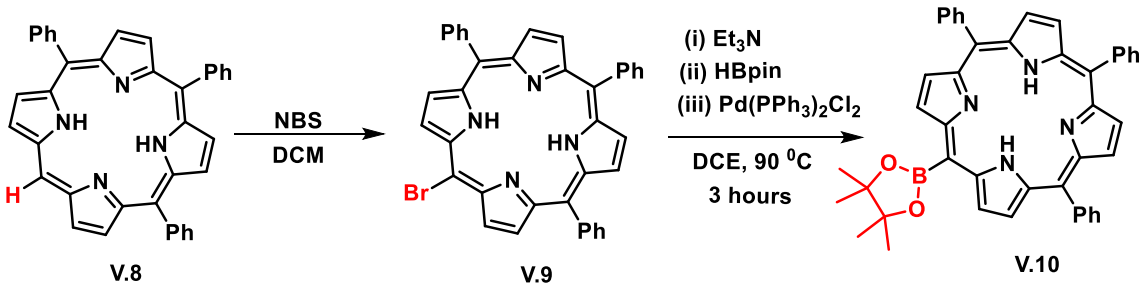

Scheme. 5.3: Synthesis of *meso*-borylated porphyrin **V.10**.

5.2 Synthesis of Isophlorin-Porphyrin Dimer V.7

The 20πe$^-$ containing isophlorin, **III.7**, was coupled with boronic acid derivative of porphyrin, **V.10**, using the optimized reaction condition of Suzukii-miyuara cross coupling[10] in presence of Pd catalyst (Scheme 5.4). After three hours of the reaction, MALDI-TOF/TOF mass spectrum revealed the formation of desired dimer **V.7**. The reaction mixture was passed through a short bed of basic alumina column and further purified via size exclusion column chromatography in toluene and **V.7** was obtained as orange color band in 20% yield.

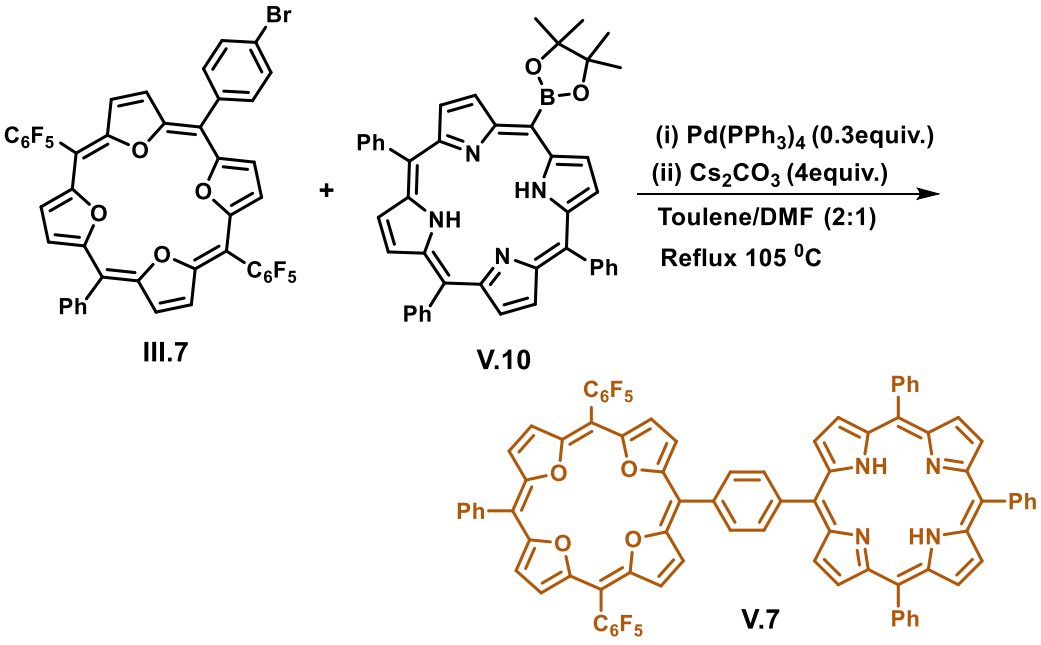

Scheme 5.4: Suzukii- Miyaura cross coupling reaction for the synthesis of Isophlorin Porphyrin dimer **V.7**.

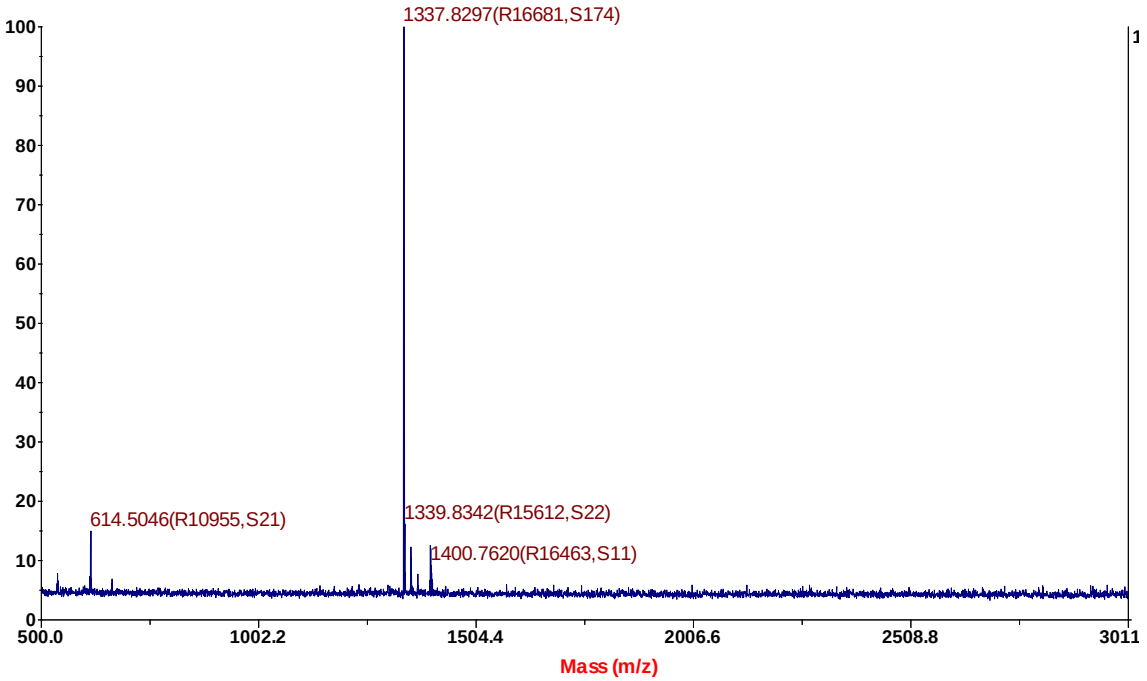

Fig. 5.3: MALDI-TOF/TOF mass spectrum of **V.7**

5.3 Characterization of dimer V.7

The molecule was characterized by appropiate several spectroscopic techniques like high-resolution mass spectrum, NMR spectra, UV-vis absorption spectroscopy.

HR-MS Spectrum of V.11

The exact composition of the molecule was confirmed by ESI TOF High-Resolution Mass Spectrum (HRMS). The parent molecule ion peak appeared at 1336.2975 along with the peak at 668.6545 (Calcd. for $C_{82}H_{42}F_{10}N_4O_4$; $[M]^+$ 1336.3046 and $[M]^{2+}$ 668.1523). supporting the formation of desired dimer **V.7**. The m/2 peaks represent the possibility of dication of dimer (Fig. 5.4).

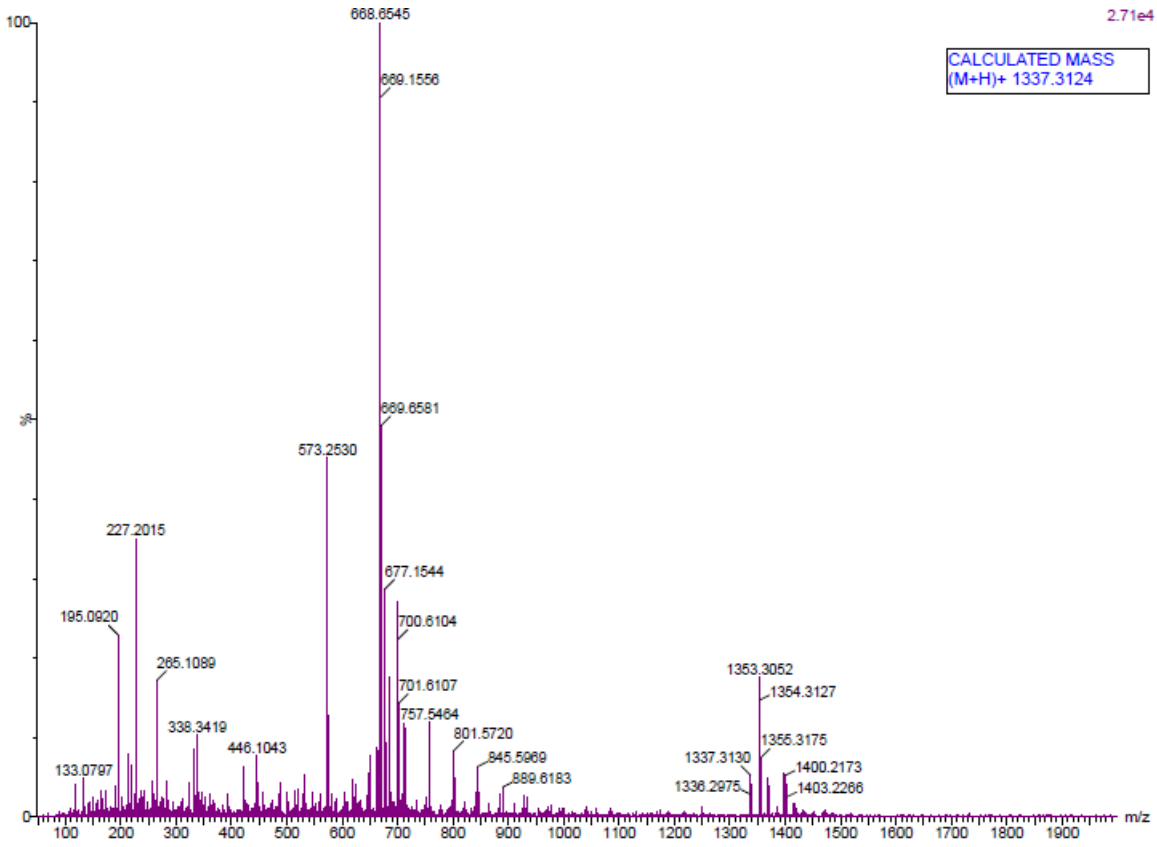

Fig. 5.4 HRMS spectrum of **V.7**.

NMR Spectrum of dimer V.7

The ^{1}H NMR spectrum of dimer was recorded at 298 K in chloroform-*d* solvent (Fig. 5.5). The obtained well resolved spectrum of **V.7** is clearly suggested the formation of desired molecule. A multiple number of signals were present in the shielded and deshielded region between δ -2.93 to 8.79 ppm. The signals in downfield regions at δ 8.78, 8.66 and 8.32 ppm for corresponding to 4H, 2H and 2H respectively represent the β C-H of pyrrole rings of the porphyrin molecule. The inner N-H protons of the porphyrin ring was found resonating in the upfield region at δ -2.93 ppm. And hence it clearly supports the diatropic ring current of 18π porphyrin ring as the outer protons were resonating in downfield region and inner protons in upfield region. In stark contrast, the four signals in upfield region at δ 3.03, 2.60, 2.56 and 2.42 ppm corresponding to two protons each belongs to β C-H of furan rings of isophlorin moiety. These signals observed in upfield region for isophlorin suggests the paratropicity of the ring. The multiple signals in between the region of δ 6.38 to 8.17 ppm for 24 protons are accorded to phenyl rings of the *meso*-substituents.

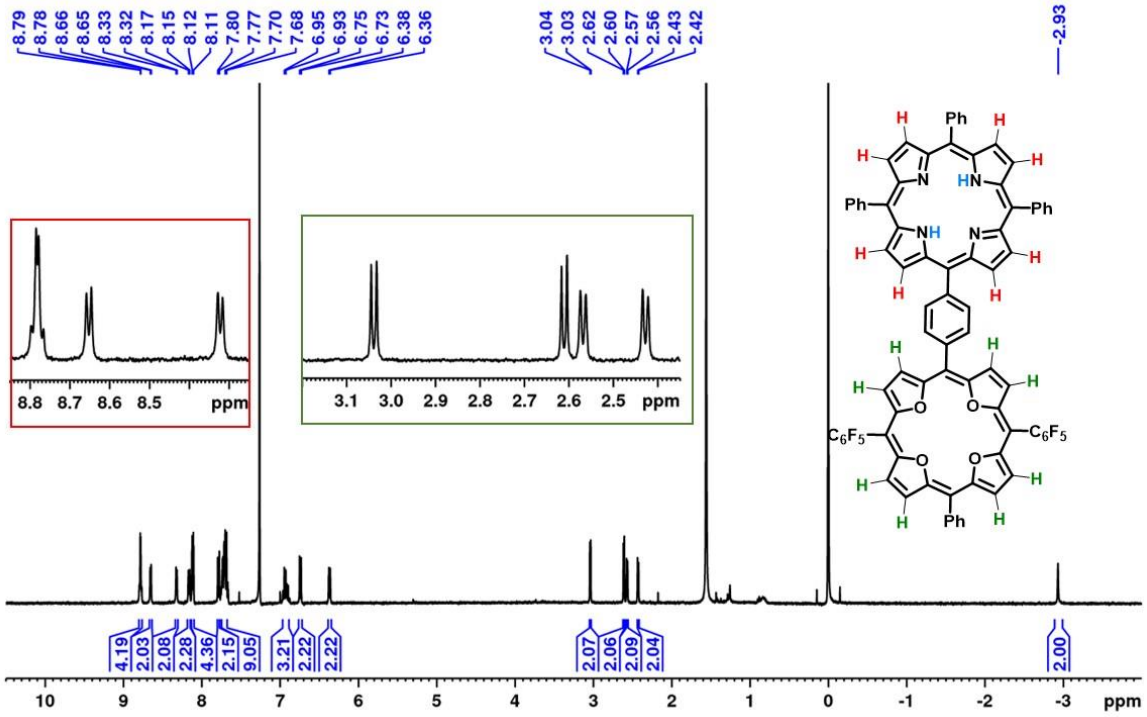

Fig. 5.5 ^{1}H NMR spectrum of **V.7** recorded in $CDCl_3$ at 298 K.

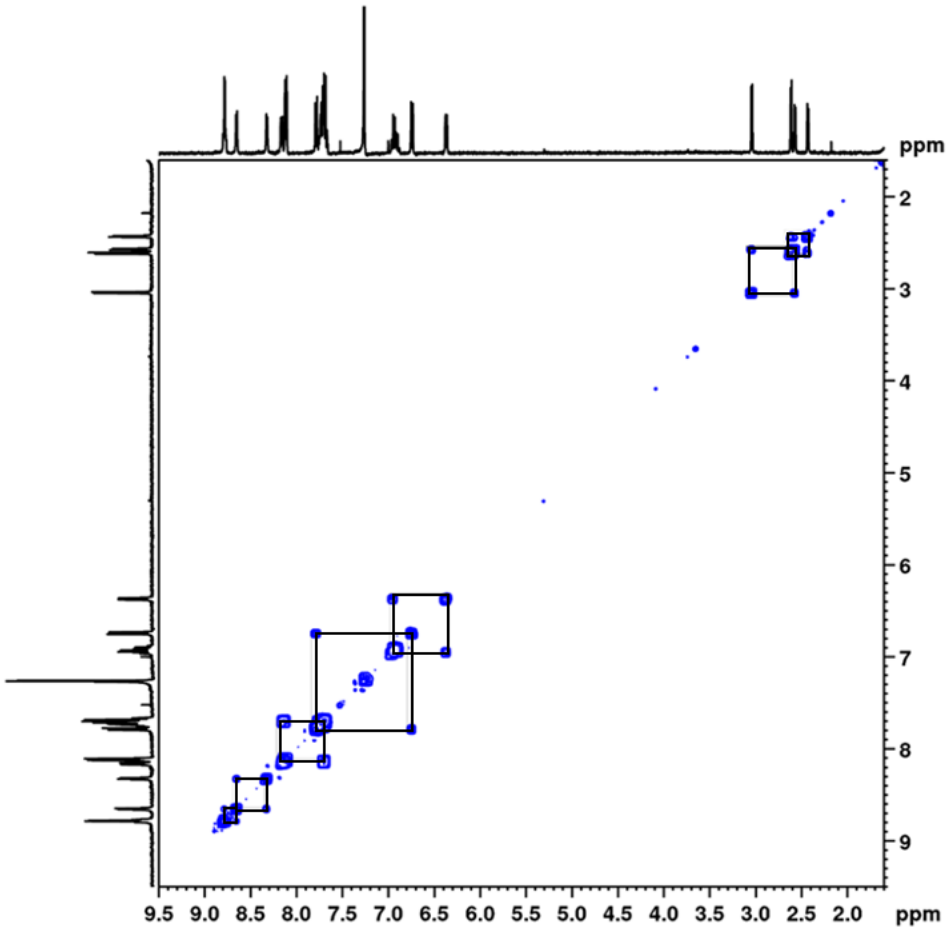

Fig. 5.6 ^{1}H -^{1}H COSY spectrum of dimer **V.7** recorded in $CDCl_3$ at 298 K.

Two-dimensional ^{1}H NMR spectroscopy (Fig. 5.6) helps to assign the correlations between the adjacent protons. The proton signal at δ 8.66 ppm was correlating with signal at δ 8.78 and 8.32 ppm and hence confirming the contribution from the porphyrin ring. The other two sets of correlation observed between the signals (3.03, 2.60 and 2.56, 2.42) ppm is assigned to isophlorin moiety. The phenyl protons were showing the three cross peaks for the 24 protons, as they were merged to each other. Therefore, the presence of signals from isophlorin moiety and porphyrin moiety confirmed poor the coupling between both the rings.

A comparative study of ^{1}H NMR spectrum shows the shift in values of NMR signals (Fig. 5.7). The β C-H of pyrrole ring of **V.7** is upfield shifted compared to its β C-H of porphyrin **V.10**. Whereas, a slight change was observed in the N-H protons signal at δ 2.80 ppm in **V.10** to 2.93 ppm in **V.7**. Also, the ^{1}H signals from isophlorin part of **V.7** are downfield shift compare to its precursor **III.7**. Due to the shielding and de-shielding of the signals in **V.7** compared to its precursor **III.7** and **V.10** it supports the electronic coupling between the isophlorin and porphyrin in **V.7**.

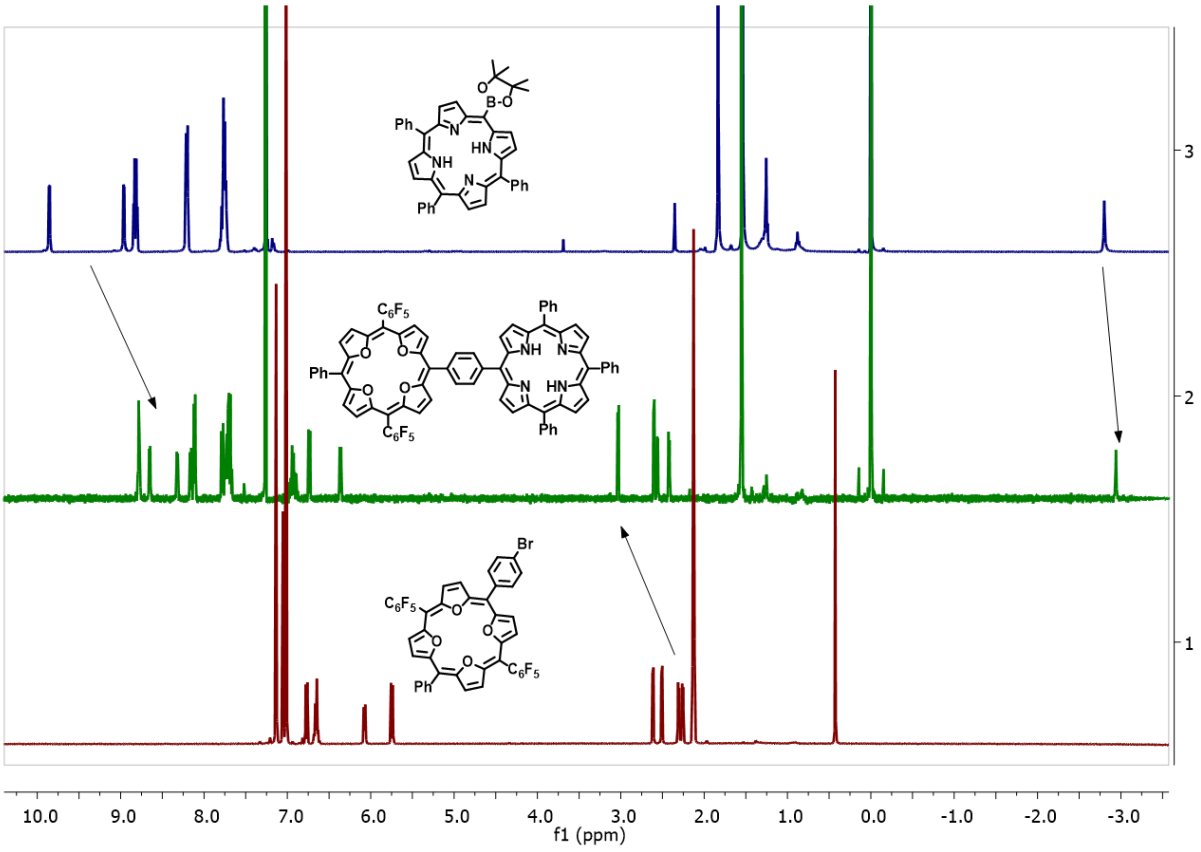

Fig. 5.7: Comparative ^{1}H NMR spectra of **V.10** (blue spectrum), **V.7** (green spectrum) and **III.7** (red spectrum).

UV-vis Absorption spectrum of V.7

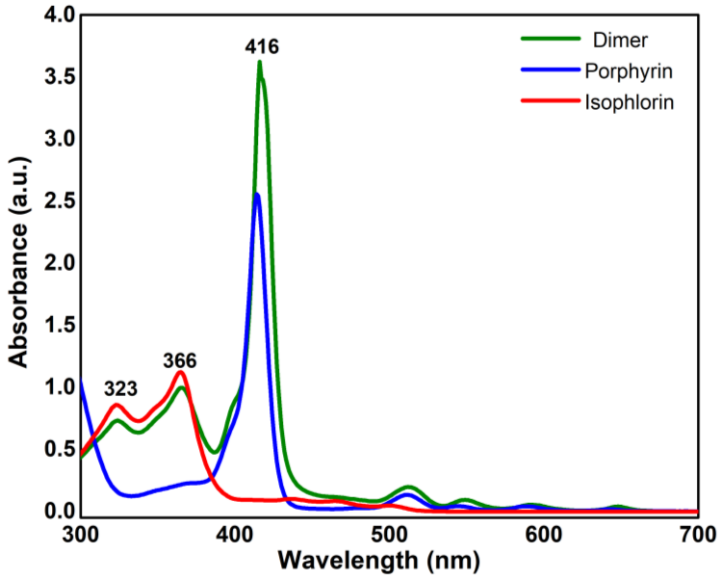

Fig. 5.8: UV-vis absorption spectrum of **V.7** (green spectrum), **V.10** (blue spectrum), and **III.7** (red spectrum) recorded in dichloromethane.

The absorption spectrum of **III.7** (Fig. 5.8) shows an intense absorption at 325 nm and 365 nm along with the Q-like bands in region between 400-500 nm. While **V.10** displayed the characteristic intense absorption at 417 nm along with four Q-like peaks, corroborating with reported porphyrins. The electronic absorption feature of dimer **V.7** (Fig. 5.8, green spectrum) displayed an intense Soret like peak at 422 nm and two blue shifted peaks at 325 and 365 nm along with four Q-band like bands at 514, 550, 590 and 644 nm. Hence electronic absorption of **V.7** holds contribution from both the isophlorin **III.7** and borylated porphyrin **V.10** moiety. It further supported the electronic exchange/coupling between isophlorin and porphyrin moiety in support of the NMR findings of **V.7**.

5.4 Quantum Chemical Calculation

The energy optimized structure of **V.7** dimer was obtained from Chem Draw structure using the B3LYP/6-31G(d,p) level of theory in DFT calculations using Gaussian 09 software.[11a] In the optimized structure (Fig. 5.9), both the isophlorin and porphyrin were arranged orthogonal to the phenylene ring. The porphyrin retains its planarity whereas, isophlorin was slightly distorted compared to its monomeric form **III.7**.

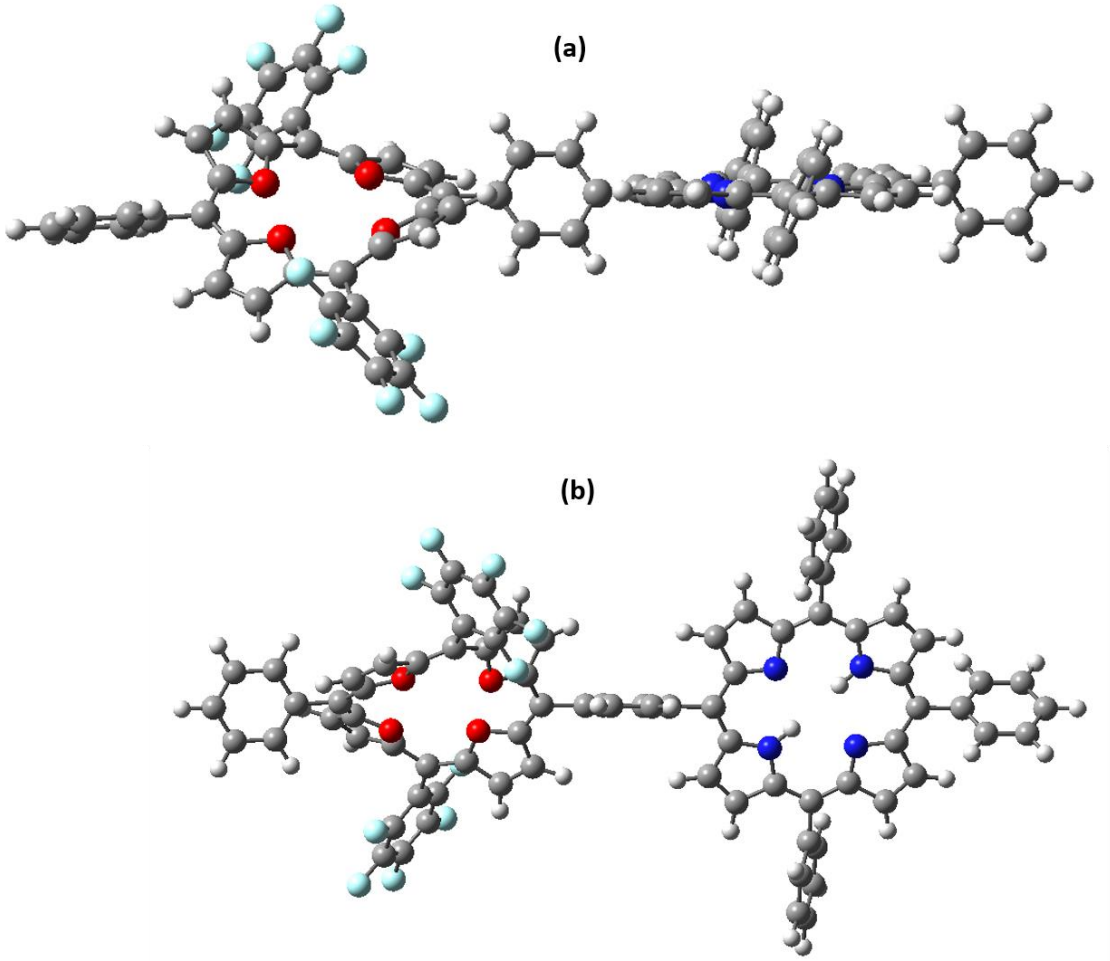

Fig. 5.9: Energy optimized structure of isophlorin-porphyrin dimer **V.7**. Images (a) and (b) represent the different orientations of the molecule.

To further validate the experimental findings from NMR and UV-vis absorbance studies, the Nuclear Independent Chemical Shift (NICS) value of the macrocycle **V.7, V.10** and **III.7** was calculated. The NICS is magnetic criterion of aromaticity and concept was first introduced by P.V.R Schleyer.[11b] The negative value of NICS represents the aromatic character of the molecule whereas, the positive value indicates the antiaromatic character. The NICS values were obtained using Gauge independent atomic orbital (GIOA) method and calculated for the dummy atom at the non-weighted mean centre of the macrocycles. Fig. 5.10, shows the NICS(0) values of all the three compounds at the centre of the ring.

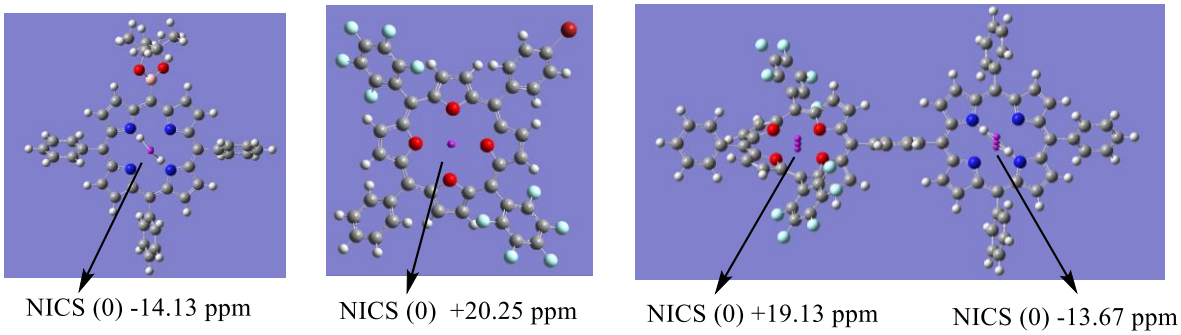

Fig. 5.10 Computed NICS(0) values of **V.10**, **III.7** and **V.7,** using the B3LYP/6-31G(d,p) level of theory.

The estimated NICS(0) value for **V.10** is -14.13 ppm confirming its aromatic behavior whereas, the **III.7**, shows the value of +20.25 ppm in support of antiaromatic character. In isophlorin-porphyrin coupled dimer **V.7**, the NICS(0) value varies in comparision to its starting units **III.7** and **V.10**. The porphyrin part of dimer **V.7** displayed the NICS(0) -13.67 ppm, suggesting the slight shielding compared to **V.10**, whereas the isophlorin part shows NICS(0) of +19.13 ppm, represent de-shielding in the antiaromatic congener compare with **III.7**. Hence varying ring current in **V.7** compared to its starting macrocycle **V.10** and **III.7** supporting its electronic coupling.

5.5 Chemical Oxidation of V.7

Two-electron oxidation of 20π tetra-oxa-isophlorin **III.7** to its 18π dicationic specie **[III.7]$^{2+}$** is described in the chapter 3. The **[III.7]$^{2+}$** was isolated and characterised through multiple spectroscopic techniques. The oxidation of phenylene bridged isophlorin-porphyrin dimer **V.7** was explored to check the feasibility of redox when both the antiaromatic and aromatic systems present in the same molecule **V.7**. The **V.7** was oxidised with Meerwein salt[12] $[Et_3O]^+[SbCl_6]^-$ and subtle a change in colour from orange to green was observed. The preliminary UV-vis absorption spectrum displayed a change in absorbance (Fig. 5.11). It showed a red shifted absorbance compared to its free base form **V.7**, hence suggesting the oxidation of **V.7** to **[V.7]$^{2+}$**.

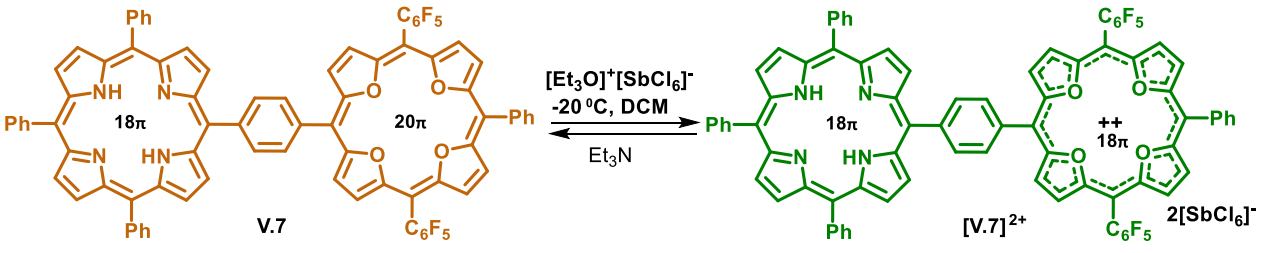

Scheme 5.5: Reversible chemical oxidation of **V.7** to **[V.7]$^{2+}$**.

UV-Visible Absorption Spectrum of $[V.7]^{2+}$

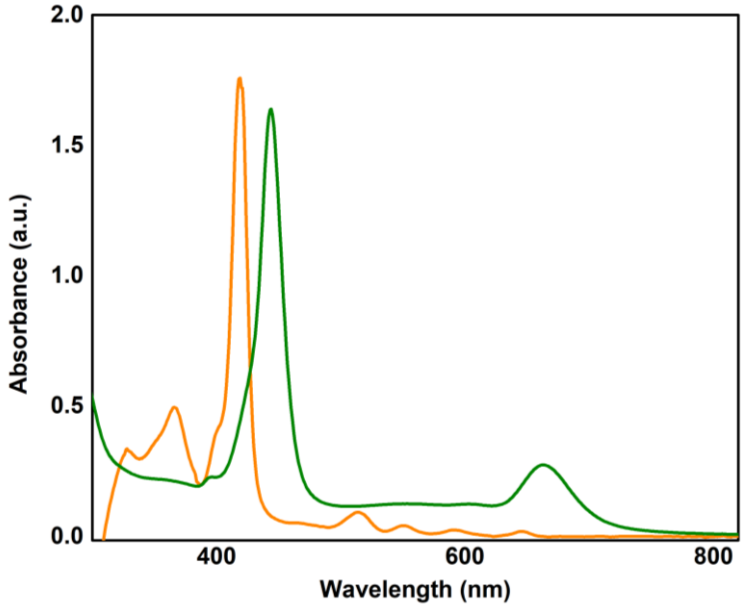

Fig. 5.11: UV-visible absorption spectrum of **V.7** (orange color) and $\mathbf{[V.7]^{2+}}$ (green color).

$\mathbf{[V.7]^{2+}}$shows the 22 nm red shifted absorption band with an intense band at 444 nm, along with broad peak at 663 nm. The Soret band was split into two bands and surprisingly, no Q-bands were observed in the spectrum. In above explained reaction (scheme 5.5), the reversible transformation of $\mathbf{[V.7]^{2+}}$ to **V.7** could be achieved by the addition of triethylamine to the solution of $\mathbf{[V.7]^{2+}}$.

NMR Studies of $[V.7]^{2+}$

The ^{1}H NMR spectrum of $\mathbf{[V.7]^{2+}}$ was recorded in 400 MHz in acetronitrile-d_3 at 298 K. The ^{1}H NMR spectral pattern of $\mathbf{[V.7]^{2+}}$ is different from **V.7**. The observed NMR displayed peaks in the downfield region along with the one broad signal at upfield region. In ^{1}H NMR spectrum of **V.7**, the signals present between 2-3 ppm for β C-H of furan rings vanished in case of $\mathbf{[V.7]^{2+}}$**.** The four doublets at δ 11.06, 10.85, 10.72 and 10.61 ppm corresponding of two protons each reflect the de-shielding of β C-H protons of furan rings. In stark contrast, the signals for β C-H protons of pyrrole rings were found to resonate in downfield region at δ 9.44, 9.39, 9.28 and 9.06 ppm. One broad signal at δ -1.76 ppm corresponding to two protons is assigned to N-H of pyrrole rings. Other four signals as multiplets were found resonating at δ 8.85, 8.80, 8.63 and 8.16 ppm corresponding to phenylene protons. A comparative study for ^{1}H NMR signals of **V.7** and $\mathbf{[V.7]^{2+}}$, shows significant change in chemical shift values of β C-H of furans rings from shielded to deshielded region in its NMR spectrum (Fig. 5.12).

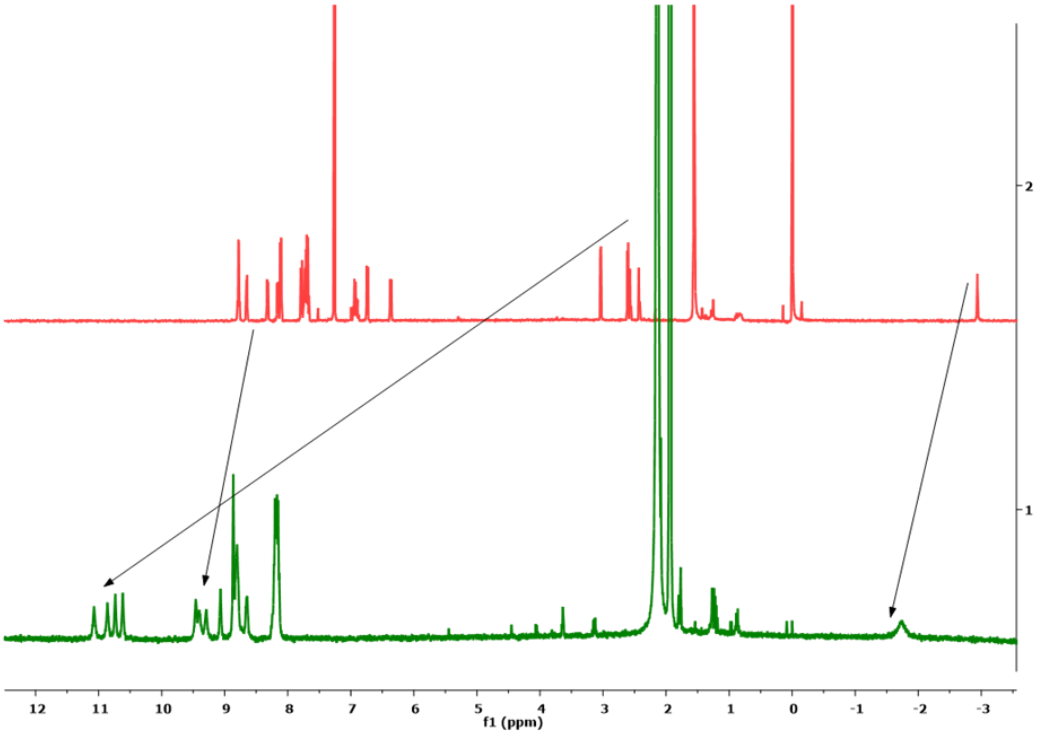

Fig. 5.12: Comparison of ^{1}H NMR spectrum of **V.7** (above) and **[V.7]**$^{2+}$(below).

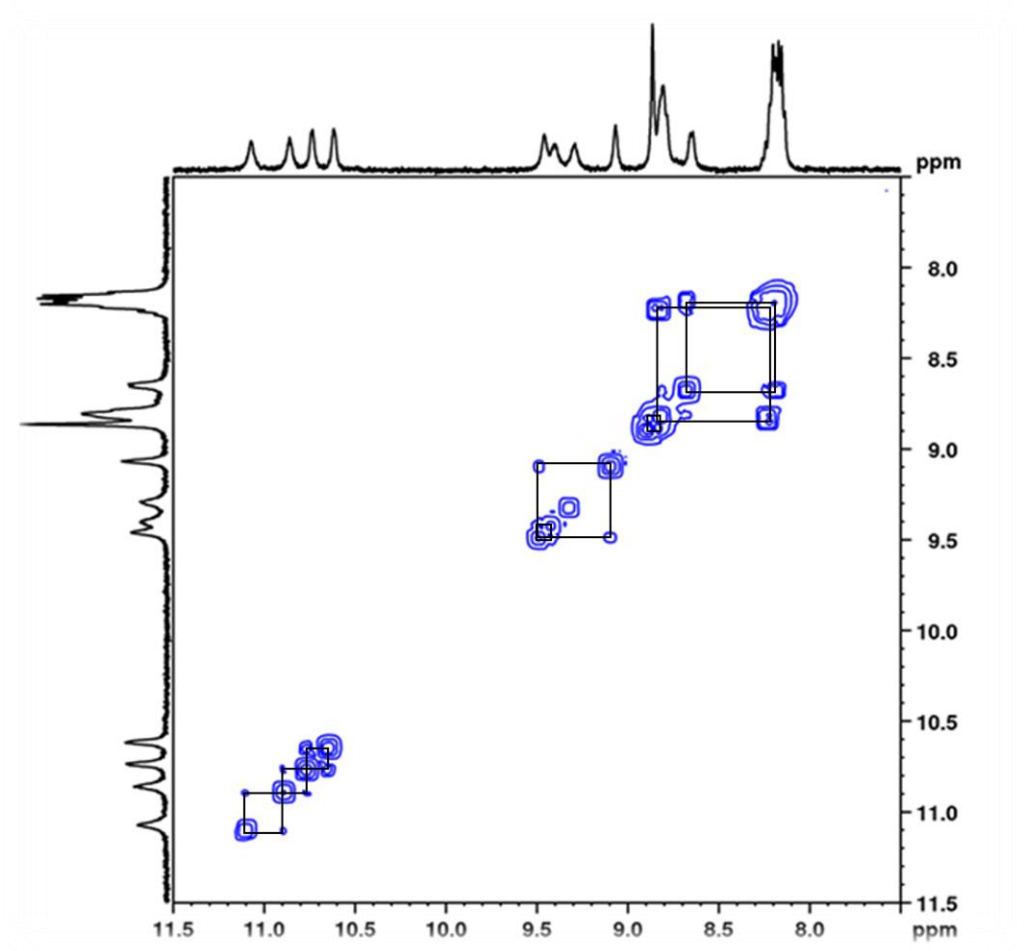

Fig. 5.13: ^{1}H -^{1}H correlation spectrum of dimer **[V.7]**$^{2+}$.

Hence, the careful inspection from ^{1}H NMR of **[V.7]$^{2+}$** suggest the selective oxidation of isophlorin moiety over the porphyrin moiety. In nutshell, the dimer, **V.7**, containing phenyl spacer between 18π aromatic specie and 20π antiaromatic specie convert to 18π neutral and 18π dicationic isophlorin upon oxidation (Scheme 5.5). Therefore, in presence of oxidising agent the antiaromatic-aromatic dimer **V.7** convert into aromatic-aromatic coupled dimer **[V.7]$^{2+}$**. Further the 2D NMR spectroscopy, reveals the correlation between the two sets of doublets (11.06, 10.85 and 10.72, 10.61) for the β C-H protons of furan rings. Similarly, three sets of correlation between the ((9.44, 9.39), (9.39, 9.28) and (9.44, 9.06)) ppm suggests the coupling of eight pyrrolic protons. The other correlations in region between 8-9 ppm correspond to phenyl ring protons (Fig. 5.13)

Therefore, compared to isophlorin dimer, **V.6**, the isophlorin-porphyrin dimer, **V.7**, is responsive towards oxidising agents and led to formation of dication **[V.7]$^{2+}$**. Hence the incorporation of electron rich isophlorin, **III.7**, in dimer **V.7**, make it more facile towards reversible redox process. Secondly, in dimer **V.7** since only isophlorin (not porphyrin) undergoes the oxidation, it was curious to study the redox nature of this dimer through electrochemical process.

5.6 Redox Behaviour of V.9

The porphyrin being 18π stable aromatic (4n+2) species, follow the (4n+2)π Huckel's rule of aromaticity. Upon oxidation/reduction it forms 4nπ species, because of electronic destabilisation, isolation and study of these molecules is not easy task. Hence there are scarce examples where porphyrins are obtained in oxidised form or as 16π species. In 2005, Yamamoto and his group reported octaethyltetraphenylporphyrin (OETPP), **V.11**, as a quiet unstable compound and which could be stored at -4 °C. To enhance the stability of **V.11**, its β substituents were replaced by the bulky group (*i*-Bu) to yield octa*iso*butyltetraphenylporphyrin (*iso*BuTPP), **V.12**. Both **V.11** and **V.12** adopted a distorted nonplanar structure confirmed through single crystal X-ray analysis, where the CH_2Cl_2 and H_2O were interacting with the macrocycles.[13] In UV-vis absorption spectra the Soret band of both **V.11** and **V.12** was blue shifted compared to its 18π porphyrin. There are few examples of 16π porphyrins **V.13**, **V.14**, **V.15** which are stabilised with metalation of its inner core.[14,15,16] Vaid and group reported the metal stabilised [Li(TPP)][BF_4] complex **V.13** having antiaromatic character, where β C-H protons were upfield shifted δ = 5.94 ppm compared to its 18 π porphyrin (δ = 8.91 ppm). It

shows an intense absorption bands at 332 and 394 nm. The detailed study of 16π system gives a general trend of distorted structure, blue shifted absorption, positive NICS value in compare to the free base 18π porphyrins.

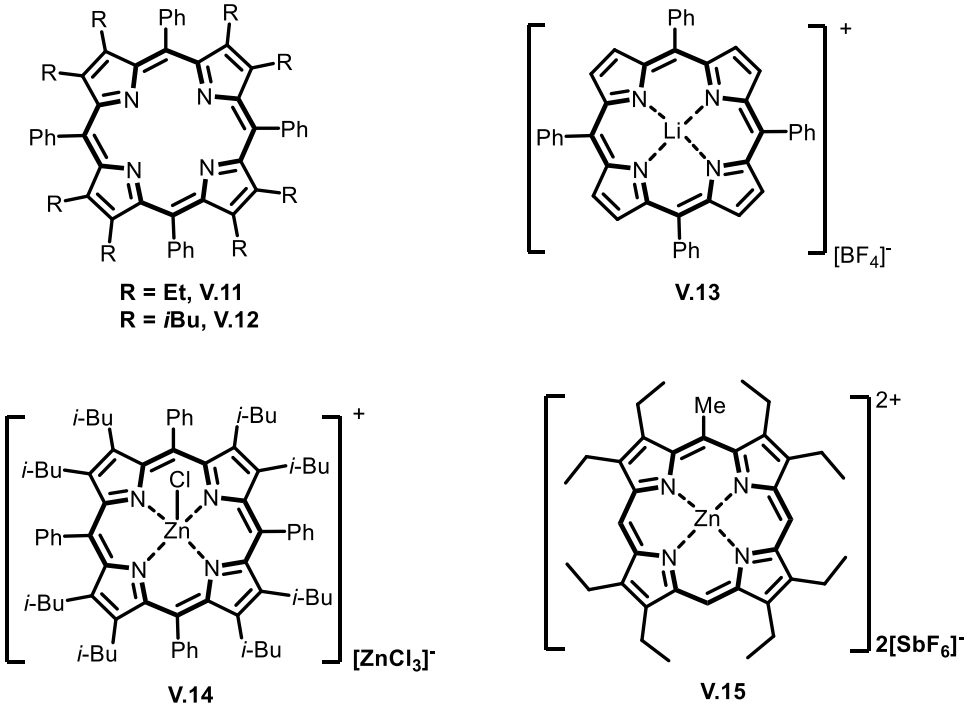

Fig. 5.14 Examples of 16π porphyrins.

All the above reported examples were found to show 16π electronic state of porphyrin and beyond that no such reports are available for e.g., 14πe$^-$ porphyrin. From a previous study of aromatic expanded porphyrins, it is observed that molecules like hexaphyrin and octaphyrins undergo four and six electron redox process respectively, via successive two step, two electron oxidation process through proton coupled electron transfer reaction.[17] Considering the same, porphyrin molecule can be expected to yield 14π species with successive two step two electron transfer reaction of 18πe$^-$ porphyrin. The 14πe$^-$ porphyrin follows the (4n+2)π Huckel's rule of aromaticity and expected to be more stabilised compare to its 16π neutral or charged species.

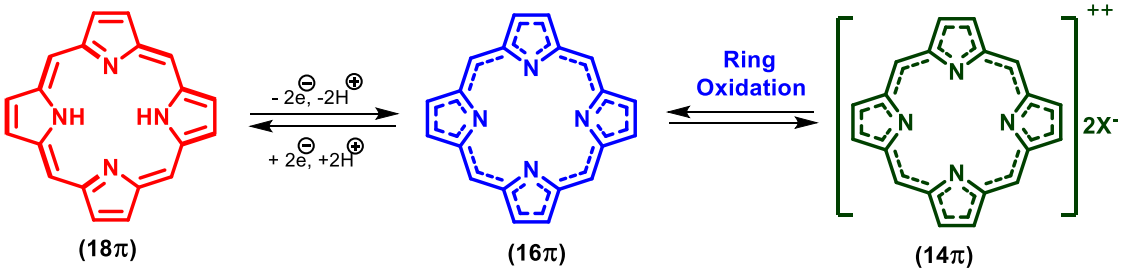

Scheme 5.6: The plausible reversible oxidation of porphyrin.

The *meso*-bromo-porphyrin **V.9** was employed to the study the reversible oxidation of 18π porphyrin. The macrocycle **V.9** was synthesized by a reported procedure through multi step synthesis.[9b]

5.7 Cyclic Voltammetry Experiment of V.9

For examing the redox behaviour of **V.9**, the cyclic voltammetry (CV) was performed using electrolyte solution 0.1 M TBAP in CH_2Cl_2 and three electrode system (calomel as reference electrode). It displayed the four reversible oxidations at 0.47, 0.70, 1.10 and 1.34 V and it was further supported by differential pulse voltammetry (DPV). The **V.9** showed four reductions at -0.44, -0.91, -1.22, -1.57 V (Fig. 5.15). Compared to (H_2TPP) tetraphenylporphyrin[18] and other metalated porphyrins[15,16] an increased number of oxidation peaks was interesting. Therefore, CV represents the possibility of four electron oxidation of 18π porphyrin **V.9** to 14π species of porphyrin. Encouraged with the electrochemistry results we performed the chemical oxidation of **V.9**.

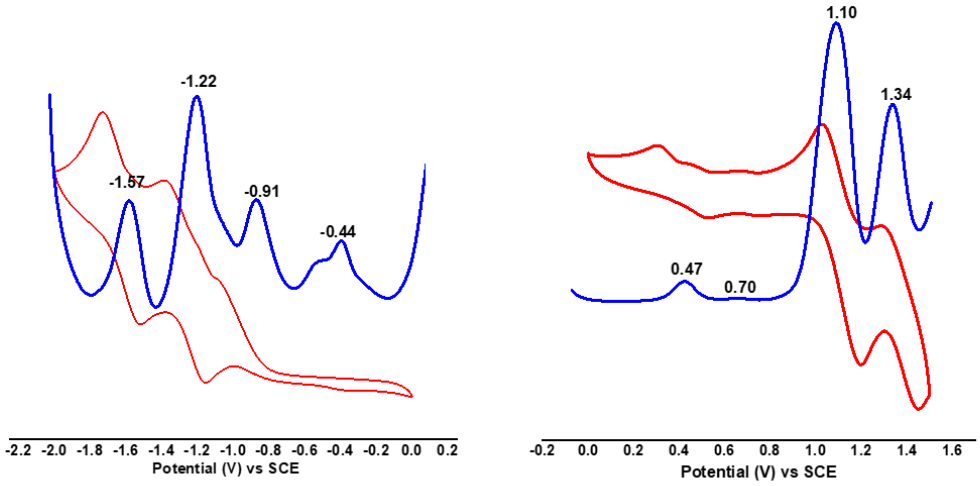

Fig. 5.15: Cyclic voltammetry (red line) and differential pulse voltammetry (blue lines) experiments of **V.9**. (a) reduction, (b) oxidation.

Chemical Oxidation of V.9

Porphyrin **V.9** upon chemical oxidation with stiochiometric excess of Meerwein salt[12] $[Et_3O]^+[SbCl_6]^-$ shows the subtle change in color from red to green and indicating the chemical oxidation suggesting the possiblity of two electrons and four electrons oxidation of macrocycle **V.9** (Scheme 5.7).

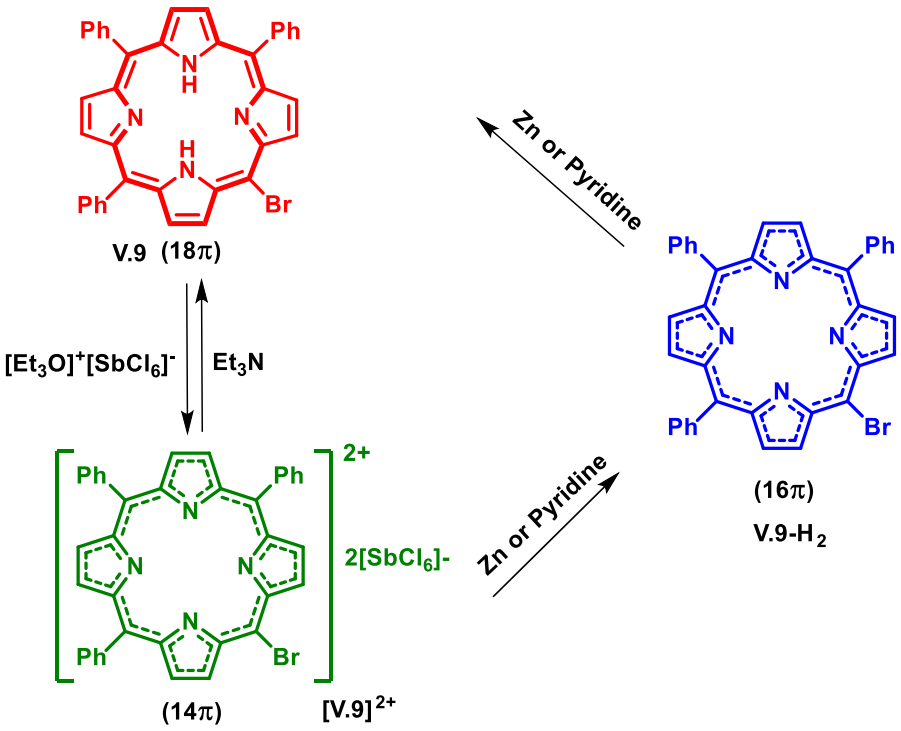

Scheme. 5.7. Possible redox stages of **V.9** through chemical oxidation.

UV-vis study of V.9 and oxidised states

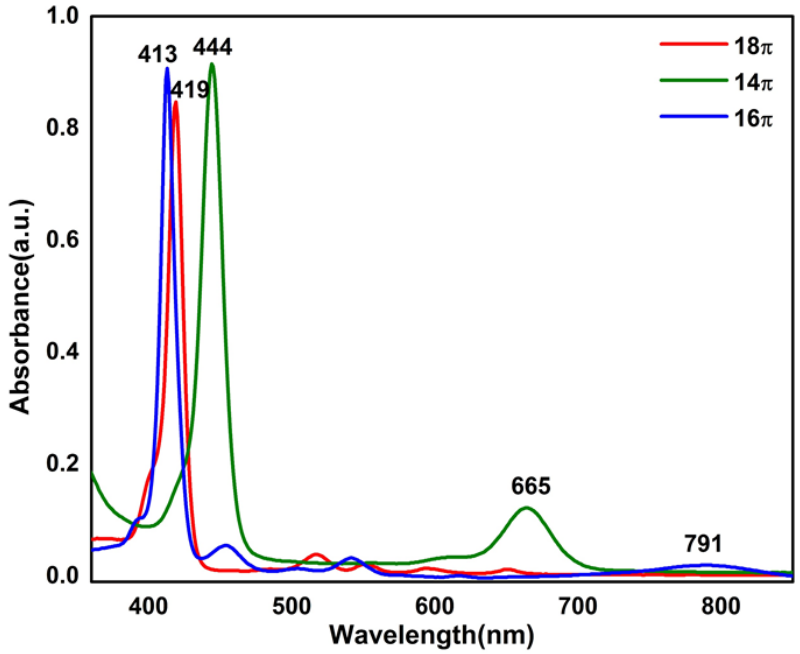

Fig. 5.16 UV-visible absorption spectrum of **V.9** (red lines) and its oxidised species.

The free base porphyrin **V.9** showed electronic absorption with a Soret-like band at 419 nm along with Q-bands at higher wavelength region between 500 - 700 nm. Whereas the oxidised species **[V.9]**$^{2+}$ displayed red shifted absorption bands, as displayed Soret like band at 444 nm along with a broad hump at 665 nm (Fig. 5.16, green line). Suprisingly, it shows the contradiction with the reported 16π porphyrins[13,14,15,16] (blue shifted Soret band). Hence, suspected the molecule **[V.9]**$^{2+}$, to be the other oxidised state rather than 16π electronic state. Curiously, we added some electron donating source to **[V.9]**$^{2+}$ and after 5 mins of stirring we observed the color change from green to orange. In electronic absorption study of the orange colour compound displayed the blue shifted absorption at 413 nm, compare to its free base porphyrin **V.9**, 18πe^{-}, and oxidised specie **[V.9]**$^{2+}$. Therefore, we suspected the orange color compound could be the intermediate state of **V.9** and **[V.9]**$^{2+}$ and it may contain 16πe^{-} (**V.9-H$_2$**). As cyclic voltammogram suggested four electron oxidation therefore **[V.9]**$^{2+}$ could be the 14π species. The macrocycle **[V.9]**$^{2+}$ was characterised with NMR and single crystal x-ray diffraction but **V.9-H$_2$** being unstable in nature, hampared the further characteristion.

5.8 ^{1}H NMR Study of [V.9]$^{2+}$

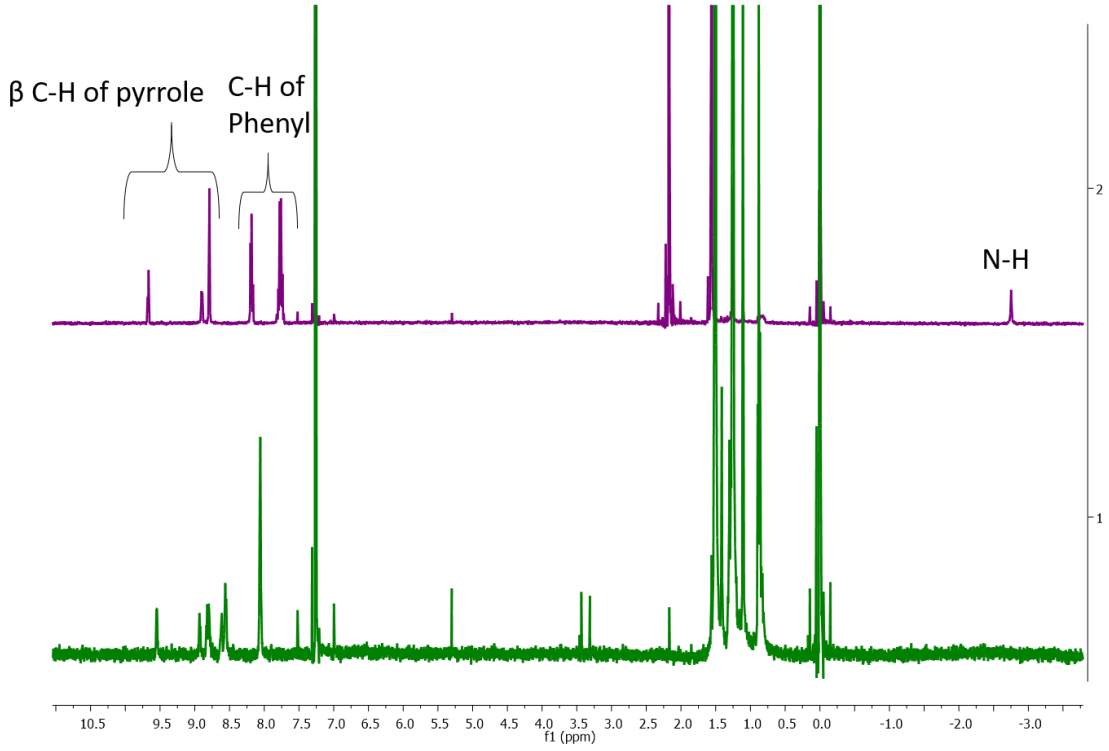

Fig. 5.17 Comparative study of ^{1}H NMR spectra of **V.9** (purple spectrum) and **[V.9]**$^{2+}$ **(**green spectrum).

V.9 is (4n+2)π aromatic molecule and its outer protons resonate in the downfield region whereas, the inner protons resonate at upfield region. The large difference between the most shielded and deshielded protons supports it diatropic ring current. The NMR spectrum of **[V.9]**$^{2+}$ was recorded in $CHCl_3$ at 298 K. It displayed peaks in the downfield regions for the β-CH protons of pyrrole rings and also for phenyl ring protons. But there no signal was observed for N-H proton in shielded region compared to its free base porphyrin **V.9** (δ = -2.74 ppm). Therefore, the absence of N-H signal shows the proton coupled electron transfer in **[V.9]**$^{2+}$. Secondly, the position of the β C-H signal is same as **V.9** and hence it represents the conversion of (4n+2)π free base to oxidised dicationic (4n+2)π species. So **[V.9]**$^{2+}$ will have 14π electrons in the conjugated backbone obtained from four electron oxidation of **V.9**.

5.9 Molecular Structure of [V.9]$^{2+}$

X-ray single crystal of the molecule was obtained by recrystallization of reaction mixture with dichloromethane. Good quality crystals was mounted and molecule crystallizes in triclinic P-1 space group.

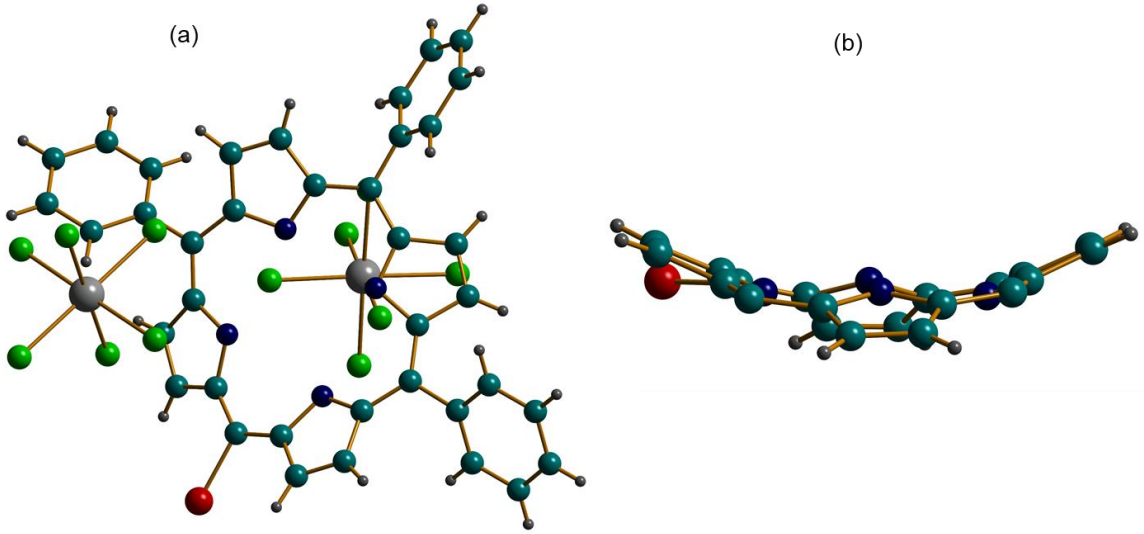

Fig. 5.18 X-ray single crystal structure of **[V.9]**$^{2+}$ **(a)** top view **(b)** side view, *meso* substituents were omitted for clarity.

The molecule **[V.9]**$^{2+}$ adopted a saddle shape and along with macrocyclic backbone, the two counter anions were present. All the nitrogen atoms are present as amine type in the core of macrocycle and *meso* substituents were almost perpendicular to plane. The presence of counter

anion suggested the ring oxidation and negative charge of counter anion balanced the two positive charge on the macrocycle (Fig. 5.18). Hence this molecule **[V.9]$^{2+}$** underwent the PCET as well as the ring oxidation and therefore lost the four electrons from macrocyclic framework. Therefore, the molecular structure confirms the 14πe^{-} dicationic species **[V.9]$^{2+}$**. In the crystal packing of **[V.9]$^{2+}$** the oxygen molecule (from water) was present to coordinate with the all four nitrogen of porphyrin ring.

5.10 Quantum Chemical Calculation

To support the experimental data, the NICS value was evaluated for **V.9**, **V.9-H$_2$** and **[V.9]$^{2+}$**. For optimised geometry, the molecular structure from XRD was taken for **V.9 and [V.9]$^{2+}$**. The initial structure for **V.9-H$_2$** was obtained with the energy optimised structure (Fig. 5.19). The optimised structure of **V.9-H$_2$** is much distorted compared to its **V.9** and **[V.9]$^{2+}$** molecule. The NICS(0) value was calculated at non-weighted mean centre of the macrocycle using B3LYP/6-31G(d, p) level of theory.

The free base porphyrin, **V.9**, shows NICS -14.05 ppm and hence aromatic in nature. For the dicationic molecule **[V.9]$^{2+}$**, estimated the NICS value of -9.60 ppm confirmed the aromatic character of **[V.9]$^{2+}$.** A decrease in NICS value supported the dicationic nature of porphyrin. Hence confirming the conversion of aromatic **V.9** to aromatic dicationic species **[V.9]$^{2+}$** through 4e^{-}oxidation of **V.9**. The **V.9-H$_2$** shows the positive NICS value and confirmed its antiaromatic characteristics (Table 5.1).

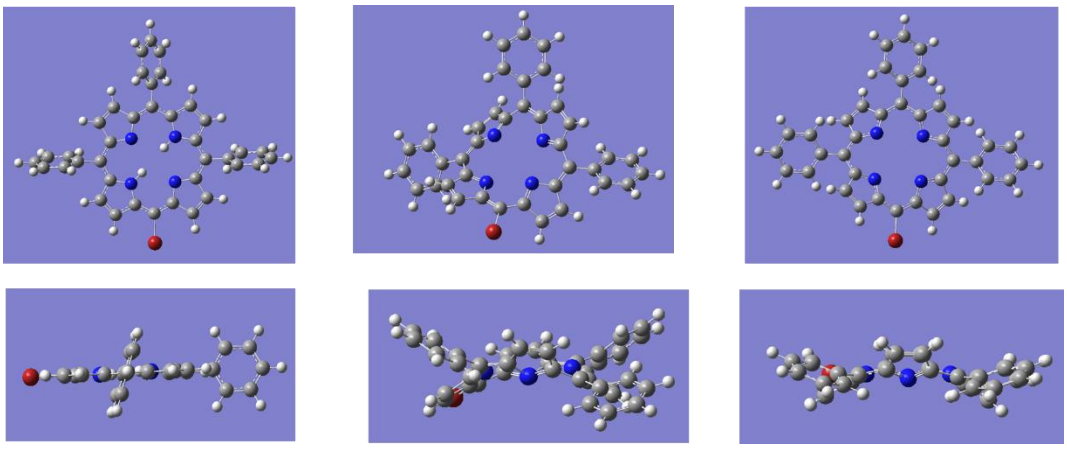

Fig. 5.19. Energy optimised structure of **V.9**, **V.9-H$_2$** and **[V.9]$^{2+}$** with B3LYP/6-31G (d,p) level of theory using DFT calculation.

Molecule	V.9	$[V.9]^{2+}$	V.9-H_2
π electrons	18π	14π	16π
Nature	Aromatic	Aromatic	Anti-Aromatic
NICS Value	-14.24 ppm	-9.60 ppm	+4.94 ppm

Table. 5.1: Molecules with their respective NICS value and their behaviour.

5.11 Conclusion

The coupling of aromatic porphyrin and antiaromatic isophlorin was carried out with Suzuki−Miyaura cross-coupling reaction. In the dimer, phenylene molecule acts as a bridge between isophlorin and porphyrin. The synthesized dimer was characterised with spectroscopic techniques and further electronic interaction between the isophlorin and porphyrin was confirmed through proton NMR and UV-vis absorption spectrum. The redox nature of dimer was studied, in the chemical oxidation, selectively isophlorin moiety gets oxidised from 20 πe^- to 18πe^-. Hence it forms the porphyrin and isophlorin dicationic dimer. Further the photophysical study of the dimer and its oxidised form is under process. During of redox study of these molecule we found the interesting properties of 18π *meso*-bromo porphyrin, it undergoes proton coupled electron transfer as well as ring oxidation process therefore, formed the 14 πe^- porphyrin dication. This is first example where porphyrin is stabilised in its lower oxidised form. The observation was supported by X-ray data and computational studies. Work to stabilize the 16 π intermediate molecule is under process.

5.12 Experimental Section

Synthetic Procedure and Characterization Dimer V.7

The two necked 25 mL round bottom flask equipped with the condenser was charged with isophlorin **III.7** (20 mg, 22.74 µmol), borylated porphyrin **V.10** (15.86 mg, 27.23 µmol), Cs_2CO_3 (14.82mg, 45.48µmol) and $Pd(PPh_3)_4$ (5.26mg, 4.55µmol) and reaction mixture was purged under N_2. The mixture of solvent dry DMF (1 mL) and dry toluene (2 mL) was added and degassed with N_2 gas then resulting mixture was stirred for 3 hours at 80°C. The progress

of reaction was checked with MALDI-TOF/TOF mass spectrum. The reaction was quenched with water and organic layer was extracted with ether and dried over Na_2SO_4. The solvent was passed with short bed of alumina column and eluent was evaporated under vacuum. Then desired compound was separated over size exclusion column in toluene on the basis of mass of the products. The desired dimer **V.7** was isolated as orange colour band in 20% yield.

HRMS (ESI) m/z: 1336.2975 and 668.6545 (Calcd. for $C_{82}H_{42}F_{10}N_4O_4$; $[M]^+$ 1336.3046 and $[M]^{2+}$ 668.1523). UV-vis (in CH_2Cl_2) λ_{max} nm: 325, 365, 422, 514, 550, 590 and 644 nm.^{1}H NMR (400 MHz in $CDCl_3$ at 298K) δ: 8.78 (m, 4H), 8.65 (d, J= 8 Hz, 2H), 8.32 (d, J= 8 Hz, 2H), 8.15 (m, 2H), 8.12 (m, 4H), 7.77 (d, J= 8 Hz, 2H), 7.70 (m, 9H), 6.95 (m, 3H), 6.73(d, J= 8 Hz, 2H), 6.36 (m, 2H), 3.03 (d, J= 4 Hz, 2H), 2.60 (d, J= 4 Hz, 2H), 2.56 (d, J= 4 Hz, 2H), 2.42 (d, J= 4 Hz, 2H), -2.93(brs, 2H).

Dimer Dication $[V.7]^{2+}$

The stoichiometric excess of $[Et_3O]^+[SbCl_6]^-$ was added to solution of **V.7** in dry and distilled dichloromethane at -20 °C and resulting solution was stirred for 20 mins at same temperature. Then the stirring was stopped and allow it to come at RT. The green color solution indicate the formation of **$[V.7]^{2+}$**. The solution was filtered in order and then concentrated under the vacuum. The resulting compound was multiple times washed with *n*-hexane and *n*-pentane to remove excess of salt. The **$[V.7]^{2+}$** was obtained in quantitative yield.

UV-vis (in CH_2Cl_2) λ_{max} nm: 448 and 665 nm. ^{1}H NMR (400 MHz in acetonitrile-d_3 at 298K) δ: 11.06 (br s, 2H), 10.85 (br s, 2H), 10.72 (br s, 2H), 10.61(br s, 2H), 9.44 (br s, 2H), 9.39 (br s, 2H), 9.28 (br s, 2H), 9.06 (br s, 2H), 8.85 (br s, 4H), 8.80 (m, 6H), 8.63 (m, 2H), 8.16(m, 2H) and -1.76 (br s,2H).

Dication porphyrin $[V.9]^{2+}$

Synthetic procedure of **$[V.9]^{2+}$** is similar to **$[V.7]^{2+}$**.

UV-vis (in CH_2Cl_2) λ_{max} nm: 444 and 665 nm. ^{1}H NMR (400 MHz in acetonitrile-d_3 at 298K) δ: 9.54 (d, J= 4 Hz, 2H), 8.92 (d, J= 4 Hz, 2H), 8.81 (m, 4H), 8.61 (m, 2H), 8.56 (m, 4H), 8.06 (m, 9H). X-ray crystal data: $(C_{38}H_{23}BrN_4)^{2+}$ $2(Cl_6\ Sb),)^-$, Triclinic, space group P -1, a = 9.918(2), b = 16.699(3), c = 18.156(4) Å, α = 114.468(5), β = 98.754(5), γ = 99.349(5); V = 2618.7(9) Å^3, Z = 2, T = 273 K, D_{calcd} = 1.865 g cm^{-3}, R_1 = 0.0880(7760), R_w (all data) = 0.2349(13054), GOF = 1.064.

Refrences

1. D. Dolphin, *The Porphyrins*, Academic press, **1978**.
2. (a) Deisenhofer, J.; Epp, O.; Miki, K.; Huber, R.; Michel, H. *J. Mol. Biol.*, **1984**, *180*, 385-398. (b) M. R. Wasielewski in M. A. Fox and **M.** Chanon (Eds.): *Photoinduced Elecfron Punsfir,* Elsevier, Amsterdam and **1988**, part A, p 161.
3. S. Nakajima, T. Nagata, K. Toriumi K. Maruyarna, and A. Osuka, *Angew. Chem. Int. Ed. Engl.* **1991**, *30*, 5, 582-584.
4. T. Nagata, A. Osuka, and K. Maruyama *J. Am. Chem. Soc*., **1990**, *112*, 3054-3059
5. H. Shimidzu and A. Osuka, *Angew. Chem. Int. Ed. Engl.* **1997**, *36*, 135-137.
6. R. G. Khoury, L. Jaquinod and K. M. Smith *Chem. Commun*., **1997,** 1057-1058**.**
7. A. Tsuda and A. Osuka, *Science,* **2001**, *293*, 79-82.
8. B. K. Reddy, S. C. Gadekar and V. G. Anand *Chem. Commun.*, **2016**, *52*, 3007-3009.
9. (a) R. D. Hartnella, A. J. Edwardsb and D. P. Arnold, *J. Porphyrins Phthalocyanines* **2002**, *6*, 695-707. (b) O. Locos, B. Basic, J. C. McMurtrie, P. Jensen, and D. P. Arnold *Chem. Eur. J.*, **2012**, *18*, 5574-5588.
10. N. Aratani and A. Osuka, *Org. Lett.*, **2001,** *3*, 4213-4216.
11. (a) Frisch, M. J.; et al. Gaussian 09, revision B.01; Gaussian, Inc.: Wallingford, CT, **2009 (b)** P. V. R. Schleyer, C. Maerker, A. Dransfeld, H. Jiao, N. J. R. van Eikema Hommes, *J. Am. Chem. Soc*. **1996**, *118*, 26, 6317-6318.
12. R. Rathore, A. S. Kumar, S. V. Lindeman, J. K. Kochi, J. *Org. Chem.*, **1998**, *63*, 5847-6682.
13. Y. Yamamoto, A. Yamamoto, S. Y. Furuta, M. Horie, M. Kodama, W. Sato, K. Y. Akiba, S. Tsuzuki, T. Uchimaru, D. Hashizume, and F. Iwasaki, *J. Am. Chem. Soc*, **2005**, *127*, 14540-14541.
14. J. A. Cissell, T. P. Vaid and G. P. A. Yap *Org. Lett.*, **2006**, *8*, 2401-2404.
15. Y. Yamamoto, Y. Hirata, M. Kodama, T. Yamaguchi, S. Matsukawa, O. K. Akiba, D. Hashizume, F. Iwasaki, A. Muranaka, M. Uchiyama, P. Chen, K. M. Kadish, and N. Kobayashi, *J. Am. Chem. Soc*., **2010**, *132*, 12627-12638.
16. T. Kakui, S. Sugawara, Y. Hirata, S. Kojima, and Y. Yamamoto, *Chem. Eur. J,*. **2011**, *17*, 7768-7771.
17. M. D. Ambhore, A. K. Basavarajappa, V. G. Anand, *Chem. Commun*., **2019**, *55*, 6763-6766.
18. H. Sun, J. C. Biffinger and S. G. DiMagno, *Dalton Trans.*, **2005**, 3148-3154.

Summary

This dissertation includes the synthesis and characterization of a wide range of core modified isophlorinoids. While the first chapter provides a comprehensive review of the literature on isophlorinoids and porphyrinoids, the second chapter discusses the synthesis of 30π planar core modified hexaphyrins with four furan and two pyrrole units. In this hexaphyrin, conjugation occurs through a skeleton structure of sp^2 hybridized carbon atoms, and the outer protons of the macrocycle are deshielded in compared to the inner protons. The 30π Huckel aromatic hexaphyrins reversibly oxidized to their 28π Mobius aromatic dication without losing their aromatic properties. Despite its twisted topology, Mobius aromatic hexaphyrin's NMR spectra revealed significant diatropic ring current. Secondly, the furan containing tetraoxa-isophlorins and octaphyrin were synthesised by the [1+1] and [2+2] condensation of dipyrromethane and furan dicarbinol respectively. Due to presence of three distinct *meso*-substituents, these macrocycles may be synthons for supramolecular chemistry. Interestingly, the octaphyrins exhibit solvatomorphism in the presence of dichloromethane and chloroform, and the conformations obtained were entirely different.

The higher membered isophlorinoids, decaphyrin were synthesised with 44π and 46π electronic circuits. Single crystal X-ray analysis reveals the completely planar nature of these giant isophlorinoids. The 44π decaphyrin has well resolved NMR signals along with symmetrical structure, yet it has a closed shell character. Whereas, the 46π aromatic decaphyrins displayed the open shell character analysed with EPR spectroscopy and quantum chemical calculations. The 42π dicationic decaphyrins were also revealed the 50% of diradical character. This observation supports the fact that as conjugation length increases, the diradical character of the molecule increases significantly; thus, 38π octaphyrin has 40% diradical character, while 46π decaphyrins has 69% diradical character.

The final chapter thoroughly discusses the synthesis of phenylene bridge isophlorin porphyrin dimer by the suzukii-Miyuara cross coupling reaction of *meso*-borylayed porphyrin and *p*-Br Ph substituted isophlorins. The dimer formed demonstrates the electronic effect of coupling on porphyrin and isophlorin. The redox studies of the isophlorin-porphyrin dimer describe the selective oxidation of 20π isophlorin to its 18π dication, i.e. dimer holding the 18π-20π electrons transforms to 18π-18π phenylene bridge dimer.

Furthermore, the redox properties of 18π porphyrins were studied; normally, the 18π porphyrins can be oxidized to up to 16π electronic states by metal assisted reactions and peripheral modifications. However, this is the first time we have demonstrated the synthesis of 14π porphyrin via the PCET followed with ring oxidation of 18π porphyrin. The aromatic features of 14π porphyrins was evaluated with the single crystal x-ray analysis and computation studies. Hence the overall thesis describes the finding of isophlorinoids as synthetic models having open shell character, polymorphic nature and along with their wide range of redox properties.

List of Publications

1- Open shell (4n + 2)π and closed shell 4nπ planar core-modified decaphyrins. Pragati Shukla, M. D. Ambhore, and V. G. Anand, *Chem. Sci.*, **2024**, *15*, 6022-6027.

Redox Assisted Reversible Aromaticity Transition between 30π Hückel and 28π Möbius Dication of a Core-Modified Isophlorinoid, Pragati Shukla, M. D. Ambhore, and V. G. Anand, *Chem. Eur. J.*, **2023**, e202203327.

2- Tailoring diradicaloid properties of expanded isophlorinoids with systematic core-modification, M. D. Ambhore, Pragati Shukla, R. G. Gonnade and V. G. Anand, *Chem. Commun.*, **2022**, *58*, 8946-8949**.**